Sulfur Speciation and Curation Considerations for the Carbonaceous Chondrite Tagish Lake and Other Meteorites

by

Miranda Celeste Holt

A thesis submitted in partial fulfillment of the requirements for the degree of

Master of Science

Department of Earth and Atmospheric Sciences

University of Alberta

Abstract

Carbonaceous chondrites contain significant abundances of sulfur components such as sulfide, sulfate, elemental sulfur (S^0), and organosulfur compounds. These are significant because questions remain regarding the role of S in the origin of life. Chondrites and all other meteorites are out of equilibrium at Earth's surface, and if stored improperly will undergo modification relatively rapidly. Additionally, analysis that modifies the form of the sample has the potential to alter its intrinsic properties. This is an important consideration when determining whether a sample can be used for multiple analyses, a necessity for future sample return missions where a limited amount of material may be available.

This thesis will: 1) Examine the Fe-Ni sulfides present in several carbonaceous chondrites to constrain their formation mechanisms and temperatures as well as the extent of aqueous alteration experienced by their parent bodies; 2) Perform chemical extractions to determine the nature of any organosulfur species which may be present within Tagish Lake; 2) Assess the extent to which the organosulfur content of Tagish Lake may have been modified following collection, storage, and processing during analysis; 3) Assess the degree to which sample heterogeneity and experimental method may influence analytical results; 4) Develop recommendations for proper curation methods for extraterrestrial materials.

As a part of this study, analysis of Fe-Ni sulfide grains within three carbonaceous chondrites, C2 Tagish Lake (TL), CM2 Aguas Zarcas (AZ), and C2 Tarda by scanning electron microscope and electron probe microanalyzer has revealed multiple morphologies, textures, and mineral phases, including some which may have formed at high temperatures of ~500-600°C within the solar nebula and some which formed at lower temperatures of ~25-135°C during parent body aqueous alteration. These temperatures of formation are based on mineral compositions plotted on Fe-Ni-S ternary diagrams, yielding the temperature of the altering fluid.

Organosulfur species provide an important record of pre- and early solar chemical reactions and parent body aqueous alteration processes. Chemical extractions designed to establish whether organosulfur species may be present within a pristine sample of Tagish Lake (specimen TL1) which has remained frozen since collection have determined that the most likely compound to be present, methane sulfonic acid, is not present within this sample in an easily accessible form. As this compound has previously been found within Tagish Lake, potential explanations for its absence in the samples studied herein, including previous extractions of samples of TL 5b and TL 11h as well as a new extraction of sample TL1, are investigated. Possible explanations include lithologic differences between samples, changes to the organosulfur or other S-species and the growth of a new mineral, gypsum, as a result of previous chemical extractions or long-term storage of samples, potential contamination, and loss of compounds during extraction and analysis as a result of the failure of existing experimental methods.

Following investigations on the effects of storage conditions into the preservation of both organic-containing stony meteorites as well as iron-based meteorites, recommendations for the storage conditions of these types of materials are made to ensure their continued preservation. In particular, storage of extraterrestrial materials in anoxic or inert atmospheres is found to be beneficial to the preservation of both carbonaceous chondrites as well as iron meteorites.

Preface

Chapter 2 of this thesis has been published as M. C. Holt and C. D. K. Herd "Fe-Ni sulfides in Tagish Lake: Implications for nebular and parent body conditions of formation" in the journal *Meteoritics and Planetary Science,* Volume 57, Issue 6, pages 1267-1287. I was responsible for the collection and analysis of the data, as well as writing and submitting the manuscript for publication. As the supervisory author, C. D. K. Herd was involved in formation and discussion of the concept, as well as responsible for significant edits to the manuscript. The supplemental tables included in the publication have been included as Appendix A.

The remainder of the chapters of this thesis are original, previously unpublished work by Miranda Holt.

Dedication

I dedicate this work to my sister Katrina, who has cared for, loved, and believed in me since the day I was born, and without who's guidance I would not have been able to accomplish all that I have. I love you. Thank you.

Acknowledgments

I would like to thank my MSc supervisor, Dr. Chris Herd for the many opportunities he has provided for me to advance my scientific and professional careers, and for his continued support throughout the entire process. The opportunity to work in Chris's lab was the beginning of my love for museums and collections, and many of the experiences I have had within this field would not have been possible without Chris, for which I am beyond grateful. It has been my privilege to be counted among the many excellent students you have and continue to nurture. I would also like to thank the other members of our lab group for their support and insights. In particular, I would like to thank Libby Tunney for her continued advice and friendship through the years of both our undergraduate and graduate studies. The chance to learn and grown with you is truly irreplaceable.

Thank you to members of my supervisory committee, Dr. Long Li, for his insights and feedback, and Dr. Rob Hilts for his continued patient assistance as I waded into the world of organic chemistry. Your confidence in me helped me gain confidence in myself. Thank you also to Dr. Thomas Chacko for serving as arm's length examiner for lending your expertise to the examination of my projects.

I would like to thank Nathan Gerein for his assistance with SEM data collection, Andrew Locock for his assistance with EPMA data collection, Patrick Hill and Libby Tunney for assistance in sub-sampling, and Mark Labbe for sample cleaning, preparation and epoxy mounting. I thank Alyssa Becker-Burns for her guidance during the completion of the iron meteorite conservation project, and the Smithsonian Natural History Museum and Natural History Museum (UK) for their input. I would also like to thank Jing Zheng from the University of Alberta and Aaron Skelhorne at MacEwan University for assistance with GC-MS data collection and reduction, Randy Whittal and Béla Reiz from the University of Alberta assistance with LC-MS data collection and interpretation, and Spencer Poulette for collection and interpretation of Raman data.

To my mom, dad, sister, and friends, who have faithfully and continually cared for and loved me during both successes and setbacks – Thank you. I could not have done this without you. Your support means more to me than I could ever express. Finally, I would like to thank my partner for believing in me even when I didn't believe in myself, and for light to my life and smiles to my face. Thank you. To everyone.

Table of Contents

List of Tables

List of Figures

Figure 3.8: Fe/S (at%) ratios of: a) The different samples of Aguas Zarcas examined in this study, as well as by Schrader et al. (2021), arranged according to increasing degree of alteration. b) The average values of examined Aguas Zarcas and Tagish Lake samples from this study, as well as average Fe/S (at%) ratios of Aguas Zarcas and CM1, CM1/2, CM2, and CI chondrites examined by Schrader et al. (2021), arranged according to increasing degree of alteration. Error bars represent one standard deviation from the mean.

Figure 4.1: Backscattered electron (BSE) images of the Tarda meteorite. a) fusion-crusted section of the Tarda matrix; b) porphyritic olivine chondrule containing dense mesostasis and sulfide-rimmed metal; c,d) several porphyritic olivine chondrules within the Tarda matrix containing porous phyllosilicates and sulfides; e,f) an example of a lithic clast containing numerous small fine-grained sulfide rings.

po= pyrrhotite-group sulfides; pn = pentlandite; alloy = Fe-Ni metal alloy.

Figure 4.2: BSE images of exsolved Fe-Ni sulfide grains including: a) lamellae and blocky pentlandite exsolved from pyrrhotite; b) pentlandite flames and lamellae exsolved from pyrrhotite; c,d) “snowflake” pyrrhotite exsolved from pentlandite; e,f) Fe-Ni metal alloy exsolved from troilite.

Figure 4.3: BSE images of a,b) unexsolved pyrrhotite and c,d) unexsolved pentlandite grains within the Tarda matrix.

Figure 4.4: BSE images of examples of “bull’s eye” sulfides within the Tarda matrix.

Figure 4.5: Compositional data from Fe-Ni sulfides in Tarda samples plotted on Fe+Co-Ni-S ternary diagrams. a) exsolved pyrrhotite-pentlandite grains at 600°C (Kosyakov et al., 2003); b) unexsolved pyrrhotite grains at 25°C (Vaughan and Craig 1997); c) unexsolved pentlandite grains at 25°C (Vaughan and Craig 1997); d) unexsolved pentlandite grains at 600°C (Kosyakov et al., 2003); e) “bull’s eye” sulfides at 25°C (Vaughan and Craig 1997).

Figure 4.6: Fe/S (at%) ratios of the of a) the examined low-Ni pyrrhotite group sulfides as compared to other aqueously altered C1 and C2 carbonaceous chondrites. Aguas Zarcas measurements are highlighted in red, Tagish Lake in blue, and Tarda in green; b) all pyrrhotite-group sulfides within Tarda samples MET11800/1 and MET11800/2 compared to individual lithologies of Tagish Lake. Tarda measurements are highlighted in red; c) pyrrhotite-group sulfides in Tarda excluding tertiary troilite formed upon atmospheric transit, compared to Tagish Lake lithologies. Tarda measurements are highlighted in red. Error bars represent one standard deviation from the mean.

Figure 5.1: Backscattered electron (BSE) images of Sample TL 8a. A) A relatively unaltered chondrule composed of Fe-rich olivine and pyrrhotite. B) A chondrule with a moderately high degree of alteration containing olivine, phyllosilicates, and magnetite. C) An unexsolved grain of pyrrhotite associated with magnetite within the sample matrix. D) A grain of pyrrhotite exhibiting exsolution of coarsened pentlandite lamella. E) A section of fusion crust containing pyrrhotite with exsolved kamacite. F) A portion of the sample matrix containing an unusually high amount of magnetite in association with a fine-grained ring of pyrrhotite.

Figure 5.2: BSE images of previously extracted powder from sample TL 11h. A,B) Portions of matrix with discernible euhedral magnetite framboids. C,D) Portions of matrix with intact euhedral olivine.

Figure 5.3: BSE images of gypsum crystals taken from the previously extracted TL 11h powder following hot water extraction. Crystal show varying amounts of this powder adhered to their surfaces.

Figure 5.4: The Raman spectrum of the white precipitate removed from sample 1.2. The black box denotes the position of the broad peak which identifies this precipitate as most likely being an amorphous Mg-sulfate.

Figure 5.5: The relative magnitudes of the peak areas of derivatized MSA peaks present in the GC-MS traces of acetonitrile extracts from Allende samples from prepared group 1.

List of Symbols and Abbreviations

At%	Atom percent
AZ	Aguas Zarcas
B.D.L.	Below detection limit
DCM	Dichloromethane
EPMA	Electron probe microanalyzer
FESEM	Field Emission Scanning Electron Microscope
GC-MS	Gas Chromatography – Mass Spectrometry
IOM	Insoluble organic matter
LC-MS	Liquid Chromatography – Mass Spectrometry
MSS	Monosulfide solid solution
MTBSTFA	N-tert-Butyldimethylsilyl-N-methyltrifluoroacetamide
NIST	National Institute of Standards and Technology
RH	Relative humidity
S^0	Elemental (zerovalent) sulfur
S_6	Hexathiane
S_8	Cyclic octaatomic sulfur
PAH	Polycyclic aromatic hydrocarbon
Pn	Pentlandite
Po	Pyrrhotite
SEM	Scanning Electron Microscope
TL	Tagish Lake
Wt%	weight percen

Chapter 1: Introduction

1.1 Introduction

Meteorites represent samples of extraterrestrial material that can provide valuable information on the conditions of the early solar system in which they were formed and whose history they preserve. An average of 2900-7300 kg of this material fall to the Earth's surface every year, ranging in size from small 10 g particles to 1 kg stones, with an average of 8.7 falls of >1 kg in mass (Bland et al., 1996). Yet many of these specimens remain unrecovered for long periods of time or may never be recovered. As a result, the quantity of extraterrestrial material available for study is limited, and often in a less-than-ideal state of preservation by the time it is retrieved. It is thus important to make careful use of and preserve these materials in a state as close to their original, unaltered state as possible. This can be achieved in part through optimizing protocols for curation of samples. When properly preserved, it is possible to gain insights into such information as the chemistry, organic content, and compositions of, as well as the geologic processes which prevailed on the bodies of the early solar system, through the study of extraterrestrial material delivered to us either as meteorites or though sample return missions. The main aims of this study are to investigate 1) the intrinsic nature of and changes to the sulfur chemistry of several members of the group of meteorites known as carbonaceous chondrites as a result of collection, storage, and study and 2) to determine ideal conditions of curation for the preservation of these and other meteorites.

1.2 Carbonaceous chondrites

Carbonaceous chondrites are a subgroup of stony meteorites which contain indigenous organic species. These meteorites can contain up to ~ 6 wt% carbon (Pearson et al., 2006), up to ~ 5 wt% of which may be organic (Wetherill and Chapman, 1988). They can be further classified into 11 groups, CI, CM, CR, CO, CV, CK, CH, CB, CY, CL, and ungrouped, according to their mineralogy and bulk chemical composition. Meteorites within these groups are given petrologic types between 1 and 6, which reflect

the degree of aqueous alteration and thermal metamorphism they have experienced, where degree of aqueous alteration increases from 3 to 1 and thermal metamorphism from 3 to 6. The meteorites utilized during the course of this study include Tagish Lake and Tarda, which are similar C2 ungrouped carbonaceous chondrites, and Aguas Zarcas, a CM2 carbonaceous chondrite. Carbonaceous chondrite groups CI and CM are known to be some of the most chemically primitive materials available for study (e.g. Huss et al., 2003). They have also experienced aqueous alteration to various degrees on their meteorite parent bodies, typically ranging between petrologic types 1 and 2 (e.g. Rubin et al., 2007, Alexander et al., 2013; Howard et al., 2015). As Tagish Lake is known to have similarities to both CM and CI groups, these groups along with Tagish Lake and Tarda are most relevant for consideration during this study.

1.3 Sulfur in Carbonaceous Chondrites

Carbonaceous chondrites contain significant abundances of sulfur components such as sulfide, sulfate, elemental sulfur (S^0), and organosulfur compounds (Burgess et al., 1991). These species are noteworthy because 1) the distribution of S between different minerals and valence states within meteorites reflects the history of the meteorite (Kaplan and Hulston, 1965); 2) The temperature of formation of Fe-Ni sulfides is one of only a few sources of information available to determine the temperature of alteration occurring on meteorite parent bodies; 3) light elements such as C, H, O, N, and S are important for the understanding of life and pre-biotic chemistry, and significant questions remain regarding the role of S in the origin of life.

1.3.1 Sulfur Speciation

Carbonaceous chondrites contain a significant amount of sulfur, ranging from ~1 – 4.4 wt% S, increasing in the order of CR < CM < CI (Burgess et al., 1991). There are a wide variety of carriers of S within C1 and C2 chondrites (e.g. elemental sulfur, sulfides such as troilite, pyrrhotite, and pentlandite, organic sulfur, and sulfates such as gypsum, tochilinite, epsomite, and bloedite; Burgess et al., 1991).

Their variety and proportions vary between C1 and C2 groups according to original mineralogy, temperature of alteration, and depth of origin on the meteorite parent body as precursor phases such as troilite are oxidized as aqueous alteration progresses (Burgess et al., 1991).

Although various studies report a range of values for both the concentrations of specific S-bearing components, in general, C1 chondrites are dominated by sulfate, C2 chondrites by elemental S, and C3 chondrites by troilite, although the distribution of phases is complex, particularly in C2 chondrites (Kaplan and Hulston, 1965). CI (Table 1.1) chondrites contain sulfate as their most abundant component, followed by elemental S, and sulfide (e.g. Burgess et al., 1991) although the sulfate proportion is likely affected by addition of terrestrial sulfate (Airieau et al, 2005), while CM chondrites (Table 1.2) contain sulfides as their phase of highest proportion, followed by sulfate, then elemental S (e.g. Burgess et al., 1991). The compositions of Fe-Ni sulfides within these meteorites can be plotted on Fe-Ni-S ternary diagrams (Figure 1.1) and compared to phase relations expected at various temperatures to determine their temperature of formation. At least a portion of this sulfate is believed to have originated during parent body aqueous alteration (Lee, 1993). The oxidation state of S in carbonaceous chondrites varies widely. Indeed, in addition to the presence of both oxidized and reduced S in mineral form as sulfate and sulfide respectively, the oxidation state of S in insoluble organic matter (IOM) can range from S^{-2} to S^{+6} within the same meteorite (Bose et al., 2017). Using a ratio of oxidized/reduced sulfur, the degree of alteration experienced by carbonaceous chondrites can be determined to be CM < CI, which is consistent with estimations given by other methodologies, such as petrographic studies (Burgess et al., 1991).

1.3.2 Sulfur isotopic Composition

Sulfur provides a unique opportunity for insight into chemical reactions as it possesses 4 stable isotopes and displays natural occurrences of both mass dependent and mass independent fractionation

(MIF) (Rai and Theimens, 2007). MIF occurs in the products of UV pyrolysis of SO_2 or H_2S (Farquhar et al., 2000). Labidi et al (2017) propose several models for incorporation of the MIF-bearing components into the CM parent body which are: 1) Incomplete photodissociation of H_2S and contemporaneous production of sulfides (troilite) and S^0, the latter of which is removed immediately following production via condensation; 2) H_2S of heterogeneous isotopic composition which has experienced some degree of photodissociation at temperatures of <500 Kelvin and condensed S^0 are trapped within ices and accreted into the CM parent body, where later melting releases the H_2S to react with any Fe-metal present. Chemically primitive meteorites may have recorded the resulting complex S-chemistry of both the early solar nebula and the parent bodies from which they are sourced (Labidi et al., 2017). The applications of the sulfur isotopes within these groups of meteorites are three-fold: 1) assessment of the sulfur chemistry of the early solar system; 2) determining the degree of aqueous alteration on the meteorite parent body and 3) elucidating the relationships between phases formed and altered during such processes.

The isotopic compositions of the various S-bearing components of carbonaceous chondrites vary between studies and specimens, however some general trends do emerge. The $\delta^{34}S$ of carbonaceous chondrites shows a trend consistent with degree of alteration such that $\delta^{34}S$ CI > $\delta^{34}S$ CM > $\delta^{34}S$ CV (Gao and Thiemens, 1993). In CI chondrites, sulfide is isotopically heaviest, followed by S^0, and sulfate is lightest (Table 1.3). In CM chondrites, typically S^0 is isotopically heaviest, followed by sulfide, with sulfate again being lightest (Table 1.4). Previous studies involving multiple CI and CM chondrites show variations in S isotopic composition to be primarily mass dependent (e.g. Gao and Thiemens, 1993; Bullock et al., 2010). This is suggested to be the result of the removal of MIF anomalies during aqueous alteration as a result of the volatility of S, anomalies being hosted in refractory phases (Gao and Thiemens, 1993) or MIF signal simply overwhelmed by “normal” isotopic signature (Rai and Thiemens, 2007). More recent analyses of CM chondrites have revealed the presence of sub-meter scale heterogeneities in MIF-

associated ^{33}S anomalies hosted primarily in S^0 or its precursor, suggesting parent body aqueous alteration did not homogenize these isotopic signatures at this scale, and that fluid flow was not pervasive in the region of CM formation (Labidi et al., 2017).

1.4 Curation of Extraterrestrial Materials

The Earth's present surface conditions are drastically different from those under which extraterrestrial materials were formed in the primordial solar nebula (Allen at al., 2011). As a result, they record valuable information regarding these early solar system conditions under which they were formed. However, contributions and changes to these materials as a result of interactions with terrestrial environments can alter the materials' intrinsic properties and obscure this information. Additionally, the limited number of the samples themselves requires that their use and preservation be carefully managed to ensure their long-term availability and valuable research contribution potential be maximized. An important aspect of this preservation involves curation.

1.4.1 Volatile-bearing Meteorites

It is of particular importance to limit the amount of terrestrial contamination experienced by volatile and organic-bearing meteorites. Organic species within such meteorites, particularly carbonaceous chondrites, may have contributed prebiotic compounds to the organic content of the early Earth (Chyba and Sagan, 1992). Therefore, determining the sources and evolution of these compounds is considered to be of great importance. This goal is complicated by the addition of terrestrial biotic and abiotic organic contaminants, a process which begins the moment the sample is collected on its parent body or passes into Earth's atmosphere (Herd et al., 2016). Additionally, alteration of the minerals and compounds within these materials through oxidation and hydrolysis or loss of volatile compounds at temperatures greater than 0°C can permanently alter the intrinsic properties of extraterrestrial samples (Herd et al., 2016). Storage of these materials at conditions which prevent contamination or alteration is crucial. Monitoring and identifying sources of contamination, and

storage at low temperature and in inert atmospheres such as Ar gas (Herd et al., 2016) are methods of curating these samples which may be implemented to reduce the effects of terrestrial contamination.

1.4.2 Iron Meteorites

Much of the focus of recent efforts in the curation of extraterrestrial material has been on preserving and preventing the contamination of the organic-molecule-bearing carbonaceous chondrites, as well as anticipating the needs of sample return missions (Herd et al., 2016). However, any extraterrestrial material is susceptible to terrestrial modification as soon as entering the Earth's atmosphere. All meteorites are out of equilibrium at Earth's surface conditions, and without proper storage, changes can occur rapidly. This truism extends beyond the chemically complex carbonaceous chondrites to even the most robust of iron meteorites.

Contamination by chlorides through handling, pollution, and exposure at the fall site prior to collection accelerates the inevitable corrosion of iron meteorites once they are exposed to the oxygen and moisture of Earth's atmosphere (Allington-Jones 2020). Iron meteorites are inherently unstable in the Earth's oxygenated atmosphere, which is drastically different from the conditions under which they have existed since formation. These meteorites will eventually deteriorate by hydrolysis and oxidation. However, careful management, handling, and control of storage conditions can slow this deterioration to a near halt, preserving their condition for the foreseeable future.

1.5 Summary and Goals

This study will: 1) Determine the nature of the S-species present in several carbonaceous chondrites to constrain their formation mechanisms and temperatures, the extent of aqueous alteration experienced by their parent bodies, and relationships between phases; 2) Assess the extent to which these characteristics have been modified following collection, storage, and processing during analysis; 3) Assess the degree to which sample heterogeneity may influence analytical results; 4) Develop

recommendations for proper curation methods and order of analysis for various extraterrestrial materials.

The conclusions of this study are anticipated to extend to other carbonaceous chondrites, providing a broader insight into processes in the early solar system.

1.6 Tables

Table 1.1: Abundance of S-bearing phases in CI chondrites. Sections marked with "-" indicate this value was not reported for a particular source.

Study	Bulk S (wt%)	Sulfide (wt%)	Sulfate (wt%)	S^0 (wt%)	Organic Sulfur
Monster et al (1965)	5.0	0.8	2.1	1.8	-
Burgess et al (1991)	2.83 to 4.38	0.15 to 0.48	2.01 to 2.10	0.17 to 0.85	0.07 to 0.09
Dreibus et al. (1995)	5.35 to 5.49	-	-	-	-
Gao and Thiemens (1993)	2.70 to 5.03	0 to 0.03	1.78 to 2.2	0.04	0.4

Table 1.2: Abundance of S-bearing phases in CM chondrites. Sections marked with "-" indicate this value was not reported for a particular source.

Study	Bulk S	Sulfide	Sulfate	S^0
Burgess et al (1991)	1.74 to 3.38 wt%	0.39 to 1.26 wt%	0.40 to 2.08 wt%	0.06 to 0.38 wt%
Dreibus et al (1995)	3.02 to 3.49 wt%	-	-	-
Gao and Thiemens (1993)	-	0.05 to 0.18 wt%	0.56 to 0.80 wt%	0.03 wt%
Labidi et al (2017)	1.72 to 3.01	8300 to 20800 ppm	1100 to 13000 ppm	800 to 5500 ppm

Table 1.3: Isotopic compositions of S-bearing phases in CI chondrites. Sections marked with "-" indicate this value was not reported for a particular source.

	Bulk			sulfide			sulfate			S^0	
Study	**$\delta^{33}S$ (‰)**	**$\delta^{34}S$ (‰)**	**$\delta^{36}S$ (‰)**	**$\delta^{33}S$ (‰)**	**$\delta^{34}S$ (‰)**	**$\Delta^{33}S$**	**$\delta^{33}S$ (‰)**	**$\delta^{34}S$ (‰)**	**$\delta^{36}S$ (‰)**	**$\delta^{33}S$ (‰)**	**$\delta^{34}S$ (‰)**
Monster et al (1965)	-	0.4	-	-	2.6	-	-	-0.9 to -1.5	-	-	1.4 to 3.0
Gao and Thiemens (1993)	-0.17	6.5 to 7.1	-0.8	3.1	6.05	-	-0.52	-1.06	-2.0	2.24	4.33
Bullock et al (2010)	-	-	-	-0.17 to 3.75	-0.6 to 6.8	-0.02 to 0.28	-	-	-	-	-
Visser et al (2019)	-	-	-	-	-3.24 to 3.40	-	-	-	-	-	-

Table 1.4: Isotopic composition of S-bearing phases in CM chondrites. Sections marked with "-" indicate this value was not reported for a particular source.

	Bulk			sulfide					sulfate					S^0				
Study	**$\delta^{34}S$ (‰)**	**$\Delta^{33}S$**	**$\Delta^{36}S$**	**$\delta^{33}S$ (‰)**	**$\delta^{34}S$ (‰)**	**$\delta^{36}S$ (‰)**	**$\Delta^{33}S$**	**$\Delta^{36}S$**	**$\delta^{33}S$ (‰)**	**$\delta^{34}S$ (‰)**	**$\delta^{36}S$ (‰)**	**$\Delta^{33}S$**	**$\Delta^{36}S$**	**$\delta^{33}S$ (‰)**	**$\delta^{34}S$ (‰)**	**$\delta^{36}S$ (‰)**	**$\Delta^{33}S$**	**$\Delta^{36}S$**
Gao and Thiemens (1993)	-	-	-	0.56 to 1.44	0.98 to 2.79	4.6 to 5.1	-	-	-0.12 to 0.22	-0.29 to 0.37	-0.3 to 0.7	-	-	2.79	5.36	10.3	-	-
Bullock et al (2010)	-	-	-	-3.53 to 3.42	-6.95 to 6.07	-	-0.23 to 0.58	-	-	-	-	-	-	-	-	-	-	-
Labidi et al (2017)	-1.11 to 0.60	-0.058 to 0.207	-0.11 to 0.22	-	-0.70 to 0.18	-	-0.070 to 0.008	-0.10 to 0.22	-	-4.54 to 1.65	-	-0.036 to 0.263	-0.33 to 0.26	-	-1.84 to 5.91	-	-0.104 to 0.256	-0.23 to 0.39
Visser et al (2019)	-	-	-	-	-8.18 to 4.16	-	-	-	-	-	-	-	-	-	-	-	-	-

1.7 Figure Captions

Figure 1.1: Fe-Ni-S ternary diagram. The area containing compositions of interest for this study is highlighted in grey.

1.8 Figures

Figure 1.1

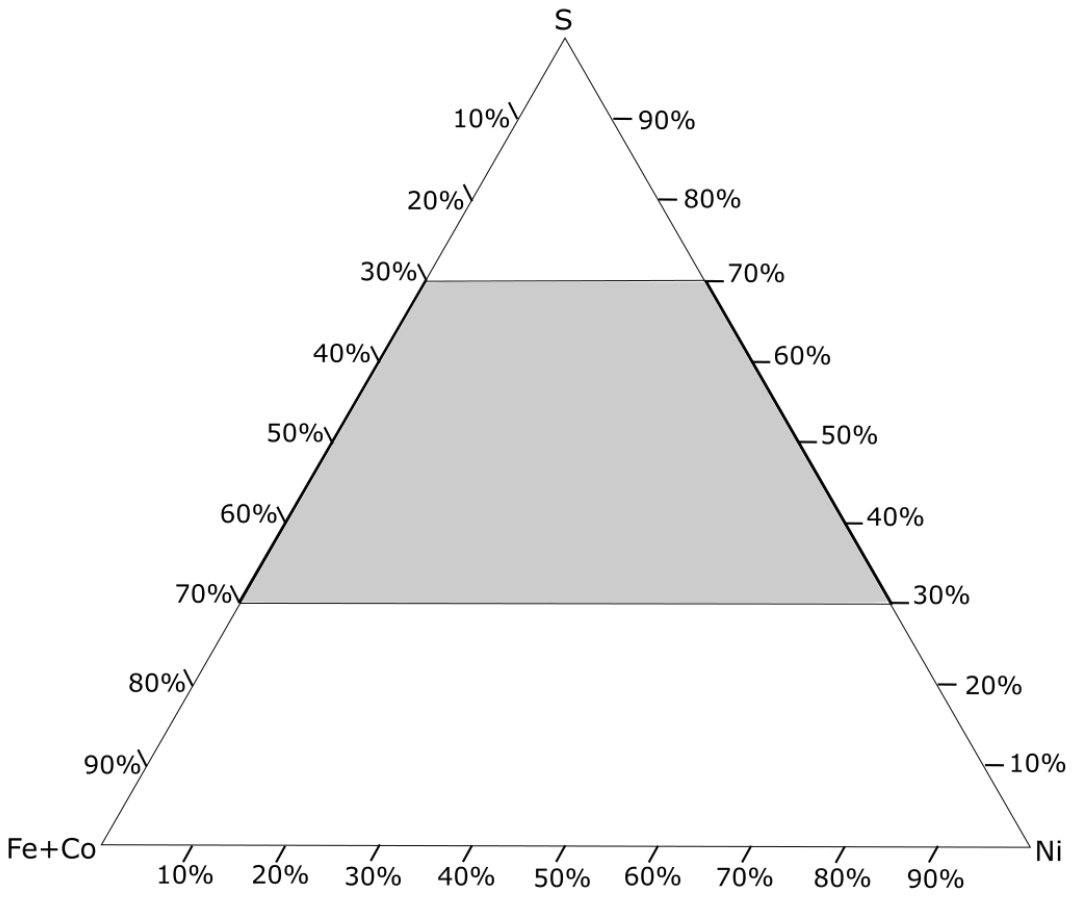

Chapter 2: Fe-Ni Sulfides in Tagish Lake: Implications for Nebular and Parent Body Conditions of Formation

Abstract

This study examined nine pristine samples representing seven lithologies of the ungrouped C2 carbonaceous chondrite Tagish Lake from the University of Alberta Meteorite Collection using scanning electron microscope (SEM) and electron probe microanalyzer (EPMA) analysis to characterize the sulfide mineralogy, textures, and compositions present. Four distinct sulfide morphologies were identified including pyrrhotite containing exsolved pentlandite, unexsolved pyrrhotite and unexsolved pentlandite, and a unique "bull's-eye" sulfide morphology. The at% Fe/Ni of the pyrrhotite grains within these samples decreases with increasing degree of alteration, and roughly places them in the alteration order of TL11v chip1 < TL4 < TL11v chip2 < TL5b ≤ TL10a < TL 11h < TL1 < TL11i. The at% Fe/Ni of low Ni (<1 wt% Ni) pyrrhotite indicates that the overall degree of alteration of Tagish Lake lies between that of CM1/2 and CI chondrites. Comparison of the composition of the sulfides to established Fe-Ni-S phase diagrams at different temperatures indicates two separate generations of sulfide formation: 1) High-temperature formation of exsolved pyrrhotite-pentlandite and much of the unexsolved pentlandite at ~500-600°C, likely by cooling of an MSS melt during chondrule formation, and 2) low-temperature formation of unexsolved pyrrhotite, some unexsolved pentlandite, pyrrhotite containing flame-like pentlandite bodies, and "bull's-eye" sulfides at ~25-100°C, likely formed during aqueous alteration events on the Tagish Lake parent body.

2.1 Introduction

The Tagish Lake meteorite is an ungrouped carbonaceous chondrite recovered from the frozen surface of the Taku Arm of Tagish Lake in British Columbia. Its fall was observed throughout the Yukon, Northwest Territories, northern British Columbia, and parts of Alaska on January 18, 2000 at 16:43 UT. The first fragments of the meteorite were recovered from the surface of the frozen lake on which it fell

by Jim Brook on January 25 and 26, 2000 (Brown et al., 2000). These specimens were wrapped in aluminium foil and placed in plastic Ziploc bags without hand contact and have been held at subzero temperatures since their collection. It is these several dozen specimens with ~0.85 kg total mass that comprise the "pristine" samples of Tagish Lake, so-called because the subzero ambient temperatures at which they have existed since their fall to Earth's surface have allowed them to remain relatively uncontaminated (Brown et al., 2000; Hildebrand et al., 2006). Analysis of this material by stepped pyrolysis of "waters" extracted from the bulk samples indicates little terrestrial signature, confirming that these samples are indeed quite pristine (Baker et al., 2002). Later collection between April 20 and May 8, 2000 provided an additional 410 fragments with various grades of degradation as a result of their immersion in meltwater (Brown et al., 2000). These later collected samples contain evidence of terrestrial contamination in both their oxygen isotopic signatures (Russell at al., 2008), and amino acids (Kminek et al., 2002). This study focuses on analysis and description of pristine samples of the Tagish Lake meteorite, hereafter referred to as Tagish Lake (TL).

Tagish Lake is an ungrouped carbonaceous chondrite with affinities to both CM and CI chondrite groups and is currently classified as petrologic type 2. This classification has been made based upon mineralogy and petrology (e.g. Simon and Grossman 2003; Zolensky et al. 2002; Boctor et al. 2003; Greshake et al. 2005; Bland et al. 2004), geochemistry (e.g. Grady et al. 2002; Mittlefehldt 2002; Nakamura et al. 2003), isotopic composition (e.g. Clayton and Mayeda 2001; Baker et al. 2002; Brandon et al. 2004; Russell et al. 2008), and organic chemistry (e.g. Pizzarello et al. 2001; Kminek et al. 2002; Pizzarello and Huang 2002; Busemann et al. 2006). Additionally, similarities between its matrix and the matrices of CR chondrites have been reported based on textures and abundance of siderite and magnetite (Zolensky et al., 2002). Tagish Lake has oxygen isotope compositions within the range of CIs (Clayton and Mayeda 2001; Russell et al., 2008), and similarly is matrix and volatile-rich (e.g. Brown et al., 2000), but contains chondrules and refractory inclusions which are more similar to CM chondrites

(Zolensky et al., 2002; Blinova et al. 2014a). Calcium-Aluminum Inclusions (CAIs) found in Tagish Lake have the same sinuous texture typically observed in CM chondrites, but alteration of these CAIs is mostly to Mg-rich serpentine, while alteration of CM CAIs typically results in Fe-rich serpentine (Zolensky et al., 2002). Additionally, the organic compounds measured in Tagish Lake do not match those within CR chondrites, and may have experienced greater parent-body aqueous and thermal processing (Pizzarello et al., 2001; Krot et al., 2002, 2005; Hilts et al. 2014). Therefore, Tagish Lake does not match any known chondrite group, and is thought to represent a possible CI precursor, or to be intermediate between CI and CM chondrites (Grady et al. 2002; Zolensky et al. 2002, 2008; Blinova et al. 2014b).

Previous examinations of Tagish Lake have described it as a heterogeneous accretionary breccia (e.g. Brown et al., 2000) and have found it to be extremely friable, have a low bulk density of 1.6g/cm^3, and be unusually porous, with a porosity of 40% (Brown et al., 2002; Ralchenko et al., 2014). The Tagish Lake meteorite is matrix supported, characterized by an opaque, dark, fine-grained matrix composed of intergrowths of Fe-bearing saponite and serpentine (Keller and Flynn, 2001; Mikouchi et al., 2001; Noguchi et al., 2002; Bland et al., 2004; Blinova eta l. 2014a). Components within the matrix include lithic fragments, sparse chondrules with 0.1-1 mm diameters and textures including altered olivine aggregates, porphyritic olivine, barred olivine, amoeboid olivine aggregates (AOAs), isolated olivine and rare pyroxene grains, rare coarse phyllosilicates and CAIs with an average diameter of 2 mm, irregular Fe-Mn-Mg-Ca carbonate nodules, magnetite, and Fe-Ni sulfides (Zolensky et al., 2002; Bland et al., 2004; Blinova et al. 2014a) primarily consisting of pyrrhotite and pentlandite (Zolensky et al., 2002; Boctor et al., 2003). The larger of these components are often surrounded by fine-grained rims, many of which contain very fine-grained Fe-Ni sulfides (Zolensky et al., 2002). The compositional ranges of olivine and pyroxene are Fa_{0-29} and Fs_{1-7}, respectively (Zolensky et al., 2002).

The Tagish Lake parent body consists of a heterogeneous precursor of anhydrous components with nebular origins which were fragmented prior to accretion and subsequently subjected to various

degrees of aqueous alteration (Blinova et al., 2014a). Samples were initially characterized as belonging to one of two main lithologies, carbonate-poor and carbonate-rich, and contain clasts of CM1-like material (Zolensky et al., 2002; Bullock et al., 2005a). The carbonate-rich lithology contains a lower abundance of magnetite and higher amounts of calcite, with almost no CAIs (Zolensky et al., 2002; Nakamura et al., 2003). The carbonates within the carbonate-poor lithology are mainly siderite, while those within the carbonate-rich lithology are primarily calcite (Nakamura et al., 2003). Izawa et al. (2010) also identified three additional "new" lithologies – magnetite, sulfide, and siderite-dominated, as well as minerals such as gypsum and talc that cannot be explained by simple mixing of the carbonate-rich and carbonate-poor lithologies, revealing Tagish Lake is even more variable in mineralogy than previously believed.

Six of the specimens included in this study have been previously examined to determine the extent of aqueous alteration experienced by the Tagish Lake parent body. These specimens, TL5b, TL11h, TL11i, TL11v, TL4, and TL10a, which are variations of the carbonate-poor lithology (Blinova et al. 2014a), span a range from type 1.6-2.0, with the lower end of this range being comparable to lesser altered members of the CM chondrite group (Gilmour et al., 2019). Tagish Lake has therefore been considered a type 1.6-2.0 ungrouped carbonaceous chondrite.

During our examination of several polished specimens of Tagish Lake, special attention was paid to the Fe-Ni sulfide minerals they contained. As these phases form, their compositions, structures, and textures are controlled by chemistry and temperature. The exsolution of pentlandite is controlled primarily by fO_2, resulting in the common association between pentlandite and FeO-rich minerals, where more oxidizing conditions result in more pentlandite and less Fe-Ni metal (Schrader et al., 2016). Additionally, the precursor sulfide phase must contain sufficient S and Ni (at least 3 wt%; Schrader et al., 2016) for exsolution to occur. Likewise, pyrrhotite composition is dependent on both fS_2 and temperature (e.g., Rau 1976; Toulmin and Barton 1964). The temperature of formation of sulfide phases

affects composition and the textures formed, such that pyrrhotite-pentlandite intergrowths form by exsolution during cooling from magmatic temperatures (>900°C), with coarse, non-linear textures developing between 610-250°C, coarse-linear from 250-150°C, and flame-shaped textures at or below 150°C (Durazzo and Taylor, 1982). Phase compositions and crystal structures can vary depending on metal-sulfur ratio and temperature (Harries and Langenhorst, 2013), and thus can be utilized to constrain closure temperature (Schrader et al., 2016).

Formation and exsolution of primary sulfides in the solar nebula occurs at high temperatures; the presence of exsolution textures would suggest the solar nebula as the likely formation environment. Potential methods of sulfide formation in the solar nebula include condensation of troilite after Fe metal through sulfidation by H_2S gas above 427°C (e.g., Grossman and Larimer 1974; Barshay and Lewis 1976; Fegley et al. 1995; Lodders 2003), which may also result in the production of pyrrhotite and pentlandite if the precursor metal was Fe-Ni metal rather than pure Fe metal (Lauretta et al.,1996a, 1996b, 1996c, 1997, 1998), or crystallization from a monosulfide solid solution (MSS) melt beginning at 1097°C, perhaps during chondrule formation (Boctor et al., 2002; Brearley and Martinez, 2010; Harries and Langenhorst, 2013; Schrader et al., 2015), which would begin exsolving to form pyrrhotite and pentlandite at about 597°C (Kitakaze et al., 2011).

Formation of sulfides during aqueous alteration on a hydrous parent body occurs at lower temperatures and has also been proposed as a potential formation mechanism (e.g. Brearley, 2006). Pentlandite may form under high fO_2 during alteration (Godlevskiy et al., 1971), and in the absence of magmatic exsolution textures indicating formation at high temperatures, its presence could suggest formation occurred via aqueous alteration by an oxidizing fluid. The oxidation of troilite at temperatures consistent with alteration on carbonaceous chondrite parent bodies can also result in the formation of magnetite, pyrrhotite, and pyrite, with the remaining unoxidized sulfide becoming increasingly Ni-enriched (Herndon et al., 1975; Bullock et al. 2005a). Sulfides may also be precipitated directly from

fluids during parent body alteration processes, with changes in solution chemistry accounting for the wide variety of textures observed (Blinova et al., 2014a; Berger et al., 2016).

Within pristine TL specimens, Blinova et al. (2014a) observed Fe-Ni sulfides as solitary subhedral to anhedral grains, including a previously unobserved "bull's-eye" morphology with a core and rim separated by a gap, or in clusters often associated with magnetite, as well as in rims with magnetite surrounding altered chondrules similar to the pure sulfide rims observed by Greshake et al. (2005). They observed sulfides both with and without exsolution textures. They found the following exsolution textures: 1) characteristic "flame" textures of pentlandite inside pyrrhotite; 2) partially coarsened *en echelon* pentlandite blades within pyrrhotite; and 3) massive pyrrhotite-pentlandite intergrowths. They also observed magnetite framboids or plaquettes in clusters with sulfides, or magnetite framboids after sulfide grains, similar to those reported by Zolensky et al. (2002). Sulfides may also be surrounded by or contain interstitial sheet silicates with sinuous textures. While these authors found no sulfide veins within any of their samples, Bullock et al. (2005b) did report such veins within a CM1 clast in Tagish Lake.

The Blinova et al. (2014a) study concluded that Tagish Lake exhibits two generations of sulfide formation. The first generation of sulfides likely formed in the solar nebula, possibly by gas-solid reactions (Lauretta et al., 1997) or metal diffusion from Ni-bearing MSS during cooling below 600°C over approximately 3000-30,000 years (Brearley and Martinez, 2010). This first generation is represented by those grains which contain exsolved pentlandite. The second generation is thought to be a result of aqueous alteration during multiple precipitation episodes at ≤100°C (Zolensky et al., 2002), and is represented by grains where pentlandite is found along pyrrhotite grain boundaries, the "bull's-eye" morphology noted, and sulfide rims surrounding highly altered chondrules. This second generation is similar to the sulfides observed by Boctor et al. (2003), which contain unexsolved Fe-Ni MSS as their primary sulfide phase.

This study had as its primary goal the systematic examination of Fe-Ni sulfide minerals within pristine samples of the Tagish Lake meteorite, including those which had not yet been thoroughly investigated. An examination of the morphologies, textures, contexts, and compositions of these minerals was conducted to determine potential formation temperatures and mechanisms, as well as any possible correlation to degree of alteration and variations in parent body conditions. Seven specimens, including six representing distinct stones (TL5b, TL11h, TL11i, TL4, TL10a, and TL1) and one composed of chips of disaggregated material (TL11v), were used to create nine epoxy mounted samples of the meteorite representing pristine lithologies with varying degrees of alteration ranging from type ~1.6-2.0 (Gilmour et al., 2019). These were examined using the scanning electron microscope (SEM) analysis and the electron probe microanalyzer (EPMA) to characterize the mineralogy, textures, and composition of the Fe-Ni sulfides present within these samples. Based on the mineralogy and compositional analysis of these phases plotted on Fe-Ni-S ternary diagrams, the temperature of formation of different phase morphologies can be elucidated (Schrader et al., 2016), and grains formed at high temperature, likely within the solar nebula, distinguished from those formed at low temperature, likely during parent body aqueous alteration. This analysis should also yield information on the temperature of the altering fluid (Berger et al., 2016), and may determine if this was consistent across samples which experienced differing temperatures of alteration.

2.2 Methods

This study was conducted using nine chips from seven pristine specimens of Tagish Lake, including prepared epoxy mounts of samples TL4 (University of Alberta specimen MET11611/P-4/1/EP) and TL10a (MET11611/P-10a/1/EP) as well as four previously described and analyzed by Blinova et al. (2014a): TL5b (MET11611/P-5b/4/EP) described as compact and coherent, with relatively abundant chondrules and light clasts; TL11v (MET11611/P-11v/4/EP), which consists of disaggregated material; TL11i (MET11611/P-11i/1-2/EP), and 11h (MET11611/P-11h/3/EP), described as a dark, dusty lithology.

The one-inch mounts were prepared using Buehler EPOKWICK two-part epoxy, polished on a Logitech WG2 polishing unit using Pellon polishing pads, diamond paste 6, 3, and 1 µm, and Engis OS type 1V lubricant (Blinova et al., 2014a), and given a conductive carbon coating.

Several new chips of specimen TL1 were obtained by subsampling the larger specimen in the Subzero Curation Facility at the University of Alberta, described by Herd et al. (2016). This pristine specimen of the Tagish Lake meteorite, which is held in storage at -28 °C within Teflon containers in a research grade freezer facility, was transferred to the Subzero Curation facility, held at -15 °C, in a freezer gel pack lined Styrofoam container that also maintains an approximately -18 °C temperature. Prior to use all instruments were cleaned with ultrapure water and HPLC dichloromethane (DCM), and where possible materials (e.g., vials, aluminium foil, and tweezers) were combusted at 450 °C for >6 hours to remove organic matter and reduce any potential contamination. Subsampling was performed using a sterile scalpel inside an argon atmosphere glove box at approximately -10 °C, and the chips obtained were collected onto aluminium foil and placed into glass vials. Two chips were chosen to be made into epoxy mounts for analysis as described above for the previously prepared samples, referred to as TL1/3 (MET11611/P-1/3/1/EP2) and TL1/6 (MET11611/P-1/6/EP).

Observations of the textures and mineralogy of the aforementioned samples were made using the Zeiss Sigma 300 VP-FESEM located within the Department of Earth and Atmospheric Sciences at the University of Alberta operating at 15 kV for Backscattered electron (BSE) imaging and energy dispersive x-ray spectrometry (EDS) analysis. Spot compositional analyses of sulfide grains within the samples were acquired over three sessions using the CAMECA SX100 electron probe microanalyzer (EPMA) located within the Earth and Atmospheric Sciences Department at the University of Alberta. Operating conditions were set to 20 keV with a beam current of 20 nA using a ZAF (Phi-Rho-Z) correction method. The counting times, standards used, and limits of detection for each element are included in Table 2.1.

Only analyses with analytical totals between 97.5 wt% and 102.5 wt% will be included in the remainder of the discussion.

2.3 Results

2.3.1 Petrography

Fe-Ni sulfides are present within all samples of Tagish Lake examined within this study. These are found dispersed throughout the matrices of samples as well as within chondrules and chondrule rims and lithic clasts. Sulfide grains located in the matrix are commonly associated with magnetite, regardless of mineralogy and morphology. Coarse-grained sulfides also commonly make up portions of the rims and interiors of chondrules containing Fe-enriched olivine. Rare examples of fine-grained (<~1-2µm) sulfide rims are present surrounding highly altered, phyllosilicate-rich and Fe-poor olivine chondrules. These more fine-grained rims closely resemble similar rims of magnetite surrounding these same types of chondrules. A variety of textures are observed, including pyrrhotite with and without exsolved pentlandite, unexsolved pentlandite, and a unique "bull's-eye" morphology previously described by Blinova et al. (2014a).

2.3.1.1. Exsolved Pyrrhotite

Grains of pyrrhotite containing exsolved pentlandite are observed in all examined sections of Tagish Lake. These grains are present in the matrices of the sections as well as in chondrule rims and interiors in chondrules with olivine of higher Fe content.

Exsolved grains display a wide variety of exsolution morphologies, including coarse non-linear (blocky or patches; Figure 2.1a,b,f) and coarse linear (Figure 2.1b), fine linear (lamellae and flames; Figure 2.1c,d,f) and fine non-linear (rods or blebs; Figure 2.2a,b), and islands of pyrrhotite within pentlandite grains or patches identified as a "snowflake" texture (Figure 2.2c,d; Brearley and Martinez, 2010; Schrader et al., 2016; Singerling and Brearley, 2018). In some cases, the distinctions between

these groups are somewhat arbitrary, but we choose a cut-off width of ~1-2 μm to distinguish between fine and coarse textures.

Coarse, non-linear exsolution morphologies, referred to previously as blocky exsolution or patches (Schrader et al., 2016; Singerling and Brearley, 2018), are roughly equant pentlandite bodies which are typically present along the grain boundaries and edges of pyrrhotite grains. Coarsened linear (Durazzo and Taylor, 1982) features are elongated in one direction but exceed the ~1-2 μm maximum widths of their fine linear counterparts (lamellae and flames). They may originate at grain boundaries, edges, cracks, or holes and penetrate into the interior of the grain or may be present solely within the interiors of pyrrhotite grains. Fine linear exsolution textures include lamellae (Schrader et al., 2016; Singerling and Brearley, 2018) or blades (Durazzo and Taylor, 1982), which consist of elongated, narrow pentlandite bodies oriented in a particular direction within the matrices of pyrrhotite grains with maximum widths of 1-2 μm. The flame texture consists of elongated, narrow pentlandite bodies with a maximum width of 1-2 μm at their widest point which originate at pentlandite grain boundaries, edges, holes, or cracks, and taper in width as they extend into the grain interiors. The occurrence of several of these flames together may result in an apparent coarsening of the exsolution feature; however, this can be distinguished from coarse linear features as this does not result in the extension of the feature significantly into the grain interior. Fine non-linear textures may be referred to as rods (Singerling and Brearley, 2018) or blebs (Schrader et al., 2016). These are fine pentlandite bodies within pyrrhotite grains that are no more than 1-2 μm in length and width which may have regular or irregular shapes. When multiple blebs are present within the same grain these may or may not be oriented in a specific direction. There are also rare occurrences of the “snowflake” texture (Figure 2.2c,d) first identified by Brearley and Martinez (2010) in CM2 TIL 91722 and observed later by Schrader et al. (2015) in CR chondrites and Singerling and Brearley (2018) in various additional CM chondrites as well. This texture is characterized by grains or coarse pentlandite exsolution features containing small blebs or islands of

pyrrhotite within their interiors, and neither a terrestrial nor experimental analogue have yet been identified (Singerling and Brearley, 2018).

Multiple exsolution textures may be observed within the same grain, and most of the examined samples contain examples of all or nearly all of the different morphologies. The occurrence of the different morphologies is summarized in Table 2.3. The various exsolution textures can be found within grains dispersed in the matrix, as well as in course-grained sulfides contained within chondrule rims and interiors - no one texture is specific to either of these occurrences, but instead they appear to be randomly distributed.

2.3.1.2 Unexsolved Pyrrhotite

The majority of samples examined also contain pyrrhotite grains without exsolved pentlandite (Figure 2.3a-d). This type of grain was not observed in samples TL4 or TL10a, which may be a result of sampling bias, a combination of the effects of small grain size, low abundances, and small sample sizes, or a difference in petrogenetic history. By comparison, grains which contain exsolved pentlandite are often associated with chondrules, making them easier to spot, and have a variety of both grain sizes present in the matrix. This may have resulted in an over-representation of exsolved grains relative to unexsolved grains in our analyses.

Unexsolved pyrrhotite grains are most abundant within the matrices of samples but may also be found within the coarse-grained sulfide rims and interiors of Fe-rich olivine chondrules and make up the rare instances of the fine-grained sulfide rims. Their morphologies are randomly distributed and vary widely from anhedral and irregular to rounded and angular.

2.3.1.3 Unexsolved Pentlandite

Also found within all samples except for TL11v and TL5b are examples of pentlandite grains which are not associated with pyrrhotite (Figure 2.3e-h). These grains are present almost exclusively as

isolated grains within the matrices of samples, and rarely within the interiors of Fe-rich olivine chondrules. They are typically angular or rounded and occasionally slightly elongated. As with the unexsolved pyrrhotite grains, they may be in relatively low abundance or absent from some samples as a result of sampling bias.

2.3.1.3 "Bull's-eye" Morphology

Present in all examined samples except for TL4, this unique morphology, first identified within samples of Tagish Lake by Blinova et al. (2014a), consists of an outer rim and core of sulfide grains separated by a gap. Previously observed samples had been rounded (Figure 2.4b,d,e,g,h), but more irregular shapes (Figure 2.4a,f), as well as examples lacking the central portion of sulfide grains (Figure 2.4c), were also observed within some samples examined here. These grains may or may not contain fine linear exsolved pentlandite. As a result of the presence of this fine exsolution as well as the small grain sizes (<~2 μm in many cases) associated with this morphology, pure compositional analyses were not possible on any of the observed cases.

2.3.2 Composition

Analyses of major and minor element compositions of Fe-Ni sulfide grains were made for eight samples of Tagish Lake. These analyses reveal the presence of both pyrrhotite and pentlandite within all samples. Some analyses return an intermediate composition, which may be attributed to either the presence of a monosulfide solid solution (MSS) phase, or to beam overlap between exsolved phases. Only analyses of pure phases were retained for discussion, therefore those where beam overlap of multiple phases is suspected are omitted. However, due to the presence of some extremely fine exsolution textures (<1-2μm), it is possible that some analyses with intermediate Ni compositions may still represent beam overlap. While Schrader et al. (2016) provide 16 wt% Ni as the boundary between pyrrhotite and pentlandite due to a sharp increase in Co content at 16 wt% Ni, this obvious sharp increase was not observed in the Tagish Lake sulfides (Figure 2.5), confirming that these sulfides with

intermediate Ni contents likely do not represent pure phases. Therefore, impure analyses were removed by determining the likelihood of beam overlap using a combination of visual analyses and Co content of the grains. The average and ranges of the retained analyses are reported in Table 2.2, as well as the Fe/S (at%) ratios of the pyrrhotite grains. All analyses are reported in Appendix A, Table A.1.

The average Fe content of the pyrrhotite in the TL samples is 58.38 ± 1.44 wt%, the average Ni is 1.63 ± 1.32 wt%, and the average S content is 39.14 ± 0.56 wt%. The total range in Fe content is 49.73-60.90 wt% with a median of 58.67 wt%, in Ni content is 0.24-9.97 wt% with a median of 1.44 wt%, and in S content is 37.29-40.16 wt% with a median of 39.15 wt%. The average Fe content of the pentlandite in the TL samples is 30.70 ± 1.92 wt%, the average Ni content is 34.05 ± 2.16 wt%, and the average S content is 33.47 ± 0.90 wt%. The total range in Fe content is 28.18-36.46 wt% with a median of 30.71 wt%, in Ni content is 28.17-36.37 wt% with a median of 34.54 wt%, and in S content is 32.47-36.78 wt% with a median of 33.19 wt%.

The average composition of pyrrhotite within grains containing exsolved pentlandite is 58.48 ± 1.17 wt% Fe, 1.56 ± 0.99 wt% Ni, and 39.02 ± 0.55 wt% S. The average composition of pentlandite within these grains is 31.48 ± 2.27 wt% Fe, 33.26 ± 2.34 wt% Ni, and 33.28 ±0.77 wt% S. The average composition of pyrrhotite grains which do not contain exsolved pentlandite is 58.18 ± 1.86 wt% Fe, 1.77 ± 1.81 wt% Ni, and 39.39 ± 0.49 wt% S. The average composition of pentlandite grains not associated with pyrrhotite is 30.49 ± 1.81 wt% Fe, and 34.26 ± 2.10 wt% Ni, and 33.53 ± 0.49 wt% S. The compositions of sulfides of different morphologies are plotted on Fe-Ni-S ternary diagrams at 25°C, 100-135°C, 500°C, and 600°C in Figures 2.6-2.8.

2.4 Discussion

2.4.1. Assessment of Degrees of alteration

The at% Fe/S ratios of low-Ni (<1 wt% Ni) pyrrhotite may be used to place CI and CM chondrites in approximate relative order of degree of alteration of CI>CM1/2>CM2, as Fe/S decreases with increasing alteration (Schrader et al., 2021). This decrease is a result of the loss of Fe in pyrrhotite, which is more susceptible to alteration than the more Ni-rich pentlandite (Singerling and Brearley, 2020) to form magnetite and Fe-rich phyllosilicates (Schrader et al., 2021). The Fe/S ratios of meteorite groups are also affected by sulfur and oxygen fugacity, sample and group heterogeneity, and thermal and aqueous alteration, and when all chondrite groups are examined, it becomes clear that Fe/S cannot always be used as a direct indication of degree of alteration but is rather a better proxy for degree of oxidation (Schrader et al., 2021). However, because the conclusion that Fe/S decreases with increasing alteration holds true for CI and CM chondrites (which experienced oxidizing conditions during the aqueous alteration of their parent bodies), and to which Tagish Lake is similar, the Fe/S ratio is utilized here to give some indication of the relative degree of alteration of the samples studied here and the meteorite as a whole.

Previous examination of the petrography (Herd et al., 2011; Blinova et al., 2014a), hydrogen abundances (Alexander et al., 2012), soluble organic content (Simkus et al., 2019), and thermogravimetric analysis and infrared transmission spectroscopy (Gilmour et al., 2019) of samples studied herein have placed them in the order of alteration of TL4 < TL5b ≤ TL10a < TL 11h < TL11i. Using the Fe/S (at%) ratios of pyrrhotite grains in each sample, this ordering can be verified, and new samples placed within this context.

Filtered data (those inferred to come from pure pyrrhotite) were used to calculate average Fe/S values for each sample. Previous studies utilized only pyrrhotite with <1 wt% Ni to calculate average Fe/S ratios for pyrrhotite, our study utilizes all available pyrrhotite measurements to provide a larger

sample size. Therefore, while these values are not directly comparable to previous studies of Fe/S ratios of other meteorite groups they provide insight into the relative degree of alteration experienced by each sample of Tagish Lake with respect to one another. The average Fe/S ratios of pyrrhotite from each sample are plotted against degree of sample alteration as determined by Gilmour et al. (2019) in Figure 2.9, which confirms the order of sample alteration of TL4 < TL5b ≤ TL10a < TL 11h < TL11i within error. Samples that were not previously placed within this order are plotted at their inferred locations within the existing order according to their relative Fe/S ratios. The new sample TL1 is thus placed between samples 11h and 11i, such that the order of increasing alteration is then TL4 < TL5b ≤ TL10a < TL 11h < TL1 < TL11i. This placement is consistent with the sample's petrologic characteristics. Chondrules present within the two chips taken from TL1 show a variety of textures, from porphyritic chondrules containing olivine and magnetite with variable amounts of phyllosilicate phases contained within fine-grained rims which represent low to moderate degrees of alteration, to more phyllosilicate-rich forms containing little to no olivine. On average these display moderate to highly altered textures similar to sample TL11h or TL11i. The sample also contains a higher abundance of magnetite framboids, platelets, and clusters, as well as more examples of the "bull's-eye" sulfide morphology previously described than other samples (Blinova et al., 2014a) within its matrix, both of which have been linked to aqueous alteration. The association of the increased abundance of these two phases suggests that the formation of the "bull's-eye" sulfides is dependent on oxygen fugacity. The ordering of samples by degree of alteration is supported by the relative absence of "bull's-eye" sulfides and unexsolved pyrrhotite and pentlandite in the less altered samples, as these morphologies may have formed as a result of deposition from an oxidizing fluid during aqueous alteration. However, the textures observed in any given sample may also be influenced by sample size and sampling bias. TL11v is a disaggregated sample including several different lithologies, likely with different degrees of alteration. The Fe/S ratios of the

two chips that comprise the sample fall towards the less altered end of the spectrum, such that the degree of alteration is TL11v chip1< TL4 < TL11v chip2 < TL5b ≤ TL10a < TL 11h < TL1 < TL11i.

The average Fe/S of low-Ni pyrrhotite from all examined samples of Tagish Lake was calculated to allow the average degree of alteration to be compared to that of CM and CI chondrites. The average Fe/S of low-Ni pyrrhotite in Tagish Lake was found to be 0.870 ± 0.017, which lies between CI chondrites (0.858 ± 0.009) and CM1/2 chondrites (0.901 ± 0.015; Schrader et al., 2021) suggesting Tagish Lake has experienced an intermediate degree of alteration and oxidation between these two groups.

2.4.2. Temperature of Equilibration

The temperature at which sulfide formation occurs affects the composition and textures of the resulting phases. By combining an examination of the textures of the sulfide grains present within the samples with compositional analyses, it is possible to determine approximate equilibration temperatures for the various textural groups of sulfides. Pyrrhotite-pentlandite intergrowths form as a result of exsolution during cooling from magmatic temperatures (>900°C), with coarse, non-linear textures developing between 610-250°C, coarse-linear from 250-150°C, and flames at or below 150°C (Durazzo and Taylor, 1982). When these textures first develop, they are small and fine, but grow and coarsen over time if temperatures remain high enough for continued exsolution to occur. At 150°C exsolution is slow, but metals can remain mobile in sulfides below temperatures of even 100°C (Etschmann et al., 2004).

The presence of high-temperature exsolution features such as blocky and coarsened linear exsolved pentlandite in sulfides present within chondrule rims and interiors suggests the formation of these sulfides at temperatures of at least 150°C and up to as high as 610°C. Because they occur in similar contexts, Fe-Ni sulfides which do not contain exsolution features that are present as large grains within chondrule rims are assumed to have formed at similar temperatures. The lack of exsolved pentlandite in

these cases may be explained by exsolution-inhibiting conditions such as a low S or Ni content in the precursor phase (Schrader et al., 2015; Schrader et al., 2016), or insufficiently high fO_2, as samples formed under conditions more reducing than about IW-2.2 will not contain pentlandite (Benedix et al., 2005). This is because the incorporation of Fe into oxidized minerals such as magnetite at higher fO_2 limits its availability for sulfide formation, which will result in the formation of more Ni-enriched sulfides such as pentlandite (Schrader et al., 2016). Sulfide grains present in the matrices of samples which contain these same exsolution textures likely formed at similarly high temperatures. Those grains within the matrix which lack exsolution, or which have pentlandite flames which may have formed below 150°C are hypothesized to have formed at temperatures below 150°C, although formation at higher temperatures cannot be ruled out completely.

The compositions and crystal structures of pyrrhotite and pentlandite vary depending on the metal to sulfur ratio and temperature (Harries and Langenhorst, 2013), and can be utilized to constrain closure temperature (Schrader et al., 2016). Fe-Ni sulfide phase formation and composition are determined by the bulk composition of the precursor monosulfide solid solution (MSS) as well as the temperature at which the system equilibrates (Harries and Langenhorst, 2013; Craig, 1973). At higher equilibration temperatures, pentlandite becomes increasingly S and Ni-enriched (Schrader et al., 2016).

Plotting Fe-Ni sulfide compositions of various textural groups against experimentally established phase diagrams for 25°C, 100-135°C, 500°C, and 600°C (Vaughan and Craig 1997; Naldrett 1989; Shewman and Clark, 1970; Kosyakov et al., 2003) allows for the testing of formation temperatures postulated above based on textural evidence. The Fe and Co content of the grains are combined for these analyses, as Fe and Co behave similarly within these minerals (Berger et al., 2016; Lauretta 2005). The majority of sulfide grains containing high-temperature exsolution textures and those present within chondrules are consistent with compositions expected from formation at temperatures of 500-600°C (Figure 2.6). Pyrrhotite grains which lack exsolved pentlandite or contain pentlandite flames originating

from grain boundaries, cracks, or holes correspond to a wider temperature range, with the majority of analyses corresponding to temperatures of 25°C or 100-135°C (Figure 2.7), indicating either that they formed at some intermediate temperature or were formed over a period of time as temperatures decreased from ~100°C to 25°C. The temperature of formation of these grains does not differ systematically according to sample of origin, but rather grains formed over the range of temperatures appear to be randomly distributed throughout the matrix. The higher temperature end of this range is consistent with the previous observations of Tagish Lake, which provide temperatures of <~100°C for the aqueous alteration which occurred on the Tagish Lake parent body (Zolensky et al. 2002; Blinova et al., 2014a; Visser et al., 2019). Several of these grains do not fit either of these low temperature phase diagrams, and are more consistent with formation at temperatures of up to 600°C. We expected unexsolved pentlandite grains to correspond to lower formation temperatures (~25-100°C), and several of the grains do correspond to the compositions predicted by the 25°C phase diagram; however, the majority of grains identified were too S-rich to have formed at these low temperatures and are better explained by formation at 500-600°C (Figure 2.8).

2.4.3. Formation Mechanisms

The formation of primary sulfides in the solar nebula is thought to have occurred either through sulfidation of Fe-Ni metal, or through direct crystallization of Fe-Ni MSS, for example during chondrule formation. Nebular equilibrium condensation models predict condensation of troilite after Fe metal above 427°C (e.g., Grossman and Larimer 1974; Barshay and Lewis 1976; Fegley et al. 1995; Lodders 2003) through sulfidation by H_2S gas via the reaction:

$$Fe\ (metal) + H_2S\ (g) = FeS\ (s) + H_2\ (g)$$ (Lauretta et al. 1996a, 1996b, 1996c)

It is, however, more likely that Fe-Ni metal formed rather than pure Fe metal (Lauretta et al., 1998), and the sulfidation of such a composition by H_2 and H_2S gases results in the production of

pyrrhotite, pentlandite, and P-rich sulfide (Lauretta et al.,1996a, 1996b, 1996c, 1997, 1998), which could later have been fragmented by collisions (Schrader et al., 2015) and incorporated into carbonaceous chondrite parent bodies. It should also be noted that pyrrhotite may form through the sulfidation of troilite in the nebula (Zolensky and Thomas, 1995), and in this case the troilite would be the primary sulfide phase, with pyrrhotite being a secondary phase, despite having formed in the solar nebula rather than within a parent body.

Alternatively, Fe-Ni-bearing sulfides could have crystallized from an MSS melt beginning at 1097°C, for instance during chondrule formation (e.g. Boctor et al., 2002; Brearley and Martinez, 2010; Harries and Langenhorst, 2013; Schrader et al., 2015). This phase is unstable at lower temperatures and will begin to exsolve to form separate pyrrhotite and pentlandite phases at about 597°C (Kitakaze et al., 2011). This exsolution results in a wide variety of textures at different temperatures, including coarse, non-linear textures between 610-250°C, coarse-linear from 250-150°C, and flames at or below 150°C (Durazzo and Taylor, 1982). What have been described as patches, blades, rods, lamellae, and blebs (Singerling and Brearley, 2018) have been observed in CM (Brearley and Martinez, 2010; Kimura et al. 2011; Harries and Langenhorst 2013; Hewins et al. 2014; Singerling and Brearley, 2018), CR (Schrader et al., 2015), CK (Schrader et al., 2016), and even CI (Berger et al., 2016) carbonaceous chondrites.

Fe-Ni sulfides exhibiting pentlandite exsolution are common components of Fe-rich olivine chondrules in Tagish Lake. The exsolution textures and composition of the pyrrhotite and pentlandite displayed by these sulfides indicates formation at temperatures of ~500-600°C, much higher than would be likely during aqueous alteration on the Tagish Lake parent body. It thus seems likely that these phases are primary sulfides and were formed by one of the high temperature processes in the solar nebula described above. Additionally, the presence of exsolved pentlandite in chondrules containing Fe-rich olivine and its absence in chondrules containing Fe-poor olivine also suggests aqueous alteration was not the source of pentlandite in these cases, as aqueous alteration would have formed pentlandite

in all chondrules, not only those containing Fe-rich olivine. This is consistent with observations made by Schrader et al. (2016), who recognized that pentlandite is commonly associated with FeO-rich minerals, and its presence in FeO-rich and absence in FeO-poor chondrules required more oxidizing conditions for the formation of sulfides in the FeO-rich chondrules, while formation during aqueous alteration would have resulted in both types containing pentlandite. The inclusion of exsolved sulfides within the interior of these chondrules suggests that crystallization from an MSS melt during chondrule formation with pentlandite exsolving upon cooling is the more likely explanation for the formation of these sulfides. Formation from an MSS melt during chondrule formation is consistent with the common occurrence of rounded sulfides both in chondrules and the meteorite matrix, with irregular shapes explained by sulfide melt crystallizing in the interstitial space between silicate minerals formed at higher temperatures (Singerling and Brearley, 2018). Fine-grained sulfide and magnetite rims may occasionally be observed surrounding other chondrules, but these lack the larger grain sizes and exsolution textures of the Fe-rich chondrule sulfides, and likely form as a result of parent body alteration in conjunction with similar magnetite chondrule rims.

The sulfides present in the matrices of the examined samples exhibiting high-temperature exsolution textures and those pentlandite grains which are not associated with pyrrhotite which have compositions consistent with formation at 500-600°C are therefore also most likely formed by crystallization and exsolution of an MSS melt during chondrule formation. These chondrules were likely later fragmented, and the sulfides incorporated into the matrix of the Tagish Lake parent body. Chondrule fragments observed within Tagish Lake provide further support for this occurrence. This is consistent with the explanations given for the formation of sulfides of similar textures found in CM chondrites (Schrader et al., 2016; Singerling and Brearley, 2018). Blinova et al. (2014a) attributed the exsolved pentlandite morphologies they observed in Tagish Lake to formation by sulfurization of Fe-Ni metal by gas-solid reactions at nebular conditions. However, because the sulfides observed herein do

not exhibit metal cores (such as the sulfide rimmed metal grains described by Singerling and Brearley (2018) in CM and CR chondrites) and are commonly observed within chondrule interiors and rims, formation by cooling of an MSS melt during chondrule formation seems a more likely explanation.

There does not appear to be any direct correlation between the presence or abundance of grains with exsolved pentlandite and the degree of alteration of any given sample. It might be expected that if their formation occurred prior to assembly of the meteorite parent body and they were later subjected to aqueous alteration and destroyed that they would only be present in the least altered samples, which is not the case. Thus, it seems likely that the abundance of these grains is related to heterogeneous distribution and concentration of sulfide phases within the parent body rather than solely the degree of alteration experienced. As sulfides exhibiting exsolution textures are commonly observed within more highly altered CM (Schrader et al., 2016; Singerling and Brearley, 2018) and even some CI (Berger et al., 2016) chondrites, they must be robust enough to survive extensive aqueous alteration, and it is therefore perhaps not surprising that they can be found within even the more highly altered samples of Tagish Lake as well.

Where there is little or no evidence of exsolution textures of pentlandite from pyrrhotite, alternative secondary mechanisms have been proposed to explain the presence of these phases within carbonaceous chondrites. One possibility is that of formation by aqueous alteration on a hydrous asteroid parent body (e.g. Brearley, 2006). Pentlandite may form under high oxygen fugacity during alteration (Godlevskiy et al., 1971), and its presence in the absence of magmatic exsolution textures could indicate formation via aqueous alteration by an oxidizing fluid. The oxidation of troilite at temperatures consistent with alteration on carbonaceous chondrite parent bodies can also result in the formation of magnetite, pyrrhotite, and pyrite, with the remaining unoxidized sulfide becoming increasingly Ni-enriched (Herndon et al., 1975; Bullock et al. 2005). Indeed, the equilibration temperatures of most pyrrhotite in CM chondrites indicates equilibration at temperatures of about 100-

135°C, which is more consistent with formation by low temperature aqueous alteration than by crystallization from a melt or high temperature metamorphism (Schrader et al., 2016). Additionally, the absence of Ni-rich sulfides in anhydrous interplanetary dust particles (IDPs) and their presence in hydrous IDPs may be used as further evidence that pentlandite may form through secondary alteration processes (Zolensky and Thomas, 1995). Sulfides may also be precipitated directly from the fluids involved in parent body alteration processes, with changes in their solution chemistry accounting for the variety of textures observed (Blinova et al., 2014a; Berger et al., 2016).

The unexsolved pyrrhotite and pentlandite grains whose compositions correspond to temperatures of formation of 25-135°C are assumed to have been formed during the aqueous alteration experienced by the Tagish Lake parent body, which likely occurred at temperatures of <100°C, consistent with the formation temperatures of these grains. The existence of fine pentlandite within pyrrhotite in "bull's-eye" sulfides, which have previously been interpreted as having formed through deposition from a fluid during multiple alteration events (Blinova et al., 2014a) suggests that low temperature exsolution or diffusion within sulfides can and does produce intergrown pyrrhotite and pentlandite textures in Tagish Lake. Pentlandite in these cases is fine (<~1-2µm) and originates at grain boundaries. This is similar to the flame exsolution morphology, suggesting that sulfide grains containing flame textures could also have formed by deposition during low temperature aqueous alteration, a possibility which is supported by the composition of these grains corresponding to formation temperatures of ~25-135°C. Previously, compositions of sulfide grains in Tagish Lake yield temperatures of formation of ~100-135°C (Visser et al., 2019), which corresponds to the high end of the range found herein. This is interpreted to be the result of the cooling of the altering fluid from which the sulfides were deposited over a period of time, or multiple episodes of aqueous alteration occurring at different temperatures.

2.5 Conclusions

An examination of the Fe-Ni sulfide grains present in nine different samples of Tagish Lake has revealed a complex history of formation and alteration.

The Fe/S ratio of low-Ni pyrrhotite in Tagish Lake is 0.870 ± 0.017, which places its average degree of alteration and oxidation between that of CI and CM1/2 chondrites. A comparison of the Fe/S ratio of pyrrhotite grains and sulfide morphologies between samples confirms the order of degree of alteration of previous samples and allows placement of the new sample TL1 such that the order of increasing alteration is now TL11v chip1<TL4<TL11v chip2< TL5b ≤ TL10a < TL11h < TL1 < TL11i. This placement of TL1 is supported by petrologic characteristics.

Tagish Lake samples contain pyrrhotite and pentlandite grains of several distinct morphologies:

1. Exsolved pyrrhotite-pentlandite grains within the sample matrices and Fe-rich olivine chondrules with exsolution morphologies (e.g. blocky, coarse linear, lamellae) and compositions consistent with formation at temperatures of 500-600°C. These grains are interpreted to have formed during chondrule formation from the cooling and exsolution of an MSS melt.
2. Isolated pentlandite grains located primarily within the matrix with compositions corresponding mostly to formation temperatures of 500-600°C likely initially formed during chondrule formation and were later incorporated into the chondrite matrix after subsequent fragmentation and accretion. Several grains have formation temperatures corresponding to 25°C, and likely formed as a result of aqueous alteration.
3. Unexsolved pyrrhotite and pyrrhotite containing pentlandite flames with compositions corresponding to formation during aqueous alteration at temperatures of 25-100°C.

4. “Bull’s-eye” sulfides composed of an exterior and interior ring of sulfides separated by a gap which may contain intergrown pyrrhotite and pentlandite with flame-like textures. These were likely deposited during multiple deposition events from an altering fluid.

Taken together these morphologies represent two distinct generations of sulfides, the first forming at higher temperatures of ~500-600°C by cooling of an MSS melt during chondrule formation, and the second by multiple episodes of deposition from a cooling aqueous fluid or multiple fluid pulses over a temperature range of ~25-100°C.

2.6 Acknowledgments

We thank Nathan Gerein for his assistance with SEM data collection, Andrew Locock for his assistance with EPMA data collection, Patrick Hill and Libby Tunney for assistance in sub-sampling, and Mark Labbe for sample preparation and epoxy mounting. Editorial handling by Adrian Brearley and review by Emma Bullock were greatly appreciated and resulted in improvements to the manuscript. Funding was provided by NSERC Grant RGPIN-2018-04902 to CDKH.

2.7 References

Alexander, C. M. O., Bowden, R., Fogel, M. L., Howard, K. T., Herd, C. D. K., & Nittler, L. R. (2012). The Provenances of Asteroids, and Their Contributions to the Volatile Inventories of the Terrestrial Planets. *Science*, *337*(6095), 721–723. https://doi.org/10.1126/science.1223474

Baker, L., Franchi, I. A., Wright, I. P., & Pillinger, C. T. (2002). The oxygen isotopic composition of water from Tagish Lake: Its relationship to low-temperature phases and to other carbonaceous chondrites. *Meteoritics & Planetary Science*, *37*(7), 977–985. https://doi.org/10.1111/j.1945-5100.2002.tb00870.x

Barshay S. S. and Lewis I. S. 1976. Chemistry of primitive solar material. *Annual Review of Astronomy and Astrophysics 14*, 81–94.

Benedix, G. K., Lauretta, D. S., & McCoy, T. J. (2005). Thermodynamic constraints on the formation conditions of winonaites and silicate-bearing IAB irons. *Geochimica et Cosmochimica Acta*, *69*(21), 5123–5131. https://doi.org/10.1016/j.gca.2005.03.048

Berger, E. L., Lauretta, D. S., Zega, T. J., & Keller, L. P. (2016). Heterogeneous histories of Ni-bearing pyrrhotite and pentlandite grains in the CI chondrites Orgueil and Alais. *Meteoritics & Planetary Science*, *51*(10), 1813–1829. https://doi.org/10.1111/maps.12721

Bland, P. A., Cressey, G., & Menzies, O. N. (2004). Modal mineralogy of carbonaceous chondrites by X-ray diffraction and Mossbauer spectroscopy. *Meteoritics & Planetary Science*, *39*(1), 3–16. https://doi.org/10.1111/j.1945-5100.2004.tb00046.x

Blinova, A. I., Zega, T. J., Herd, C. D. K., & Stroud, R. M. (2014a). Testing variations within the Tagish Lake meteorite-I: Mineralogy and petrology of pristine samples. *Meteoritics & Planetary Science*, *49*(4), 473–502. https://doi.org/10.1111/maps.12271

Blinova, A. I., Herd, C. D. K., & Duke, M. J. M. (2014b). Testing variations within the Tagish Lake meteorite-II: Whole-rock geochemistry of pristine samples. *Meteoritics & Planetary Science*, *49*(6), 1100–1118. https://doi.org/10.1111/maps.12303

Boctor, N. Z., Kurat, G., & Alexander, C. M. O. D. (2003). Sulfide-Oxide Assemblage in Tagish Lake Carbonaceous Chondrite. *34th Lunar and Planetary Science Conference*, abstract no. 1705. http://adsabs.harvard.edu/abs/2003LPI....34.1705B

Boctor, Nabil Z., Kurat, G., Alexander, C. M. O., & Prewitt, C. T. (2002). Sulfide Mineral Assemblages in Boriskino CM Chondrite. *33rd Lunar and Planetary Science Conference*, abstract no. 1534.

Brandon, A. D., Humayun, M., Puchtel, I. S., & Zolensky, M. E. (2005). Re-Os isotopic systematics and platinum group element composition of the Tagish Lake carbonaceous chondrite. *Geochimica Et Cosmochimica Acta*, *69*(6), 1619–1631. https://doi.org/10.1016/j.gca.2004.10.005

Brearley A. J. (2006) The action of water. In *Meteorites and the Early Solar System II* (eds. D. S. Lauretta and H. Y. McSween). University of Arizona Press, Tucson, pp. 584–624.

Brearley, A. J., & Martinez, C. (2010). Ubiquitous Exsolution of Pentlandite and Troilite in Pyrrhotite from the TIL 91722 CM2 Carbonaceous Chondrite: A Record of Low Temperature Solid State Processes. *41st Lunar and Planetary Science Conference*, abstract no. 1689.

Brown, P. G., Hildebrand, A. R., Zolensky, M. E., Grady, M., Clayton, R. N., Mayeda, T. K., Tagliaferri, E., Spalding, R., MacRae, N. D., Hoffman, E. L., Mittlefehldt, D. W., Wacker, J. F., Bird, J. A., Campbell, M. D., Carpenter, R., Gingerich, H., Glatiotis, M., Greiner, E., Mazur, M. J., McCausland, P. JA., Plotkin, H., Mazur, T. R. (2000). The fall, recovery, orbit, and composition of the Tagish Lake meteorite: A new type of carbonaceous chondrite. *Science*, *290*(5490), 320–325. https://doi.org/10.1126/science.290.5490.320

Brown, P. G., ReVelle, D. O., Tagliaferri, E., & Hildebrand, A. R. (2002). An entry model for the Tagish Lake fireball using seismic, satellite and infrasound records. *Meteoritics & Planetary Science*, *37*(5), 661–675. https://doi.org/10.1111/j.1945-5100.2002.tb00846.x

Bullock, E. S., Gounelle, M., Lauretta, D. S., Grady, M. M., & Russell, S. S. (2005a). Mineralogy and texture of Fe-Ni sulfides in CI1 chondrites: Clues to the extent of aqueous alteration on the CI1 parent body. *Geochimica Et Cosmochimica Acta*, *69*(10), 2687–2700. https://doi.org/10.1016/j.gca.2005.01.003

Bullock, E. S., Grady, M. M., Russell, S. S., & Gounelle, M., (2005b). Fe-Ni Sulphides Within a CM1 Clast in Tagish Lake. *36th Lunar and Planetary Science Conference,* abstract no.1883.

Busemann, H., Young, A. F., Alexander, C. M. O., Hoppe, P., Mukhopadhyay, S., & Nittler, L. R. (2006). Interstellar chemistry recorded in organic matter from primitive meteorites. *Science*, *312*(5774), 727–730. https://doi.org/10.1126/science.1123878

Clayton, R. N., & Mayeda, T. K. (2001). Oxygen Isotopic Composition of the Tagish Lake Carbonaceous Chondrite. *32nd Lunar and Planetary Science Conference*, abstract no. 1885. http://adsabs.harvard.edu/abs/2001LPI....32.1885C

Craig J. R. 1973. Pyrite-pentlandite assemblages and other low temperature relations in the Fe-Ni-S system. *American Journal of Science* 273-A:496–510.

Durazzo, A., & Taylor, L. (1982). Exsolution in the Mss-Pentlandite System—Textural and Genetic-Implications for Ni-Sulfide Ores. *Mineralium Deposita*, *17*(3), 313–332.

Etschmann, B., Pring, A., Putnis, A., Grguric, B. A., & Studer, A. (2004). A kinetic study of the exsolution of pentlandite $(Ni, Fe)_9S_8$ from the monosulfide solid solution (Fe, Ni)S. *American Mineralogist*, *89*(1), 39–50. https://doi.org/10.2138/am-2004-0106

Fegley, B., Jr., Lauretta, S. D., & Kremser, T. D. (1995). *The origin of troilite and pyrrhotite in chondrites: I. Iron sulfide formation kinetics in H_2S-H_2 gas mixtures. 20th Symposium on Antarctic Meteorites*, 59–62.

Gilmour, C. M., Herd, C. D. K., & Beck, P. (2019). Water abundance in the Tagish Lake meteorite from TGA and IR spectroscopy: Evaluation of aqueous alteration. *Meteoritics & Planetary Science*, *54*(9), 1951–1972. https://doi.org/10.1111/maps.13362

Godlevskiy M. N., Likhachev A. P., Chuvikina N. G., and Andronov A. D. (1971) Hydrothermal synthesis of pentlandite. *Dokl. Akad. Nauk. SSSR* 196, 146-149.

Grady, M. M., Verchovsky, A. B., Franchi, I. A., Wright, I. P., & Pillinger, C. T. (2002a). Light element geochemistry of the Tagish Lake CI2 chondrite: Comparison with CI1 and CM2 meteorites. *Meteoritics & Planetary Science*, *37*(5), 713–735. https://doi.org/10.1111/j.1945-5100.2002.tb00851.x

Grady, M. M., Verchovsky, A. B., Franchi, I. A., Wright, I. P., & Pillinger, C. T. (2002b). Light element geochemistry of the Tagish Lake CI2 chondrite: Comparison with CI1 and CM2 meteorites. *Meteoritics & Planetary Science*, *37*(5), 713–735. https://doi.org/10.1111/j.1945-5100.2002.tb00851.x

Greshake, A., Krot, A. N., Flynn, G. J., & Keil, K. (2005). Fine-grained dust rims in the Tagish Lake carbonaceous chondrite: Evidence for parent body alteration. *Meteoritics & Planetary Science*, *40*(9–10), 1413–1431. https://doi.org/10.1111/j.1945-5100.2005.tb00410.x

Grossman L. and Larimer J. W. 1974. Early chemical history of the solar system. *Reviews of Geophysics and Space Physics, 12*, 71–103.

Grossman L. and Larimer J. W. 1974. Early chemical history of the solar system. *Reviews of Geophysics and Space Physics, 12*, 71–103.

Harries, D., & Langenhorst, F. (2013). The nanoscale mineralogy of Fe,Ni sulfides in pristine and metamorphosed CM and CM/CI-like chondrites: Tapping a petrogenetic record. *Meteoritics & Planetary Science*, *48*(5), 879–903. https://doi.org/10.1111/maps.12089

Herd, C. D. K., Blinova, A., Simkus, D. N., Huang, Y., Tarozo, R., Alexander, C. M. O., Gyngard, F., Nittler, L. R., Cody, G. D., Fogel, M. L., Kebukawa, Y., Kilcoyne, A. L. D., Hilts, R. W., Slater, G. F., Glavin, D. P., Dworkin, J. P., Callahan, M. P., Elsila, J. E., De Gregorio, B. T., & Stroud, R. M. (2011). Origin and Evolution of Prebiotic Organic Matter As Inferred from the Tagish Lake Meteorite. *Science*, *332*(6035), 1304–1307. https://doi.org/10.1126/science.1203290

Herd, C. D. K., Hilts, R. W., Skelhorne, A. W., & Simkus, D. N. (2016). Cold curation of pristine astromaterials: Insights from the Tagish Lake meteorite. *Meteoritics & Planetary Science*, *51*(3), 499–519. https://doi.org/10.1111/maps.12603

Herndon J. M., Rowe M. W., Larson E. E., and Watson D. E. (1975) Origin of magnetite and pyrrhotite in carbonaceous chondrites. *Nature, 253*, 516–518.

Hewins, R. H., Bourot-Denise, M., Zanda, B., Leroux, H., Barrat, J.-A., Humayun, M., Goepel, C., Greenwood, R. C., Franchi, I. A., Pont, S., Lorand, J.-P., Cournede, C., Gattacceca, J., Rochette, P., Kuga, M., Marrocchi, Y., & Marty, B. (2014). The Paris meteorite, the least altered CM chondrite so far. *Geochimica Et Cosmochimica Acta*, *124*, 190–222. https://doi.org/10.1016/j.gca.2013.09.014

Hildebrand, A. R., McCausland, P. J. A., Brown, P. G., Longstaffe, F. J., Russell, S. D. J., Tagliaferrii, E., Wacker, J. F., & Mazur, M. J. (2006). The fall and recovery of the Tagish Lake meteorite. *Meteoritics & Planetary Science*, *41*(3), 407–431. https://doi.org/10.1111/j.1945-5100.2006.tb00471.x

Izawa, M. R. M., Flemming, R. L., King, P. L., Peterson, R. C., & McCausland, P. J. A. (2010). Mineralogical and spectroscopic investigation of the Tagish Lake carbonaceous chondrite by X-ray diffraction and infrared reflectance spectroscopy. *Meteoritics & Planetary Science*, *45*(4), 675–698. https://doi.org/10.1111/j.1945-5100.2010.01043.x

Keller, L. P., & Flynn, G. J. (2001). Matrix Mineralogy of the Tagish Lake Carbonaceous Chondrite: TEM and FTIR Studies. *32nd Lunar and Planetary Science Conference,* Abstract no. 1639. http://adsabs.harvard.edu/abs/2001LPI....32.1639K

Kimura, M., Grossman, J. N., & Weisberg, M. K. (2011). Fe-Ni metal and sulfide minerals in CM chondrites: An indicator for thermal history. *Meteoritics & Planetary Science*, *46*(3), 431–442. https://doi.org/10.1111/j.1945-5100.2010.01164.x

Kitakaze, A., Sugaki, A., Itoh, H., & Komatsu, R. (2011). A Revision of Phase Relations in the System Fe-Ni-S From 650 Degrees to 450 degrees C. *Canadian Mineralogist*, *49*(6), 1687–1710. https://doi.org/10.3749/canmin.49.6.1687

Kminek, G., Botta, O., Glavin, D. P., & Bada, J. L. (2002). Amino acids in the Tagish Lake meteorite. *Meteoritics & Planetary Science*, *37*(5), 697–701. https://doi.org/10.1111/j.1945-5100.2002.tb00849.x

Kosyakov V. I., Sinyakova E. F. and Shestakov V. A. (2003). Dependence of sulfur fugacity on the composition of phase associations in the Fe–FeS–NiS–Ni system at 873 K. *Geochem. Int. 7*, 660–669.

Krot, A. N., Hutcheon, I. D., Yurimoto, H., Cuzzi, J. N., McKeegan, K. D., Scott, E. R. D., Libourel, G., Chaussidon, M., Aleon, J., & Petaev, M. I. (2005). Evolution of oxygen isotopic composition in the inner solar nebula. *Astrophysical Journal*, *622*(2), 1333–1342. https://doi.org/10.1086/428382

Krot, A. N., Meibom, A., Weisberg, M. K., & Keil, K. (2002). The CR chondrite clan: Implications for early solar system processes. *Meteoritics & Planetary Science*, *37*(11), 1451–1490. https://doi.org/10.1111/j.1945-5100.2002.tb00805.x

Lauretta, D. (2005). Sulfidation of an Iron–Nickel–Chromium–Cobalt– Phosphorus Alloy in 1% H_2S–H_2 Gas Mixtures at 400–1000°C. *Oxidation of Metals*, *64*, 1–22. https://doi.org/10.1007/s11085-005-5703-4

Lauretta, D. S., Kremser, D. T., & Fegley, B. (1996a). The rate of iron sulfide formation in the solar nebula. *Icarus*, *122*(2), 288–315. https://doi.org/10.1006/icar.1996.0126

Lauretta, D. S., Lodders, K., & Fegley, B. (1997). Experimental simulations of sulfide formation in the solar nebula. *Science*, *277*(5324), 358–360. https://doi.org/10.1126/science.277.5324.358

Lauretta, D. S., Lodders, K., & Fegley, B. (1998). Kamacite sulfurization in the solar nebula. *Meteoritics & Planetary Science*, *33*(4), 821–833. https://doi.org/10.1111/j.1945-5100.1998.tb01689.x

Lauretta, Dante S., Fegley, B., Jr., Lodders, K., & Kremser, D. T. (1996b). The kinetics and mechanism of iron sulfide formation in the solar nebula. *Antarctic Meteorite Research*, *9*, 111.

Lauretta, Dante S., Kremser, D. T., & Fegley, B., Jr. (1996c). A comparative study of experimental and meteoritic metal-sulfide assemblages. *Antarctic Meteorite Research*, *9*, 97.

Lodders, K. (2003). Solar system abundances and condensation temperatures of the elements. *Astrophysical Journal*, *591*(2), 1220–1247. https://doi.org/10.1086/375492

Mikouchi, T., Kasama, T., Zolensky, M. E., & Tachikawa, O. (2001). Transmission Electron Microscopy of the Matrix Minerals in the Tagish Lake Carbonaceous Chondrite. *32nd Lunar and Planetary Science Conference,* Abstract no. 1371. http://adsabs.harvard.edu/abs/2001LPI....32.1371M

Mittlefehldt, D. W. (2002). Geochemistry of the ungrouped carbonaceous chondrite Tagish Lake, the anomalous CM chondrite Bells, and comparison with CI and CM chondrites. *Meteoritics & Planetary Science*, *37*(5), 703–712. https://doi.org/10.1111/j.1945-5100.2002.tb00850.x

Nakamura, T., Noguchi, T., Zolensky, M. E., & Tanaka, M. (2003). Mineralogy and noble-gas signatures of the carbonate-rich lithology of the Tagish Lake carbonaceous chondrite: Evidence for an accretionary breccia. *Earth and Planetary Science Letters*, *207*(1–4), 83–101. https://doi.org/10.1016/S0012-821X(02)01127-5

Naldrett A. J. (1989) *Magmatic Sulphide Deposits*. Oxford University Press, Oxford.

Schrader, D. L., Davidson, J., McCoy, T. J., Zega, T. J., Russell, S. S., Domanik, K. J., & King, A. J. (2021). The Fe/S ratio of pyrrhotite group sulfides in chondrites: An indicator of oxidation and implications for return samples from asteroids Ryugu and Bennu. *Geochimica et Cosmochimica Acta*, *303*, 66–91. https://doi.org/10.1016/j.gca.2021.03.019

Noguchi, T., Nakamura, T., & Nozaki, W. (2002). Mineralogy of phyllosilicate-rich micrometeorites and comparison with Tagish Lake and Sayama meteorites. *Earth and Planetary Science Letters*, *202*(2), 229–246. https://doi.org/10.1016/S0012-821X(02)00777-X

Pizzarello, S., & Huang, Y. S. (2002). Molecular and isotopic analyses of Tagish Lake alkyl dicarboxylic acids. *Meteoritics & Planetary Science*, *37*(5), 687–696. https://doi.org/10.1111/j.1945-5100.2002.tb00848.x

Pizzarello, S., Huang, Y. S., Becker, L., Poreda, R. J., Nieman, R. A., Cooper, G., & Williams, M. (2001). The organic content of the Tagish Lake meteorite. *Science*, *293*(5538), 2236–2239. https://doi.org/10.1126/science.1062614

Ralchenko, M., Britt, D. T., Samson, C., Herd, C. D. K., Herd, R. K., and McCausland, P. J. A., 2014. Bulk Physical Properties of the Tagish Lake Meteorite Frozen Pristine Fragments *45th Lunar and Planetary Science Conference* Abstract no. 1021

Rau, H. (1976). Energetics of Defect Formation and Interaction in Pyrrhotite Fe1-Xs and Its Homogeneity Range. *Journal of Physics and Chemistry of Solids*, *37*(4), 425–429. https://doi.org/10.1016/0022-3697(76)90024-X

Russell, S. D. J., Longstaffe, F. J., King, P. L., & Larson, T. E. (2008). *Whole-Rock, Clay Mineral, and Olivine Oxygen and Hydrogen Isotope Compositions of the Tagish Lake Carbonaceous Chondrite*. *39*, 1709.

Schrader, D. L., Connolly, H. C., Lauretta, D. S., Zega, T. J., Davidson, J., & Domanik, K. J. (2015). The formation and alteration of the Renazzo-like carbonaceous chondrites III: Toward understanding the genesis of ferromagnesian chondrules. *Meteoritics & Planetary Science*, *50*(1), 15–50. https://doi.org/10.1111/maps.12402

Schrader, D. L., Davidson, J., & Mccoy, T. J. (2016). Widespread evidence for high-temperature formation of pentlandite in chondrites. *Geochimica Et Cosmochimica Acta*, *189*, 359–376. https://doi.org/10.1016/j.gca.2016.06.012

Shewman, R. W., & Clark, L. A. (1970). Pentlandite phase relations in the Fe–Ni–S system and notes on the monosulfide solid solution. *Canadian Journal of Earth Sciences*, *7*(1), 67–85. https://doi.org/10.1139/e70-005

Simkus, D. N., Aponte, J. C., Elsila, J. E., Hilts, R. W., McLain, H. L., & Herd, C. D. K. (2019). New insights into the heterogeneity of the Tagish Lake meteorite: Soluble organic compositions of variously altered specimens. *Meteoritics & Planetary Science*, *54*(6), 1283–1302. https://doi.org/10.1111/maps.13276

Simon, S. B., & Grossman, L. (2003). Petrography and mineral chemistry of the anhydrous component of the Tagish Lake carbonaceous chondrite. *Meteoritics & Planetary Science*, *38*(5), 813–825. https://doi.org/10.1111/j.1945-5100.2003.tb00044.x

Singerling, S. A., & Brearley, A. J. (2018). Primary iron sulfides in CM and CR carbonaceous chondrites: Insights into nebular processes. *Meteoritics & Planetary Science*, *53*(10), 2078–2106. https://doi.org/10.1111/maps.13108

Singerling, S. A., & Brearley, A. J. (2020). Altered primary iron sulfides in CM2 and CR2 carbonaceous chondrites: Insights into parent body processes. *Meteoritics & Planetary Science*, *55*(3), 496–523. https://doi.org/10.1111/maps.13450

Toulmin P. and Barton P. B. Jr. 1964. A thermodynamic study of pyrite and pyrrhotite. *Geochimica et Cosmochimica Acta 28*, 641–671.

Vaughan D. J. and Craig J. R. 1997. Sulfide ore mineral stabilities, morphologies, and intergrowth textures. In *Geochemistry of Hydrothermal Ore Deposits*, 3rd edn., edited by Barnes H. L. New York: John Wiley and Sons. pp. 367–434.

Visser, R., John, T., Patzek, M., Bischoff, A., & Whitehouse, M. J. (2019). Sulfur isotope study of sulfides in CI, CM, C2(ung) chondrites and volatile-rich clasts—Evidence for different generations and reservoirs of sulfide formation. *Geochimica et Cosmochimica Acta*, *261*, 210–223. https://doi.org/10.1016/j.gca.2019.06.046

Zolensky, M. E., & Thomas, K. L. (1995). Iron and iron-nickel sulfides in chondritic interplanetary dust particles. *Geochimica et Cosmochimica Acta*, *59*(22), 4707–4712. https://doi.org/10.1016/0016-7037(95)00329-0

Zolensky, M. E., Nakamura, K., Gounelle, M., Mikouchi, T., Kasama, T., Tachikawa, O., & Tonui, E. (2002). Mineralogy of Tagish Lake: An ungrouped type 2 carbonaceous chondrite. *Meteoritics & Planetary Science*, *37*(5), 737–761. https://doi.org/10.1111/j.1945-5100.2002.tb00852.x

Zolensky, Michael E., Krot, A. N., & Benedix, G. (2008). Record of low-temperature alteration in asteroids. In G. J. MacPherson, D. W. Mittlefehldt, J. H. Jones, & S. B. Simon (Eds.), *Oxygen in the Solar System* (Vol. 68, pp. 429–462). Mineralogical Soc Amer & Geochemical Soc. https://doi.org/10.2138/rmg.2008.68.15

2.8 Tables

Table 2.1: Counting times, standards, and detection limits for each of the elements analysed during EPMA analysis.

Element	Counting Time	Standard	Detection Limit (wt%)		
			08-Mar	18-Mar	19-Mar
Si	60	KAlSi3O8 sanidine Itrongay	0.007	0.007	0.007
Cr	30	Cr2O3 chromium oxide Alfa	0.009	0.010	0.009
Fe	30	Pyrrhotite Fe7S8	0.014	0.013	0.014
Co	30	Cobalt Co	0.019	0.018	0.019
Ni	30	Ni nickel CrC C_U	0.018	0.021	0.015
Mn	30	Alabandite MnS	0.013	0.013	0.013
P	30	Apatite, Durango	0.010	0.010	0.009
S	60	Marcasite FeS2	0.012	0.013	0.013

Table 2.2: Major and minor element compositions of Fe-Ni sulfides in Tagish Lake.

Sample	Mineral	Number of analyses		Si (wt%)	Cr (wt%)	Fe (wt%)	Co (wt%)	Ni (wt%)	Mn (wt%)	P (wt%)	S (wt%)	Total (wt%)	Fe/S (at%)
11h	Pyrrhotite	6	range	b.d.l[1] - 0.03	0.02 - 0.12	58.08 - 59.34	b.d.l. - 0.15	1.67 - 2.65	b.d.l. - 0.06	b.d.l.	39.50 - 39.94	99.51 - 101.06	0.836 - 0.862
			average	0.02	0.05	58.81	0.03	1.91	0.03	0.00	39.73	100.57	0.850
			1σ	0.01	0.03	0.55	0.06	0.37	0.02	0.00	0.21	0.56	0.010
	Pentlandite	8	range	b.d.l. - 0.21	0.01 - 0.05	29.48 - 30.95	0.75 - 1.49	33.89 - 36.12	b.d.l. - 0.01	b.d.l.	32.57 - 34.07	97.70 - 100.89	0.504 - 0.524
			average	0.03	0.03	30.29	1.07	35.17	0.00	0.00	33.62	100.20	0.517
			1σ	0.07	0.01	0.55	0.28	0.68	0.00	0.00	0.45	1.07	0.007
11i	Pyrrhotite	9	range	0.01 - 0.20	0.03 - 0.13	49.73 - 59.28	b.d.l. - 0.15	0.91 - 9.97	b.d.l. - 0.04	b.d.l. - 0.01	38.63 - 39.91	98.79 - 99.93	0.739 - 0.874
			average	0.05	0.07	57.22	0.07	2.91	0.02	0.00	39.18	99.51	0.839
			1σ	0.06	0.03	3.37	0.06	3.15	0.02	0.00	0.35	0.41	0.050
	Pentlandite	5	range	b.d.l - 0.02	b.d.l - 0.04	28.19 - 36.46	0.61 - 0.79	28.17 - 36.24	b.d.l - 0.02	b.d.l	33.35 - 34.86	98.06 - 100.36	0.485 - 0.600
			average	0.00	0.02	31.17	0.69	33.44	0.00	0.00	33.82	99.14	0.529
			1σ	0.01	0.02	3.31	0.07	3.21	0.01	0.00	0.60	0.82	0.048
11v chip 1	Pyrrhotite	5	range	0.03 - 0.82	0.04 - 0.32	57.79 - 60.22	b.d.l	0.61 - 2.80	b.d.l. - 0.27	b.d.l.	37.29 - 39.24	97.70 - 100.54	0.869 - 0.902
			average	0.21	0.15	59.29	0.00	1.19	0.11	0.00	38.50	99.45	0.884
			1σ	0.34	0.14	1.04	0.00	0.91	0.12	0.00	0.78	1.13	0.012
11v chip 2	Pyrrhotite	2	range	0.11 - 0.12	0.04 - 0.05	57.76 - 58.64	b.d.l.	2.40 - 2.89	b.d.l. - 0.03	b.d.l.	38.38 - 38.57	99.18 - 99.81	0.864 - 0.873
			average	0.12	0.05	58.20	0.00	2.65	0.02	0.00	38.48	99.50	0.869
			1σ	0.01	0.01	0.62	0.00	0.35	0.02	0.00	0.13	0.45	0.006
4	Pyrrhotite	12	range	b.d.l. - 0.01	0.02 - 0.05	57.94 - 60.90	b.d.l. - 0.11	0.36 - 2.64	b.d.l. - 0.03	b.d.l.	37.92 - 38.82	99.00 - 99.92	0.861 - 0.921
			average	0.00	0.04	59.04	0.02	1.84	0.01	0.00	38.44	99.39	0.882
			1σ	0.00	0.01	0.82	0.03	0.68	0.01	0.00	0.29	0.25	0.017
	Pentlandite	5	range	b.d.l. - 0.06	0.01 - 0.05	28.52 - 35.15	0.69 - 1.27	29.47 - 36.30	b.d.l.	b.d.l.	32.47 - 32.88	97.64 - 98.40	0.504 - 0.617
			average	0.01	0.03	31.37	0.90	33.16	0.00	0.00	32.64	98.11	0.552
			1σ	0.03	0.01	3.45	0.24	3.39	0.00	0.00	0.17	0.39	0.058
5b	Pyrrhotite	24	range	0.01 - 0.15	0.01 - 0.55	57.77 - 59.36	b.d.l. - 0.09	0.45 - 1.63	b.d.l. - 0.06	b.d.l.	38.26 - 39.44	97.77 - 99.51	0.844 - 0.881
			average	0.04	0.07	58.64	0.04	0.87	0.03	0.00	38.84	98.53	0.867
			1σ	0.03	0.11	0.44	0.03	0.35	0.02	0.00	0.28	0.43	0.010
10a	Pyrrhotite	7	range	b.d.l. - 0.05	0.03 - 0.16	53.09 - 59.20	b.d.l. - 0.08	1.51 - 6.42	b.d.l. - 0.07	b.d.l.	38.85 - 39.57	99.22 - 100.52	0.770 - 0.867
			average	0.01	0.08	57.95	0.01	2.41	0.03	0.00	39.23	99.72	0.848
			1σ	0.02	0.04	2.15	0.03	1.77	0.03	0.00	0.24	0.48	0.034
	Pentlandite	2	range	b.d.l.	0.03 - 0.04	30.71 - 30.87	0.79	33.41 - 33.55	0.02	b.d.l.	33.12 - 33.13	98.09 - 98.39	0.532 - 0.535
			average	0.00	0.04	30.79	0.79	33.48	0.02	0.00	33.13	98.24	0.534
			1σ	0.00	0.01	0.11	0.00	0.10	0.00	0.00	0.01	0.21	0.002

1/3	Pyrrhotite	12	range	b.d.l. - 0.34	0.03 - 0.35	56.99 - 59.60	b.d.l. - 0.18	0.24 - 3.13	b.d.l. - 0.14	b.d.l. - 0.06	39.06 - 39.90	98.06 - 100.34	0.823 - 0.862
			average	0.04	0.16	58.47	0.05	1.08	0.05	0.01	39.58	99.43	0.848
			1σ	0.10	0.15	0.98	0.06	0.82	0.05	0.02	0.27	0.61	0.014
	Pentlandite	4	range	b.d.l.	0.02 - 0.04	31.00 - 32.48	0.43 - 1.01	30.02 - 34.23	b.d.l. - 0.01	b.d.l.	33.16 - 36.78	99.22 - 99.85	0.501 - 0.543
			average	0.00	0.03	31.74	0.59	32.18	0.00	0.00	35.02	99.56	0.521
			1σ	0.00	0.01	0.68	0.28	2.04	0.01	0.00	1.50	0.30	0.018
1/6	Pyrrhotite	24	range	b.d.l. - 0.10	0.02 - 0.12	55.78 - 59.34	b.d.l. - 0.26	0.91 - 4.61	b.d.l. - 0.07	b.d.l.	39.00 - 40.16	98.91 - 100.72	0.821 - 0.863
			average	0.02	0.06	58.19	0.09	1.78	0.02	0.00	39.62	99.77	0.843
			1σ	0.02	0.03	0.96	0.07	0.90	0.02	0.00	0.33	0.53	0.011
	Pentlandite	9	range	b.d.l.	0.01 - 0.11	28.26 - 30.99	0.69 - 0.80	33.51 - 36.37	b.d.l.	b.d.l.	32.80 - 33.26	98.15 - 99.31	0.494 - 0.539
			average	0.00	0.03	29.95	0.76	34.86	0.00	0.00	33.01	98.61	0.521
			1σ	0.00	0.03	1.08	0.04	1.10	0.00	0.00	0.16	0.47	0.018
total	Pyrrhotite	101	range	b.d.l - 0.82	0.01 - 0.55	49.73 - 60.90	b.d.l. - 0.26	0.24 - 9.97	b.d.l. - 0.27	b.d.l. - 0.06	37.29 - 40.16	97.70 - 101.06	0.739 - 0.921
			average	0.04	0.08	58.38	0.05	1.63	0.03	0.00	39.14	99.35	0.856
			median	0.02	0.06	58.67	0.03	1.44	0.02	b.d.l.	39.15	99.46	0.860
			1σ	0.09	0.09	1.44	0.06	1.32	0.04	0.01	0.56	0.85	0.025
	Pentlandite	33	range	b.d.l. - 0.21	b.d.l. - 0.11	28.19 - 36.46	0.43 - 1.49	28.17 - 36.37	b.d.l. - 0.02	b.d.l.	32.47 - 36.78	97.64 - 100.89	0.485 - 0.617
			average	0.01	0.03	30.70	0.83	34.05	0.00	0.00	33.47	99.09	0.527
			median	b.d.l.	0.02	30.71	0.79	34.54	b.d.l.	b.d.l.	33.19	99.05	0.521
			1σ	0.04	0.02	1.92	0.24	2.16	0.01	0.00	0.90	1.00	0.031

[1]b.d.l. = below detection limit

Table 2.3: Summary of the Fe-Ni sulfide occurrences observed in each sample of Tagish Lake.

	Po with Exsolved Pn								
Sample	**Blocky**	**Coarse Linear**	**Lamella**	**Blebs**	**Flames**	**Snowflake**	**Unexsolved Po**	**Unexsolved Pn**	**Bull's Eye**
TL11h	x			x	x	x	x	x	x
TL11i	x	x	x	x	x		x	x	x
TL11v			x	x	x		x		x
TL4	x	x	x	x	x			x	
TL5b	x	x			x		x		x
TL10a		x	x	x	x			x	x
TL1/3	x			x	x		x	x	x
TL1/6	x	x	x	x	x		x	x	x

2.9 Figure Captions

Figure 2.1: Backscattered electron (BSE) images of exsolved pyrrhotite-pentlandite grains within the matrix and chondrules of Tagish Lake samples. A variety of exsolution textures are shown including: a) blocky exsolution; b) blocky and coarse linear; c) lamellae; d) flames; e,f) blocky, lamellae, flames.

po = pyrrhotite, pn = pentlandite, mag = magnetite.

Figure 2.2: BSE images of po-pn grains with magnified fine exsolution textures including: a,b) blebs of pn in mo; c,d) snowflake texture.

po = pyrrhotite, pn = pentlandite.

Figure 2.3: BSE images of unexsolved Fe-Ni sulfides from samples of Tagish Lake (a-d: pyrrhotite; e-h: pentlandite).

Figure 2.4: BSE images of "bull's eye" sulfides from samples of Tagish Lake.

Figure 2.5: Co vs Ni (wt%) for all Fe-Ni sulfide data collected. Data which were retained for analysis are shown as filled circles; data which were filtered to remove analyses with suspected phase overlap are shown as open symbols.

Figure 2.6: Compositional data from sulfides containing course pentlandite exsolution textures plotted on Fe+Co-Ni-S ternary diagrams at 500°C (Shewman and Clark, 1970) and 600°C (Kosyakov et al., 2003).

Figure 2.7: Compositional data from sulfides containing pentlandite flames or without pentlandite exsolution plotted on Fe+Co-Ni-S ternary diagrams at 25°C (Vaughan and Craig 1997) and 100-135°C (Naldrett 1989).

Figure 2.8: Compositional data from isolated pentlandite grains plotted on on Fe+Co-Ni-S ternary diagrams at 25°C (Vaughan and Craig 1997), 100-135°C (Naldrett 1989), 500°C (Shewman and Clark, 1970) and 600°C (Kosyakov et al., 2003)

Figure 2.9: Fe/S (at%) ratios of the examined Tagish Lake samples arranged according to increasing degree of alteration. Error bars represent one standard deviation from the mean.

2.10: Figures

Figure 2.1.

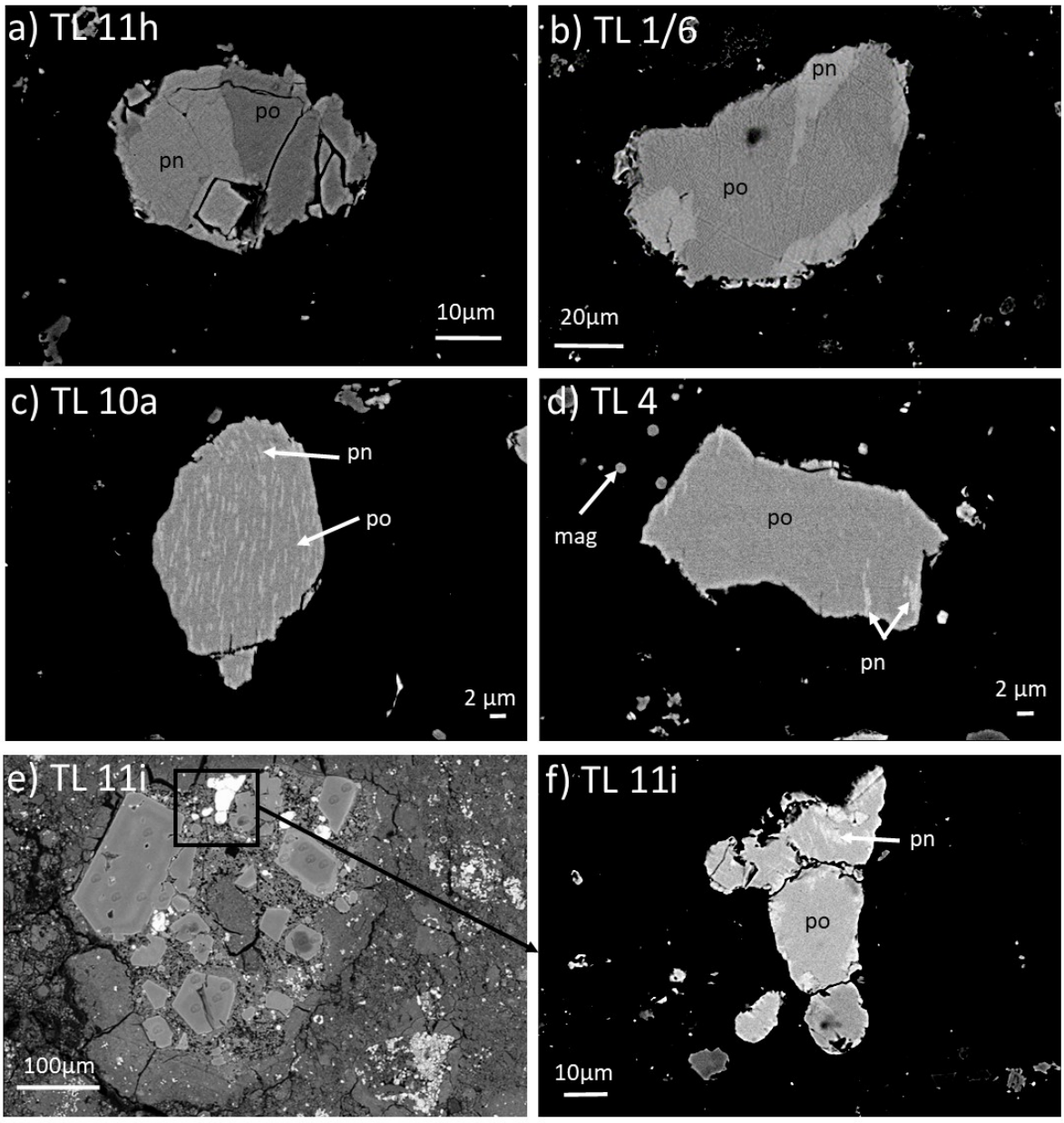

Figure 2.2.

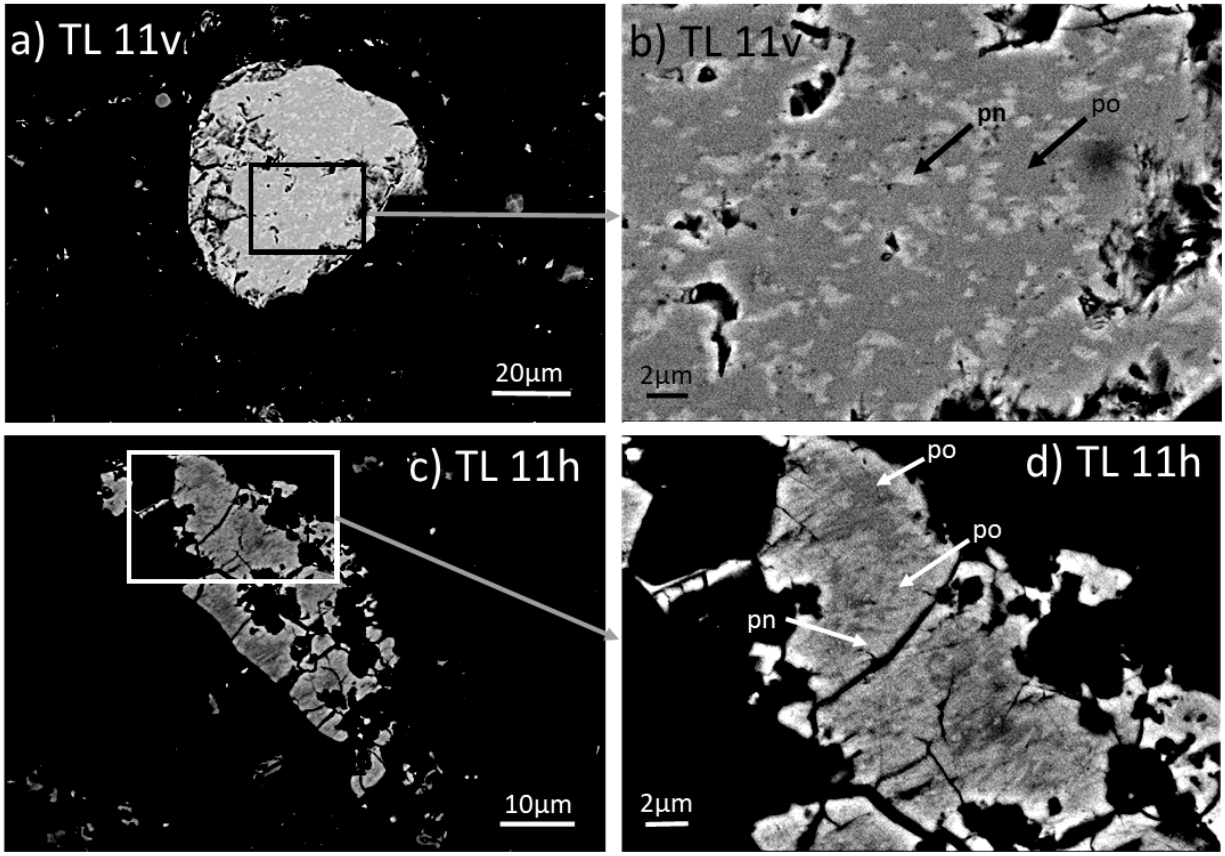

Figure 2.3.

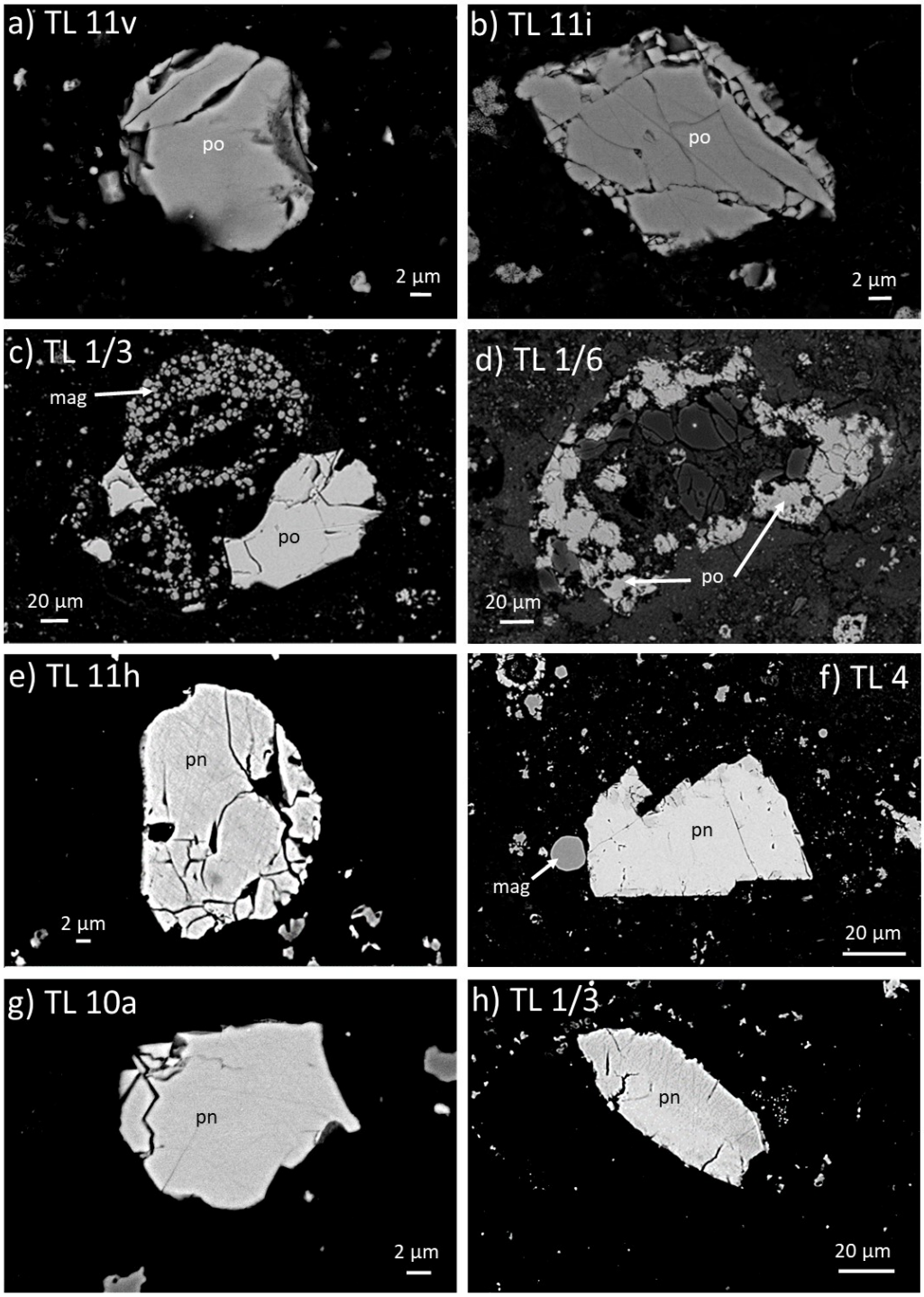
a) TL 11v
po
2 µm
b) TL 11i
po
2 µm
c) TL 1/3
mag
po
20 µm
d) TL 1/6
po
20 µm
e) TL 11h
pn
2 µm
f) TL 4
pn
mag
20 µm
g) TL 10a
pn
2 µm
h) TL 1/3
pn
20 µm

Figure 2.4.

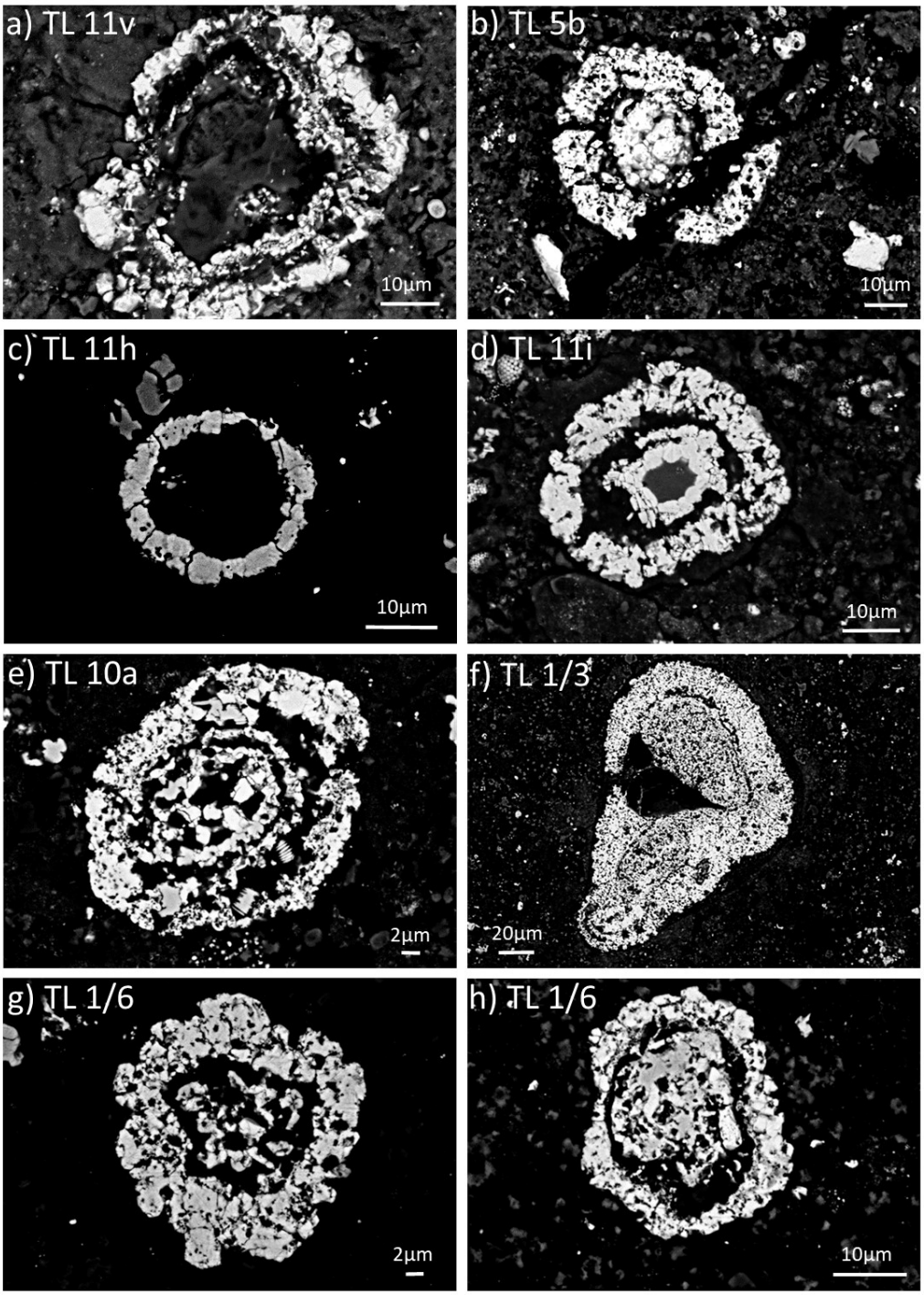
a) TL 11v
10µm
b) TL 5b
10µm
c) TL 11h
10µm
d) TL 11i
10µm
e) TL 10a
2µm
f) TL 1/3
20µm
g) TL 1/6
2µm
h) TL 1/6
10µm

Figure 2.5.

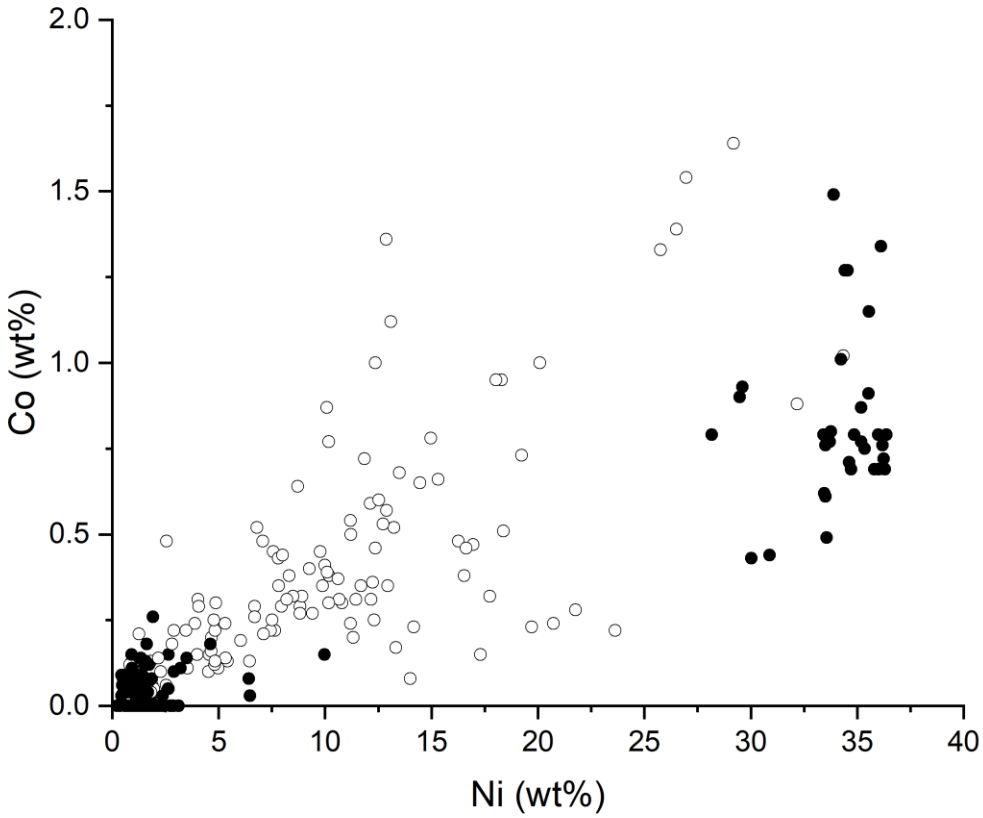

Figure 2.6.

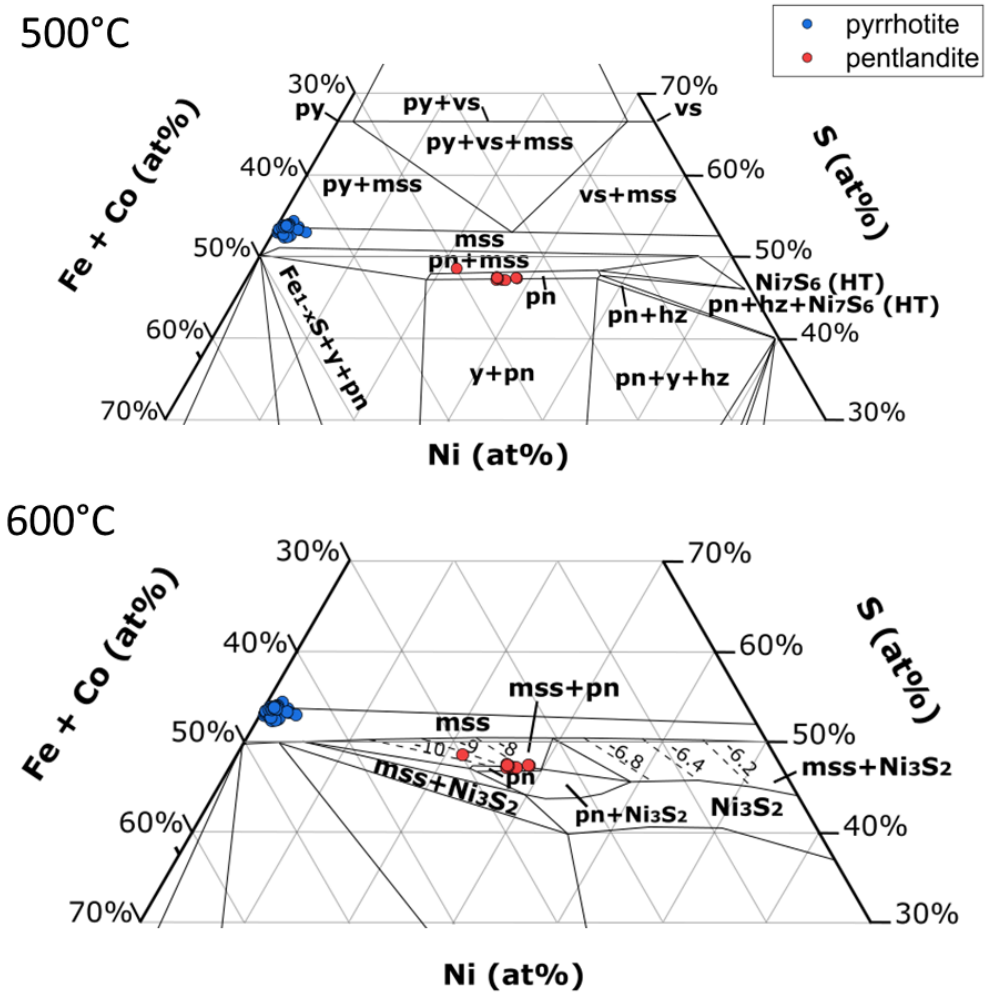
500°C
pyrrhotite
pentlandite
30%
70%
py
py+vs
vs
py+vs+mss
40%
60%
py+mss
vs+mss
S (at%)
Fe + Co (at%)
mss
50%
50%
pn+mss
Ni7S6 (HT)
pn
pn+hz
pn+hz+Ni7S6 (HT)
60%
40%
Fe1-xS+y+pn
y+pn
pn+y+hz
70%
30%
Ni (at%)
600°C
30%
70%
40%
60%
S (at%)
Fe + Co (at%)
mss+pn
mss
50%
50%
-10
-9
-8
-6.8
-6.4
-6.2
mss+Ni3S2
pn
mss+Ni3S2
pn+Ni3S2
Ni3S2
60%
40%
70%
30%
Ni (at%)

Figure 2.7.

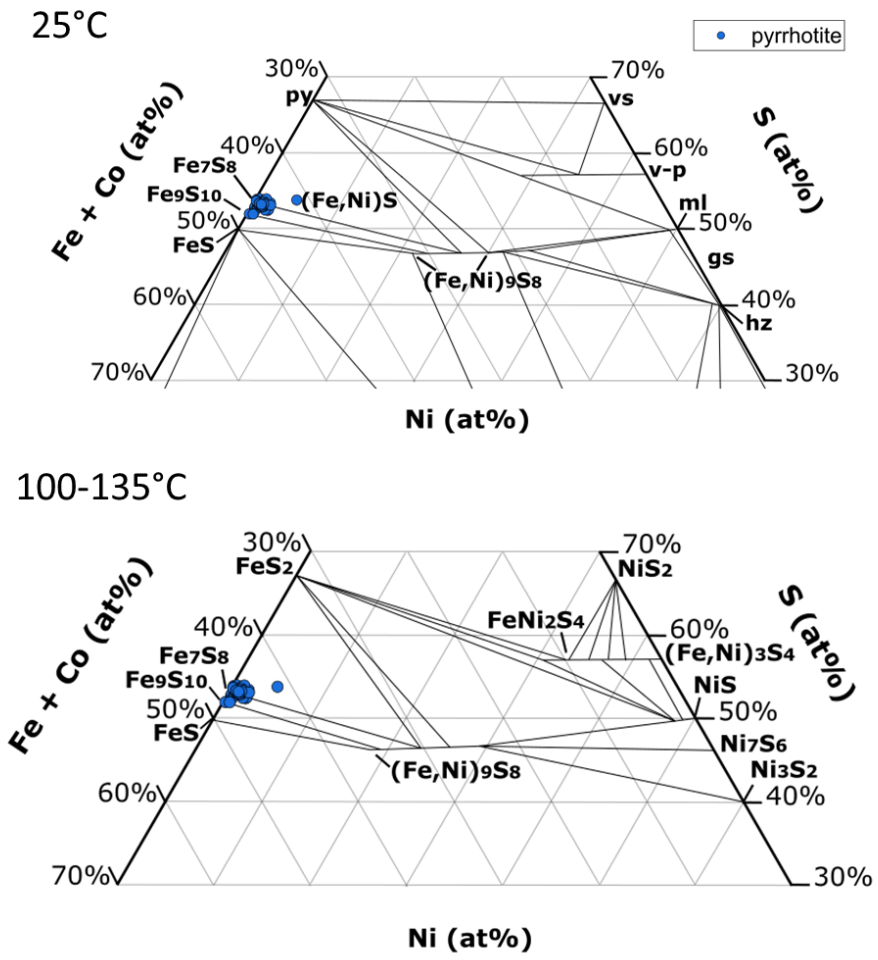
25°C
pyrrhotite
30%
70%
py
vs
40%
60%
Fe7S8
v-p
Fe9S10
(Fe,Ni)S
ml
50%
50%
FeS
gs
(Fe,Ni)9S8
60%
40%
hz
70%
30%
Fe + Co (at%)
S (at%)
Ni (at%)
100-135°C
30%
70%
FeS2
NiS2
FeNi2S4
40%
60%
(Fe,Ni)3S4
Fe7S8
Fe9S10
NiS
50%
50%
FeS
Ni7S6
(Fe,Ni)9S8
Ni3S2
60%
40%
70%
30%
Fe + Co (at%)
S (at%)
Ni (at%)

Figure 2.8.

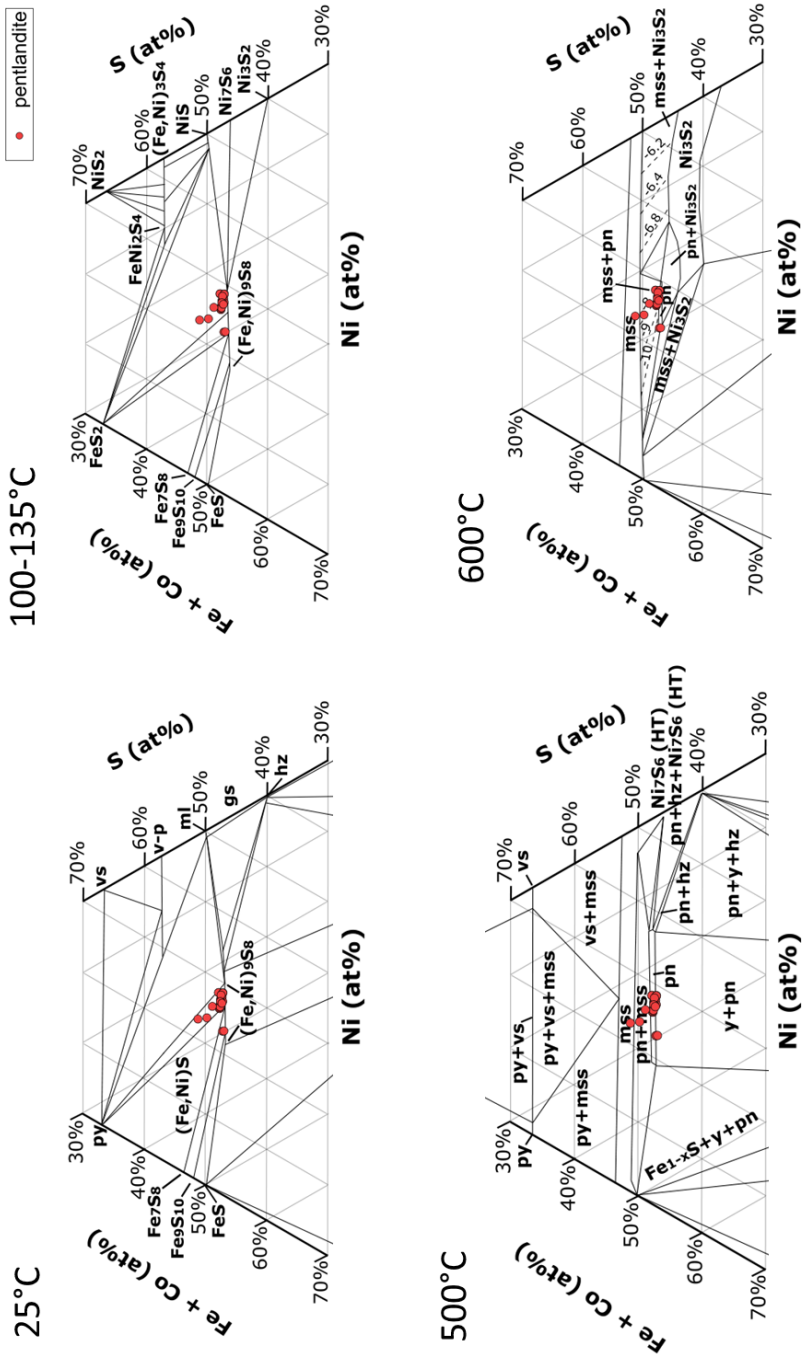
pentlandite
100-135°C
25°C
600°C
500°C
S (at%)
Ni (at%)
Fe + Co (at%)
NiS2
(Fe,Ni)3S4
NiS
Ni7S6
Ni3S2
FeS2
FeNi2S4
Fe7S8
Fe9S10
FeS
(Fe,Ni)9S8
vs
v-p
ml
gs
hz
py
(Fe,Ni)S
mss+pn
mss
mss+Ni3S2
pn+Ni3S2
-6.2
-6.4
-6.6
-6.8
-9
-10
Ni7S6 (HT)
pn+hz+Ni7S6 (HT)
pn+hz
pn+y+hz
vs+mss
py+vs
py+vs+mss
py+mss
pn+mss
pn
y+pn
Fe1-xS+y+pn

Figure 2.9.

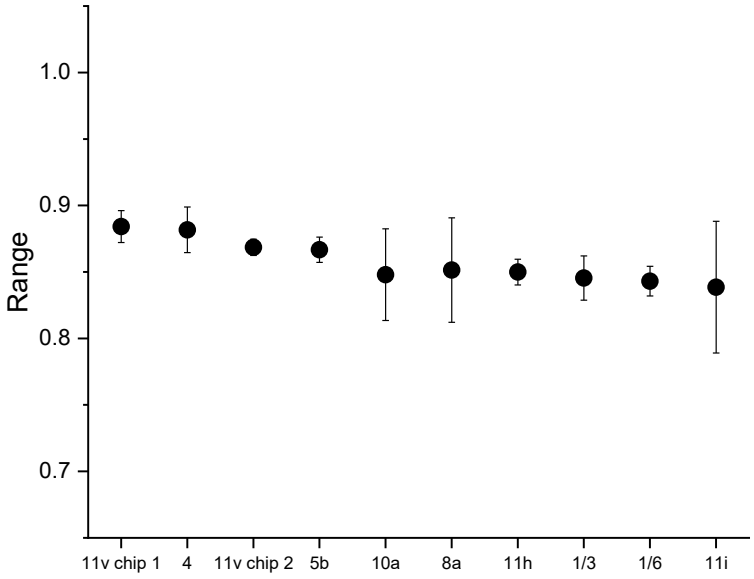

Chapter 3: Fe-Ni Sulfides in Aguas Zarcas: Implications for Nebular and Parent Body Conditions of Formation

3.1 Introduction

Aguas Zarcas is classified as a CM2 carbonaceous chondrite (Meteoritical Bulletin Database, 2021; Takir et al., 2020). This meteorite fell in the San Carlos county of Costa Rica on April 23, 2019. Eleven kilograms of meteorites were recovered in the next 6 days prior to the area receiving rainfall and has thus experienced little terrestrial weathering, after which a further ~16 kg was collected (Meteoritical Bulletin Database, 2021). Aguas Zarcas is in fact a complex breccia found to be composed of at least 5 different lithologies, described by Kerraouch et al (2021a) as: 1) a primitive, metal-rich lithology with petrologic characteristics similar to CR and CM chondrites but different oxygen isotopic composition and chondrule size/abundance that may be related to an impact event between early CM and CR parent bodies; 2) a primitive, metal-rich lithology more closely related to CM chondrites; 3) a CM-related lithology with oxygen isotopic compositions overlapping CM compositions that is likely to be related to CM chondrites and experienced similar aqueous alteration; 4) a CM breccia with clasts of various sub-types, classified as C1/2; 5) a C1 lithology which has a different phyllosilicate composition and may or may not be related to CMs. While the chondrule abundances of these lithologies differ from the chondrule-rich and chondrule-poor lithologies initially described in the Meteoritical Bulletin, one of the metal-rich lithologies may correspond the originally identified chondrule-rich lithology and one of the CM-related lithologies may correspond to the chondrule-poor lithology (Kerraouch et al., 2021a). An additional compact lithology composed of flattened, elongated chondrules showing a strong preferred orientation along with fractures within the chondrite matrix, determined to be the result of high (15-20 GPa) shock pressure experienced during hypervelocity impact was later described by Yang et al. (2021). The coexistence of this highly shocked lithology with other, non shocked lithologies requires transportation and mixing of lithologies within the Aguas Zarcas (AZ) parent body, perhaps by impact ejection and reaccretion (Yang et al., 2021).

Spectral characteristics of Aguas Zarcas samples indicate the various lithologies between specimens have experienced moderate to high degrees of aqueous alteration, falling between CM1, CM1/2, and CM2 classifications (Davidson et al., 2020). Phyllosilicates comprise ~74-85% of the volume of AZ samples, supporting the conclusion that samples have experienced moderate degrees of aqueous alteration (Davidson et al., 2020). Other phases identified within AZ include olivine, pyroxene, magnetite, calcite, minor amounts of metal, and the Fe-Ni sulfides pyrrhotite and pentlandite, the compositions of which indicate formation by low-temperature aqueous alteration (Davidson et al., 2020). Chondrules have been observed to have rims or contain sulfide minerals and metal, similar to chondrules typical of CR2 chondrites, particularly within the metal-rich lithologies (Kerraouch et al., 2020; Kerraouch et al., 2021b). Sulfides may occur as isolated grains or as aggregates of grains, pentlandite may occur as exsolution from pyrrhotite, and sulfide grains may contain metal inclusions (Kerraouch et al., 2020; Kerraouch et al., 2021a). Concentric, “cauliflower-like” sulfide-oxide aggregates occur isolated within the matrix and on the exteriors of chondrules, and may contain relict metal in their cores (Kerraouch et al., 2021a).

This study focused on examining and characterizing the morphologies and compositions of Fe-Ni sulfide phases within five polished, epoxy-mounted samples of AZ to constrain their temperatures and mechanisms of formation. The sulfides are compared across the three lithologies identified within the samples – chondrule-rich, chondrule-poor, and metal-rich (Figure 3.1) - and between other CM2 chondrites and the C2 ungrouped chondrite Tagish Lake. The Fe/S (at%) ratio of low-Ni (<1 wt% Ni) pyrrhotite in AZ is used to compare the degree of aqueous alteration these lithologies experienced on the AZ parent body to those of other C1 and C2 carbonaceous chondrites.

3.2 Methods

Subsampling of AZ specimens for epoxy mounting was conducted under clean room conditions using instruments cleaned with ultrapure water and HPLC-grade dichloromethane (DCM), and where possible (i.e., for the vials, aluminium foil, and tweezers) combusted at 450°C for >6 hours to reduce the potential for contamination. Samples were collected onto aluminum foil and stored in glass vials until use. Epoxy mounting procedures, SEM and EPMA operating conditions and standards are the same as those used during previous analysis of Tagish Lake samples, and are given in Chapter 2. Only analyses with analytical totals between 97.5 wt% and 102.5 wt% will be included in the remainder of the discussion.

3.3 Results

3.3.1 Petrography

Five specimens of AZ were examined during the course of the study. Samples MET11791/1 and MET11791/3 are from the University of Alberta Meteorite Collection, and were originally obtained from Mendy Ouzillou (Skyfall Meteorites), with the former collected pre-rain and the latter collected post-rain. Three additional samples, AZ-PT1, AZ-PT2, and AZ-PT3, are pre-rain specimens obtained from the Meteorite Market. Four of these, AZ-PT1, AZ-PT2, AZ-PT3, and MET11791/3, comprise a mixture of both a chondrule-rich and a subordinate chondrule-poor lithology (Figure 3.1a, b). One specimen, MET11791/1, consists of an unusual metal-rich lithology (Figure 3.1c). Fe-Ni sulfides were found within all of these samples. Fe-Ni Sulfide grains are present both as isolated grains within the matrices of the examined samples and within chondrule interiors and rims; however, their abundance is higher in the matrix than in chondrules. Several of the sulfide grains in both the chondrules and matrices of specimens AZ-PT1, AZ-PT2, AZ-PT3, and MET11791/3 show evidence of alteration (Figure 3.2), having a fairly porous texture and producing compositional analyses with low total wt% and significant impurities of Si, Cr, Mn, and P that are not expected within Fe-Ni sulfides. Compared with sulfides observed in

Tagish Lake, there is less association between sulfide and magnetite in AZ, which has a lower abundance of magnetite visible in the matrix overall. A similar variety of textures are observed in the AZ sulfides as in Tagish Lake, including exsolved pyrrhotite-pentlandite grains, unexsolved pyrrhotite and pentlandite, as well as the "bull's-eye" morphology first identified by Blinova et al. (2014a) in Tagish Lake. Examples and explanations of these textures in Tagish Lake are found in Chapter 2.

3.3.1.1 Exsolved pyrrhotite-pentlandite

A few exsolved sulfide grains are observed as isolated grains within the AZ sample matrices. These grains primarily exhibit fine textures (<~2 μm in diameter) including lamellae, blebs, and flames of pentlandite within pyrrhotite (Figure 3.3a, b, e, f, g, h), as well as wormy exsolution of pyrrhotite from pentlandite similar to the "snowflake" texture (Figure 3.3c, d) first described by Brearley and Martinez (2010).

3.3.1.2 Unexsolved Pyrrhotite

Pyrrhotite grains which lack exsolution features comprise the majority of sulfide grains observed within the AZ samples examined (Figure 3.4). These grains occur both within chondrules as well as within the sample matrices but are more common within the matrix. They occur as angular to rounded grains, several of which exhibit the unusual porous texture previously noted.

3.3.1.4 Unexsolved Pentlandite

Several examples of pentlandite grains not associated with pyrrhotite are observed within the matrix of samples AZ-PT1, AZ-PT2, AZ-PT3, and MET11791/3 (Figure 3.5). The observed grains often occur within close proximity to chondrules containing altered, porous sulfide grains, as components of dense, round, phyllosilicate-rich objects, or isolated in the matrix. They are typically fairly angular in nature and contain several fractures.

3.3.1.5 "Bull's-Eye" Sulfides

One instance of the "bull's-eye" sulfide morphology first observed in samples of Tagish Lake by Blinova et al. (2014a) was observed in specimen MET11791/1 (Figure 3.6), here exhibiting the expected morphology of an outer and inner ring of sulfides separated by an incomplete gap. The center ring appears to have nucleated around a pre-existing, non-sulfide grain. Unlike those grains observed within TL, however, the example found in AZ had a sufficiently large grain size and lacked exsolved pentlandite, allowing for a pure compositional analysis to be obtained.

3.3.2 Composition

Analysis of the major and minor element compositions of the Fe-Ni sulfide grains present indicates that they are composed of primarily pyrrhotite and pentlandite, with several examples of an intermediate monosulfide solid solution (MSS) phase. Suspected impure analyses caused by beam overlap of multiple phases were removed from consideration in the same manner as described previously for Tagish Lake in Chapter 2. The resulting ranges and averages of the filtered data are reported in Table 3.1. All analyses are reported in Appendix B, Table B.1.

The data represent 26 pyrrhotite and 19 pentlandite measurements from the chondrule-rich specimen examined, and 15 pyrrhotite measurements from the metal-rich specimen. The average Fe content of the pyrrhotite in the AZ samples is 60.09 ± 0.72 wt%, the average Ni is 1.08 ± 0.62 wt%, and the average S content is 38.51 ± 0.38 wt%. The total range in Fe content is 58.00-61.71 wt% with a median of 60.26 wt%, in Ni content is 0.21-2.43 wt% with a median of 0.94 wt%, and in S content is 37.51-39.25 wt% with a median of 38.60 wt%. The average Fe content of the pentlandite in the AZ samples is 32.44 ± 1.90 wt%, the average Ni content is 32.42 ± 1.28 wt%, and the average S content is 33.28 ± 0.33 wt%. The total range in Fe content is 29.69-35.96 wt% with a median of 31.84 wt%, in Ni content is 29.49-33.71 wt% with a median of 33.01 wt%, and in S content is 32.66-33.72 wt% with a median of 33.39 wt%.

The compositions of the exsolved and unexsolved pyrrhotite, pentlandite, and "bull's-eye" sulfide grains are plotted on Fe-Ni-S ternary diagrams at 100-135°C (Naldrett 1989) and 500°C (Shewman and Clark, 1970) in Figure 3.7.

3.4 Discussion

3.4.1 Degree of Aqueous Alteration

The Fe/S (at%) ratio of low-Ni (<1 wt% Ni) pyrrhotite grains can be used as measure of the relative degree of aqueous alteration for carbonaceous chondrites (Schrader et al. 2021). The Fe-content of pyrrhotite is expected to decrease with increasing aqueous alteration as Fe is incorporated into magnetite and phyllosilicates, a trend which holds true for CM and CI chondrites, where the Fe/S ratio of low-Ni pyrrhotite increases in the order of CI<CM1/2<CM2 (Schrader et al., 2021).

The Fe/S (at%) ratio of low-Ni pyrrhotite grains in both the metal-rich and metal-poor AZ lithologies are reported in Table 3.1. The average Fe/S (at%) of low-Ni pyrrhotite in both AZ and TL samples examined during this study as well as values for AZ, CM1, CM1/2, CM2, and CI chondrites obtained by Schrader et al. (2021) are plotted in order of increasing degree of alteration according to their Fe/S ratios in Figure 3.8. From this plot it is clear that: 1) AZ sulfides have a relative degree of alteration comparable to that of CM1/2 chondrites, as was concluded by Schrader et al. (2021); 2) The Fe/S ratios of the pyrrhotite from the different lithologies examined during this study differ slightly from one another and significantly from that obtained by Schrader et al. (2021) for the same meteorite.

Given that AZ is in reality not simply made up of a single CM2 lithology as suggested by its classification, but is in fact a breccia made up of multiple lithologies spanning the range of degrees of alteration between that of CM1 and CM2 chondrites, it is not surprising that, on average, the degree of alteration indicated by the Fe/S ratio of its pyrrhotite grains lies between CM1 and CM2 chondrites with CM1/2 chondrites. It is thus also unsurprising that the various samples examined by these and other

authors have been shown by this method to have experienced slight differences in their degree of alteration. Indeed, this method of assessing degree of alteration is further confirmation of the heterogeneity within AZ. The different degrees of alteration preserved between samples suggest that the samples experienced distinct alteration histories which were not later overprinted or reset by a common alteration event, prior to being incorporated into the AZ meteorite. Rather, the records of their unique alteration histories are retained.

Notably, the Fe/S ratio of the metal-rich lithology found in this study lies within the range of Fe/S ratios defined by the metal-poor samples, despite previous suggestion that this unusual lithology is more primitive (Kerraouch et al., 2021a) than coexisting lithologies. This result implies that the aqueous alteration history experienced by the different samples is not directly controlled by sample lithology, but instead can vary slightly independently of lithologic makeup. Therefore, the aqueous alteration history reflected by these results likely does not correspond to differences in the sources of these various lithologies, but more likely reflects slight variations in degree of alteration on the AZ parent body itself. This may be explained by a single common aqueous alteration event on the AZ parent body overprinting any signals from earlier alteration events which may have been experienced by the individual lithologies prior to their assembly into the AZ parent body. The range of degrees of alteration between samples of AZ could then be explained by the location of these samples on the AZ parent body itself, with more highly altered samples being sourced from locations closer to the source of this altering event, and less altered samples being sourced from farther away.

3.4.2 Temperature of Formation

The temperatures of formation of sulfides in AZ were constrained using a combination of textural and compositional analysis. The Fe-Ni-S compositions of the examined grains plotted on ternary diagrams for the Fe-Ni-S system at 100-135°C and 500°C (Figure 3.7; Naldrett 1989; Shewman and Clark,

1970) and presence or absence of various exsolution textures were used to determine and approximate temperature of formation for each group.

Although the exsolution features observed within the AZ sulfides examined are primarily <~1-2 μm in width, too fine for compositional analyses to be obtained on most grains, the presence of exsolution lamellae and blebs of pentlandite within pyrrhotite suggest formation of these grains at temperatures of at least 150-250°C (Durazzo and Taylor, 1982) or higher, similar to grains within the TL samples examined which display pentlandite-pyrrhotite exsolution. The composition of TL sulfides verifies this high-temperature formation of up to ~600°C. Those grains where exsolution features are large enough to allow their composition to be determined best match the composition predicted by the 500°C diagram (Figure 3.7a). Likewise, the composition of the unexsolved pentlandite grains are too S-rich to have formed at low temperatures between 100-135°C, and are more consistent with formation at ~500°C (Figure 3.7b), as was similarly seen in the TL pentlandite examined. The majority of the sulfide grains present within the AZ samples are unexsolved pyrrhotite, and the composition of these grains corresponds well to the 100-135°C ternary diagram (Figure 3.7c), a lower temperature of formation with is consistent with their texture. The “bull’s-eye” sulfide found within sample MET11791/1 is of sufficient grain size to allow for compositional analysis, a first for this morphology during the course of this study. Its composition is most consistent with formation at 100-135°C (Figure 3.7d), the same temperature as the unexsolved pyrrhotite grains, confirming the hypothesis that these grains are formed at low temperature.

The range of temperatures of formation obtained in this study is similar to the majority of Fe-Ni sulfide grains observed within other CM2 chondrites (Schrader et al., 2016,), including the lower limit of the temperatures of formation, which likely corresponds to the temperature of the altering fluid on the AZ parent body. This indicates that, while AZ is a complex breccia of multiple lithologies with varying degrees of alteration, the altering event(s) that formed these sulfides occurred at similar temperatures

as those experienced by other CM2 chondrites. In contrast, these temperatures are not consistent with those experienced by either TL, as revealed in this study, or some CI chondrites, where low temperature unexsolved pyrrhotite may form at temperatures as low as ~25°C (Berger et al., 2016).

3.4.3 Formation Mechanisms

Like the Fe-Ni sulfides found within other CM chondrites, those within AZ are divided into two distinct groups – those formed at high temperatures of up to 500-600°C, and those formed at low temperatures of ~100-135°C, the latter of which are in much greater abundance. These groups must have distinct methods of formation to account for the presence of both in the same meteorite.

The formation of sulfides at high temperature has been attributed to either sulfidation of Fe-Ni metal or crystallization of a monosulfide solid solution (MSS) liquid. The high temperature sulfides in AZ, the exsolved pyrrhotite-pentlandite grains and unexsolved pentlandite, are similar in texture, occurrence, and temperature of formation to grains observed during the study of TL samples reported in Chapter 2, and similarly lack metal cores. This suggests that the most likely mechanism of formation of these grains is likewise crystallization of an MSS melt during chondrule formation, with later fragmentation and incorporation into the AZ matrix.

The second group of sulfides, the unexsolved pyrrhotite and “bull’s-eye” morphology, formed at lower temperatures of 100-135°C, which is more consistent with formation by aqueous alteration on the meteorite parent body than in the solar nebula. This conclusion provides evidence to support the Blinova et al. (2014a) hypothesis that the “bull’s-eye” morphology formed by deposition from a fluid during parent body aqueous alteration, and is consistent with the temperature of equilibration of similar pyrrhotite grains within other CM chondrites examined by Schrader et al. (2016) believed to have formed during low-temperature aqueous alteration. While this “bull’s eye” morphology is similar in appearance to the “cauliflower-like” sulfide-oxide aggregates noted in AZ by Kerraouch et al. (2021a),

such “cauliflower-like” grains are interpreted by Barth et al. (2018) to have formed at ~400-550°C in the solar nebula by gas-solid interactions, rather than during aqueous alteration. The “cauliflower-like” grains differ from the low-temperature “bull’e eye” sulfides in their Fe/Ni ratios, which match expected ratios for the aforementioned higher formation temperature, as well as their association with accessory metal, silicate, and phosphate phases. The “bull’s eye” sulfides, conversely, have compositions more consistent with lower temperatures of formation (Figure 3.7d), and are not associated with these phases.

3.5 Conclusion

The Fe-Ni sulfide grains present within two samples of the Aguas Zarcas meteorite and their lithologies represent a complex history of formation, and their morphologies and compositions reveal information about their formation and alteration histories.

The Fe/S (at%) ratio of the low-Ni pyrrhotite grains was used to place the various lithologies of AZ into an order of relative degree of alteration with other moderately altered carbonaceous chondrites. The relative order of alteration of these groups is CM2 (Schrader et al., 2021) < AZ (Schrader et al., 2021) < CM1/2 (Schrader et al., 2021) < AZ (this study) < TL < CI (Schrader et al., 2021).

The sulfide grains present within AZ represent two distinct generations of sulfide formation, which increasing evidence suggests is common to all moderately altered carbonaceous chondrites such as CM and CI chondrites (Schrader et al., 2016), as well as Tagish Lake (Holt and Herd, 2022, Chapter 2). The first of these is the high-temperature generation, which likely formed between 500-600°C during crystallization of an MSS melt during chondrule formation and is represented in AZ by exsolved pyrrhotite-pentlandite and unexsolved pentlandite grains. The second of these is the low temperature generation, which formed at ~100-135°C, likely during parent body aqueous alteration. This second generation includes most unexsolved pyrrhotite as well as the distinctive “bull’s-eye” morphology

previously identified in TL. The temperature of formation of this second generation is consistent with results for previous CM2 chondrites. This temperature of formation does not vary between different samples regardless of the degree of alteration they experienced, which suggests that degree of alteration is not directly correlated to alteration temperature. The range in degree of alteration experienced within a meteorite group and variations in degree of alteration within single meteorites such as Aguas Zarcas could be the result of differences in the length of time aqueous alteration continued at a particular location on the meteorite parent body, or differences in proximity of the source locations of different specimens to the source of the altering event.

3.6 Tables

Table 3.1: Major and minor element compositions of Fe-Ni sulfides in Aguas Zarcas.

Sample	Mineral	Number of Analyses		Si	Cr	Fe	Co	Ni	Mn	P	S	Total	Fe/S
				wt%	wt%	wt%	wt%	wt%	wt%	wt%	wt%	wt%	at%
MET11791-1	pyrrhotite	15	range	b.d.l. - 0.39	0.01 - 0.68	58.00 - 60.61	b.d.l. - 0.24	0.42 - 2.43	b.d.l. - 0.10	b.d.l. - 0.01	37.51 - 39.25	98.72 - 100.50	0.872 - 0.917
			average	0.05	0.15	59.77	0.05	1.34	0.02	0.00	38.29	99.68	0.896
			1σ	0.10	0.18	0.69	0.10	0.67	0.03	0.00	0.50	0.53	0.015
AZ-PT2	pyrrhotite	3	range	b.d.l. - 0.03	0.02 - 0.05	59.42 - 60.34	0.03 - 0.05	0.59 - 0.84	b.d.l. - 0.01	b.d.l.	38.46 - 38.58	98.98 - 99.46	0.884 - 0.901
			average	0.01	0.03	59.95	0.04	0.69	0.00	0.00	38.51	99.24	0.894
			1σ	0.02	0.02	0.48	0.01	0.13	0.01	0.00	0.07	0.24	0.009
	pentlandite	3	range	b.d.l. - 0.12	0.03 - 0.04	30.51 - 33.56	0.65 - 2.16	31.42 - 33.21	b.d.l. - 0.01	b.d.l.	32.94 - 33.29	98.66 - 99.33	0.526 - 0.585
			average	0.04	0.03	32.53	1.18	32.05	0.00	0.00	33.09	98.93	0.565
			1σ	0.07	0.01	1.75	0.85	1.01	0.01	0.00	0.18	0.36	0.033
AZ-PT1	pyrrhotite	6	range	b.d.l. - 0.02	0.02 - 0.04	59.21 - 61.71	b.d.l. - 0.14	0.21 - 1.71	b.d.l. - 0.08	b.d.l.	38.15 - 38.88	98.98 - 100.84	0.886 - 0.911
			average	0.01	0.03	60.51	0.04	0.89	0.01	0.00	38.69	100.18	0.898
			1σ	0.01	0.01	0.95	0.06	0.61	0.03	0.00	0.28	0.65	0.009
	pentlandite	6	range	b.d.l. - 0.16	0.02 - 0.04	29.69 - 34.24	0.63 - 1.89	31.22 - 33.66	b.d.l.	b.d.l.	32.83 - 33.51	97.86 - 99.76	0.515 - 0.589
			average	0.05	0.03	31.21	1.30	32.95	0.00	0.00	33.27	98.82	0.538
			1σ	0.06	0.01	1.66	0.64	0.91	0.00	0.00	0.29	0.74	0.028
AZ-PT3	pyrrhotite	11	range	b.d.l. - 0.01	0.01 - 0.05	59.00 - 60.74	b.d.l. - 0.22	0.49 - 2.35	b.d.l.	b.d.l.	38.46 - 38.86	99.55 - 100.55	0.878 - 0.903
			average	0.01	0.03	60.08	0.09	1.24	0.00	0.00	38.62	100.06	0.893
			1σ	0.01	0.01	0.54	0.08	0.58	0.00	0.00	0.13	0.33	0.008
	pentlandite	8	range	b.d.l. - 0.14	0.02 - 0.04	30.28 - 35.96	0.49 - 1.71	29.49 - 33.71	b.d.l.	b.d.l. - 0.02	32.66 - 33.72	97.96 - 100.60	0.532 - 0.622
			average	0.04	0.03	32.95	0.88	32.25	0.00	0.00	33.27	99.42	0.569
			1σ	0.05	0.01	2.01	0.38	1.64	0.00	0.01	0.39	0.84	0.034
MET11791-3	pyrrhotite	6	range	b.d.l. - 0.04	b.d.l. - 0.06	59.29 - 61.02	b.d.l. - 0.05	0.34 - 0.94	b.d.l.	b.d.l.	38.13 - 38.91	98.43 - 100.29	0.892 - 0.909
			average	0.01	0.02	60.57	0.01	0.54	0.00	0.00	38.66	99.81	0.900
			1σ	0.02	0.03	0.67	0.02	0.23	0.00	0.00	0.28	0.71	0.005
	Pentlandite	2	range	b.d.l. - 0.01	0.04 - 0.06	33.26 - 34.62	0.45 - 0.69	31.03 - 33.06	b.d.l.	b.d.l.	33.60 - 33.64	99.99 - 100.47	0.568- 0.592
			average	0.01	0.05	33.94	0.57	32.05	0.00	0.00	33.62	100.23	0.580
			1σ	0.01	0.01	0.96	0.17	1.44	0.00	0.00	0.03	0.34	0.017
total	pyrrhotite	41	range	b.d.l. - 0.39	b.d.l. - 0.68	58.00 - 61.71	b.d.l. - 0.24	0.21 - 2.43	b.d.l. - 0.10	b.d.l. - 0.01	37.51 - 39.25	98.43 - 100.84	0.872 - 0.917

		average	0.02	0.07	60.09	0.05	1.08	0.01	0.00	38.51	99.84	0.896
		median	0.01	0.03	60.26	b.d.l.	0.94	b.d.l.	b.d.l.	38.60	100.01	0.896
		1σ	0.06	0.12	0.72	0.08	0.62	0.02	0.00	0.38	0.56	0.011
pentlandite	19	range	b.d.l. - 0.16	0.02 - 0.06	29.69 - 35.96	0.45 - 2.16	29.49 - 33.71	b.d.l. - 0.01	b.d.l.	32.66 - 33.72	97.86 - 100.60	0.515 - 0.622
		average	0.04	0.03	32.44	1.03	32.42	0.00	0.00	33.28	99.24	0.560
		median	0.02	0.03	31.84	0.74	33.01	b.d.l.	b.d.l.	33.39	99.29	0.552
		1σ	0.05	0.01	1.90	0.56	1.28	0.00	0.00	0.33	0.80	0.032

3.7 Figure Captions

Figure 3.1: a) A backscattered electron (BSE) image of a chondrule-rich portion of sample AZ PT2; b) A BSE image of a chondrule-poor portion of sample AZ PT2; c) A BSE image of the unusual metal-rich lithology in sample MET11791-1.

Figure 3.2: BSE images of porous sulfides is sample AZ PT2.

Figure 3.3: BSE images of exsolved pyrrhotite-pentlandite grains within the matrix of Aguas Zarcas samples. The textures observed include a, b, e, f, g, h) lamellae, blebs, and rods; c,d) “snowflake” texture. po = pyrrhotite, pn = pentlandite

Figure 3.4: BSE images of unexsolved pyrrhotite grains within samples of Aguas Zarcas. po = pyrrhotite, pn = pentlandite, alloy = Fe-Ni metal

Figure 3.5: BSE images of isolated pentlandite grains within samples of Aguas Zarcas.

Figure 3.6: BSE images of the “bull’s eye” sulfide grain identified in AZ sample MET11791-1.

Figure 3.7: Compositional data from: a) Exsolved pyrrhotite- pentlandite grains plotted on an Fe+Co-Ni-S ternary diagram at 500°C (Shewman and Clark, 1970); b) Isolated pentlandite grains plotted on an Fe+Co-Ni-S ternary diagram at 500°C (Shewman and Clark, 1970); c) Isolated pyrrhotite grains plotted on

an Fe+Co-Ni-S ternary diagram at 100-135°C (Naldrett 1989); d) “Bull’s-eye” sulfides grains plotted on an Fe+Co-Ni-S ternary diagram at 100-135°C (d; Naldrett 1989).

Figure 3.8: Fe/S (at%) ratios of: a) The different samples of Aguas Zarcas examined in this study, as well as by Schrader et al. (2021), arranged according to increasing degree of alteration. b) The average values of examined Aguas Zarcas and Tagish Lake samples from this study, as well as average Fe/S (at%) ratios of Aguas Zarcas and CM1, CM1/2, CM2, and CI chondrites examined by Schrader et al. (2021), arranged according to increasing degree of alteration. Error bars represent one standard deviation from the mean.

3.8 Figures

Figure 3.1:

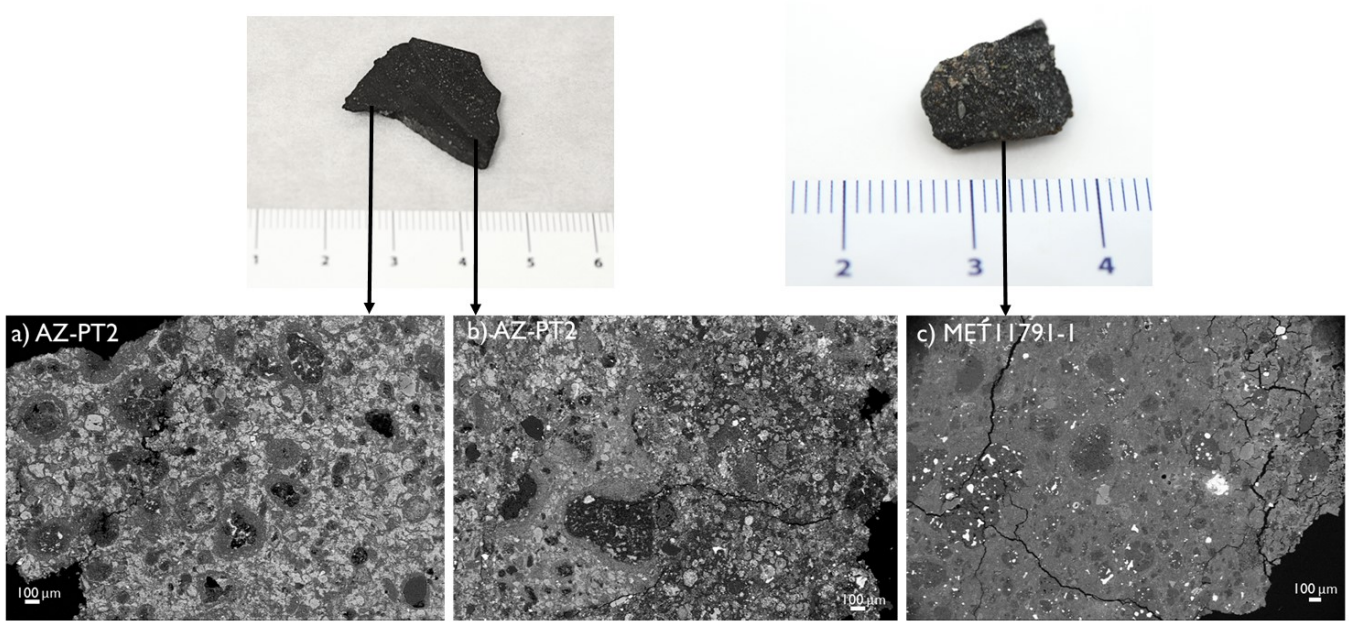

Figure 3.2:

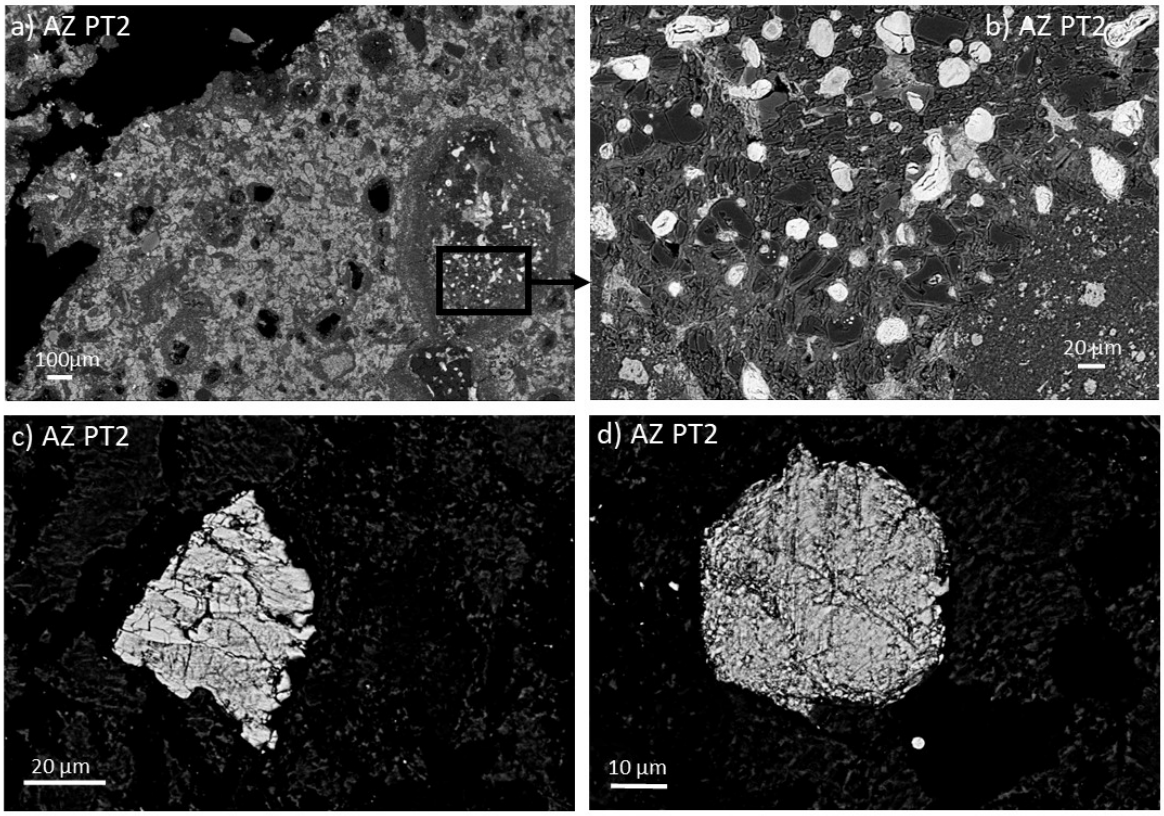

Figure 3.3:

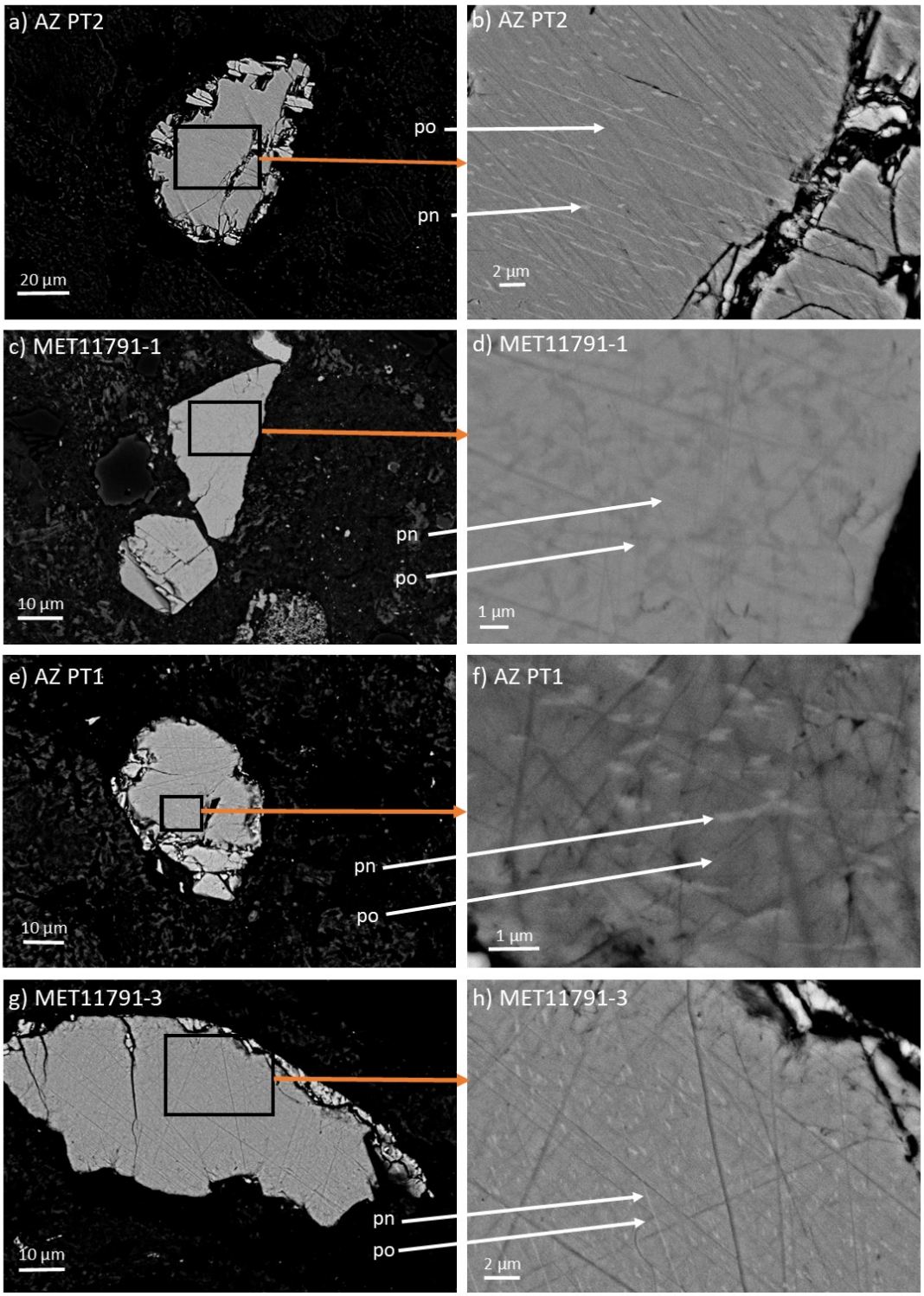
a) AZ PT2
po
pn
20 µm
b) AZ PT2
2 µm
c) MET11791-1
pn
po
10 µm
d) MET11791-1
1 µm
e) AZ PT1
pn
po
10 µm
f) AZ PT1
1 µm
g) MET11791-3
pn
po
10 µm
h) MET11791-3
2 µm

Figure 3.4:

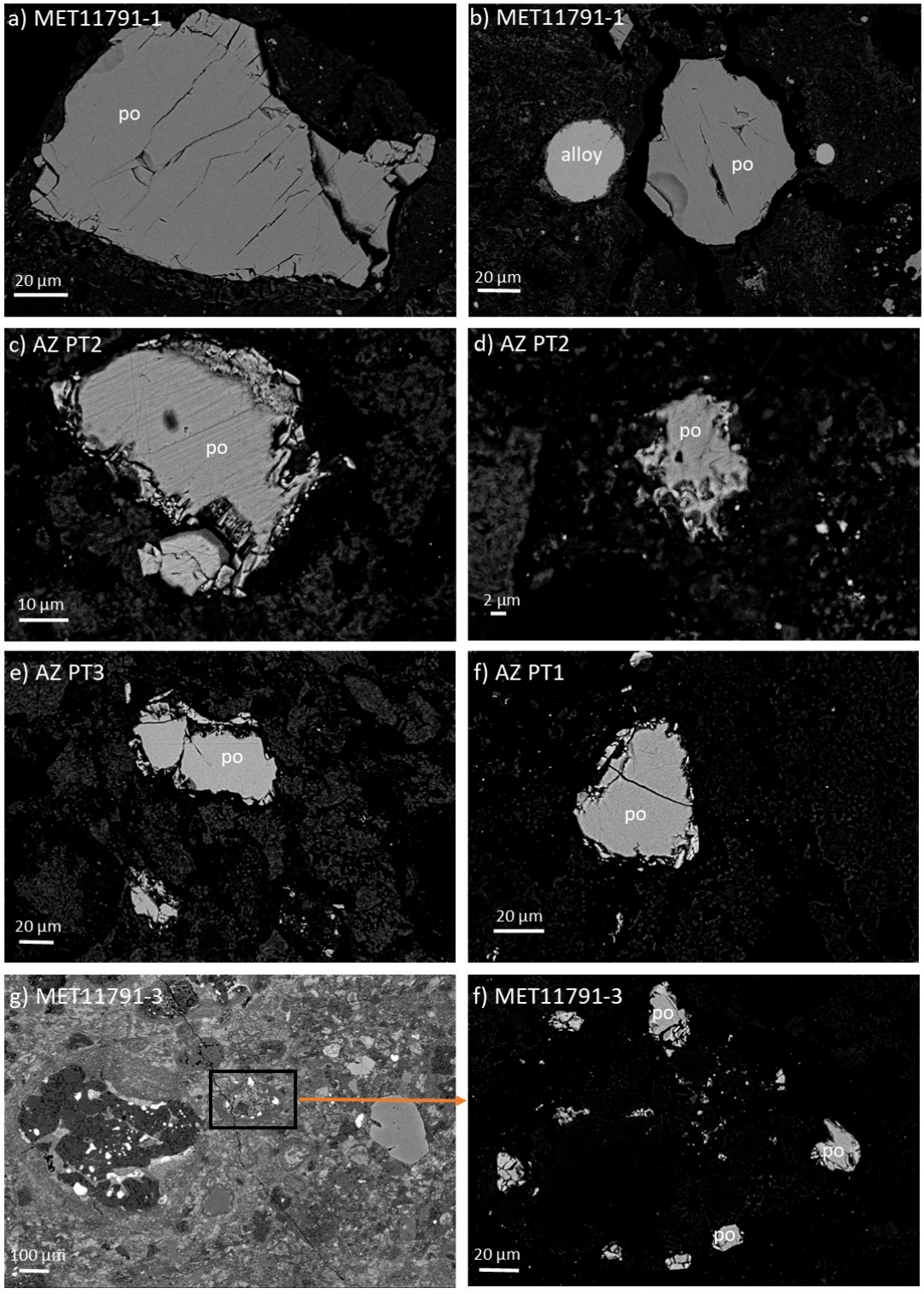
a) MET11791-1
po
20 µm
b) MET11791-1
alloy
po
20 µm
c) AZ PT2
po
10 µm
d) AZ PT2
po
2 µm
e) AZ PT3
po
20 µm
f) AZ PT1
po
20 µm
g) MET11791-3
100 µm
f) MET11791-3
po
po
po
20 µm

Figure 3.5:

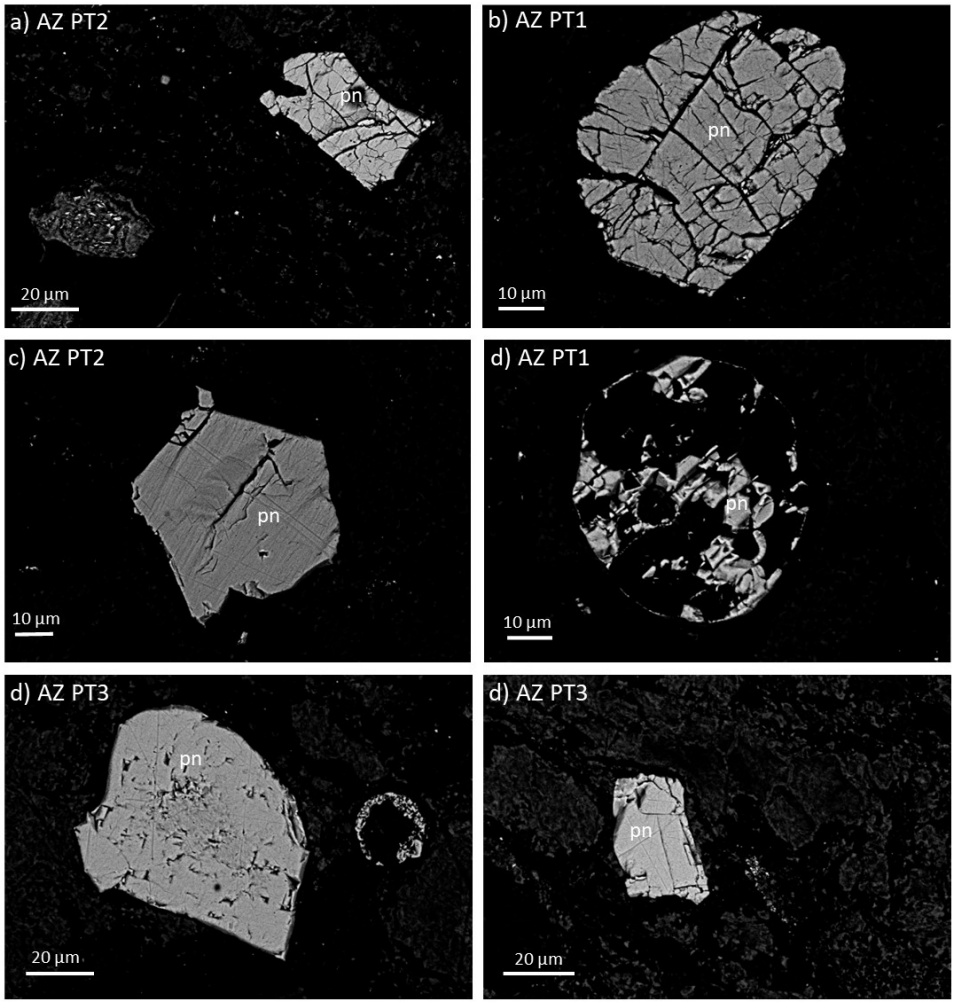
a) AZ PT2
pn
20 µm
b) AZ PT1
pn
10 µm
c) AZ PT2
pn
10 µm
d) AZ PT1
pn
10 µm
d) AZ PT3
pn
20 µm
d) AZ PT3
pn
20 µm

Figure 3.6:

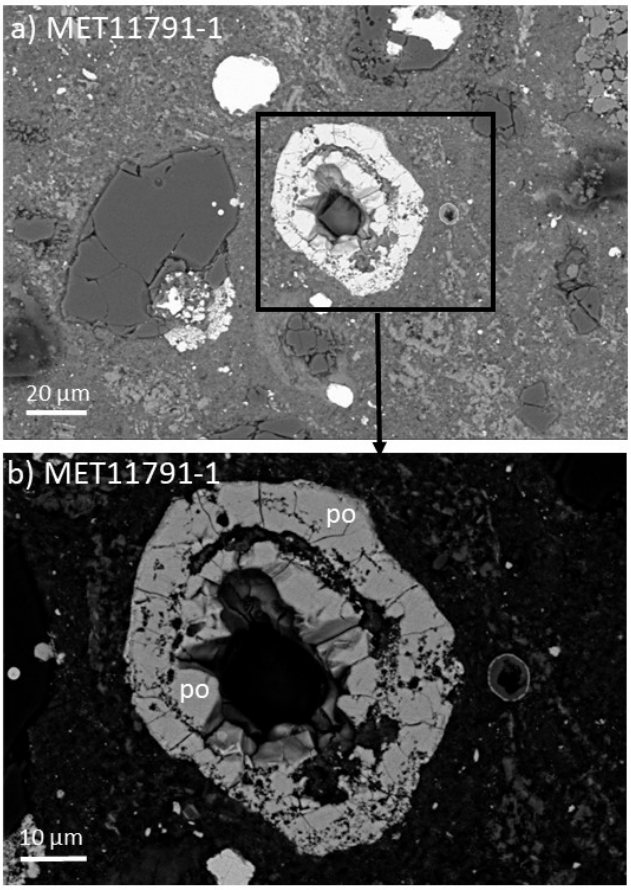

Figure 3.7:

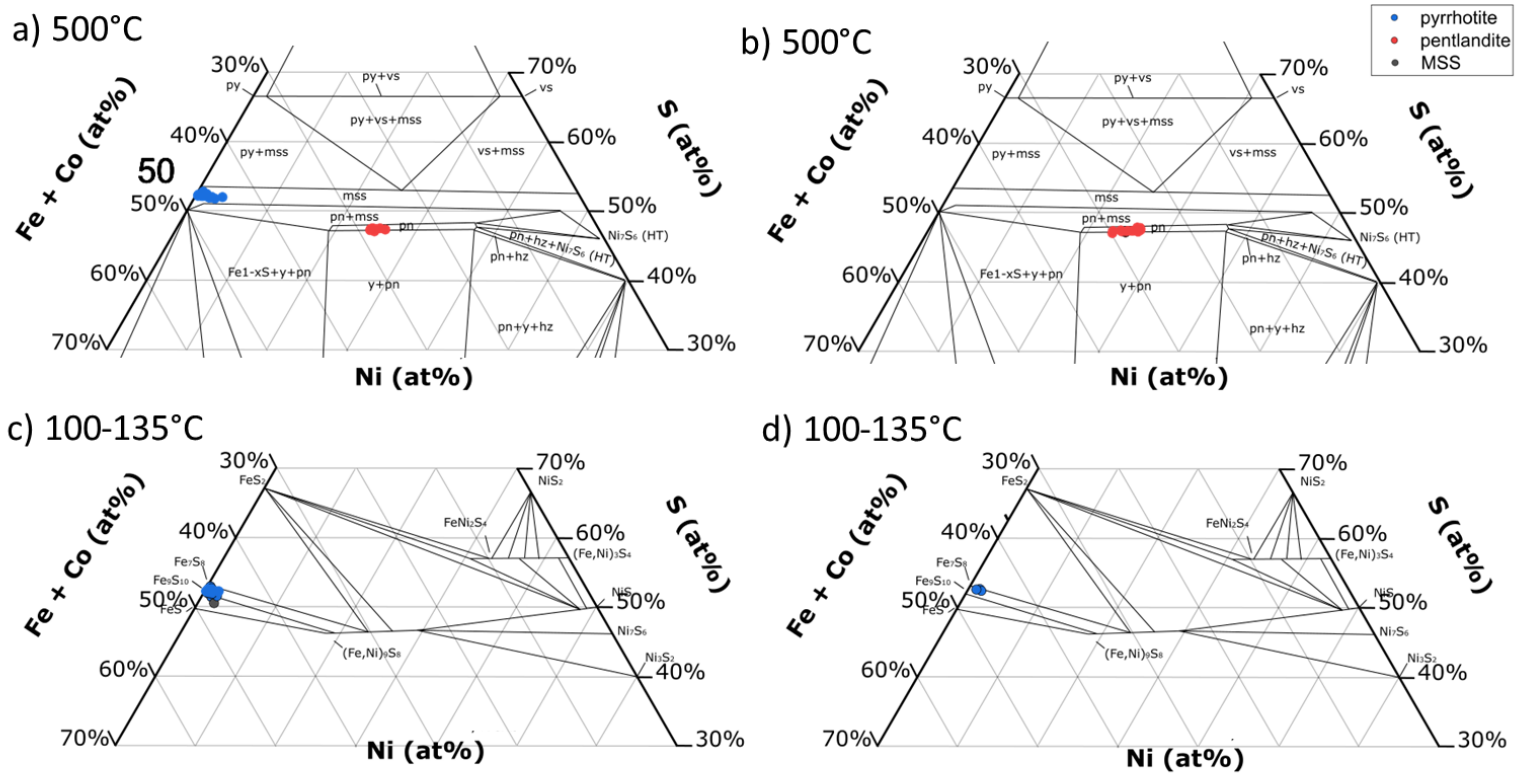
a) 500°C
b) 500°C
c) 100-135°C
d) 100-135°C
pyrrhotite
pentlandite
MSS
Fe + Co (at%)
Ni (at%)
S (at%)
30%
40%
50%
60%
70%
py
vs
py+vs
py+vs+mss
py+mss
vs+mss
mss
pn+mss
pn
Ni7S6 (HT)
pn+hz+Ni7S6 (HT)
pn+hz
Fe1-xS+y+pn
y+pn
pn+y+hz
FeS2
NiS2
FeNi2S4
(Fe,Ni)3S4
Fe7S8
Fe9S10
FeS
NiS
Ni7S6
(Fe,Ni)9S8
Ni3S2

Figure 3.8:

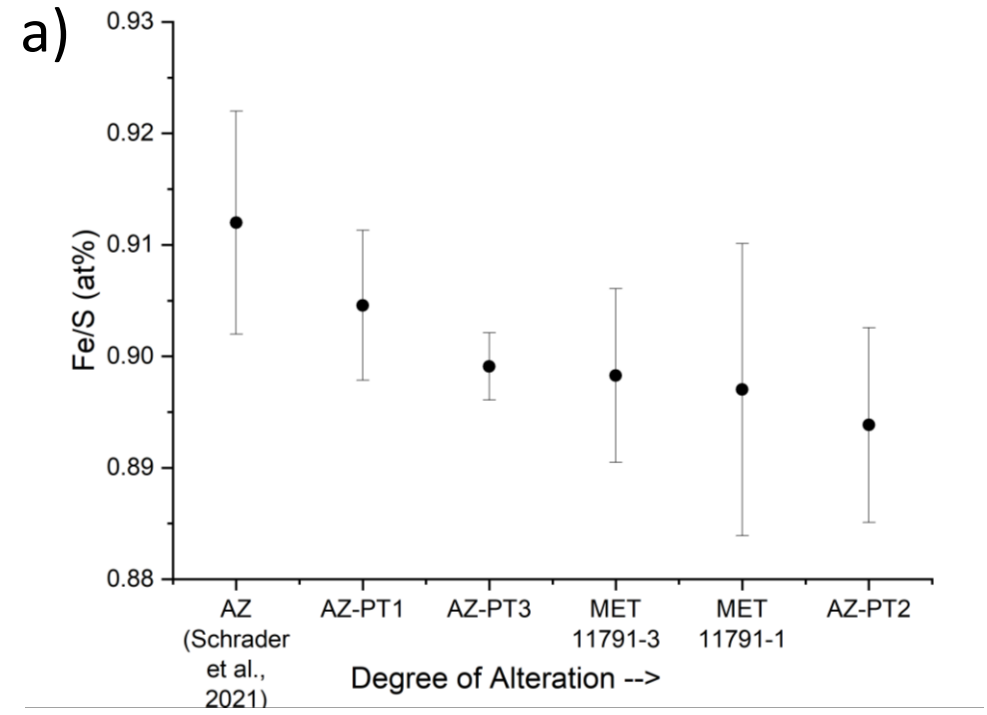
a)
0.93
0.92
0.91
0.90
0.89
0.88
Fe/S (at%)
AZ (Schrader et al., 2021)
AZ-PT1
AZ-PT3
MET 11791-3
MET 11791-1
AZ-PT2
Degree of Alteration -->

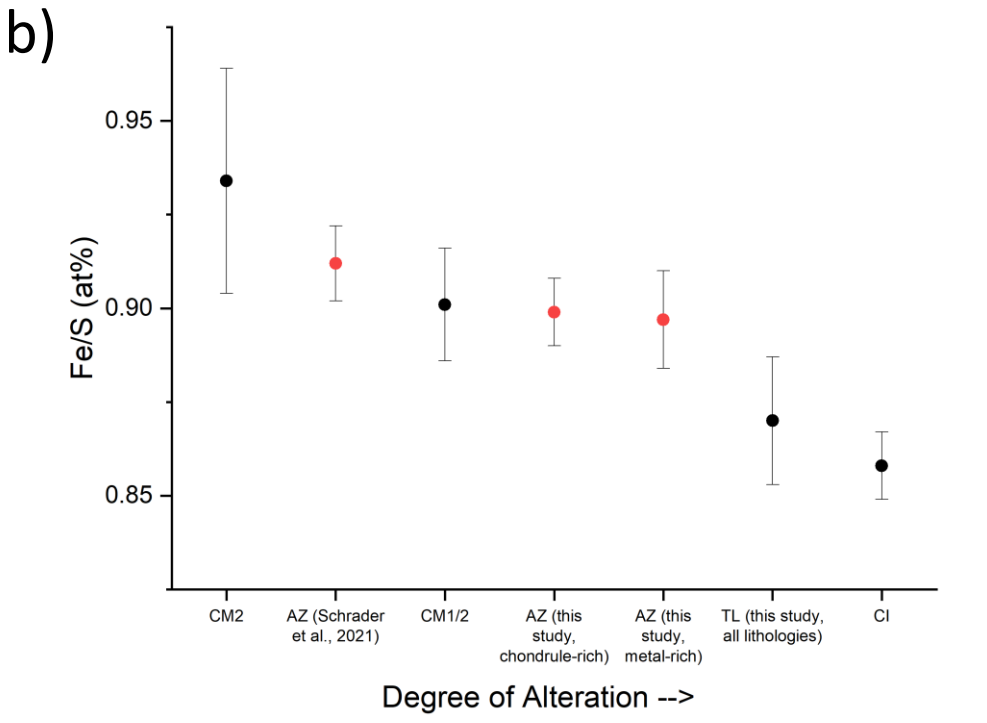
b)
0.95
0.90
0.85
Fe/S (at%)
CM2
AZ (Schrader et al., 2021)
CM1/2
AZ (this study, chondrule-rich)
AZ (this study, metal-rich)
TL (this study, all lithologies)
CI
Degree of Alteration -->

Chapter 4: Fe-Ni Sulfides in Tarda: Implications for Nebular and Parent Body Conditions of Formation and Comparison to Ungrouped C2 Tagish Lake

4.1 Introduction

The ungrouped C2 chondrite Tarda was observed to fall on the 25th of August, 2020 in the Moroccan desert, and was located the following day, with collection occurring shortly thereafter. The recovered specimens are somewhat friable and low density, and the meteorite was determined to be a breccia composed in majority of a fine-grained matrix (~80 vol%) dominated by serpentine and smectite phyllosilicates, with some magnetite framboids, platelets, and spherules, troilite, pyrrhotite, pentlandite, carbonates, olivine, chromite, and rare kamacite (Chennaoui Aoudjehane et al., 2021). Set within the matrix are small chondrules and chondrule fragments consisting mainly of forsterite with minor spinel, some of which are partially replaced by Fe-Mn dolomite, siderite, and phyllosilicates or mantled by forsterite dust, isolated forsterite grains, very fine ameboid olivine aggregates (AOAs), and other clasts (Chennaoui Aoudjehane et al., 2021). The mineralogy, compositions, and petrology of the various chondrules, matrix, and other components outlined above are consistent with petrologic type 2.

The Tarda meteorite shows some similarities to CI, CY, and CR groups. Tarda's oxygen isotopic composition has similar but lower $\Delta^{17}O$ values to both CI and CY groups (Chennaoui Aoudjehane et al., 2021), and an indistinguishable $\varepsilon^{34}Cr$ signature from CR chondrites (Dey et al. 2021). However, the presence of chondrules, enrichment in REEs and refractory elements and depletion in volatile elements, high phyllosilicate content, and H, C, and O isotopic compositions rule out Tarda belonging to any of these groups (Marrocchi et al., 2021). It has therefore been classified as ungrouped.

Notably, Tarda shares similarities in mineralogy, O, H, N, C, and Cr isotopic composition (Chennaoui Aoudjehane et al., 2021; Marrocchi et al., 2021; Dey et al., 2021), and REE composition and bulk chemistry (Marrocchi et al., 2021) to Tagish Lake. However, early examinations of Tarda suggests it may have a greater abundance of chondrules and anhydrous silicates than Tagish Lake as well as fewer

carbonates, implying it has experienced a lower degree of aqueous alteration, while its $\Delta^{17}O$ is also higher than that of Tagish Lake, which typically implies it has experienced a higher degree of alteration (Dey et al., 2021). This contradiction requires further investigation.

This study seeks to characterize the Fe-Ni sulfide minerals present within the Tarda meteorite, represented by three polished epoxy mounts from fresh specimens. The morphology and textures of these phases were characterized in order to elucidate their temperatures and mechanisms of formation, and for comparison to the similar ungrouped type 2 carbonaceous chondrite Tagish Lake. The Fe/S (at%) ratio of the Tarda pyrrhotite-group sulfides was compared to other C1 and C2 carbonaceous chondrites to define their relative degrees of alteration, following Schrader et al. (2021).

4.2 Methods

Three separate polished epoxy mounts were made from two individual fragments of the Tarda meteorite from the University of Alberta Meteorite Collection. Sample MET11800/1 ("Tarda A") yielded two epoxy mounts – MET11800/1/EP1 and MET11800/1/EP2. A second sample, MET11800/2 ("Tarda B") provided one mount – MET11800/2/EP1. The subsampling of these specimens took place under cleanroom conditions using the same methodology as described previously for Aguas Zarcas in Chapter 3. The Tarda samples were impregnated with EPO-TEK® 301 two-part epoxy under vacuum to create the 1-inch mounts. As the Tarda samples are especially susceptible to slacking in water and, following several attempts at polishing the epoxy-mounted samples using the methodology outlined in Chapter 2, it was found that these methods resulted in almost immediate disintegration of the matrix of the sample. It was therefore necessary to dry polish these samples without the use of liquid water or lubricants, using silicon carbide sandpaper of 600 to 4000 grit. These samples were then examined by SEM and analysed by EPMA using the same methodology as previously described for both Tagish Lake and Aguas Zarcas.

4.3 Results

4.3.1 Petrography

While the focus of this study was on the Fe-Ni sulfide minerals present, the general textures and mineralogy of the samples were noted as well. These aspects were of particular interest because Tarda has yet to be thoroughly examined and described, especially in comparison to Tagish Lake, with which Tarda may share similar origins. Therefore, a general overview of the petrography of Tarda is presented here. The matrices of the Tarda samples (Figure 4.1a, e) are composed primarily of fine-grained phyllosilicates with abundant magnetite framboids as well as subordinate amounts of lithic fragments, Fe-Ni sulfides, isolated olivine grains and moderately well-preserved porphyritic olivine chondrules. Within this population of chondrules, examples of chondrules containing both recrystallized, dense mesostasis (Figure 4.1b) and porous phyllosilicate interstitial material (Figure 4.1c, d) are observed, most similar in texture to chondrules in Tagish Lake samples 5b and 10a as described by Blinova et al. (2014a). Chondrules containing Fe-Ni sulfide grains are rare but present, as are those with fine-grained magnetite and Fe-Ni sulfide rims. Overall, chondrule and sulfide abundances are generally lower, while magnetite framboids are in higher abundance in Tarda than in any Tagish Lake samples examined during the course of this study.

Fe-Ni sulfides in Tarda exist as both fine (~1-2 μm) grains and fine-grained rings (Figure 4.1e, f), as well as larger (≥ ~10 μm) grains which may or may not contain exsolution (Figure 4.2, 4.3). Examples of the “bull’s eye” sulfides (Figure 4.4) first observed in Tagish Lake (Blinova et al., 2014a) are found in Tarda as well. In general, Fe-Ni sulfides are more abundant within the sample matrices than in chondrules or chondrule rims. There is little association between the occurrence of sulfide and magnetite grains, apart from several magnetite-sulfide chondrule rims. Nearly all of the sulfide grains found within Tarda samples are highly fractured, likely as a result of the polishing process and the

extreme friability of the Tarda samples themselves. The most notable groups of sulfide morphologies are outlined below.

4.3.1.1 Exsolved Sulfides

Examples of relatively coarse (≥ ~10 μm in diameter) Fe-Ni sulfide grains containing exsolution are occasionally found both within the sample matrices and within chondrules and chondrule rims. Both pentlandite exsolved from pyrrhotite and Fe-Ni metal exsolved from pyrrhotite are observed.

Pentlandite exsolution from pyrrhotite occurs primarily as blocky (Figure 4.2a) and flame-like (Figure 4.2b) exsolution at the edges of grains and occasional lamellae of pentlandite within pyrrhotite are observed (Figure 4.2a). At least one example of the "snowflake" texture of pyrrhotite exsolved from pentlandite, first described by Brearley and Martinez (2010), was observed within sample MET11800/1/EP1 (Figure 4.2c, d). Fine exsolution features are comparatively rare. However, as a result of the fractured nature of many of the Fe-Ni sulfides found in Tarda, it is often difficult to discern whether such features may be present, even in larger grains. It is therefore possible that, while fine exsolution such as blebs or lamellae are indeed present within the Fe-Ni sulfides of Tarda, they are simply indiscernible as a result of the poor preservation of many of these grains.

Kamacite (mean composition 88.25±4.93 wt% Fe, 10.59±4.55 wt% Ni) is exsolved from near end-member composition troilite and highly Ni-rich sulfide. The exsolved metal occurs as one or more rounded or blocky inclusions up to ~10 μm in size within the larger sulfide grain (Figure 4.2 e, f). These assemblages occur most often as large grains (>~50 μm) in the sample matrix, near the edges of the samples within the fusion crust, typically forming a semi-continuous chain through and mantling this fusion crust. Occasionally similar metal-sulfide grains are found within chondrules as well, occurring as rounded pyrrhotite grains with metal alloy cores (Figure 4.1b).

4.3.1.2 Unexsolved sulfides

Unexsolved pyrrhotite and pentlandite occur primarily as fine grains (~1-2 μm) disseminated throughout the sample matrices. Such grains are typically too fine to have their compositions accurately measured by EPMA, precluding identification of these grains as pyrrhotite or pentlandite. Larger unexsolved grains similar in size to the exsolved pyrrhotite-pentlandite grains described above also occur in both the matrices of samples and within chondrules (Figure 4.4). Compositional analyses of these grains confirms that both pyrrhotite and pentlandite unexsolved grains exist within the Tarda samples.

4.3.1.3 Fine-grained Rings and "Bull's Eye" Sulfides

Abundant fine-grained rings which may or may not surround other components or dense areas of phyllosilicate are common within the matrix of Tarda as well as within lithic fragments (Figure 4.1e, f). These differ from the "bull's eye" sulfides noted in Tagish Lake (Blinova et al., 2014a) as they are typically smaller in diameter (<~5 μm) and lack the characteristic multi-ring morphology of these unique sulfides. Several "bull's eye" sulfides occur in Tarda as well (Figure 4.4), both with the typical rounded, multi-ring morphology as well as more irregular shapes. These assemblages range in size from ~10 μm to over 100 μm in diameter.

4.3.2 Composition

As a result of the fractured nature of many Fe-Ni sulfide grains in combination with the small size of many grains present, compositional analysis of the majority of Fe-Ni sulfide grains, particularly fine grains and rings within the matrices of samples, was not possible.

Spot EPMA analyses of the major and minor elemental compositions of Fe-Ni sulfides identified during SEM analysis with sufficient grain size (≥ ~2 μm) reveals that the majority of these consist of pyrrhotite and pentlandite. Several troilite grains containing small blebs of exsolved kamacite are also observed; these and other pyrrhotite-group sulfides are referred to collectively as pyrrhotite. Impure

analyses and those with total wt% outside the 97.5-102.5% range were removed from consideration and will not be discussed further. Such analyses were relatively common compared to similar studies of Aguas Zarcas and Tagish Lake specimens due to the small grain size of the majority of sulfides in Tarda. Troilite containing exsolved kamacite are also removed from consideration, for reasons which are discussed in sections 4.4.2 and 4.4.3. The resulting filtered data along with ranges and average values are presented in Table 4.1. All analyses are reported in Appendix C, Table C.1.

The average Fe content of the pyrrhotite in the Tarda samples is 57.98 ± 2.44 wt% with a median of 59.96 wt%, the average Ni is 2.06 ± 2.44 wt% with a median of 0.93 wt%, and the average S content is 39.13 ± 0.71 wt% with a median of 39.28 wt%. The total range in Fe content is 50.98-63.68 wt%, in Ni content is 0.23-9.47 wt%, and in S content is 34.00-40.07 wt%. The average Fe content of the pentlandite in Tarda is 33.46 ± 2.86 wt% with a median of 32.79 wt%, the average Ni content is 30.02 ± 3.59 wt% with a median of 30.54 wt%, and the average S content is 34.27 ± 0.69 wt% with a median of 34.31 wt%. The total range in Fe content is 28.81-37.95 wt%, in Ni content is 23.52-35.36 wt%, and in S content is 33.15-35.29 wt%. These data represent 23 pyrrhotite and 18 pentlandite analyses across all three samples of Tarda examined.

The compositions of coarse-grained exsolved and unexsolved Fe-Ni sulfides and “bull’s eye” sulfides are plotted on Fe+Co-Ni-S ternary diagrams at 25°C (Vaughan and Craig 1997) and 600°C (Kosyakov et al., 2003) in Figure 4.5.

4.4 Discussion

4.4.1 Degree of Alteration

The degree of aqueous alteration experienced by the Tarda meteorite was compared to that of other aqueously altered C1 and C2 carbonaceous chondrites using the petrography of various

components such as chondrules, magnetite, and sulfides, as well as the composition of these Fe-Ni sulfides.

The chondrules within Tarda are primarily porphyritic olivine with low to moderate amounts of recrystallized dense mesostasis and/or phyllosilicate, magnetite, and sulfides within their interiors. These textures are similar to those within low to moderately altered specimens of Tagish Lake, particularly TL5b and TL10a (Blinova et al., 2014a). However, the large amounts of magnetite framboids and "bull's eye" and ring sulfides within the meteorite matrices seem to suggest a much higher degree of alteration than the textures of the chondrules, more similar to the abundances of magnetite within Tagish Lake specimen TL1, a highly altered lithology with ample amounts of magnetite in its matrix. Petrography alone is thus an unreliable indicator of the relative degree of alteration of the Tarda meteorite.

A more precise method of determining relative degree of alteration may be that of comparing Fe/S (at%) ratios of pyrrhotite in Tarda and other aqueously altered carbonaceous chondrites. This method was utilized by Schrader et al. (2021) on low-Ni pyrrhotite grains to place various groups of carbonaceous chondrites into a relative order of alteration. These authors found that this methodology was most reliable for CM and CI chondrites, as the Fe/S ratio of pyrrhotite is not directly controlled by degree of alteration, but rather by oxidation. As the conditions of aqueous alteration on CM and CI parent bodies are relatively oxidizing, the Fe/S ratios of their pyrrhotite grains can generally be utilized as a proxy for degree of alteration. Similarly, our study has shown that the Fe/S ratio of pyrrhotite in various Tagish Lake lithologies confirms, within error, the sequence of relative degree of alteration of these lithologies determined by previous studies (Holt and Herd 2022; Herd et al., 2011; Blinova et al., 2014a; Alexander et al., 2012; Simkus et al., 2019; Gilmour et al., 2019). It is therefore reasonable to assume that any CM, CI, or similar meteorite which has experienced oxidation during aqueous alteration can be placed into this pre-established order of degree of alteration put forth by Schrader et al. (2021)

and amended to include Tagish Lake (Holt and Herd 2022) and subsequent samples. It is into this framework that we propose to place Tarda.

The Fe/S (at%) ratios of the pyrrhotite grains in the three Tarda samples analysed are reported in Table 3.1. The average Fe/S (at%) ratios of low-Ni pyrrhotite in the Tarda, Tagish Lake, and Aguas Zarcas samples examined during the course of this study, as well as CM, CI, and Aguas Zarcas average values from Schrader et al. (2021) are plotted in Figure 4.6a. These samples and groups are arranged in order of increasing degree of alteration according to these values, with a decrease in Fe/S ratio corresponding to an increase in degree of alteration, as Fe is increasingly incorporated into magnetite and phyllosilicates (Singerling and Brearley, 2020; Schrader et al., 2021). This plot confirms that Tarda has, on average, experienced a higher degree of aqueous alteration than Tagish Lake, and a lower degree of alteration than CI chondrites. This sequence is more consistent with the degree of alteration implied by the magnetite abundance of the samples than by the textures of their chondrules. Distinct lithologies of Tagish Lake contain chondrules with a range of textures, and it is only the result of a sufficiently large sample size and chondrule abundance in these lithologies that enough can be examined to define their average degree of alteration. As the Tarda samples examined during this study are smaller, with fewer chondrules, it is perhaps not surprising that they do not give an accurate picture of the alteration history of their host lithology. Conversely, the magnetite content of the Tarda matrix remains relatively consistent throughout and between samples, providing a more reliable metric for assessment.

4.4.2 Temperature and Mechanisms of Formation

The textures and compositions of the Fe-Ni sulfide groups in Tarda can be utilized to constrain the likely temperatures and mechanisms of formation of these various groups. The compositions of the main groups of sulfides have been plotted on experimentally established Fe-Ni-S ternary diagrams at 25°C (Vaughan and Craig 1997) and 600°C (Kosyakov et al., 2003) according to the normalized weight

percent of these elements in Figure 4.5. Fe and Co content are combined for these plots as these elements behave similarly within the Fe-Ni sulfide minerals represented (Berger et al., 2016; Lauretta 2005). These plots, in combination with the presence or absence of particular exsolution features and grain morphologies, allow temperature and mechanism of formation to be estimated.

The exsolved pyrrhotite-pentlandite grains present within Tarda primarily have coarse, non-linear blocky exsolution, a texture which forms at temperatures of between 610-250°C upon cooling from magmatic temperatures of >900°C (Durazzo and Taylor, 1982). Subordinate amounts of linear exsolution such as lamellae, forming between 250-150°C, and flames, forming at or below 150°C (Durazzo and Taylor, 1982), are also found in some pyrrhotite-pentlandite grains. The textures of these grains, as well as the compositions of the coexisting pyrrhotite and pentlandite, plotted in Figure 4.5a, are most consistent with formation at ~600°C. This high temperature of formation has been associated with formation either by sulfidation of Fe-Ni metal within the solar nebula, or cooling and crystallization of a monosulfide solid solution (MSS) melt. As, with one exception of a rounded sulfide grain within a chondrule, the exsolved grains observed in Tarda lack the metal cores which may be expected to remain upon formation of sulfides by sulfidation of metal, the most likely mechanism of formation for these grains is crystallization from an MSS, perhaps during chondrule formation. The anomalous sulfide-rimmed metal grain may indeed have formed by sulfidation.

The origins of the sulfide-metal exsolved grains are distinct from that of the pyrrhotite-pentlandite exsolved grains. In the samples of Tarda examined they are only observed within the thin layers of fusion crust present at the edge of the sample. Additionally, they are only found within one sample of Tagish Lake – sample 8a, which is composed of several small, partially fusion crusted chips. These grains are thus likely related to the fusion crust itself. Indeed, according to Genge and Grady (1999), metal and sulfide often occur within fusion crusts as droplets and menisci on vesicles in carbonaceous chondrites, and a sulfide-enriched layer can be found within CM, CI, CV, and CO

chondrites beneath the outer melted fusion crust layer. Such grains include troilite-metal and Ni-rich-sulfide-metal assemblages. These authors conclude their formation is likely the result of the formation of immiscible metallic and silicate liquids by melting of pre-existing phases such as metal, sulfide, and chromite. Given the similar occurrence, compositions, and textures of the sulfide-metal grains in both Tarda and Tagish Lake 8a, it is likely they have similar origins. A more complete overview of sample TL8a is given in Chapter 5.

The compositions of the majority of the various unexsolved pyrrhotite grains (Figure 4.5b) as well as the "bull's eye" sulfides (Figure 4.5e) with sufficient grain sizes to allow for analysis by EPMA within the Tarda samples best match predictions of the 25°C ternary diagram. This is consistent with the temperatures of formation of similar grains within Tagish Lake. This lower temperature is more consistent with formation during aqueous alteration on the meteorite parent body than either formation by sulfidation or crystallization from a melt and suggests the Tarda and Tagish Lake parent bodies experienced similar temperatures during such alteration. While the very fine (<~ 1-2 µm) grains and rings within the Tarda matrices are too small to analyse by EPMA, their similar textures and occurrences suggest similar formation mechanisms. In the case of the fine-grained rings, they may have been directly deposited by the altering fluid, nucleated on a pre-existing component of the matrix, or may be the result of alteration and dissolution of the central portion of a pre-existing sulfide grain, leaving dense phyllosilicate material behind.

The compositions of the unexsolved pentlandite grains within Tarda are varied. While some do correspond to compositions predicted by the 25°C ternary (Figure 4.5c), many are too S-rich to have formed at the same low temperatures as the unexsolved pyrrhotite and "bull's eye" sulfides, and are more consistent with formation at higher temperatures of ~600°C (Figure 4.5d). Therefore, this population of grains must contain representatives of both formation mechanisms outlined above. Those formed at high temperatures likely formed in a similar manner as the exsolved pyrrhotite-pentlandite

grains, by crystallization from an MSS during chondrule formation, with later fragmentation resulting in the incorporation of isolated grains into the meteorite matrix. Those grains which correspond best to the lower temperature of formation of ~25°C were likely formed during the same aqueous alteration event which formed the pyrrhotite and "bull's eye" sulfides.

4.4.3 Comparison with Tagish Lake

Tarda has been classified as a C2 ungrouped carbonaceous chondrite, similar in mineralogy, O, H, N, C, and Cr isotopic composition (Chennaoui Aoudjehane et al., 2021; Marrocchi et al., 2021; Dey et al., 2021), and REE composition and bulk chemistry (Marrocchi et al., 2021) to Tagish Lake. However, early studies have failed to agree on: 1) whether Tarda is more or less aqueously altered than Tagish Lake; 2) whether they may be sourced from the same parent body. Even in our own study conflicting results between the estimates of aqueous alteration arose depending on the method used.

To investigate these discrepancies further, the average Fe/S (at%) ratios of pyrrhotite in all individual lithologies of Tagish Lake are plotted along with those from both Tarda "A" (MET11800/1/EP1 and MET11800/1/EP2) and Tarda "B" (MET11800/2/EP1) in Figure 4.6. When all analysed grains of pyrrhotite group sulfides in Tarda are considered (Figure 4.6b), MET11800/2/EP1 falls in the mid range of the degree of alteration established for Tagish Lake, while MET11800/1 falls towards the lower degree of aqueous alteration end of this spectrum. This placement, particularly of MET11800/1, is inconsistent with both the petrography and the placement of Tarda as a whole with respect to Tagish Lake and other carbonaceous chondrites based on the average Fe/S (at%) ratio of their low-Ni pyrrhotite grains. However, when the analyses of the near end member troilite with Fe/S ratios greater than one, representing sulfide grains containing exsolved metal alloy, are excluded the average Fe/S (at%) ratio of MET11800/1 shifts from 0.869 to 0.849. This changes the position of the specimen in the order of alteration from a low degree of alteration, between TL4 and TL11v chip 2 (Figure 4.6b), to a higher degree of alteration, between TL11h and TL1/3 (Figure 4.6c). These grains should indeed be removed

from consideration during this analysis as they only formed upon entry into Earth's atmosphere and their Fe/S ratios would not have been affected by parent body alteration. As was the case when using petrology to establish degree of alteration it is apparent that outlier values, in this instance the sulfide-alloy grains formed during atmospheric entry rather than the pre-accretionary chondrules, can significantly skew the results away from the expected. The higher degree of alteration is more consistent with what is expected based on the abundance of magnetite in the Tarda samples, suggesting that it is the more accurate estimation of degree of alteration.

Tarda and Tagish Lake do overlap in terms of their degree of alteration, one line of evidence which may be used to support the suggestion that they are sourced from the same parent body. However, when Tarda samples are compared to Tagish Lake samples of similar degrees of alteration, discrepancies begin to emerge. The Tarda samples examined here contain fewer chondrules and more magnetite than Tagish Lake samples of comparable degree of alteration. Tarda also contains a higher number of secondary sulfides such as "bull's eye" and fine-grained ring sulfides and fewer exsolved sulfides than Tagish Lake. The friability of the Tarda samples and their susceptibility to disintegration during polishing, a characteristic not shared by Tagish Lake, suggests there may be differences in their matrix compositions as well. In addition to the differences observed in the samples utilized in this study, previous studies have noted differences in chondrule, anhydrous silicate, and carbonate abundances, as well as $\Delta^{17}O$ values between Tarda and Tagish Lake (Dey et al., 2021). The conditions of aqueous alteration – both the temperature and degree of alteration - experienced by both Tarda and Tagish Lake are similar enough to support the hypothesis that they may be sourced from the same parent body. However, significant differences have been observed between Tarda and Tagish Lake samples which have experienced similar degrees of alteration, as noted in the studies mentioned above as well as in our own examination. When taken together one possible explanation for these observations is that Tarda may represent yet another lithology of the relatively heterogeneous Tagish Lake parent body.

4.5 Conclusion

The mineralogy, compositions, and textures of the Fe-Ni sulfides within the Tarda meteorite provide valuable insights into the complex history of formation and alteration of these grains as well as into its relationship to other meteorites, particularly to the very similar Tagish Lake.

The Fe/S (at%) ratio of the low-Ni pyrrhotite within Tarda allows it to be compared to other aqueously altered carbonaceous chondrite groups. These ratios establish a relative order of alteration such that CM2 (Schrader et al., 2021) < Aguas Zarcas (Schrader et al., 2021) < CM1/2 (Schrader et al., 2021) < Aguas Zarcas (Chapter 3) < TL (Holt and Herd, 2022; Chapter 2) < Tarda (this study) < CI (Schrader et al., 2021). When the two samples examined herein are compared with the distinct Tagish Lake lithologies directly, the relative order of alteration of these lithologies is TL11v chip1 <TL4 < TL11v chip2 < TL5b ≤ Tarda B ≤ TL10a ≤ TL8a < TL11h < Tarda A < TL1 < TL11i. This reveals that the Tarda samples fall towards the more highly altered end of the range established previously for Tagish Lake.

Tarda contains three distinct groups of Fe-Ni sulfides:

1) Primary sulfides represented by exsolved pyrrhotite-pentlandite grains within the sample matrices and chondrule interiors and rims and several unexsolved pentlandite grains. These grains formed between ~500-600°C, likely by crystallization on an MSS melt during chondrule formation.
2) Secondary sulfides represented by unexsolved pyrrhotite and pentlandite, “bull’s eye”, and ring sulfides primarily located in the sample matrices. These grains formed at ~25°C, likely during aqueous alteration on the meteorite parent body. This temperature of alteration is similar to that experienced by Tagish Lake according to the composition of its own secondary sulfides.

3) Tertiary sulfides represented by troilite and high-Ni sulfides containing exsolved metal alloy located within the fusion crusts of the samples, likely formed by the formation of immiscible silicate and metallic liquids during melting or partial melting of pre-existing phases during atmospheric transit.

Tarda and Tagish Lake do overlap in terms of the degree and temperature of alteration they have experienced, conditions which are distinct from CM and CI chondrites, suggesting they may have originated from a shared, unique parent body. However, when the petrology of Tarda and Tagish Lake samples of similar degrees of alteration are compared, discrepancies in their chondrule textures, magnetite abundances, and Fe-Ni sulfides emerge. When considered along with previous inconsistent observations between the two meteorites, it seems increasingly likely that, while the two meteorites may indeed be sourced from a single parent body, these meteorites are representative of several distinct lithologies present within the Tarda-Tagish Lake parent body.

4.6 Tables

Table 4.1: Major and minor element compositions of Fe-Ni sulfides in Tarda

Sample	Mineral	Number of Analyses		Si	Cr	Fe	Co	Ni	Mn	P	S	Total	Fe/S
				wt%	wt%	wt%	wt%	wt%	wt%	wt%	wt%	wt%	at%
MET11800/1/1	pyrrhotite	11	range	0.01 - 0.15	0.02 - 0.84	53.88 - 59.97	b.d.l. - 0.74	0.23 - 6.11	b.d.l. - 0.28	b.d.l. - 0.03	38.91 - 40.07	99.11 - 100.69	0.790 - 0.873
			average	0.04	0.15	58.51	0.12	1.49	0.04	0.00	39.63	99.99	0.848
			1σ	0.04	0.24	2.00	0.24	1.97	0.08	0.01	0.40	0.54	0.028
	pentlandite	11	range	b.d.l. - 0.26	0.02 - 0.08	28.81 - 36.70	0.85 - 2.04	26.04 - 35.36	b.d.l. - 0.04	b.d.l. - 0.02	33.15 - 35.29	98.30 - 100.84	0.500 - 0.613
			average	0.09	0.04	32.89	1.39	30.89	0.01	0.00	34.22	99.55	0.551
			1σ	0.09	0.02	2.49	0.44	3.05	0.02	0.01	0.68	0.95	0.034
MET11800/1/2	pyrrhotite	5	range	b.d.l. - 0.19	0.02 - 0.05	52.92 - 60.26	b.d.l. - 0.69	0.93 - 6.76	b.d.l. - 0.07	b.d.l.	34.00 - 39.60	98.37 - 100.23	0.803 - 0.890
			average	0.05	0.03	57.88	0.21	2.42	0.04	0.00	39.04	99.67	0.851
			1σ	0.08	0.01	2.87	0.28	2.46	0.03	0.00	0.73	0.76	0.031
	pentlandite	2	range	0.12 - 0.13	0.04 - 0.14	31.24 - 37.39	1.10 - 1.34	25.37 - 31.53	b.d.l.	b.d.l.	33.50 - 35.14	97.77 - 99.27	0.536 - 0.611
			average	0.13	0.09	34.32	1.22	28.45	0.00	0.00	34.32	98.52	0.573
			1σ	0.01	0.07	4.35	0.17	4.36	0.00	0.00	1.16	1.06	0.053
MET11800/2/1	pyrrhotite	7	range	0.04 - 0.35	0.02 - 0.22	50.98 - 59.18	b.d.l. - 0.26	0.82 - 9.47	b.d.l. - 0.06	b.d.l.	37.64 - 38.86	97.94 - 99.20	0.764 - 0.882
			average	0.13	0.09	57.22	0.07	2.69	0.01	0.00	38.42	98.62	0.855
			1σ	0.10	0.09	2.91	0.10	3.20	0.03	0.00	0.39	0.47	0.041
	pentlandite	1	range	-	-	-	-	-	-	-	-	-	-
			average	0.28	0.05	37.95	1.66	23.52	b.d.l.	0.25	34.69	98.40	0.628
			1σ	-	-	-	-	-	-	-	-	-	-
Total	pyrrhotite	23	range	b.d.l. - 0.35	0.02 - 0.84	50.98 - 63.68	b.d.l. - 0.74	0.23 - 9.47	b.d.l. - 0.28	b.d.l. - 0.03	34.00 - 40.07	97.94 - 100.69	0.764 - 0.890
			average	0.07	0.10	57.98	0.12	2.06	0.03	0.00	39.13	99.50	0.851
			median	0.03	0.04	58.96	0.03	0.93	0.02	b.d.l.	39.28	99.58	0859
			1σ	0.08	0.17	2.44	0.21	2.44	0.06	0.01	0.71	0.82	0.031
	pentlandite	18	range	b.d.l. - 0.28	0.02 - 0.14	28.81 - 37.95	0.85 - 2.04	23.52 - 35.36	b.d.l. - 0.04	b.d.l. - 0.25	33.15 - 35.29	97.77 - 100.84	0.500 - 0.628
			average	0.11	0.05	33.46	1.39	30.02	0.01	0.02	34.27	99.32	0.560
			median	0.08	0.04	32.79	1.34	30.54	b.d.l.	b.d.l.	34.31	99.41	0.549
			1σ	0.10	0.03	2.86	0.40	3.59	0.01	0.07	0.69	1.00	0.040

4.7 Figure Captions

Figure 4.1: Backscattered electron (BSE) images of the Tarda meteorite. a) fusion-crusted section of the Tarda matrix; b) porphyritic olivine chondrule containing dense mesostasis and sulfide-rimmed metal; c,d) several porphyritic olivine chondrules within the Tarda matrix containing porous phyllosilicates and sulfides; e,f) an example of a lithic clast containing numerous small fine-grained sulfide rings.

po= pyrrhotite-group sulfides; pn = pentlandite; alloy = Fe-Ni metal alloy.

Figure 4.2: BSE images of exsolved Fe-Ni sulfide grains including: a) lamellae and blocky pentlandite exsolved from pyrrhotite; b) pentlandite flames and lamellae exsolved from pyrrhotite; c,d) "snowflake" pyrrhotite exsolved from pentlandite; e,f) Fe-Ni metal alloy exsolved from troilite.

Figure 4.3: BSE images of a,b) unexsolved pyrrhotite and c,d) unexsolved pentlandite grains within the Tarda matrix.

Figure 4.4: BSE images of examples of "bull's eye" sulfides within the Tarda matrix.

Figure 4.5: Compositional data from Fe-Ni sulfides in Tarda samples plotted on Fe+Co-Ni-S ternary diagrams. a) exsolved pyrrhotite-pentlandite grains at 600°C (Kosyakov et al., 2003); b) unexsolved pyrrhotite grains at 25°C (Vaughan and Craig 1997); c) unexsolved pentlandite grains at 25°C (Vaughan and Craig 1997); d) unexsolved pentlandite grains at 600°C (Kosyakov et al., 2003); e) "bull's eye" sulfides at 25°C (Vaughan and Craig 1997).

Figure 4.6: Fe/S (at%) ratios of the of a) the examined low-Ni pyrrhotite group sulfides as compared to other aqueously altered C1 and C2 carbonaceous chondrites. Aguas Zarcas measurements are highlighted in red, Tagish Lake in blue, and Tarda in green; b) all pyrrhotite-group sulfides within Tarda samples MET11800/1 and MET11800/2 compared to individual lithologies of Tagish Lake. Tarda

measurements are highlighted in red; c) pyrrhotite-group sulfides in Tarda excluding tertiary troilite formed upon atmospheric transit, compared to Tagish Lake lithologies. Tarda measurements are highlighted in red. Error bars represent one standard deviation from the mean.

4.8 Figures

Figure 4.1

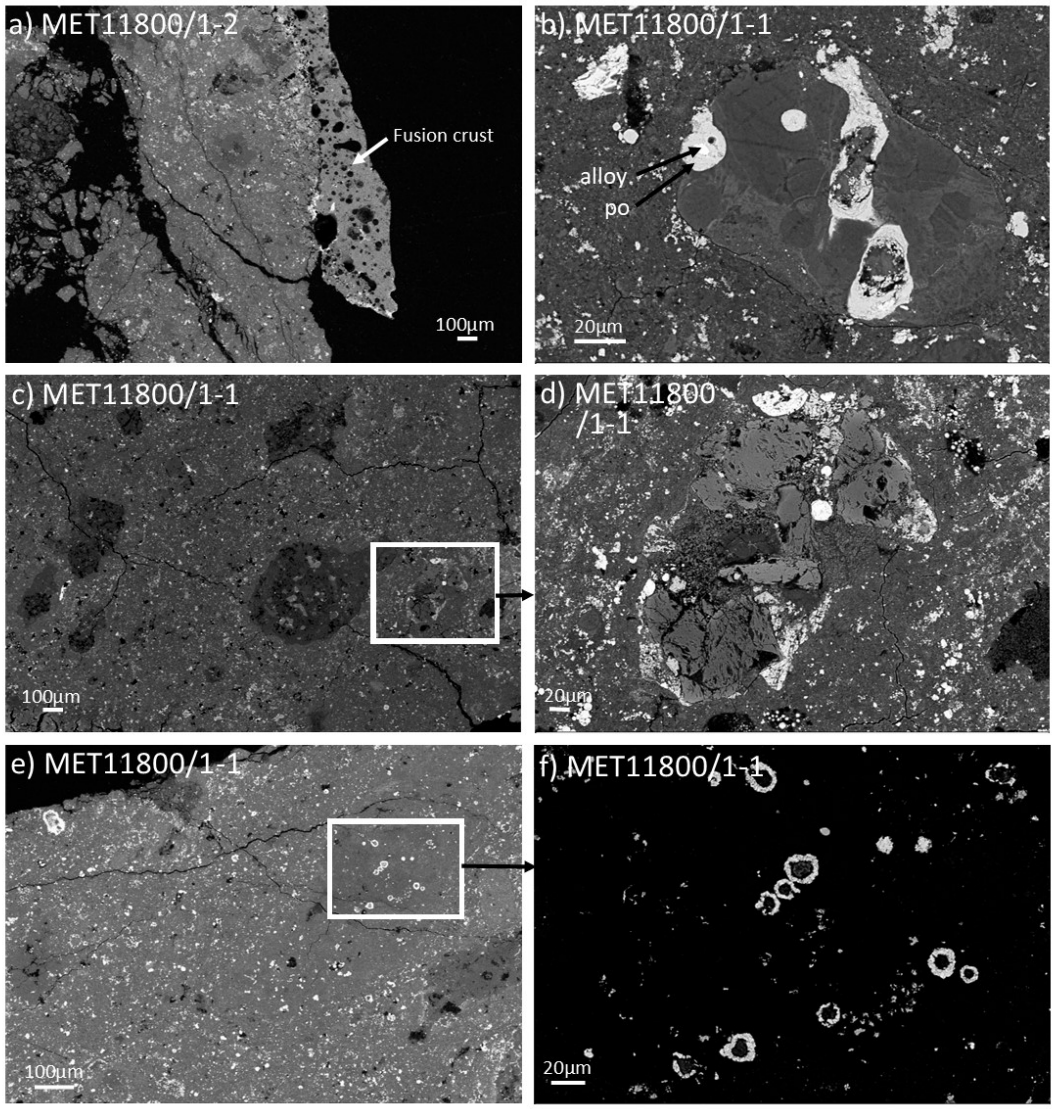

Figure 4.2

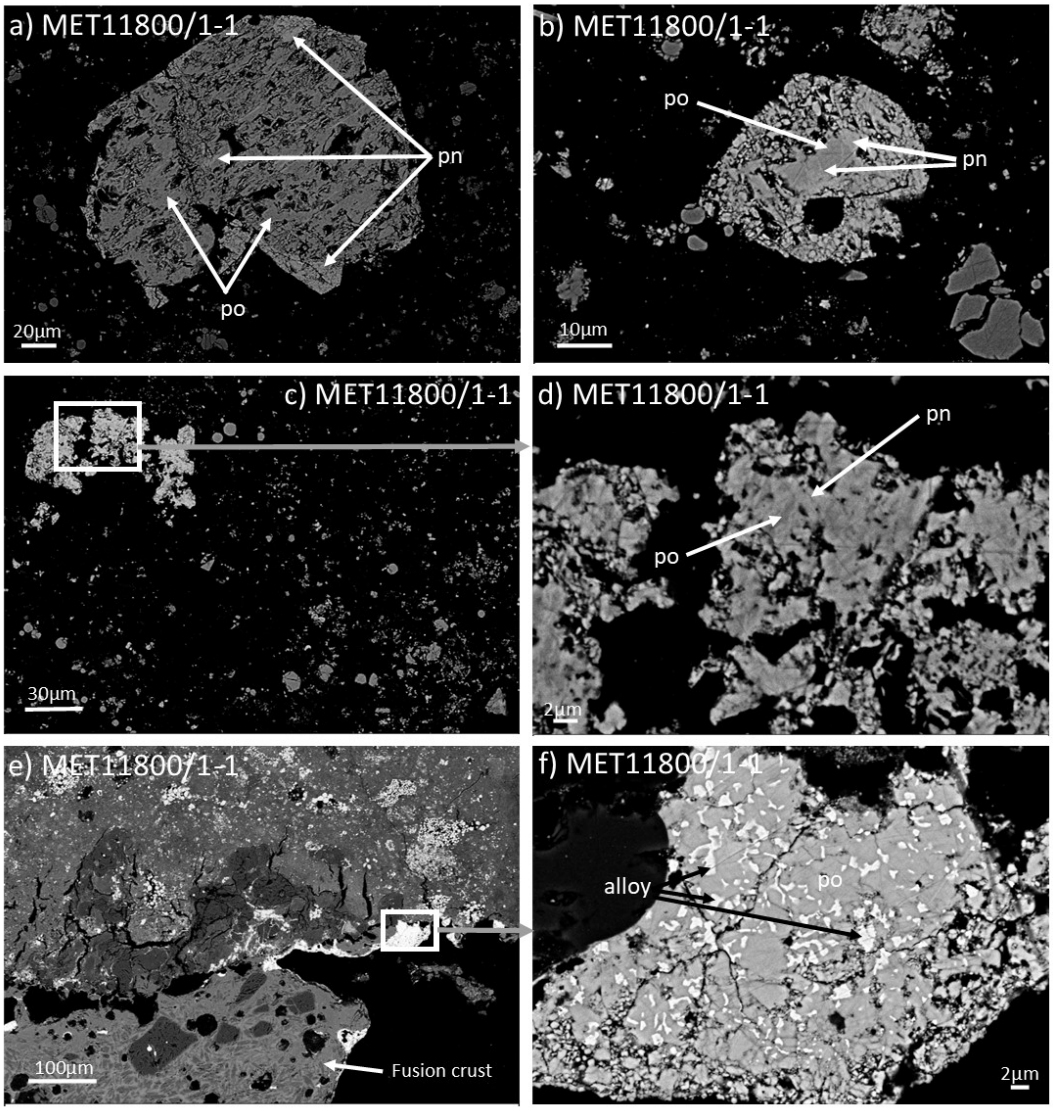
a) MET11800/1-1
pn
po
20µm
b) MET11800/1-1
po
pn
10µm
c) MET11800/1-1
30µm
d) MET11800/1-1
pn
po
2µm
e) MET11800/1-1
100µm
Fusion crust
f) MET11800/1-1
alloy
po
2µm

Figure 4.3

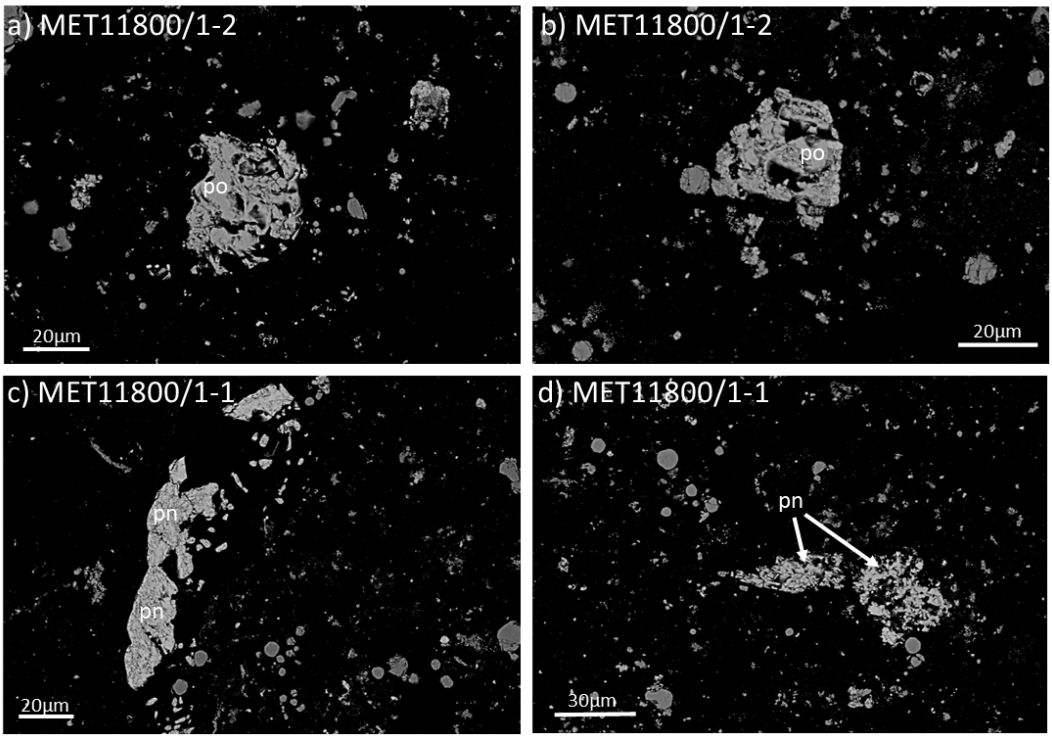
a) MET11800/1-2
po
20µm
b) MET11800/1-2
po
20µm
c) MET11800/1-1
pn
pn
20µm
d) MET11800/1-1
pn
30µm

Figure 4.4

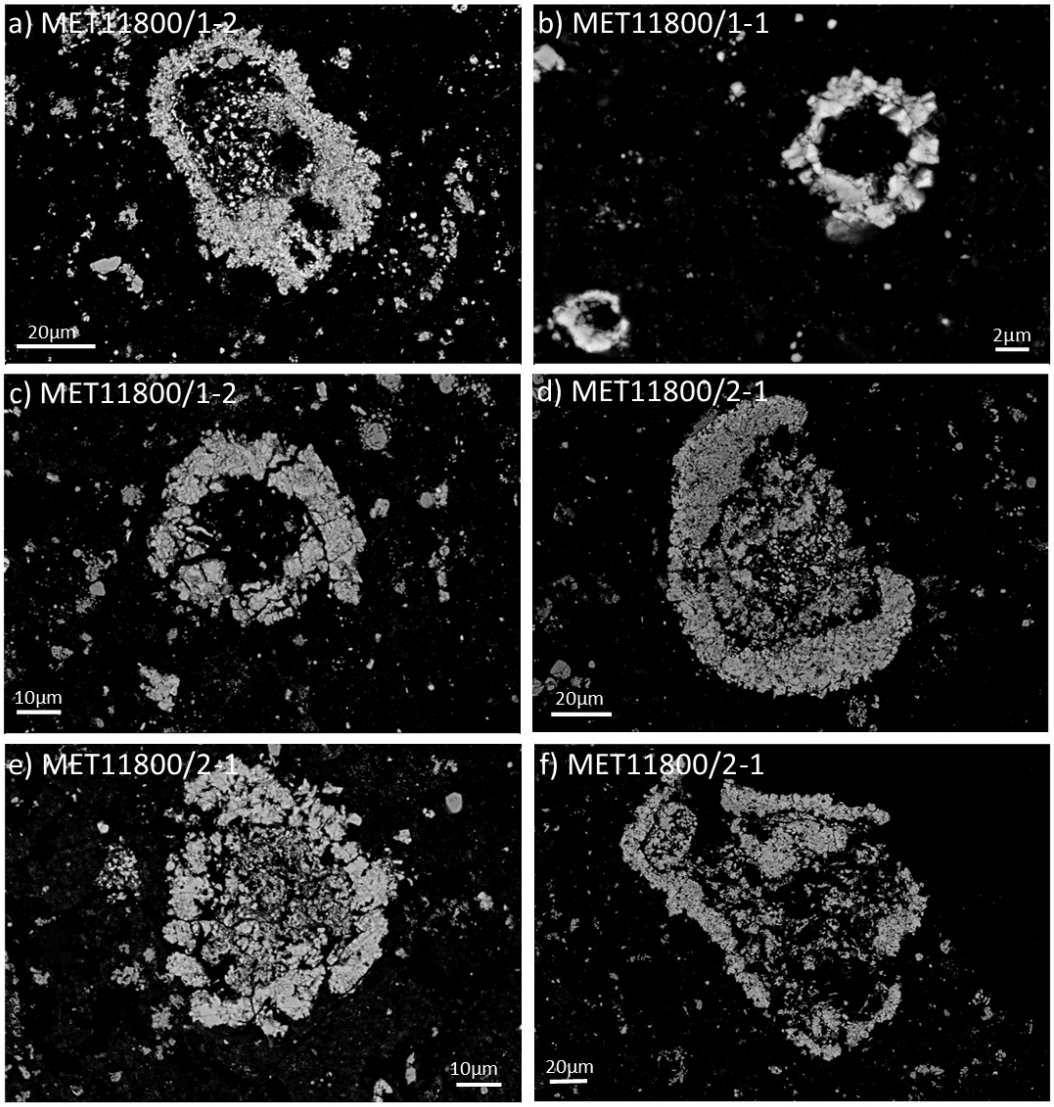
a) MET11800/1-2
20µm
b) MET11800/1-1
2µm
c) MET11800/1-2
10µm
d) MET11800/2-1
20µm
e) MET11800/2-1
10µm
f) MET11800/2-1
20µm

Figure 4.5

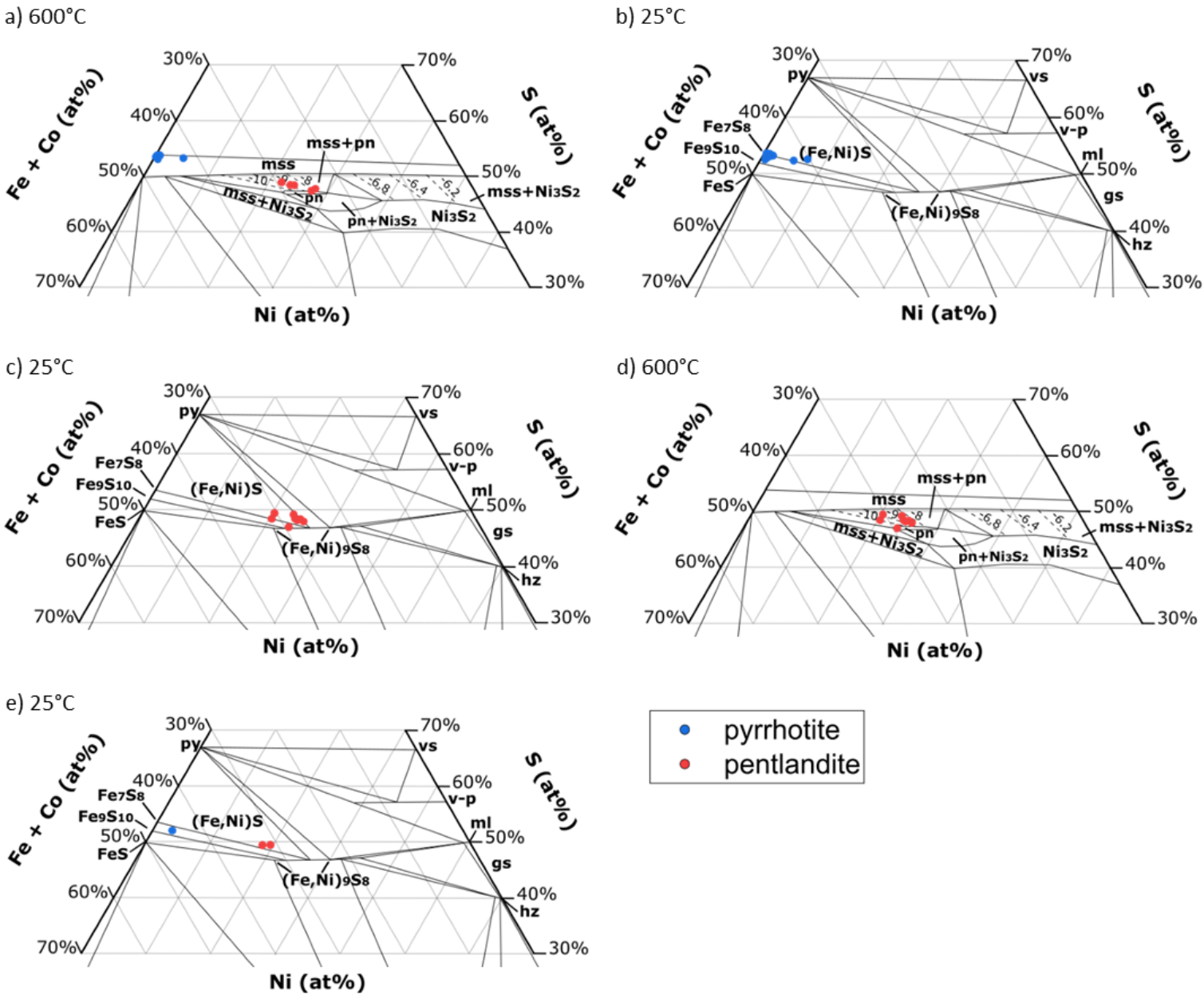
a) 600°C
b) 25°C
c) 25°C
d) 600°C
e) 25°C
Fe + Co (at%)
Ni (at%)
S (at%)
30%
40%
50%
60%
70%
mss
mss+pn
pn
mss+Ni3S2
pn+Ni3S2
Ni3S2
py
vs
Fe7S8
Fe9S10
(Fe,Ni)S
FeS
v-p
ml
gs
(Fe,Ni)9S8
hz
pyrrhotite
pentlandite

Figure 4.6

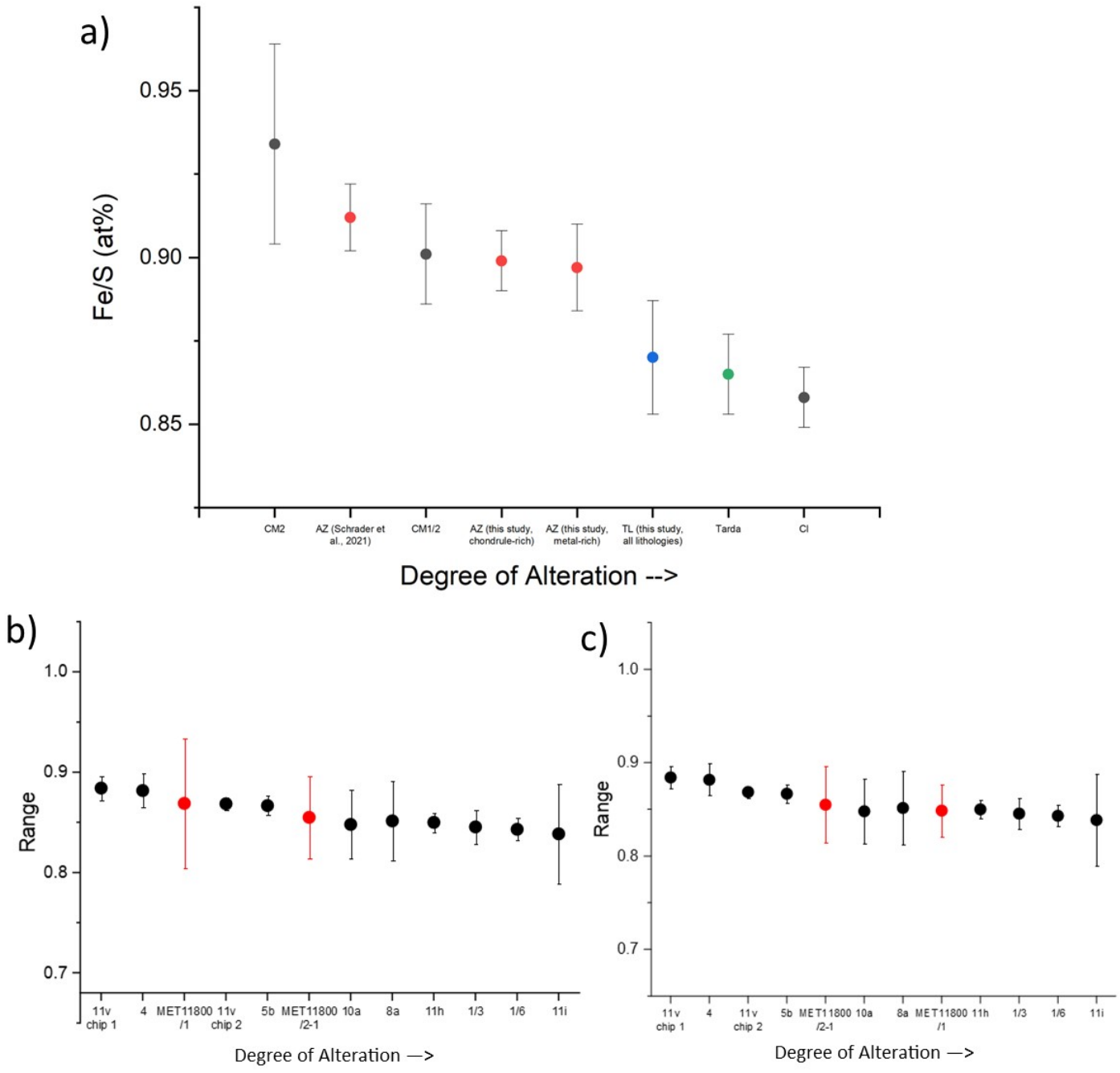
a)
Fe/S (at%)
0.95
0.90
0.85
CM2
AZ (Schrader et al., 2021)
CM1/2
AZ (this study, chondrule-rich)
AZ (this study, metal-rich)
TL (this study, all lithologies)
Tarda
CI
Degree of Alteration -->
b)
Range
1.0
0.9
0.8
0.7
11v chip 1
4
MET11800 /1
11v chip 2
5b
MET11800 /2-1
10a
8a
11h
1/3
1/6
11i
Degree of Alteration —>
c)
Range
1.0
0.9
0.8
0.7
11v chip 1
4
11v chip 2
5b
MET11800 /2-1
10a
8a
MET11800 /1
11h
1/3
1/6
11i
Degree of Alteration —>

Chapter 5: Investigation of the Effects of Lithology, Sample Storage, and Sample Processing on the Organosulfur Content of Tagish Lake

5.1 Introduction

The Tagish Lake meteorite, a C2-ungrouped carbonaceous chondrite, has been found to be rich in both soluble (SOM) and insoluble organic matter (IOM), with nearly 3 wt% total organic matter (Herd et al., 2011) and a concentration of between ~100 ppm of (Pizzarello et al., 2001) to greater than 600 ppm (Simkus et al., 2019) soluble organic compounds. Soluble organic species found in Tagish Lake include mono- and dicarboxylic acids, pyridine carboxylic acids, dicarboximides, sulfonic acids, and trace amounts of aliphatic and aromatic hydrocarbons, amino acids, amines, and amides (Pizzarello et al., 2001) many of which are of prebiotic interest (Herd et al., 2011). Differences in the concentrations and compositions of soluble organic compounds found in each of the lithologies examined may be explained by these lithologies having experienced differing degrees of aqueous alteration (Herd et al., 2011; Hilts et al., 2014; Simkus et al., 2019).

Organosulfur compounds provide an important record of pre- and early solar chemical reactions, as well as parent body aqueous alteration processes (Aponte et al., 2020). However, organosulfur species have not yet been seen in either the hot water extracts (Glavin et al., 2012) or the DCM extracts (Hilts et al., 2014) of other Tagish Lake samples examined in previous studies. Cooper et al. (1992) have proposed that sulfonic acids are the organosulfur species that should have the highest abundances within carbonaceous chondrites as parent-body aqueous alteration of labile sulfate esters and other polar, sulfur-bearing compounds would result in their conversion to sulfonic acids. Sulfonic acids are known to be among the organic components within at least some lithologies of Tagish Lake (Pizzarello et al., 2001) and are the most abundant sulfur-bearing compounds in the Tagish Lake soluble organic matter. Pizzarello et al. (2001) found a ca. 20 ppm concentration of methane sulfonic acid (MSA), which appears to be the most abundant sulfonic acid in Tagish Lake, from a hot water extract of

a 4.5 g powdered sample of a pristine TL specimen labelled as TL8a. The total concentration for the soluble organic matter in TL8a was determined to be ~100 ppm, which is a much lower organic content than some other examined specimens (Hilts et al., 2014; Simkus et al., 2019). The relative degree of alteration of the Pizzarello et al. (2001) sample has not yet been established. It is possible that the presence of MSA in TL8a and its absence from other samples is a result of lithologic differences in degree of alteration experienced by these samples. To investigate this possibility further the lithology of TL8a and its degree of aqueous alteration relative to previously examined samples must be characterized, and whether any MSA remains present in the previously extracted sample or is present in a fresh, unextracted sample of Tagish Lake must be determined.

The presence of MSA in the sample examined by Pizzarello et al. (2001) suggests it is possible they may be present in other samples of Tagish Lake. Because sulfonic acids are water-soluble the hot-water extractions previously performed by Glavin et al. (2012) may have removed them from these powdered TL samples. It is possible that these compounds were oxidized during hot water extraction, and that their oxidation is the source of the euhedral gypsum crystals first identified by Cosette Gilmour in the powdered residue of sample MET11611/P-11h/2 following the completion of the hot water extraction. Alternatively, since the hot water extraction did not employ a derivatizing agent, polar compounds such as MSA may have escaped analysis by the GC-MS method used, even if they were extracted from the powdered sample during one of these analyses. Therefore, to provide a complete inventory or organic compounds present, a new method of extraction not previously utilized on these samples is required to recover these compounds, if they are present. It is also necessary to characterize what effects these previous extractions may have had on the samples, to determine whether a failure in experimental methods is the reason for the absence of MSA or other organosulfur compounds in the suite of organic molecules recovered.

The discrepancy between TL8a organic content and those of other TL samples could therefore be explained in several ways including: 1) Heterogeneity of organic content between different specimens of TL, including due to storage conditions; 2) Oxidation of any organosulfur compounds present during or prior to leaching with hot water; 3) Inability of the methods used to capture and analyse any organosulfur species present (e.g., polar compounds not detected during analysis, species below detection limit of the analytical instruments). A new experimental methodology was therefore designed to reveal whether the apparent absence of soluble organosulfur species within our examined samples is due to a failure of experimental methods or because the sulfonic acid content of the samples is indeed below the detection limits of the instrument.

The primary goals of this work are to: 1) Determine the relative degree of alteration of the sample of Tagish Lake examined by Pizzarello et al. (2001), referred to as TL8a; 2) Determine whether oxidation of MSA or other sulfur-bearing species may be the source of sulfur in the sulfate crystals observed following the initial hot water extraction of TL11h (Glavin et al., 2012); 3) extract and identify any organosulfur species or other organic compounds present in the previously leached samples of Tagish Lake specimens TL5b and TL11h as well as a pristine sample of the Tagish Lake specimen TL1.

5.2 Methods

5.2.1 SEM and EPMA of TL8a

Several fusion-crusted chips of sample TL8a were selected for textural and compositional analysis. These chips were oriented so that the interior of the meteorite would be exposed upon subsequent epoxy mounting. The 1-inch epoxy mount of these chips was created in the same manner as previously described for similar mounts of TL samples in Chapter 2.

The textural analysis of this sample was conducted using backscattered electron (BSE) imaging on the Zeiss Sigma 300 VP-SEM in the University of Alberta Earth and Atmospheric Sciences Department

operating at 15 kV. Compositional analysis was conducted within the University of Alberta Earth and Atmospheric Sciences Department using the CAMECA SX100 electron probe microanalyzer (EPMA) operating at 20 keV with a beam current of 20nA using ZAF (Phi-Rho-Z) correction method. Standards used are the same as described in Chapter 2.

5.2.2 SEM of TL11h Powder

A portion of the powdered sample of TL11h that remained after the initial hot water (Glavin et al., 2012) and DCM (Hilts et al., 2014) extractions was taken for textural examination by SEM. Additionally, a small amount of the gypsum crystals separated from sample TL11h following hot water extraction was taken for mounting and examination. These two samples were mounted on double-sided carbon tape and examined on the Zeiss Sigma 300 VP-SEM operating at 25 kV for energy dispersive x-ray spectrometry (EDS) analysis under variable pressure (VP) conditions.

5.2.3 Initial Soluble Organosulfur Extraction

The first round of chemical extractions we performed was conducted using a 1:1 solution of methanol and toluene. Approximately 35 mL of this solution was combined with the previously extracted powders of TL11h (two samples of MET11611/P-11h/2 weighing 0.242 g and 0.942 g, samples a and b respectively) and TL5b (one sample of MET11611/P-5b/5 weighing 1.698 g) inside sealed vials in an ultrasonic bath. These vials were then centrifuged to separate the supernatant from the solid material, which was reduced to a volume of 0.2mL under a stream of N_2 gas and analysed by gas-chromatography mass spectrometry (GC-MS). These analyses were performed at MacEwan University following the sample procedures for analysis and compound identification for this instrument as outlined in Tunney et al. (2022a).

5.2.4 Allende Sample Preparation and Storage

Prior to their application to Tagish Lake samples, the experimental methods outlined below were first tested on samples of the meteorite Allende which had been artificially doped with MSA. One

stone of Allende (MET7100/A-121) was selected for subsampling for this purpose. The subsample was taken using a hammer and chisel, then powdered with an agate mortar and pestle and homogenized using a 150 µm sieve. The powder was then combusted overnight to remove any intrinsic or contaminant organic molecules that may have been present. Originally, this combustion was done at 450°C, however subsequent sample preparations used a combustion temperature of 200°C to avoid dehydrating any phyllosilicates which may be present in the sample. In total, three sets of samples were prepared for storage:

1) Allende powder combusted at 450°C. Each 1 g sample of powder had 1.5 mL of 50 ppm MSA solution in water added to it prior to storage.
2) Allende powder combusted at 200°C. Each 1 g sample of powder had 0.4 mL of pure MSA added to it to wet the sample prior to storage.
3) Allende powder combusted at 200°C. Each 1 g sample of Allende powder had 6 µL of 20 ppm MSA solution in water added to it, which was then dried under Ar gas, resulting in 100 ppm MSA in Allende. These samples were then stored.

To test the effects of storage conditions on the physiochemical retention of MSA the prepared samples of Allende + MSA were stored in one of several locations between 72 hours and 1 month:

1) A Class 1000 clean room, which provides general storage of the University of Alberta Meteorite Collection.
2) The primary storage facility of TL specimens at the University of Alberta, consisting of a Forma model 3670 single chamber laboratory freezer which maintains an internal temperature of ~-28°C (Herd et al., 2016).

3) The low-temperature chamber portion of the Subzero Curation Facility for Astromaterials at the University of Alberta, which maintains an internal temperature of ~-18°C. The specifications of which are given in Herd et al. (2016).
4) The inert argon atmosphere glovebox housed within the above mentioned low-temperature chamber of the Subzero Curation Facility for Astromaterials. Specifications for this glovebox are given in Herd et al. (2016).

The specifics of sample preparation, storage time, and storage conditions of each of the prepared samples used for extraction are outlined in Table 5.1.

5.2.5 Raman Spectroscopy

Raman spectroscopy was conducted on a LabRam Evolution HR spectrometer using a 532 nm laser at 100% power and a 1500 groove/cm grating. Exposure was for 10 seconds for 3 accumulations.

5.2.6 Experimental Extraction, Derivatization, and GC-MS Analysis

To determine the effects of storage conditions, storage time, and extraction method on MSA retention and retrieval, several extraction methods were tested on the prepared Allende. Sample extracts were analysed via GC-MS using an Agilent 6890N equipped with a HP-5MS column of 30 m length, 0.25 µm film thickness, and 250 µm internal diameter following the same procedures of detection and identification as outlined for this instrument in Tunney et al. (2022a).

The first stage of these experiments was to determine the effectiveness of our chosen derivatizing agent, N-*tert*-butyldimethylsilyl-*N*-methyltrifluoroacetamide (MTBSTFA), at derivatizing MSA and related compounds. For this, a three-fold excess of MTBSTFA was added to lab-grade samples of MSA, sulfuric acid, and $NaHSO_4^-$ in dried, deoxygenated acetonitrile. The glass ampules were then sealed and heated at 60°C for 4 hours, after which the contents were analysed by GC-MS at MacEwan University, as described above.

Preliminary experiments were conducted using Allende samples from prepared group 1, as well as several 1 g samples of silica powder prepared in the same manner. Both hot water and acetonitrile were tested as potential solvents for extraction. For each extraction, 8-10 mL of the chosen solvent were added to the vial containing the prepared sample. The solvent was then transferred to a test tube and centrifuged at 4600 rpm for 5 minutes to separate the supernatant, which was transferred to a round-bottomed flask and roto-evaporated at ~80°C to dryness. To collect the sample for GC-MS analysis, ~3 mL of dried, deoxygenated acetonitrile was added to each round bottomed flask containing the sample residues. The resulting solutions were then transferred to GC vials, 23 µL of MTBSTFA was added to each vial and the vials were heated at 60°C for 4 hours, after which the contents were analysed by GC-MS. These analyses were performed at MacEwan University as described above.

A second set of experiments designed to determine the lowest amount of MTBSTFA needed to derivatize all MSA present in the samples was then completed using Allende samples from prepared group 2. Each solid sample was mixed with 10 mL of dried, deoxygenated acetonitrile. One mL of each of the three resulting solutions was transferred to three 2-mL GC vials, where 1.35, 2.70, and 4.05 times excess MTBSTFA was added into solution. The vials were then sealed and heated to ~60°C for 4 hours, following which the solutions were diluted 4-fold and a liquid-liquid extraction with hexane performed to leave any underivatized MSA behind. These samples were then analysed by GC-MS at the University of Alberta on an Agilent 5975C using a HP-5MS column that was 30 m in length, 0.25 µm in film thickness, and 250 µm in internal diameter, following the procedure outlined for this instrument in Tunney et al. (2022a).

5.2.7 LC-MS Analysis

To test the sensitivity of the Liquid chromatography–mass spectrometry (LC-MS) analytical method toward sulfonic acids, a 100 ppm stock solution of MSA in acetonitrile was prepared. Diluted solutions with concentrations of 500, 50, 5, and 0.5 ppb MSA were created using acetonitrile and 25 mM

Ammonium Formate pH 4.5 as solvents. These solutions were injected in 1 µL quantities into the Orbitrap exploris 240 located within the Department of Chemistry at the University of Alberta in MS (mass spectrometry) mode using a HILIC Z column to collect HRAM (high resolution accurate mass) MS data.

Following these experiments, the same methodology was applied to extracts of the Allende samples from prepared group 3. These extractions were performed by adding 5 mL of acetonitrile to each vial containing the Allende powder and agitating the contents for 5 minutes. The contents of these vials were allowed to settle, and the acetonitrile supernatant transferred to an empty vial. Initial experiments on samples stored for 72 hours utilized filter paper during this step to remove Allende powder which had not yet settled out of solution, while later experiments using samples stored for 1 month did not. This process was then repeated a second time, and the total 10 mL of acetonitrile evaporated down to 1.5 mL under a stream of Ar gas and transferred to an LC vial. In both cases, the samples were passed through a 0.2 µm filter prior to injection. The contents of these vials were analyzed by LC-MS as outlined above.

5.2.8 Extraction of Tagish Lake

Once the viability of the acetonitrile-extraction and LC-MS analysis techniques described for retrieval and analysis of MSA had been verified using the doped Allende + MSA samples, a similar method of extraction and analysis was devised for Tagish Lake. A 0.84 g sample of specimen TL1 was taken by subsampling of a larger specimen as described in Chapter 2. This subsample was then powdered with an agate mortar and pestle, and the powder given the sample number MET11611/P-1/9.

An acetonitrile extraction was performed as above, with 5 mL of acetonitrile added to the vial containing the TL powder, the vial agitated for 5 minutes before the contents were allowed to settle and the solvent being transferred to a separate vial. This process was then repeated a second time before

being evaporated under a stream of Ar gas to a volume of ~ 1.5 mL and transferred to an LC vial for analysis. Filter paper was not used in the extraction of the TL powder; however, the sample was filtered with a 0.2 μm filter prior to injection into the LC-MS. Following extraction with acetonitrile, the remaining TL powder was dried under a stream of Ar gas. A second extraction utilizing 5 mL of dichloromethane (DCM) was then performed, the sample agitated for 5 minutes and allowed to settle, and ~2 mL of the DCM supernatant transferred to a separate GC vial for analysis by GC-MS.

LC-MS analysis of the acetonitrile sample was performed by injecting the sample into the Orbitrap exploris 240 in MS mode using both C18 and HILIC Z columns to collect HRAM MS data. Both Electrospray ionization (ESI) MS negative mode and positive ion mode were tested as ionization sources for this analysis. GC-MS analysis of the DCM extract was performed at the University of Alberta as described above.

5.3 Results

5.3.1 Petrography

5.3.1.1 TL 8a

The SEM and EPMA analyses of the epoxy-mounted chips of sample TL8a were used to examine the textures and compositions of various components within these chips, with focus placed primarily on the chondrules and sulfides they contained. BSE images (Figure 5.1) were used to examine chondrules within the sample to determine the degree of alteration of their interiors using the state of preservation of the olivine grains they contain. Intact grains which have not been altered to phyllosilicates are indicative of lower degrees of alteration. The TL8a chondrules are porphyritic olivine type with a limited range of degrees of alteration, with nearly all containing a mixture of both phyllosilicates and relict olivine grains in various proportions. Several examples show very little alteration of olivine (Figure 5.1a), while others have olivine nearly entirely replaced by phyllosilicates (Figure 5.1b). The partial replacement of olivine by phyllosilicates results in an increase in the porosity of chondrule interiors. The

majority of chondrules within the sample are composed of Fe-poor olivine; however, one example of a relatively Fe-enriched, unaltered olivine chondrule containing pyrrhotite was observed (Figure 5.1a). Chondrules typically also have a dense, fine-grained rim, with some having an additional fine-grained magnetite rim or magnetite within their interiors (Figure 5.1b). The majority of Fe-Ni sulfide grains within TL 8a are unexsolved pyrrhotite grains within the matrix (Figure 5.1c, f). These include relatively large (> ~10 μm in diameter), isolated grains (Figure 5.1c) as well as numerous fine-grained rings (Figure 5.1f). Grains which do exhibit exsolution display textures of blocky and flame-like exsolution of pentlandite along the edges of pyrrhotite grains, as well as pentlandite lamellae within pyrrhotite grain interiors (Figure 5.1d). Within one section of fusion crust, grains on kamacite exsolved from pyrrhotite are present (Figure 5.1e). The matrix itself is texturally consistent with a composition of primarily phyllosilicates, and contains lithic fragments, isolated silicate grains, and abundant magnetite framboids as isolated grains, rings, and clusters (Figure 5.1f).

EPMA analysis was performed on Fe-Ni sulfide grains of sufficient size (≥ ~2μm in diameter) to determine their major and minor element compositions, as well as the Fe/S (wt%) ratios of these grains. The results of this analysis are reported in Table 5.2. A sharp increase from <15 wt% Ni to >30 wt% Ni separates the majority of analyses obtained into two distinct groups; the group low in Ni corresponds to pyrrhotite (Schrader et al., 2016), while the group high in Ni corresponds to pentlandite. Five analyses lie between these groups, with Ni contents between 19.32-22.28 wt%. These are likely representative of impure analyses caused by beam overlap of multiple phases and therefore were removed from consideration. Additionally, the grain of pyrrhotite which contains exsolved kamacite was most likely formed upon atmospheric transit, and therefore its composition is not representative of its pre-terrestrial history, and these analyses are therefore also excluded from consideration. Following the removal of these analyses as well as those with total wt% values outside the range of 97.5-102.5%, a total of 57 pyrrhotite and 4 pentlandite measurements were retained. The resulting average Fe content

of the pyrrhotite the sample is 55.39 ± 3.48 wt%, the average Ni is 5.55 ± 3.59 wt%, and the average S content is 38.28 ± 0.81 wt%. The total range in Fe content is 45.64-59.89 wt%, in Ni content is 1.22-13.96 wt%, and in S content is 36.84-39.83 wt%. The average Fe content of the pentlandite in the TL samples is 31.24 ± 0.60 wt%, the average Ni content is 34.53 ± 0.76 wt%, and the average S content is 33.41 ± 0.17 wt%. The total range in Fe content is 30.59-32.01 wt%, in Ni content is 33.41-35.08 wt%, and in S content is 33.17-33.57 wt%.

5.3.1.2 TL 11h Powders

BSE images of the extracted TL11h powder (Figure 5.2) and the sample of gypsum grains (Figure 5.3) removed from this powder were taken to identify any intact components remaining or new mineral growth following hot water extraction, as well as any significant changes the original components may have undergone. As a result of the powdering and extraction processes the majority of the sample examined, consisting primarily of phyllosilicate matrix, appears as irregular, fluffy-looking clumps within which little else is discernable. The most readily identifiable component within the matrix are magnetite framboids as isolated grains as well as clusters (Figure 5.2a,b). Their characteristic rounded shapes do not appear to have been altered during powdering and extraction, though some clusters may have been broken up, resulting in an increase in isolated framboids. Also identifiable but in lower abundance are intact olivine grains (Figure 5.2c,d) which may have initially isolated within the matrix or may be portions of chondrules which were broken up upon powdering of the sample. No obvious Fe-Ni sulfide grains were identified within the sample.

BSE images of the gypsum crystals reveal them to be elongated, euhedral grains which are greater than 100 μm in diameter in their narrowest dimension and may be up to several millimeters in length (Figure 5.3). Their large size confirms their formation following sample powdering, as this procedure would have broken up the large grains. The euhedral nature of the grains suggest they likely

precipitated from solution following extraction, consistent with their first observation following the hot water extraction.

5.3.2 Methanol-Toluene Extractions

The compounds found in the previously leached Tagish Lake samples 11h and 5b samples are listed in Table 5.3. The majority of the compounds identified in the initial methanol-toluene extracts are common terrestrial contaminants introduced by fuels, pharmaceuticals, and plasticizers (Tunney et al., 2020; Tunney at al., 2022a,b). However, several other intrinsic species were also identified, including polycyclic aromatic hydrocarbons (PAHs) and two allotropes of elemental sulfur, hexathiane (S_6) and octaatomic sulfur (S_8). Several of these species were also detected in previous extractions of the samples, suggesting that a single round of chemical extractions cannot provide quantitative results of the organic content of a sample, but rather provides a lower limit of compound concentration. No organosulfur compounds were observed during this stage of analysis.

5.3.3 Experimental Extractions, Derivatization, and GC-MS Analysis

The initial tests of our GC methodology of derivatizing MSA, sulfuric acid, and $NaHSO_4^-$ using MTBSTFA in dried, deoxygenated acetonitrile revealed that both the MSA and sulfuric acid species could be derivatized and recovered from these solutions. Therefore, MTBSTFA was used in future experiments to retrieve organosulfur species that contain acidic hydrogens.

Extractions of the various Allende group 1 samples using both hot water and dried, deoxygenated acetonitrile as solvents derivatized with MTBSTFA were all performed under the same conditions as outlined above. Only one sample, namely that which was stored within the Ar atmosphere glovebox for only 72 hours and extracted with hot (~80°C) water, precipitated a white powder on the interior of the round-bottomed flask in which the extraction was performed. This powder was removed and analysed using Raman spectroscopy and is likely an amorphous Mg-sulfate based on the position of peaks in its Raman spectrum (Figure 5.4). The formation of this precipitate must have been the result of

oxidation of the added MSA or another intrinsic S-bearing Allende component during the extraction, as sulfate is not among the known S-bearing compounds intrinsic to Allende (Bose et al., 2017). This confirms that such a hot water extraction can result in the formation of sulfate grains, such as the gypsum crystals recovered from TL11h following its initial hot water extraction.

The experimental extractions of Allende group 1 prepared samples revealed that MTBSTFA preferentially reacted with any water present in the samples or solutions during derivatization, rather than with the MSA present, increasing the amount of derivatizing agent required for complete derivatization of MSA. As a result, the GC-MS analyses of these samples were dominated by hydrolyzed derivatives of MTBSTFA. The full results of these experiments are reported in the Appendix of this chapter. The derivatized MSA produced comparatively small peaks, some of which were not initially identified by the analytical software used. The relative areas of the largest of these peaks (with retention time of ~6.1 minutes) for the various samples are plotted in Figure 5.5. These relative peak sizes are similar across many of the samples analysed, however it was difficult to determine whether this similarity was a true reflection of the MSA content of each sample following storage, or if there simply had not been enough MTBSTFA present to derivatize the water as well as the full amount MSA present in the sample. Therefore, it was necessary to test what amount of derivatizing agent needed to react with and retrieve any and all MSA present in the samples following storage.

The second round of acetonitrile extractions conducted on group 2 prepared Allende samples was therefore designed to determine the quantity of MTBSTFA necessary to react with the total amount of MSA originally added to the samples during their preparation. GC-MS analyses were completed for each of three samples which had 1.35 times, 2.70 times, and 4.05-fold excess MTBSTFA added to react with the amount of MSA each initially contained. The relative areas and heights of largest peaks returned for the derivatized MSA compound (at a retention time of ~6.1 minutes) for each of these three samples are shown in Figure 4.6. From these results it is clear that the 2.70 times and 4.05 times

excess samples show similar, strong peaks of derivatized MSA, while the 1.35 times excess sample has a much smaller peak. This implies that both the 2.70 times and 4.05 times excess MTBSTFA were sufficient to derivatize all MSA present in these samples, as there is little change in the peak sizes between these two samples, despite the additional quantity of MTBSTFA present in the 4.05 times excess sample. When only 1.35 times excess MTBSTFA is added to the sample, however, the peak is much smaller, implying that this quantity of MSA is not sufficient to derivatize all MSA present in the sample. Therefore, it is likely that the 23 µL of MTBSTFA added to the prepared group 1 Allende samples may not have been sufficient to derivatize all MSA present in these samples, and additional testing would be necessary to determine the effects of storage conditions on the retention of MSA.

Because of the difficulty in working with a derivatizing agent so sensitive to the water content of the chosen solvent, as well as to achieve a lower detection limit of the desired compounds, a new method of extraction and analysis was devised – viz. one based on LC-MS analysis.

5.3.4 LC-MS Analysis

Prior to the final extraction and analysis of the doped Allende samples, the LC technique was first tested on stock solutions of MSA dissolved in acetonitrile. These analyses produced strong, easily discernable peaks at a retention time of ~1.30 minutes for concentrations as low as 0.5 ppb. Concentrations of 0.5, 5, 50, and 500 ppb were analysed, and the resulting peak areas and heights used to construct calibration curves. These plots are presented in Figure 5.7.

The final round of acetonitrile extractions was performed on samples of Allende from prepared group 3 and the extracts were analysed by LC-MS. MSA concentrations in each of these samples were calculated using both the peak area and peak height calibration curves described above. The results of this analysis are reported in Table 5.4. The relative areas and heights of these peaks are also plotted in Figure 5.8. From these results it is clear that in the short-term period of 72 hours, storage of samples in

either the freezer or glovebox offers comparable retention of MSA, while cleanroom storage results in a significant decrease in MSA content over the storage period. However, when the storage period was increased to a length of one month, while the retention of MSA by the Allende sample stored within the glovebox remained high, the MSA concentration remaining within the cleanroom sample was significantly elevated in comparison to the sample which had been stored in the freezer. The implications and possible explanations for this observation are discussed below. The considerable difference in the magnitude of the amounts of MSA recovered from the two sets of samples is most likely attributed to differences in the experimental method, where the extraction of the first set of samples employed a step using filter paper, while the second did not. Further experimentation using identical methods will be necessary to determine whether any decrease in the MSA concentration in the samples occurs over extended periods of storage.

5.3.5 Tagish Lake DCM and Acetonitrile Extractions

LC-MS analysis of the acetonitrile extract of the TL1 sample using the HILIC column identified several salt clusters, perhaps because the extraction technique did not employ any desalting procedures, but did not uncover any organic compounds. The C18 column identified 8 compounds in positive mode and 18 compounds in negative mode. These results are summarized in Table 5.5. Although sample analysis in MS mode alone does not allow for direct compound identification because it does not provide compound structures, some inferences can be made regarding these compounds. A comparison with the results of Simkus et al. (2019) reveals none of the compounds identified during this study have been found in previous SOM extractions of sample TL1. The presence of oxygen in the compounds we extracted suggests they may be carboxylic acids or their derivatives, which have been identified in high abundance in numerous previous studies of Tagish Lake (e.g. Pizzarello et al., 2001; Hilts et al., 2014, Simkus et al., 2019). It is also possible that any number of these compounds may be the result of terrestrial contamination. While TL 1 is among the samples of Tagish Lake considered to be

pristine, contamination prior to collection, during storage, or processing and extraction in an open atmosphere may have occurred despite best efforts at proper curation.

A total of 3 species were identified in the DCM extract of TL 1 by GC-MS. The species detected are hexathiane (S_6) and cyclic octaatomic sulfur (S_8), two allotropes of elemental sulfur, both of which have been identified in previous GC-MS analyses of various Tagish Lake samples and are thought to be intrinsic (Hilts et al., 2014), as well as 2,2'-Methylenebis[6-(1,1-dimethylethyl)-4-(1-methylpropyl)phenol]. The most common use of this compound is as a solvent stabilizing agent, and we therefore may expect that it was introduced to the sample by the DCM solvent itself. However, an analysis of a blank sample of DCM did not contain this compound. While these results are somewhat puzzling, it is possible that contamination of the sample may have occurred sometime prior to the DCM extraction. The compound may have been present in the acetonitrile utilized during the first extraction of the sample, or may have come from contaminated lab equipment which came into contact with the sample.

5.4 Discussion

5.4.1 Degree of Alteration of Sample TL 8a

Based primarily on the degree of alteration of the chondrules within sample TL8a, which typically contain both olivine and phyllosilicates, with the former in greater quantities than the latter, this sample is most similar in degree of alteration to the previously examined samples TL10a, TL5b, and TL11h. The mean Fe/S ratio of all pyrrhotite grains within TL8a is 0.830, lower than that of any previously examined sample. This suggests TL8a is of a higher degree of alteration, since the Fe/S ratio of pyrrhotite decreases with increasing alteration as Fe from pyrrhotite is incorporated into magnetite and Fe-rich phyllosilicates (Schrader et al., 2021). However, pyrrhotite grains in these previous samples typically contained significantly lower Ni content. The higher Ni content of the TL8a pyrrhotite may be the result of impure analyses caused by beam overlap between pyrrhotite and sub-micron sized

exsolved pentlandite which is not perceptible in the BSE images. For a more direct comparison between TL8a and previous samples, only pyrrhotite grains with Ni content of <7 wt% were used to determine an Fe/S ratio of pyrrhotite which is less likely to be contaminated by pentlandite; this Ni content was used because the majority of pyrrhotite grains in previous samples contained <7 wt% Ni, and this value represented a break in Ni content of the TL8a pyrrhotite between 5.93 wt% Ni and 7.16 wt% Ni. This new ratio of 0.855 is between that of TL11h (0.850) and TL5b (0.867), a position which is more consistent with the estimation of degree of alteration based on the texture of the TL8a chondrules.

Together these observations reveal that the previously uncharacterized petrology of TL8a places it within the known range of degrees of alteration of previously examined TL samples. As such, the number, concentrations, and types of organic compounds it contains should be similar to these samples. Previous studies have suggested that minimal to moderate aqueous alteration such as that of samples TL5b, TL11h and TL1 is optimal for the synthesis and preservation of organic molecules such as amino acids (Herd et al., 2011; Glavin et al., 2012; Hilts et al., 2014; Simkus et al., 2019). These samples are similar in degree of alteration to TL8a. Therefore, lithologic differences between samples are likely not the main contributor to differences in their organic contents.

It follows that, as MSA was found within TL8a, it should also be present within one of these other samples. However, neither the methanol-toluene extraction of TL5b and TL11h nor the acetonitrile and DCM extractions of TL1 conducted in this study revealed the presence of any detectable amount of MSA. Previous extractions of TL5b and TL11h (Glavin et al., 2012; Hilts et al., 2014; Simkus et al., 2019) have similarly failed to show the presence of any MSA. It is possible that the larger amount of TL8a (4.5 g) utilized for organic extraction by Pizzarello et al. (2001) resulted in the ability to detect a greater number of compounds. However, the detection limits of the LC-MS technique employed for the analysis of the TL1 acetonitrile extract are far lower than the 20 ppm MSA originally reported for TL8a (Pizzarello et al., 2001). Therefore, even extractions using a smaller sample quantity should be able to

detect a compound in such high abundance, if it is present. Another explanation besides sample lithology must be found to explain this discrepancy.

5.4.2 Storage and Implications for Curation

One possible alternative explanation for the absence of MSA in TL samples 5b, 11h, and 1 is the loss of MSA from these samples over time as a result of volatilization or, and perhaps more likely, oxidation during storage. The freezer in which these samples have been stored since their collection is held at ~-28°C, however there are no atmospheric controls on the storage environment.

The results of the MSA-doped Allende experiments suggest that while in the short-term, storage within an environment where temperature is controlled but which is open to Earth's atmosphere results in a high rate of MSA preservation, over longer periods the performance of this method of storage decreases. This is perhaps the result of the high amount of air circulation within the freezer of the Subzero Curation Facility resulting in increased evaporation of the MSA from the sample, as the lids of the samples where intentionally left unsealed during storage to expose them to their environments. While there are some doubts as to the validity of the results of the month-long experiment – the concentration of MSA retained in the cleanroom sample being close to that preserved by the glovebox, and significantly higher than that preserved in the freezer seems dubious at best – if these results do indeed reflect reality, they suggest that atmospheric control is at least as important for the preservation of organic molecules as temperature control. As the atmosphere in the facility in which Tagish Lake specimens have been stored is not controlled, it is possible that the nearly 16 years of storage within this facility has resulted in the loss of certain compounds such as MSA. If any MSA remained in samples TL5b and TL11h at the time of their initial extractions (Glavin et al., 2012; Hilts et al., 2014) it likely went undetected during these analyses, which did not employ the derivatizing agent MTBSTFA to retrieve polar compounds.

Contrary to freezer storage alone, in both the short-term and long-term experiments, the samples stored within the glovebox maintained a relatively high concentration of MSA. Based on these results, it is advisable that for samples which may contain any organic molecules or other volatiles be stored within controlled atmospheric conditions with an inert gas such as Ar and limited air flow to maintain these compounds for the longest amount of time possible. While it may not always be possible to control the initial collection and storage conditions of meteorites, which may be found and collected by inexperienced individuals after great lengths of time, long-term storage of valuable samples within research collections in such a manner should be considered. Additionally, any sample return missions should be planned and constructed in such a way as to collect and hold samples indefinitely within a sealed environment which will not be exposed to Earth's atmosphere.

Alternatively, MSA may have been a terrestrial contaminant in sample TL8a. A high proportion of the organic compounds detected within recently collected samples are now known to be terrestrial contaminants (Tunney et al., 2020; Tunney et al., 2022a, b). It is possible that a similar statement may be true for Tagish Lake, and that the MSA in TL8a may be one of these contaminants. This is supported by the detection of MSA in a blank sample of Allende + acetonitrile prepared and analysed under the sample conditions as samples of Allende from prepared group 3 despite heating of the Allende powder to remove any previous organic compounds. The presence of the MSA in these blanks is likely the result of cross contamination from the laboratory equipment used. However, MSA is not among the terrestrial contaminants which have previously been detected within samples processed by our laboratory (Tunney et al., 2020, Tunney et al., 2022a, b), suggesting it is not a commonly occurring contaminant within our own laboratory. However, MSA is produced in large quantities worldwide, in addition to having been found in terrestrial ice cores (Isaksson et al., 2005). Therefore, it is highly probable that the MSA found within TL8a is not intrinsic, and may represent contamination of the sample within the laboratory which prepared and analyzed TL8a. Investigation of the isotopic signatures of any MSA found within TL

samples may be able to determine its origin, as the isotopic ratios of terrestrial MSA (Siauw and Norman, 2006) are expected to be quite different from any extraterrestrial organosulfur compounds.

5.4.3 Chemical Extraction and Production of Sulfate

Another possible explanation for the absence of MSA from the samples examined during the course of this study is loss during chemical extraction and subsequent analysis. This may have occurred during past extractions of TL5b and TL11h by one of two mechanisms: 1) Oxidation of MSA to form sulfate during hot water extraction; 2) MSA recovered during extraction, but not detected during GC-MS analysis because no derivatizing agent was used, as discussed above.

This first mechanism could explain the formation of gypsum in the powdered residue of TL11h following hot water extraction. Indeed, oxidation of MSA to sulfate by aerosolized Cl_2^- and hydroxyl radicals has been documented in terrestrial atmospheric environments, with aqueous-phase reactions proceeding more quickly than gas-phase reactions, and the lifetime of MSA ranging from days to weeks (Mungall et al., 2018).

The sulfur within the recovered gypsum must have been sourced from one or more of the S-bearing components within Tagish Lake itself, as the extraction did not employ any S-bearing components. Organosulfur compounds, sulfides, and elemental sulfur are all possible sources of this sulfur. If MSA was indeed the S-source for these gypsum crystals, a possibility which is supported by the formation of the amorphous Mg-sulfate precipitate from one doped Allende sample during hot water extraction, it would explain the absence of MSA in this sample. If this is indeed the case, it would suggest that sample TL11h initially contained MSA or some other S-bearing species, while TL5b and TL1 did not. It is not clear at this time what the true source of sulfur is within these crystals. Further testing will be required before a definitive answer can be found.

5.4.4 Potential Problems with Methodology

It is also possible that, despite the use of various extraction solvents and analytical techniques, the methods employed during this study are not suitable for extracting MSA, or perhaps are not sensitive enough to detect this compound in very low concentrations. MSA is water-soluble and thus should have been easily identified once a derivatizing agent was employed. However, it is possible that the MSA detected by Pizzarello et al. (2001) in TL8a had, prior to extraction, initially been part of a larger molecule which decomposed during extraction, and which may not be soluble in any of our chosen solvents. If this is the case, this initial organosulfur compound may still be present within the samples of TL examined during this study, and more aggressive extraction techniques may yet recover them.

5.4.5 LC-MS for Astrobiology – Two Steps Forward, One Step Back

Several compounds in sample TL1 with chemical formulas yet unseen in previous analyses were identified during the course of this study by LC-MS, however these could not be positively identified as LC-MS analysis does not provide structural information. These results show that the application of LC-MS analysis to the detection of organic molecules in extraterrestrial materials has both benefits and drawbacks.

The detection limit of compounds such as MSA is much lower for LC-MS than for the same compounds using GC-MS. A derivatizing agent is not required to recover polar compounds using LC-MS, thereby avoiding the complications resulting from using MTBSTFA and other derivatizing agents. Finally, solvents such as water can be injected directly into the instrument, a feature which may prove particularly useful in sample return missions from icy bodies. However, as seen in this analysis, the technique cannot provide structural information, making identification difficult and time consuming. Compounds must be run in MS MS mode and compared to a known standard; therefore, the compounds of interest must be known or hypothesized in advance. While a database to aid in identification, mzCloud, does exist, it is not nearly as extensive as the NIST database for GC-MS data and

there is no software available to check results against this database. Each result must be individually manually searched. Additionally, because experimental conditions can vary widely for LC-MS analyses, it is possible that, even if a particular compound is present within the database, if the experimental conditions utilized during the generation of the database entry were different than those utilized on the sample of interest, it may still be impossible to generate a match.

LC-MS analysis has the potential to recover a myriad of organic compounds present in extraterrestrial materials which have thus far gone undetected because of their low concentrations, as well as to simplify the procedure by eliminating the need for derivatizing agents. However, significant advancements in the mzCloud database will be needed before the LC-MS technique could be routinely applied. In its current state, with the use of a standard LC-MS analysis could be used to confirm the presence of a compound of interest within a sample, but may not yet be the preferred choice for exploratory analyses of unknown compounds, at least until a larger database is generated.

5.5 Conclusion

Despite numerous attempts and the utilization of both GC-MS and LC-MS methodologies, neither MSA nor any other organosulfur compound were found within any of the three samples of Tagish Lake (TL5b, TL11h, and TL1) examined during this study. MSA has been found in one sample of Tagish Lake, TL8a, which, based on the texture and composition of its chondrules and Fe-Ni sulfides respectively, has a similar degree of alteration to TL samples 5b and 11h, suggesting lithologic differences are not the primary reason for the absence of MSA within these samples. It is possible that the storage of these samples within an atmosphere open to the environment since their collection resulted in the oxidation or volatilization and loss of compounds such as MSA, a hypothesis supported by a decrease over time in the concentration of MSA within a sample of Allende which had been artificially doped with MSA and stored in a freezer for one month. The relatively high retention of MSA

by a similar sample stored within an Ar atmosphere glovebox suggests storage in an inert atmosphere within a sealed vessel may be a preferable method of long-term storage for Tagish Lake and similar samples, as well as specimens recovered during return sample missions. It is also possible that any MSA initially present within samples TL5b and TL11h may have been recovered during their initial chemical extractions, but the polar compound went undetected as no derivatizing agent was employed. Gypsum crystals which formed in the reside of TL11h following the how water extraction may have resulted from the oxidation of MSA or other S-bearing components during the extraction. Future isotopic studies may shed light on the true source of sulfur within these crystals. It is also possible that the MSA within TL8a was initially part of a larger compound which was not susceptible to our methods of extraction, and more aggressive techniques may be necessary to recover such compounds. For all of these reasons, while soluble organosulfur compounds have yet to be detected by any of the employed methodologies within this study, their presence within Tagish Lake cannot be ruled out. Further testing to determine the rate at which MSA is lost during storage and more aggressive extraction techniques may establish whether MSA or an MSA precursor may be present in other samples of Tagish Lake, and if these species prove to be absent, may provide additional insights into the reasons it has only been detected in a singular sample. In particular, there is a strong possibility that the MSA found in the TL8a extract by Pizzarello et al., (2001) might have been a terrestrial contaminant rather than an intrinsic component.

5.6 Tables

Table 5.1: Summary of the preparation, storage conditions, and extraction procedures of the artificially doped Allende samples.

Sample	Sample Group	Heating Temperature	Storage Location	Storage Time	MSA solution Concentration	Quantity of Solution Added	Extraction Method	Quantity of MTBSTFA Added
Silica + MSA	0.1	450	Ar glovebox	72 hours	50 ppm	1.5 mL	acetonitrile	23µL
Silica + MSA	0.2	450	Tagish Lake Storage Freezer	72 hours	50 ppm	1.5 mL	acetonitrile	23µL
Allende + MSA	1.1	450	Ar glovebox	72 hours	50 ppm	1.5 mL	acetonitrile	23µL
Allende + MSA	1.2	450	Ar glovebox	72 hours	50 ppm	1.5 mL	hot water	23µL
Allende + MSA	1.3	450	Tagish Lake Storage Freezer	72 hours	50 ppm	1.5 mL	acetonitrile	23µL
Allende + MSA	1.4	450	Tagish Lake Storage Freezer	72 hours	50 ppm	1.5 mL	hot water	23µL
Allende + MSA	1.5	450	Ar glovebox	1 month	50 ppm	1.5 mL	acetonitrile	23µL
Allende + MSA	1.6	450	Tagish Lake Storage Freezer	1 month	50 ppm	1.5 mL	acetonitrile	23µL
Allende + MSA	2.1	200	Ar glovebox	72 hours	pure	0.4 mL	acetonitrile	0.30 mL
Allende + MSA	2.2	200	Ar glovebox	72 hours	pure	0.4 mL	acetonitrile	0.59 mL
Allende + MSA	2.3	200	Ar glovebox	72 hours	pure	0.4 mL	acetonitrile	0.89 mL
Allende + MSA	3.1	200	Cleanroom	72 hours	20 ppm	6 µL	acetonitrile	none
Allende + MSA	3.2	200	Subzero Curation Facility Freezer	72 hours	20 ppm	6 µL	acetonitrile	none
Allende + MSA	3.3	200	Ar glovebox	72 hours	20 ppm	6 µL	acetonitrile	none
Allende + MSA	3.4	200	Cleanroom	1 month	20 ppm	6 µL	acetonitrile	none
Allende + MSA	3.5	200	Subzero Curation Facility Freezer	1 month	20 ppm	6 µL	acetonitrile	none
Allende + MSA	3.6	200	Ar glovebox	1 month	20 ppm	6 µL	acetonitrile	none

Table 5.2: Major and minor element compositions of Fe-Ni sulfides in sample TL 8a.

Mineral	Si (wt%)	Cr (wt%)	Fe (wt%)	Co (wt%)	Ni (wt%)	Mn (wt%)	P (wt%)	S (wt%)	Total (wt%)	Fe/S (at%)
pyrrhotite	0.04	0.08	49.73	1.07	11.33	0.03	b.d.l.	37.81	100.10	0.755
	0.07	0.06	57.41	0.23	2.08	b.d.l.	0.02	38.96	98.83	0.846
	0.24	0.04	56.63	0.24	3.56	b.d.l.	b.d.l.	37.31	98.03	0.871
	0.08	0.04	58.30	0.03	2.29	b.d.l.	b.d.l.	38.60	99.35	0.867
	0.07	0.04	58.11	0.05	1.69	0.01	b.d.l.	39.03	99.00	0.855
	0.03	0.09	58.14	0.03	2.72	0.08	0.01	38.75	99.84	0.861
	0.01	0.08	57.87	0.10	3.13	0.13	b.d.l.	39.15	100.49	0.849
	0.01	0.07	57.91	0.09	2.54	0.12	b.d.l.	39.22	99.96	0.848
	b.d.l.	0.05	59.34	b.d.l.	1.22	0.02	0.01	39.83	100.47	0.856
	0.02	0.03	58.89	b.d.l.	1.44	0.01	b.d.l.	39.55	99.95	0.855
	b.d.l.	0.04	59.33	b.d.l.	1.71	0.01	b.d.l.	39.33	100.42	0.866
	0.02	0.04	55.71	0.20	4.93	0.02	b.d.l.	39.35	100.27	0.813
	0.03	0.03	54.66	0.31	5.80	0.03	b.d.l.	39.40	100.25	0.796
	0.04	0.13	55.15	0.09	7.27	0.01	0.02	38.71	101.42	0.818
	0.03	0.45	58.82	b.d.l.	1.77	0.01	0.06	38.20	99.34	0.884
	0.18	0.05	50.12	0.55	11.45	0.02	0.01	36.99	99.37	0.778
	0.06	0.03	49.08	0.58	12.40	0.01	b.d.l.	37.26	99.43	0.756
	0.04	0.03	46.93	0.82	13.96	b.d.l.	b.d.l.	37.54	99.30	0.718
	0.16	0.2	55.89	0.26	4.76	b.d.l.	b.d.l.	37.87	99.14	0.847
	0.07	0.22	54.60	0.46	5.93	0.01	0.01	38.43	99.75	0.816
	0.01	0.06	56.28	0.59	5.13	0.02	b.d.l.	38.01	100.10	0.850
	0.15	0.05	54.28	0.71	5.18	0.01	b.d.l.	37.15	97.53	0.839
	0.03	0.05	55.97	0.47	4.88	0.01	0.01	38.10	99.53	0.843
	0.04	0.02	54.48	0.29	7.34	b.d.l.	b.d.l.	37.87	100.04	0.826
	0.01	0.02	54.34	0.25	7.33	0.01	b.d.l.	37.79	99.76	0.825
	0.02	0.02	53.39	0.20	8.23	b.d.l.	b.d.l.	37.65	99.51	0.814
	0.06	0.03	50.92	0.32	9.66	0.01	0.01	37.43	98.45	0.781
	0.21	0.10	54.66	0.15	7.16	0.08	b.d.l.	36.84	99.21	0.852
	0.01	0.08	55.10	0.20	7.35	0.09	b.d.l.	37.26	100.10	0.849
	0.01	0.07	54.79	0.22	7.63	0.11	b.d.l.	37.43	100.28	0.840
	0.04	0.08	57.69	0.36	4.20	0.01	0.01	37.32	99.71	0.887
	0.04	0.15	54.23	0.67	7.59	b.d.l.	b.d.l.	37.19	99.87	0.837
	0.06	0.05	56.36	0.17	5.66	0.05	b.d.l.	37.95	100.30	0.853
	0.01	0.06	48.28	0.62	11.48	0.02	b.d.l.	37.19	97.66	0.745
	0.03	0.12	59.89	0.04	1.34	0.02	b.d.l.	38.86	100.29	0.885
	0.01	0.13	59.60	0.04	1.80	0.01	0.01	38.74	100.33	0.883
	0.01	0.02	52.61	0.88	8.72	0.03	0.02	38.04	100.33	0.794
	0.02	0.03	50.91	1.13	10.09	0.02	b.d.l.	37.74	99.94	0.774
	0.06	0.02	52.25	0.87	8.35	0.02	b.d.l.	37.79	99.35	0.794

	0.03	0.04	56.11	0.28	5.07	b.d.l.	b.d.l.	38.14	99.66	0.845
	0.03	0.04	53.73	0.44	7.36	b.d.l.	b.d.l.	38.13	99.72	0.809
	0.02	0.05	58.64	b.d.l.	1.35	b.d.l.	b.d.l.	39.48	99.54	0.853
	0.04	0.06	58.40	b.d.l.	1.74	0.01	b.d.l.	39.29	99.54	0.853
	0.13	0.05	58.30	b.d.l.	1.33	0.05	0.02	39.06	98.95	0.857
	0.01	0.04	51.98	0.44	9.93	0.01	b.d.l.	37.67	100.07	0.792
	0.07	0.05	50.65	0.45	10.30	0.01	b.d.l.	37.23	98.77	0.781
	0.06	0.06	51.83	0.36	9.56	0.02	0.01	37.54	99.43	0.793
	0.02	0.12	57.15	b.d.l.	4.70	0.03	b.d.l.	38.21	100.23	0.859
	b.d.l.	0.13	58.84	b.d.l.	3.31	0.03	b.d.l.	38.22	100.54	0.884
	0.01	0.15	58.47	b.d.l.	3.43	0.02	0.01	38.21	100.29	0.879
	b.d.l.	0.11	57.45	0.09	3.02	0.09	b.d.l.	39.32	100.08	0.839
	0.02	0.12	45.64	0.69	13.34	0.04	b.d.l.	38.12	97.97	0.687
	b.d.l.	0.10	59.43	b.d.l.	1.29	0.08	0.01	39.40	100.31	0.866
	0.04	0.05	58.74	b.d.l.	1.75	b.d.l.	0.01	39.27	99.85	0.859
	0.02	0.09	57.29	0.16	2.84	0.10	0.01	39.00	99.49	0.843
	0.02	0.07	58.15	0.12	2.37	0.06	b.d.l.	39.31	100.08	0.849
	0.16	0.06	57.53	0.10	2.47	0.08	b.d.l.	38.44	98.83	0.859
average	0.05	0.08	55.39	0.29	5.55	0.03	0.00	38.28	99.66	0.830
1σ	0.05	0.07	3.48	0.30	3.59	0.03	0.01	0.81	0.75	0.043
pentlandite	0.03	0.03	31.01	0.77	35.08	b.d.l.	0.01	33.57	100.48	0.530
	0.03	0.03	32.01	0.54	33.41	0.03	b.d.l.	33.47	99.52	0.549
	0.01	0.01	30.59	0.78	34.78	b.d.l.	b.d.l.	33.41	99.59	0.526
	0	0.03	31.33	0.56	34.86	b.d.l.	b.d.l.	33.17	99.96	0.542
average	0.02	0.03	31.24	0.66	34.53	0.01	0.00	33.41	99.89	0.537
1σ	0.02	0.01	0.60	0.13	0.76	0.02	0.01	0.17	0.44	0.011

Table 5.3: Organic and inorganic compounds detected in the 1:1 methanol-toluene extractions of Tagish Lake sample TL 11h and TL 5b. All compound identifications are best matches from the NIST database. Compounds which are thought to be intrinsic are denoted with square brackets. All other compounds are thought to be terrestrial contaminants. Compounds are classified as either intrinsic or contaminants based on the likelihood of a given compound being sourced from a terrestrial environment as well as comparison with previous literature.

Sample	Retention Time	Quality	Compound
MET11611/P-11h/2 a	3.185	91	toluene
	3.948	91	toluene
	4.264	91	toluene
	4.569	91	ethylbenzene
	4.590	81	ethylbenzene
	4.656	87	p- Xylene
	4.689	70	Benzene, 1,3-dimethyl-
	7.936	78	tridecane
	9.407	11.5	hydrazinecarboxylic acid, phenylmethyl ester
	17.121	10	[Quinoline, 7-chloro-4-nitro-, 1-oxide]
	19.584	91	[cyclic octaatomic sulfur]
	20.423	2	methane
	21.589	12	[Fumaric acid, 4-chlorobenzyl undecyl ester]
	22.308	2	ammonia
	22.635	23	Silicic acid, diethyl bis(trimethylsilyl) ester
	28.781	47	2-(Decyloxycarbonyl)benzoic acid
	29.107	43	Phthalic acid, 2-ethoxyethyl decyl ester
	34.185	9	3-Methyl-2,3-dihydro-benzo[b]thiophene-3-carboxylic acid, methyl ester
MET11611/P-11h/2 b	3.185	91	toluene
	3.937	89	toluene
	3.948	91	toluene
	3.991	94	toluene
	4.264	91	toluene
	4.569	91	ethylbenzene
	4.591	87	ethylbenzene
	4.667	91	Benzene, 1,3-dimethyl-
	4.689	70	Benzene, 1,3-dimethyl-
	7.936	80	undecane
	9.407	64	dodecane
	7.936	78	Heptadecane, 2,6,10,14-tetramethyl-
	11.161	11.2	benzeneethanol, alpha-methyl-
	13.395	24.5	2-6-lutidine-4-[benzyloxy]-3,5-dichloro-
	14.648	94	Diethyl Phthalate

	18.625	27	Benzene, 1-bromo-3-chloro-
	19.562	94	[Cyclic octaatomic sulfur]
	19.573	91	[Cyclic octaatomic sulfur]
	26.427	1	water
	30.807	50	1,2-Benzenedicarboxylic acid, dinonyl ester
MET11611/P-5b/5	3.174	91	toluene
	3.185	90	toluene
	3.937	90	toluene
	3.98	94	toluene
	4.264	90	toluene
	4.569	91	ethylbenzene
	4.591	70	ethylbenzene
	4.667	87	p-Xylene
	4.689	70	o-Xylene
	7.936	80	undecane
	8.982	10.2	benzeneethanol, alpha-methyl
	9.407	31.7	benzaldehyde, 3-benzyloxy-2-fluoro-4methoxy
	9.756	78	Ethanol, 2-phenoxy-
	10.093	56	2-Propanol, 1-[1-methyl-2-(2-propenyloxy)ethoxy]-
	12.948	45.6	2-0-benzyl-d-arabinose
	14.495	51	diethyltoluamide
	14.648	97	Diethyl Phthalate
	14.931	34.4	[hexathiane]
	15.127	56.3	ethaneperoxoic acid, cyanodiphenylmethyl ester
	16.261	31.4	thiosulfuric acid (H2S2O3), S-2(2-ccyclopropylamino)-2iminoethyl) ester
	19.595	91	[cyclic octaatomic sulfur]
	19.726	34.7	[fluoranthene]
	20.227	40	[pyrene]
	20.336	62.4	5-benzyloxypyrimadine-2-carboxylic acid
	21.098	47	2-Propenoic acid, 2-cyano-3-(4-methylphenyl)-, ethyl ester
	31.003	59	1,2-Benzenedicarboxylic acid, dinonyl ester

Table 5.4: Peak areas and heights for MSA peaks in doped Allende samples from prepared group 3 as well as samples of known MSA concentration in acetonitrile used to produce calibration curves. The calculated MSA concentrations of the doped Allende samples based on these curves are also given.

				MSA Concentration (ppb)	
Sample	**RT (min)**	**Peak Area**	**Peak Height**	**Using Area**	**Using Height**
0.5 ppm MSA	1.29	273334.28	105822.6	-	-
5 ppm MSA	1.30	634657.66	285468.4	-	-
50 ppm MSA	1.30	8893647.86	3572776	-	-
500 ppm MSA	1.30	108619504.26	40178543	-	-
72-hour blank	1.27	370420.65	176161.7	5.05	4.17
3.1	1.28	6239168.16	2582267	31.91	34.02
3.2	1.28	23950210.97	9544420	112.99	120.38
3.3	1.27	22373760.23	8592326	105.77	108.57
1 month blank	1.22	2610788.87	11209121	15.30	141.03
3.4	1.24	150269957.50	58573498	691.24	728.53
3.5	1.25	74454269.22	30429279	344.18	379.43
3.6	1.25	156918353.90	58745239	721.67	730.66

Table 5.5: Compounds detected in the acetonitrile extraction of sample MET11611/P-1/9.

C18 Column Negative Mode				
Retention Time (min)	**Mass (A_0)**	**[M-H]-**	**Mass Difference (ppm)**	**Formula**
4.18	436.1931	435.1858	0.54	C17H30N3O10
4.43	356.2351	355.2279	1.82	C23H32O3
4.61	284.1776	283.1704	2.23	C19H24O2
4.7	354.2195	353.2122	1.83	C23H30O3
4.76	372.2301	371.2228	1.99	C23H32O4
4.98	340.2402	339.233	0.71	C23H32O2
5.31	460.2996	459.2923	2.12	C19H44N2O10
5.57	356.2351	355.2279	0.31	C23H32O3
C18 Column Positive Mode				
Retention Time (min)	**Mass (A_0)**	**[M+H]+**	**Mass Difference (ppm)**	**Formula**
2.49	110.0732	111.0804	1.3	C7H10O
2.84	124.0888	125.0961	0.99	C8H12O
3.26	166.0994	167.1067	0.51	C10H14O2
3.32	179.0735	180.0808	0.32	C13H9N
3.74	338.2246	339.2319	1.04	C23H30O2
3.85	408.1549	409.1622	1.16	C22H25NaO6
4.19	260.1776	261.1849	0.46	C17H24O2
4.44	253.2406	254.2478	0.24	C16H31NO
4.51	246.162	247.1693	0.65	C16H22O2

4.57	279.2562	280.2635	0.65	C18H33NO
4.58	255.2562	256.2635	0.21	C16H33NO
4.7	281.2719	282.2791	0.06	C18H35NO
4.83	283.3875	284.2948	0.96	C18H37NO
4.86	284.214	285.2213	0.86	C20H28O
4.9	302.2246	303.2319	0.91	C20H30O2
4.99	176.1201	177.1274	0.55	C12H16O
5.13	337.3345	338.3417	1.6	C22H43NO
5.16	342.2923	343.2995	1.69	C24H38O

5.7 Figure Captions

Figure 5.1: Backscattered electron (BSE) images of Sample TL 8a. A) A relatively unaltered chondrule composed of Fe-rich olivine and pyrrhotite. B) A chondrule with a moderately high degree of alteration containing olivine, phyllosilicates, and magnetite. C) An unexsolved grain of pyrrhotite associated with magnetite within the sample matrix. D) A grain of pyrrhotite exhibiting exsolution of coarsened pentlandite lamella. E) A section of fusion crust containing pyrrhotite with exsolved kamacite. F) A portion of the sample matrix containing an unusually high amount of magnetite in association with a fine-grained ring of pyrrhotite.

Figure 5.2: BSE images of previously extracted powder from sample TL 11h. A,B) Portions of matrix with discernible euhedral magnetite framboids. C,D) Portions of matrix with intact euhedral olivine.

Figure 5.3: BSE images of gypsum crystals taken from the previously extracted TL 11h powder following hot water extraction. Crystal show varying amounts of this powder adhered to their surfaces.

Figure 5.4: The Raman spectrum of the white precipitate removed from sample 1.2. The black box denotes the position of the broad peak which identifies this precipitate as most likely being an amorphous Mg-sulfate.

Figure 5.5: The relative magnitudes of the peak areas of derivatized MSA peaks present in the GC-MS traces of acetonitrile extracts from Allende samples from prepared group 1.

Figure 5.6: The relative magnitudes of the peak areas of derivatized MSA peaks present in the GC-MS traces of acetonitrile extracts from Allende samples from prepared group 2.

Figure 5.7: Calibration curves calculated using the peak heights and areas of MSA peaks present in the LC-MS traces of solutions of known concentration of MSA in acetonitrile.

Figure 5.8: The relative magnitudes of the calculated peak areas and heights of MSA peaks present in the LC-MS traces of acetonitrile extracts from Allende samples from prepared group 3.

5.8 Figures

Figure 5.1

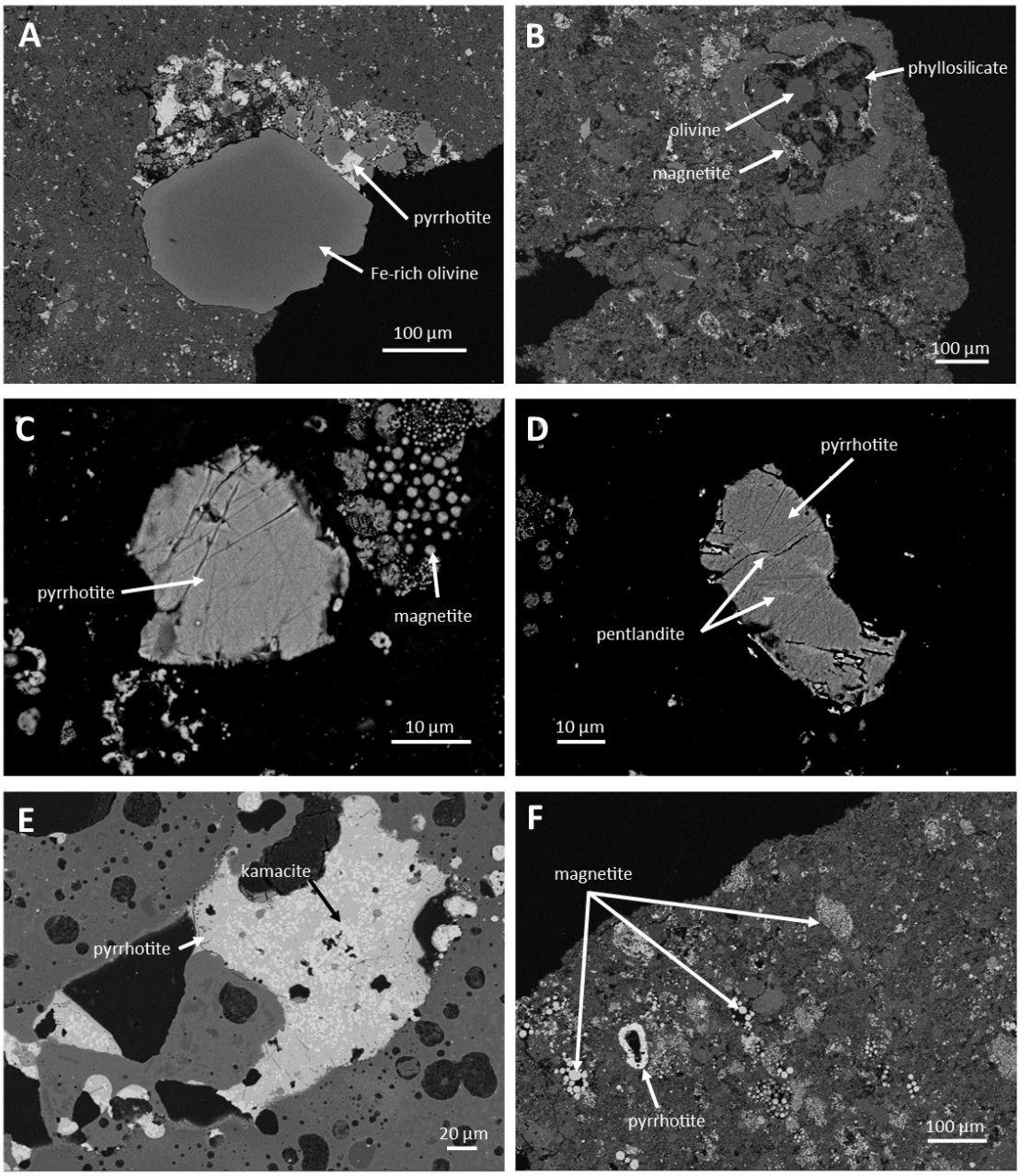

Figure 5.2

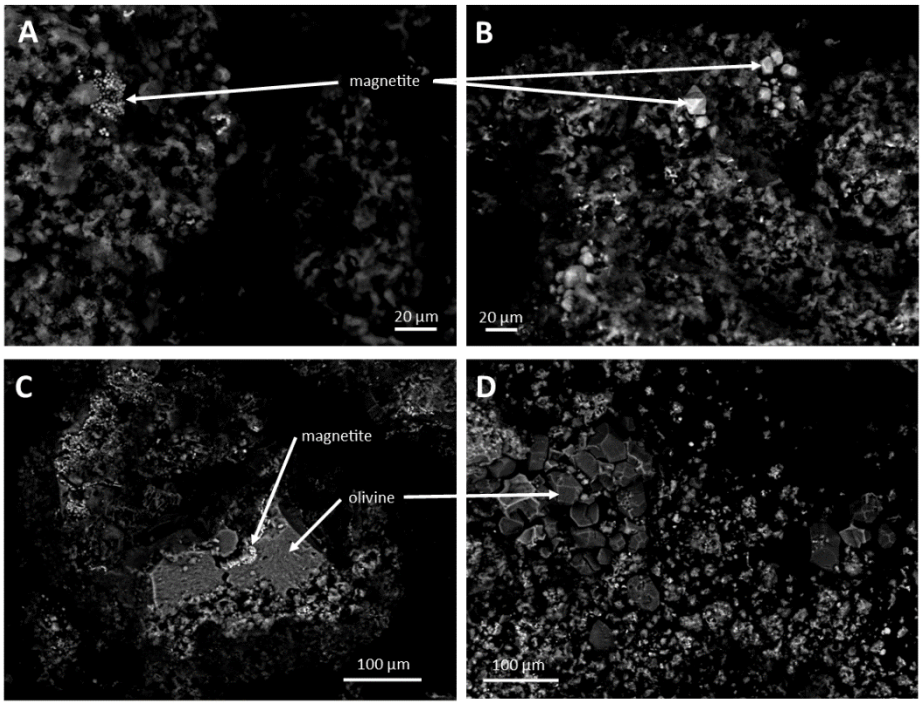

Figure 5.3

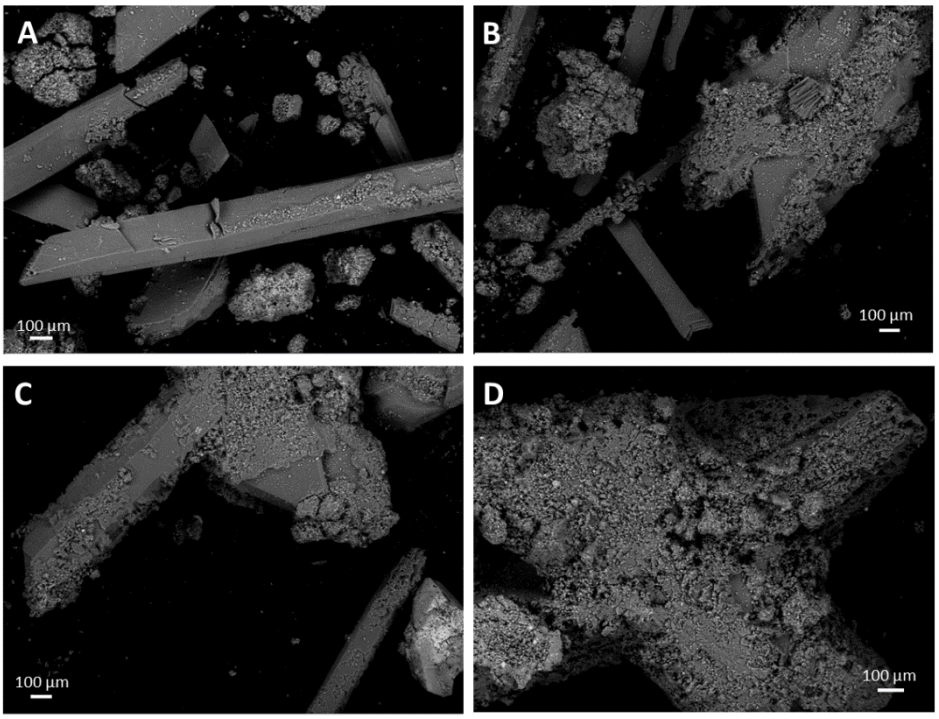

Figure 5.4

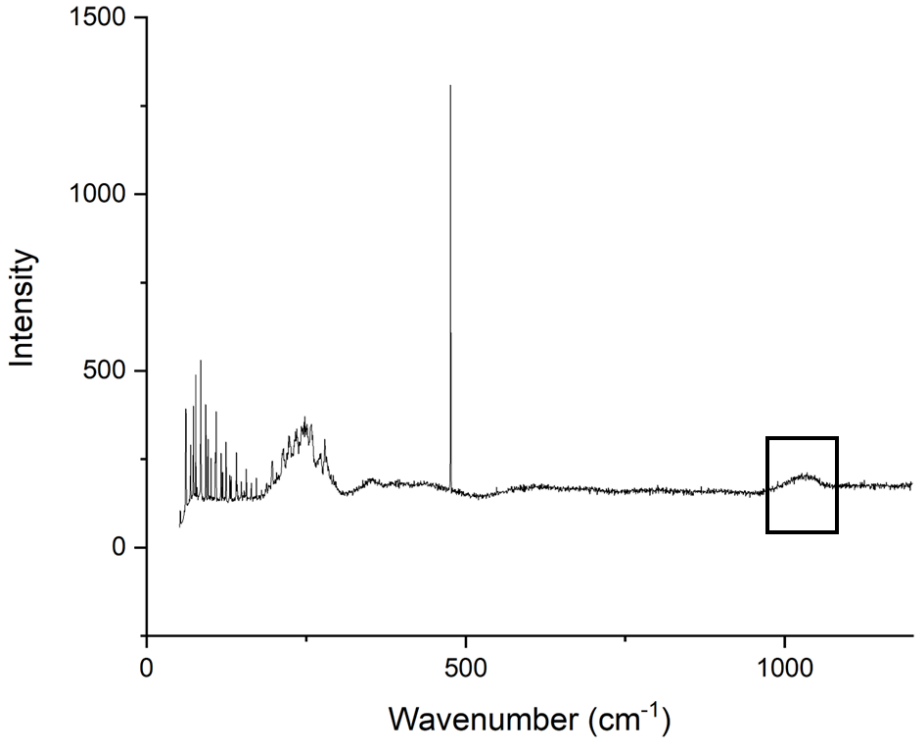

Figure 5.5

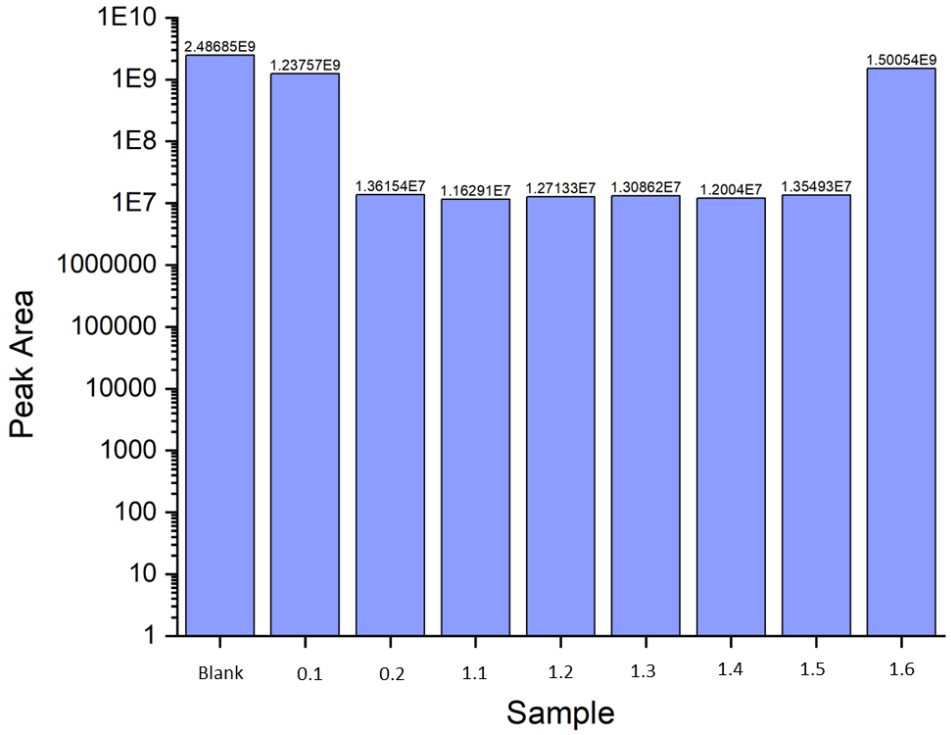

Figure 5.6

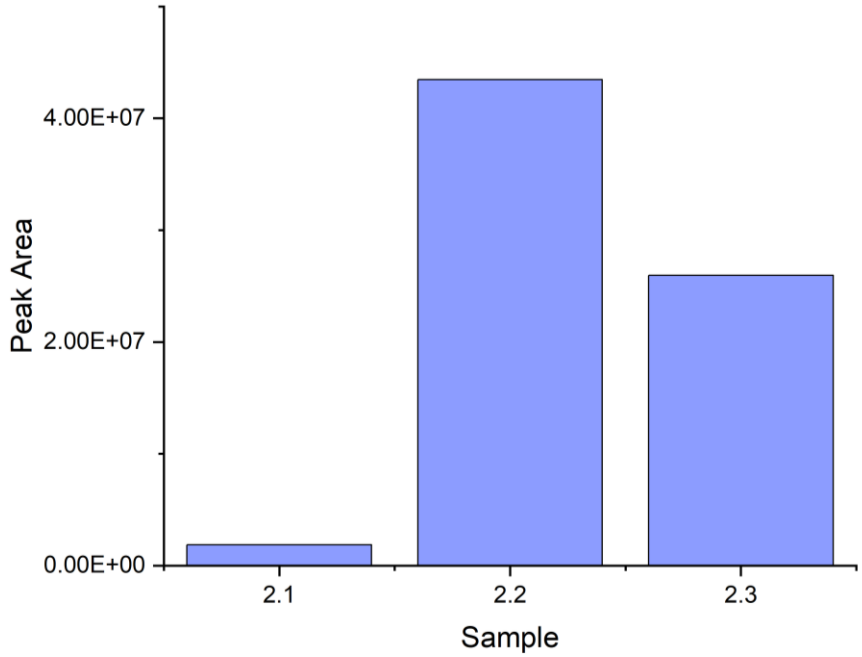

Figure 5.7

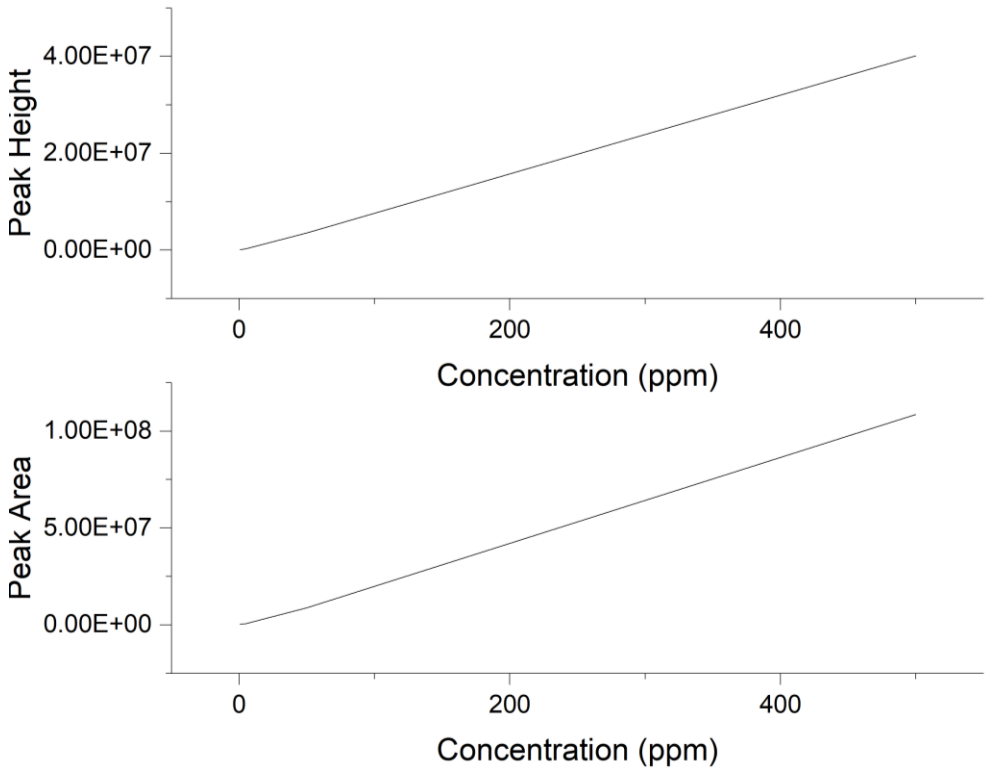

Figure 5.8

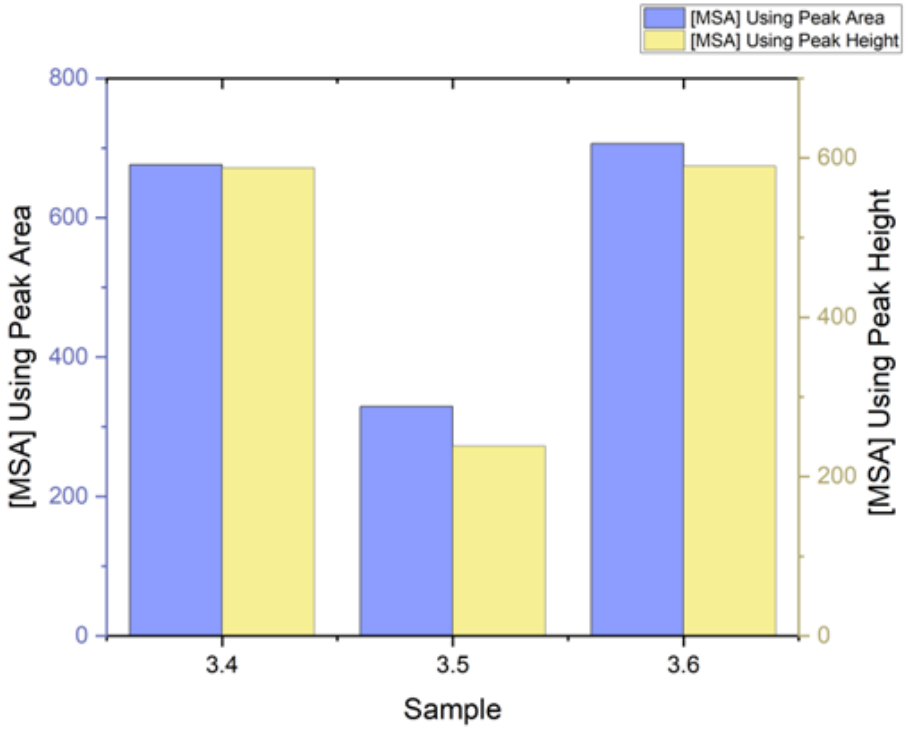
[MSA] Using Peak Area
[MSA] Using Peak Height
800
600
400
200
0
600
400
200
0
[MSA] Using Peak Area
[MSA] Using Peak Height
3.4
3.5
3.6
Sample

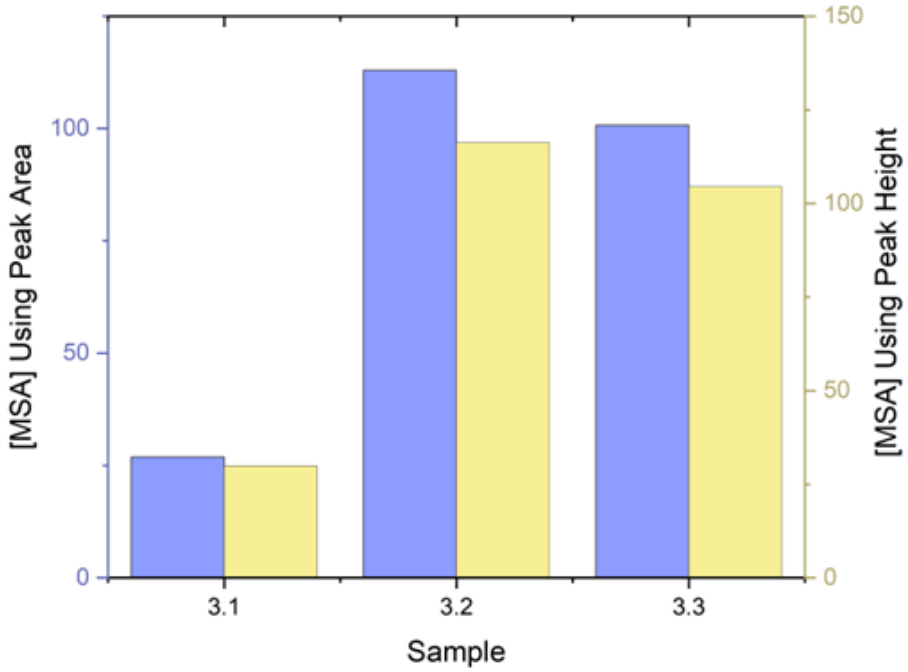
100
50
0
150
100
50
0
[MSA] Using Peak Area
[MSA] Using Peak Height
3.1
3.2
3.3
Sample

Chapter 6: Conservation Conditions for Iron Meteorites: Application to the University of Alberta Meteorite Collection

6.1 Purpose

The University of Alberta Meteorite Collection contains a large number of iron and stony-iron meteorites. Numerous specimens among the over 600 iron and stony-iron meteorite specimens within the collection are known to experience ongoing active corrosion (Figure 7.1) despite the use of a dehumidifier to control the relative humidity within the collection storage area, a leading factor in the rusting of iron objects. The storage area consists of a Class 1000 clean room; curation conditions are outlined in Herd et al., 2016.

These specimens are composed primarily or partially of iron-nickel alloys and are vulnerable to corrosive attack as soon as they fall to the Earth's surface, where they may not be collected for many years. Exposure to terrestrial surface conditions results in corrosion which forms mineral products such as goethite, lepidocrocite, maghemite, magnetite, and akaganéite (β-FeOOH) in the presence of chloride ions, which may penetrate into the interior of the meteorite along grain boundaries and cracks (Sjøgren and Buchwald, 1991). Ni-rich taenite and Ni-poor kamacite are intergrown in these meteorites, and kamacite is selectively attacked relative to taenite (Sjøgren and Buchwald, 1991). Corrosion of these meteorites is slightly more complex because the additional phases add nickel, sulfur, and phosphorus, which may influence pH levels (Sjøgren and Buchwald, 1991). This corrosion does not cease automatically when the meteorites are collected from the field and will continue during storage unless preventative measures are taken. Corrosion-causing chlorides are ubiquitous throughout the environments meteorites are likely to be recovered from, and so it is likely that any iron meteorite may be contaminated and require treatment (Allington-Jones, 2020). Similar conservation procedures for archeological iron artifacts typically involve stabilization treatments and/or environmental controls (Rimmer et al., 2013).

Chemical stabilization treatments have not been proven to be 100% effective at removing chloride ions and halting corrosion. These techniques also carry with them the potential for chemical agents to contaminate the meteorite surface, as well as penetrate into the meteorite interior and cause changes to their mineralogy. Additionally, the high heat and pressures associated with some of these treatment options may alter the specimens' metallurgical characteristics (Mardikian, 2006) in ways that have not been sufficiently investigated, especially with regards to meteorites. For this reason, as well as because the techniques described above can require significant costs and infrastructure to implement, as well as being time consuming when considering the scale of the collection, such treatments are not recommended for broad implementation at this time. As a result, the recommendations in this chapter will focus on preventative measures such as climate control and the establishment of microclimates. However, chemical treatment of specific specimens where corrosion poses a significant threat to their integrity could be considered in the future if environmental measures fail to halt corrosion and stabilize their conditions, if such measures are deemed appropriate. Further investigation of the effects of these treatments on iron meteorites is needed before any invasive chemical treatments should be considered on a broader scale. These techniques, as well as methods of environmental control, are outlined below.

The purpose of this chapter is to provide guidance for the storage of iron-based meteorites in the University of Alberta Meteorite Collection, based on review of the current literature and a survey of storage methods in two other institutions. Recommendations are made on the methods and next steps to undertake for the conservation of these objects. A pilot program was initiated involving 25 specimens within the Meteorite Collection. Preliminary results from this program are included.

6.2 Chemical Stabilization treatments

A variety of desalination techniques have been developed to reduce the chloride ion levels which contribute to the corrosion of many iron objects through the formation of akaganéite (β-FeOOH):

6.2.1 Alkaline Soaking

Soaking iron objects in alkaline solutions (commonly solutions of NaOH, KOH, or alkaline sulfite) increases their porosity, allowing the solution to penetrate into the object, and remove and replace corrosion-causing chloride ions, transforming troublesome corrosion products such as akageneite into more stable minerals like goethite, feroxyhyte, ferrihydrite, and magnetite, which do not contain chlorides (Kergourlay et al., 2011). This method is widely used and is proven to reduce the amount of chloride ions present, but the many variables involved produce inconsistent results, and treatment times are long (Mardikian, 2006).

6.2.2 Cathodic Polarization in Alkaline Solutions

Electrochemical techniques are relatively commonly used in the cleaning and stabilization of iron artifacts. These involve immersing the object in alkaline solutions and applying a potential (typically corresponding to the maximum of the reduction and oxidation peaks for the cathodic and anodic potentials respectively) where the object acts as the cathode, with stainless steel commonly used as the anode, to create passivation of the iron metal through the formation of a stable mineralogy (Degrigny, 2010). This method serves primarily to speed treatment when compared with simple alkaline soaking (Kergourlay et al., 2011), however it is still fairly time consuming and can alter the appearance of and pose risks to the treated objects (Mardikian, 2006; Scarlett, 2016).

6.2.3 Gaseous Reduction

Gaseous reduction functions similarly to the cathodic polarization technique described above, but rather than using alkaline fluids as the electrolyte, this technique employs hydrogen gas (Sjøgren and Buchwald., 1991). The hydrogen gas is capable of penetrating along cracks and fissures in the metal to depths of 5-15 mm below the surface, where is reacts with chloride ions, which are then removed as hydrogen chloride gas, transforming akaganeite to magnetite and/or maghemite and goethite to magnetite (Sjøgren and Buchwald., 1991). No physical erosion or changes in the meteorite structure

were observed in tested specimens, except that some transformed corrosion products lost coherence, and the objects were considered stable even after exposure to a relative humidity (RH) of >95% for 10 days (Sjøgren and Buchwald., 1991).

6.2.4 Subcritical Fluids

The use of the subcritical treatment technique involves highly pressurized water heated above its normal atmospheric boiling point to between 100°C and 374°C, which remains in a liquid state as a result of pressurization (Drews et al., 2013). The resulting change in properties facilitates effective and more rapid extraction of chloride ions because: 1) the increase in diffusivity of ions by almost an order of magnitude increases the rate of Cl^- and OH^- exchange; 2) the decreased viscosity allows for more rapid penetration of the fluid into and removal of Cl^- from the material undergoing treatment; 3) fluid transport increases with the decreased density of the water; 4) wetting and penetration of the water into the object is increased as a result of the decrease in surface tension (Drews et al., 2013). Treatment in this manner using deionized water alone is not sufficient to remove Cl^- and halt corrosion, and the addition of a portion of NaOH to produce an alkaline solution is necessary to stop active corrosion from continuing immediately following treatment (Drews et al., 2013). The exact amount of time required for treatment is affected by the temperature and pH of the solution as well as eluent flow rate (Drews et al., 2013, González et al., 2013), however when compared with specimens treated by simple soaking in alkaline solutions with and without cathodic polarization, this method of treatment requires less time - typically less than 10 days, while traditional techniques can require up to 6 months (Mardikian et al., 2009) - and is at least as or more effective at halting active corrosion following treatment (Drews et al., 2013) while requiring a much lower concentration of caustic be used (González et al., 2013). This form of treatment also results in the transformation of akaganéite to more stable minerals such as hematite, magnetite, and goethite without damaging graphitized layers or separating corrosion layers from core

metal on treated objects (González et al., 2013), and treated samples have remained stable even when exposed to 100% RH conditions for over 7 years (González et al., 2013).

6.2.5 Supercritical Fluids

Supercritical fluid treatments employ fluids maintained above the temperature and pressure of their critical points. When CO_2 fluid heated to a minimum of 60°C was used to dewater iron artifacts, delamination was delayed by ~6 months, at which time objects began to rehydrate and corrode (Scarlett, 2016). When dewatering was combined with impregnation and coating with a polymer sealant, delamination did not occur. The addition of NaOH to the fluid may allow for removal of chloride ions as well, providing an efficient method of dechlorination at lower temperatures than utilized in subcritical fluid treatments (Scarlett, 2016).

6.2.6 Surface Treatments

The application of surface treatments, when undertaken, is usually done following some other form of chemical treatment. Such surface treatments may include air-drying oils and inhibitors (Sjøgren and Buchwald., 1991), such as coatings of tannic acid (Selwyn and Logan, 1993; Allington-Jones, 2020), or coating with polymer sealant (Scarlett, 2016). These techniques have proven relatively successful, but also introduce foreign chemicals to the surfaces, and in some cases interiors, of the objects. Treated objects require continued monitoring as the surface treatments alone do not solve the underlying causes of corrosion and may require reapplication.

6.3. Environmental Control

A second main approach to dealing with the challenges posed by the corrosion of iron metals is to control the environment in which they are stored. This may be undertaken in combination with chemical treatment methods, or as an alternative, non-invasive option. Because corrosion requires the combination of the presence of soluble salts, oxygen, and water, removing or controlling any one of these factors will prevent the continued active corrosion of iron (Thunberg et al., 2021). Environmental

controls focus on reducing either the water or oxygen available for corrosion, or both. Corrosion ceases completely below 12% RH, and rises continually above this threshold (Watkinson and Lewis, 2005). All iron artifacts can therefore safely be stored below 11% RH, with most stable below 19% RH unless akaganeite has already been formed, slow corrosion rates at <30% RH, and rapid corrosion above 50% RH (Rimmer et al., 2013). A precise safe level of oxygen is not firmly established, but the Natural History Museum (London, UK) recommends anoxic environments for the storage of iron meteorites maintain oxygen levels below 3% (Allington-Jones, 2020). The various methods employed to maintain these conditions in either case will be discussed.

6.3.1 Room-level Climate Control

Controlling the relative humidity, temperature, and air circulation in collections storage spaces is an important factor in the conservation of all museum collections, especially in those which are vulnerable to deterioration as a result of unsafe levels or fluctuations in any of these factors. Conditions which are appropriate for other types of materials may not be appropriate for iron objects, and vice versa. A survey of collections practitioners revealed that the majority treat metal objects separate from non-metal objects, drying them either by air drying or using silica gel, and storing in environments which are climate-controlled through the use of high volume air conditioning (HVAC), dehumidifiers, or conservation heating to maintain low RH levels, sometimes combined with other measures, such as the use of microclimates (Thunberg et al., 2021).

6.3.2 Microclimates

When controlling the entire storage environment in which iron objects are kept is either not possible or not sufficient, the implementation of microclimates may be considered. These involve segregating an object or a number of objects within plastic (polyethylene or polypropylene) boxes or bags with desiccants or oxygen absorbers to control RH and oxygen levels.

6.3.3 Desiccants

When creating desiccated microenvironments, boxes with no gaps, large lock-to-seal ratios, stiff locks on all four sides, and easily deformable gaskets are ideal for maximum air tightness, and silica gel should be distributed in thin layers across a series of bags, with a weight-to-volume ratio of silica gel chosen to achieve the desired lowest RH and maintenance schedule (on average, with 50% ambient RH, 44g/L will achieve a lowest RH of 7%, increasing to 15% after 3 months; 88g/L will achieve 2%, increasing to 15% after 7 months; 176g/L will achieve 1%, increasing to 15% after 12 months' 352g/L will achieve 0%, increasing to 15% after 48 months; Thunberg et al., 2021). Since even the most suitable storage boxes are not completely air- and water vapor-tight, the RH within these microclimates must be monitored, and silica gel regenerated relatively frequently to maintain low RH levels. Additionally, it may take up to 24 hours for RH to drop below 10% when silica gel is employed as the desiccant (Paterakis and Mariano, 2013).

6.3.4 Anoxic Environments

An alternative to desiccated storage, oxygen-free microclimates can be established using heat-sealed Escal™ film to enclose iron objects with the Revolutionary Preservation (RP) System™ oxygen absorbing RP-A agent, which is capable of establishing a microenvironment with <10% RH and an oxygen concentration below 0.1% within less than 18 hours (Paterakis and Mariano, 2013). The microclimates created by the RP/Escal™ should last at least 5 years, possibly up to 20, compared with the annual regeneration required for silica gel storage (Paterakis and Hickey-Friedman, 2011), assuming a good seal, no damage to the film, and enough RP agent was used (Mathias et al., 2004). Escal™ film is recommended over other barriers as it has very low rates of both water and oxygen migration and is transparent (Mathias et al., 2004). As an alternative to heat sealing, specialized sealing clips are available for the Escal™ film, which show slightly more erratic rates of oxygen absorption but maintain their seal

for at least 12 months and provide better access to objects (Paterakis and Mariano, 2016). While Escal™ film can be resealed after opening, the RP-A agent must be replaced following any exposure to air.

6.3.5 N_2 atmosphere

Another method of establishing a controlled environment is that of isolating specimens within a gaseous nitrogen (or other inert gas) atmosphere. The resultant anoxic environment should prevent further corrosion of these specimens. This technique has been employed for select specimens at the Smithsonian Natural History Museum, the Natural History Museum (UK), as well as the NASA Johnson Space Center (JSC) (McCubbin et al., 2019). According to personal communications, this technique has proven effective at halting corrosion since its implementation in both cases. If a nitrogen atmosphere is to be used to create an anoxic storage environment, monitoring of the nitrogen levels within the storage space is required to ensure no undetected leaks occur to ensure the space remains safe to work in.

6.4 Recommendations

Following completion of the above review of current literature, as well as a survey of storage methods in two other institutions (Appendix E), the next step in the treatment process was to complete an inventory of the collection to determine which specimens and how many require treatment. This assessment was done using criteria such as the presence of active corrosion and severity of corrosion, sample stability, as well as the research and cultural values of specimens, as applicable. These criteria are outlined in the accompanying rubric for assessment in Appendix E. Future recommendations for how to proceed with regards to collection-wide conservation may be dependent on the number of specimens found to be requiring treatment, as well as space and budget available to implement any required changes.

Because the collection space which houses the iron meteorites currently also plays host to a number of stony meteorites such as carbonaceous chondrites, which require a higher RH (~35-45%)

compared to iron meteorites (Allington-Jones, 2020), it is recommended that the target RH for the space remain within this window through the use of a dehumidifier (Figure 7.2), with corrosion controlled through the establishment of microclimates. Based on the findings of this review, it is recommended that anoxic storage environments be implemented within the collection. This is because maintaining RH at or below the necessary 11% through the use of silica gel desiccant alone requires more rigorous upkeep and monitoring. An appropriate oxygen scavenger, such as the RP-A agent, on the other hand, can be chosen to maintain low oxygen and RH levels for longer periods of time.

To address the most immediate needs of the collection, and assess the effectiveness of the microclimate technique, a pilot project was implemented following the inventory of the collection. This project employs Escal™ film and RP-A agent to isolate individual corroded meteorite specimens within anoxic and low RH environments and prevent further corrosion. An ideal, long-term solution to the problem of corroding in the Meteorite Collection requires a more holistic approach. Isolating each individual specimen within its own microclimate is not only time consuming, but limits access to these specimens, as to retrieve them requires breaking the seal of the Escal™ film, and subsequent replacement of the RP-A agent upon resealing. Additionally, specimens which are not experiencing active corrosion may be able to be safely stored at slightly higher RH (~19%). A more practical approach may be to separate the iron meteorites from the remainder of the collection in a separate environment where RH and/or oxygen levels more suitable for iron objects can be maintained. Suggestions include the use of a desiccator or nitrogen or other inert atmosphere cabinet, which would make the specimens more accessible than if stored within sealed Escal™ bags. This approach would require sufficient funding to acquire the cabinet, as well as a monitored storage space, to ensure safe levels of nitrogen or other gas such as argon are maintained (if an inert atmosphere cabinet is chosen). If this approach is not feasible, the Escal™/RP system could be employed throughout the entire collection.

6.5 Implementation

6.5.1 Materials List

The materials needed for the proposed pilot project are:

- Escal™ film
    - Available in 160mm, 240mm, 480mm, 1000mm x 100m rolls through Mitsubishi Gas Chemical
    - for purchase by the meter through CXD International (7.69-16.07 GPBP/meter)
- RP-A agent sachets
    - Available in 100ml, 300ml, 500ml, and 2000ml capacities in 40 packs of 25 sachets each (20 packs of 5 for 2000ml capacity) from Mitsubishi Gas Chemical
    - Available in individual packs of 25 sachets from CXD International (39.50-123.00 GBP)
    - Available in 40, 20, and individual packs of 25 from ConservationSupportSystems ($36.23 - $1051.50)
- Oxygen indicators
    - Pink/blue coloured oxygen indicator tablets available from Mitsubishi Gas Chemical in packages of 500
    - Oxygen indicator tablets and indicator eyes available from ConservationSupportSystems ($6.06-$7.48)
    - Oxygen meter should be considered if precise reading of oxygen levels is desired
        - E.g. MOCON OpTech-O2 Platinum oxygen meter
- Heat sealer and/or RP clips
    - Escal™/RP clips available from Mitsubishi Gas Chemical
    - Escal™/RP Clips available from CXD International (6.50 GBP)

- Meteorite Collection is already in possession of a heat-sealer which was found to be appropriate

6.5.2 Collection inventory

The first step in the implementation of the recommendations described above was a complete inventory of all iron and stony-iron meteorites in the University of Alberta collection, including polished and unpolished slices, epoxy mounts and thin sections, and completely or partially fusion crusted specimens. A list of samples was complied, and a visual examination of each sample was performed to determine whether corrosion was present on the sample surface, and to what extent.

Samples where advanced stages of active corrosion were present and significant enough to pose a threat to the physical integrity of the specimen were given a priority one rating (Figure 6.1). Such damage could include flaking, cracking, weeping, blistering, and delamination. Flaking and cracking were observed most often in this category, with several specimens (especially of the Whitecourt meteorite) showing evidence of blistering as well. In total, 42 specimens were placed in this category, requiring immediate intervention and treatment to prevent further damage. Samples where evidence of active corrosion was present, but not yet extensive enough to threaten sample integrity were given a priority two rating. This group includes specimens partially or completely covered in surface corrosion which has not yet progressed beyond this stage. In total 335 specimens were placed in this category. The third and final category included specimens with no signs of active corrosion. 43 specimens were placed in this category. These results are summarized in Table 6.1.

The large number of specimens in the priority one and two groups necessitated a way to prioritize treatment even among these groups. Group one was addressed first. Specimens from group one which have been in the collection for less than ten years were considered unstable, and were chosen for the treatment pilot project outlined below.

6.5.3 Project Plan

The University of Alberta Meteorite Collection is housed within a Class 1000 clean room (Figure 6.2), the curation conditions of which are outlined in (Herd et al., 2016). Prior to this study, all meteorites in this area were stored within stainless-steel geological specimen cabinets on Volara™-lined stainless-steel trays (Herd et al., 2016). Each specimen was enclosed within 2 polyethylene resealable bags, which were then placed within Volara™ lined friction-fit lidded plastic boxes (Herd et al., 2016). The relative humidity (RH) had originally been controlled using a small dehumidifier which had ceased to function some time ago. During this project, the dehumidifier was replaced and set to maintain the RH at or below 30%.

The specimens chosen for the pilot project were removed from their current storage location to be heat-sealed within an Escal™ film pouch cut to size and enclosed with RP-A sachets and an oxygen indicator to assess whether oxygen is present. They may be stored with or without protective the rigid plastic boxes they had previously been stored in, depending on the size the specimen once enclosed in Escal™. Several polished specimens whose faces were obscured by extensive surface corrosion were cleaned to expose their polished and/or etched surfaces prior to being enclosed in the Escal™ film. This was done by submerging the samples in CLR® (Calcium Limescale & Rust Remover) - a solution primarily composed of water, lactic acid, and gluconic acid – scrubbing the polished faces with a brush to remove the rust, sonicating the samples in water, and finally heating them to ~60°C for < 1 hour to dryness. This process is outlined in Figure 6.3. Specimens in the pilot project are planned to be monitored for at least one year following enclosure to verify the effectiveness of the technique at halting corrosion.

To determine the effectiveness of the chosen treatment plan, a direct comparison with an untreated specimen is necessary. For this, two polished slices taken from the same stone of the Pinawa meteorite and prepared at the same time by the same methods are used to directly compare the effects of the microclimate storage against those of storage at ambient conditions. One of the specimens was

sealed as described above, with the other stored unsealed as before, both within the collection clean room storage facility (Figure 6.4). The RH of the space will be continually monitored, with a dehumidifier used to maintain it at or below 30%. The condition of these slices will be assessed periodically to determine whether any new or worsening corrosion has occurred. The result of this monitoring will be used to determine what measures may be put in place for other iron-based meteorites in the collection.

6.8 Preliminary Results

The treated samples were placed into storage on August 2, 2022. The first evaluation of the stored Pinawa samples was completed on October 3, 2022. Few changes to the overall appearance of either sample occurred after 2 months in storage, with only moderate amounts of pre-existing surface rust on the underside of both samples, and a small amount of surface rusting on the face of the unsealed sample. However, the bag holding the unsealed sample of Pinawa has been slightly discoloured by a small amount of surface rust which has rubbed off of the sample and onto the interior of the bag. No such stain was observed on the sealed sample. The second, more recent evaluation of the stored samples was completed on January 6, 2023. At the time of this examination, a small amount of surface rust had appeared on the sealed sample. No noticeable changes had occurred to the unsealed sample. It is likely that rusting in the winter months is slow because the RH of the surrounding atmosphere is low. Rusting may accelerate in the summer months when RH is generally higher. Sample monitoring should be continued periodically during this time. The conditions of each of the samples at each evaluation are shown in Figure 6.5.

6.9 Conclusions

The conservation and treatment methods of iron meteorites outlined above are paramount to ensuring that iron-based materials remain intact for the foreseeable future for the purposes of display

as well as scientific research. It is inevitable that iron-based specimens will deteriorate over time; however, this eventuality can be delayed indefinitely with proper care and storage measures.

The potential success of the pilot project measures outlined above over a year of monitoring is expected to reinforce the theory that anoxic storage conditions are beneficial in the conservation of iron meteorites. Assuming this is the case, two options for long-term anoxic storage of the entire body of iron and stony-iron meteorites within the UAlberta collection are proposed:

1. Enclosure of all specimens individually within Escal™ film with RP-A agent.
2. Storage of all specimens in an inert atmosphere cabinet.

These measures will ensure that the University of Alberta Meteorite Collection can maintain and grow the abundance of valuable iron-based samples it contains for many years to come.

6.10 Tables

Table 6.1: Number of specimens in each condition category

Condition	Number of Specimens
Priority 1, unstable	33
Priority 1, total	42
Priority 2	335
Priority 3	43

6.11 Figure Captions

Figure 6.1: Examples of highly corroded iron meteorites from the University of Alberta Meteorite Collection. Top: Aletai (MET11840/2); Bottom left: Campo del Cielo (MET11610/4-1); Bottom right: Whitecourt (MET11617/401).

Figure 6.2: University of Alberta Meteorite Collection clean room.

Figure 6.3: Steps in the treatment process for iron meteorites in the Ualberta Meteorite Collection.

Figure 6.4: Top: Two slices of the meteorite Pinawa prepared for storage using old (MET11756/4; left) and new (rMET11756/3; right) curation procedures. Bottom: The storage location of these slices within the collection storage space.

Figure 6.4: Changes observed in the Pinawa samples (left: MET11756/4; right: MET11756/3) over the monitoring period. The unsealed sample is shown on the left, the sealed sample on the right.

6.12 Figures

Figure 6.1

Figure 6.2

Figure 6.3

Survey and Select

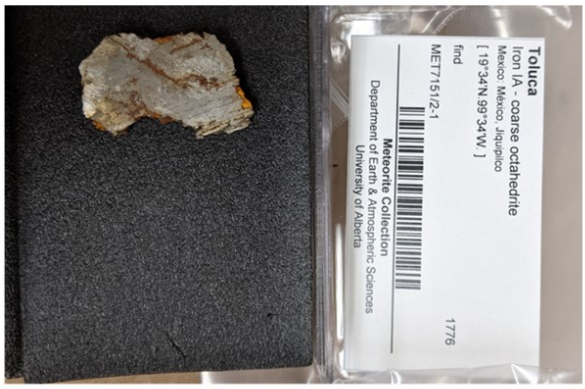

Clean with CLR (polished specimens only)

Package and Store

Figure 6.4


Pinawa
IAB-MG iron
Canada: Manitoba
[50° 12.746'N, 95° 57.058'W]
find
MET11756/4
Meteorite collection
Oxy/Eye
DO NOT EAT
RP
Agent
DO NOT OPEN
DO NOT EAT
MITSUBISHI GAS CHEMICAL
RPSystem™
Oxygen Absorbent Without Affecting Moisture
0 cm 1 2 3 4 5 6 7
UNIVERSITY OF ALBERTA
EDMONTON·ALBERTA·CANADA
Department of Earth & Atmospheric Sciences

Figure 6.5

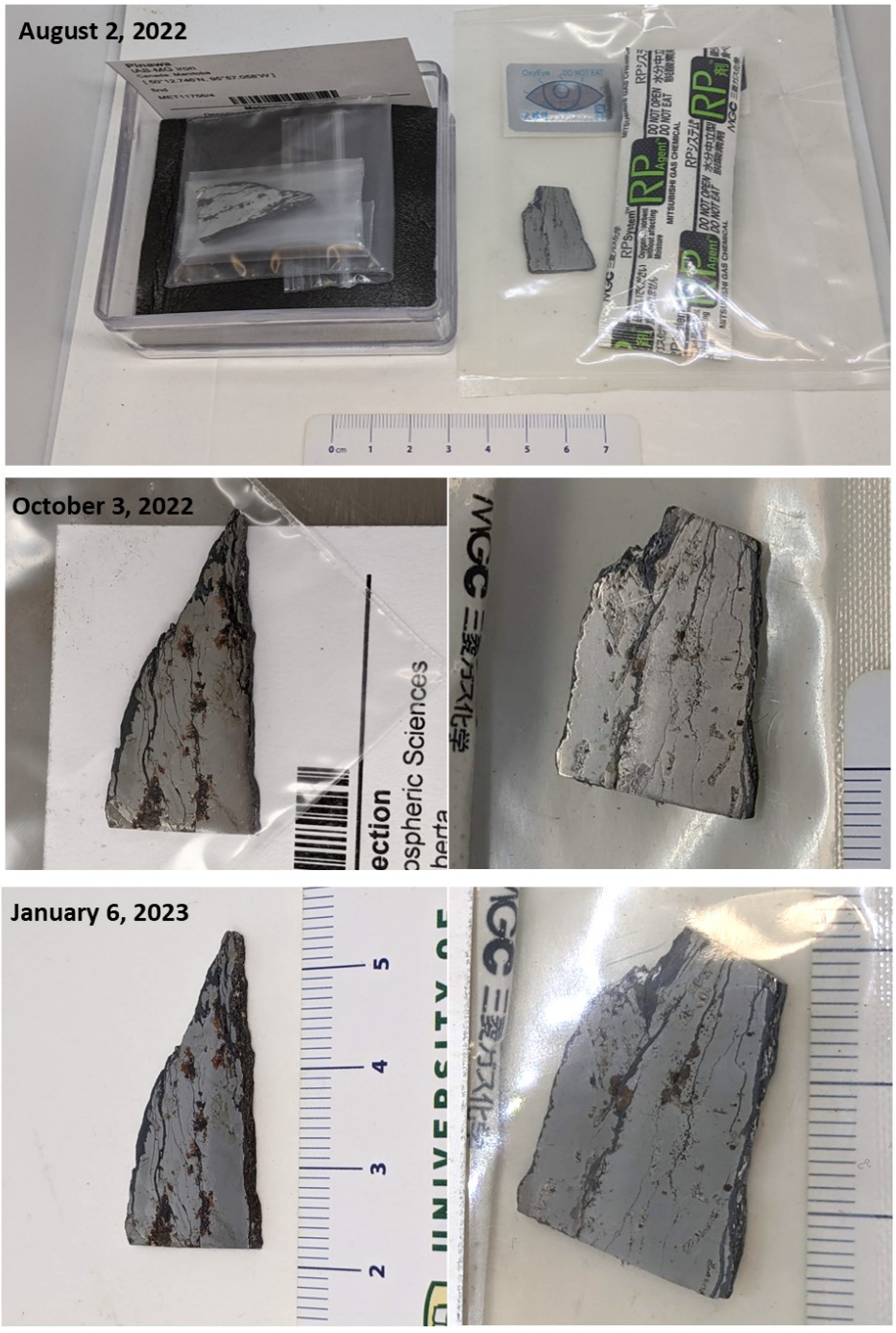

Chapter 7: Thesis Conclusions and Future Work

7.1 Conclusions and Implications

The study of the sulfur-bearing species within Tagish Lake, Aguas Zarcas, and Tarda, as well as the effects of storage conditions of both stony and iron meteorites have revealed much regarding the intrinsic nature of these materials, as well as how they may be altered by improper storage and handling, including:

- C2 chondrites such as those examined during this study typically contain two distinct generations of Fe-Ni sulfide. The first generation likely formed between ~500-600°C during chondrule formation from the cooling of an MSS melt, with or without exsolution of pentlandite from pyrrhotite. The second generation likely formed between ~25-135°C during aqueous alteration by one or more deposition events from an altering fluid

- The Fe/S ratios of low-Ni pyrrhotite within the carbonaceous chondrites examined can be used to place them in a relative order of degree of aqueous alteration. This order is CM2 (Schrader et al., 2021) < Aguas Zarcas (Schrader et al., 2021) < CM1/2 (Schrader et al., 2021) < Aguas Zarcas (Chapter 3) < TL (Holt and Herd, 2022; Chapter 2) < Tarda (Chapter 4) < CI (Schrader et al., 2021).

- Tagish Lake sample 8a has a relative degree of aqueous alteration comparable to that of samples TL 11h and TL 5b.

- To date, organosulfur species have only been observed in the Tagish Lake sample TL 8a (Pizzarello et al., 2001) in the form of MSA. MSA was not observed in any of the samples analysed during this study. While this could be the result of lithologic differences between samples, it is also possible that any MSA which was initially present in these samples may have deteriorated in storage, or been lost during extraction by oxidation to sulfate, or during previous GC-MS analyses when no derivatizing agent was

used. It is also quite conceivable that the MSA found by Pizzarello et al., (2001) is a terrestrial contaminant, since MSA is produced in large quantities worldwide.

- To ensure optimum preservation of organic species and volatiles within extra-terrestrial materials, meteorites and samples collected during return missions should be collected and stored within sealed vessels, preferably in inert atmospheres.

- Any analysis which modifies the form of the sample such as chemical extraction has the potential to alter its intrinsic properties, as is the case with the growth of new gypsum crystals following hot water extraction in the residue of sample TL 11h. Therefore, proper order of analysis should be carefully considered when planning projects to minimize the effects of changes caused by previous analyses on future analytical results. This is vital to ensure that a minimum amount of sample will be consumed over successive analyses, a necessity for studies involving future sample return missions, where a limited amount of material will be available for study. When such analyses are unavoidable, careful records should be kept on sample history to ensure the origin of any alterations can be traced.

- Even more robust types of meteorites such as iron meteorites are susceptible to alteration and deterioration once exposed to Earth's surface. To control and limit this deterioration, storage in an anoxic, low RH environment is ideal.

7.2 Future Work

To determine whether oxidation of MSA may have resulted in the formation of gypsum crystals following the hot water extraction of sample TL 11h, the source of the sulfur in these crystals must be determined. Isotopic analyses of these gypsum crystals, as well as the S-bearing components within both the leached TL 11h residue and a fresh, non-leached sample of TL1 are planned to elucidate this source. The S isotopic composition of the various S-bearing components will be determined by performing a bulk chemical extraction according to the procedures of Labidi et al. (2017) to measure ^{32}S,

^{33}S, ^{34}S, and ^{36}S and determine the isotopic ratios of Fe-Ni sulfides, elemental sulfur, and any sulfate that may be present in both samples. These analyses should reveal any nucleosynthetic anomalies in ^{33}S and ^{36}S (Gao and Thiemens, 1993), as well as depletion or enrichment in light or heavy S isotopes in a particular phase.

The corresponding ratios of each S-bearing phase will be compared between the leached and unleached samples. If one particular component is found to be relatively enriched in heavy isotopes in the leached powder compared to the unleached powder, this implies it is the source of sulfur in the gypsum grains, as these grains would scavenge the lighter isotopes of sulfur, leaving the remaining phase from which the sulfur was sourced relatively enriched in heavy isotopes. Therefore, these gypsum grains should also have a lighter isotopic composition than the component from which they scavenged the sulfur in the leached powder. Since the temperature of formation of the terrestrial sulfates is known – the leaching with hot water occurred at 100°C – it should be possible to determine the mass dependent fractionation which would have occurred at this temperature and use the measured composition of the sulfate grains to back-calculate what the initial isotopic composition of the S-source should be. This value can be compared to those found for the components in the unleached sample. If the isotopic compositions of each of the examined components remain relatively unchanged between the leached and unleached powders, then it is possible that the source of S in the post-extraction gypsum crystals may have been from organosulfur compounds, such as MSA, or other S-bearing species present in the initial sample.

Finally, the gypsum grains should have inherited any mass-independent fractionation (MIF) signal which may have been present in their precursor phase. The presence of a MIF signal ($\Delta^{33}S$ and $\Delta^{36}S$) should be examined in each component of the unleached TL powder and compared to that of the sulfate grains to determine whether the S in the sulfate was sourced primarily from sulfides or S^0 (Labidi et al., 2017). If The MIF signal in the post-extraction gypsum grains does not match either the sulfide or

S^0 signals from the unleached powder, the most likely source of sulfur in these grains is any organosulfur compounds which may have been present in the initial sample prior to leaching.

Bibliography

Airieau, S. A., Farquhar, J., Thiemens, M. H., Leshin, L. A., Bao, H., & Young, E. (2005). Planetesimal sulfate and aqueous alteration in CM and CI carbonaceous chondrites. *Geochimica et Cosmochimica Acta*, *69*(16), 4167–4172. https://doi.org/10.1016/j.gca.2005.01.029

Alexander, C. M. O., Bowden, R., Fogel, M. L., Howard, K. T., Herd, C. D. K., & Nittler, L. R. (2012). The Provenances of Asteroids, and Their Contributions to the Volatile Inventories of the Terrestrial Planets. *Science*, *337*(6095), 721–723. https://doi.org/10.1126/science.1223474

Alexander, C. M. O., Howard, K. T., Bowden, R., & Fogel, M. L. (2013). The classification of CM and CR chondrites using bulk H, C and N abundances and isotopic compositions. *Geochimica et Cosmochimica Acta*, *123*, 244–260. https://doi.org/10.1016/j.gca.2013.05.019

Allen, C., Allton, J., Lofgren, G., Righter, K., & Zolensky, M. (2011). Curating NASA's extraterrestrial samples—Past, present, and future. *Chemie Der Erde-Geochemistry*, *71*, 1–20. https://doi.org/10.1016/j.chemer.2010.12.003

Allington-Jones, L. (2020). Weep no more: Conservation of an iron-nickel meteorite from Canyon Diablo, Arizona. *Journal of Natural Science Collections*, 83–91.

Aponte, J. C., McLain, H. L., Simkus, D. N., Elsila, J. E., Glavin, D. P., Parker, E. T., Dworkin, J. P., Hill, D. H., Connolly, H. C., & Lauretta, D. S. (2020). Extraterrestrial organic compounds and cyanide in the CM2 carbonaceous chondrites Aguas Zarcas and Murchison. *Meteoritics & Planetary Science*, *55*(7), 1509–1524. https://doi.org/10.1111/maps.13531

Baker, L., Franchi, I. A., Wright, I. P., & Pillinger, C. T. (2002). The oxygen isotopic composition of water from Tagish Lake: Its relationship to low-temperature phases and to other carbonaceous chondrites. *Meteoritics & Planetary Science*, *37*(7), 977–985. https://doi.org/10.1111/j.1945-5100.2002.tb00870.x

Barshay S. S. and Lewis I. S. 1976. Chemistry of primitive solar material. *Annual Review of Astronomy and Astrophysics 14*, 81–94.

Barth, M. I. F., Harries, D., Langenhorst, F., & Hoppe, P. (2018). Sulfide–oxide assemblages in Acfer 094—Clues to nebular metal–gas interactions. *Meteoritics & Planetary Science*, *53*(2), 187–203. https://doi.org/10.1111/maps.12992

Benedix, G. K., Lauretta, D. S., & McCoy, T. J. (2005). Thermodynamic constraints on the formation conditions of winonaites and silicate-bearing IAB irons. *Geochimica et Cosmochimica Acta*, *69*(21), 5123–5131. https://doi.org/10.1016/j.gca.2005.03.048

Berger, E. L., Lauretta, D. S., Zega, T. J., & Keller, L. P. (2016). Heterogeneous histories of Ni-bearing pyrrhotite and pentlandite grains in the CI chondrites Orgueil and Alais. *Meteoritics & Planetary Science*, *51*(10), 1813–1829. https://doi.org/10.1111/maps.12721

Bland, P. A., Cressey, G., & Menzies, O. N. (2004). Modal mineralogy of carbonaceous chondrites by X-ray diffraction and Mossbauer spectroscopy. *Meteoritics & Planetary Science*, *39*(1), 3–16. https://doi.org/10.1111/j.1945-5100.2004.tb00046.x

Bland, P., Smith, T., Jull, A., Berry, F., Bevan, A., Cloudt, S., & Pillinger, C. (1996). The flux of meteorites to the Earth over the last 50,000 years. *Monthly Notices of the Royal Astronomical Society*, *283*, 551–565.

Blinova, A. I., Zega, T. J., Herd, C. D. K., & Stroud, R. M. (2014a). Testing variations within the Tagish Lake meteorite-I: Mineralogy and petrology of pristine samples. *Meteoritics & Planetary Science*, *49*(4), 473–502. https://doi.org/10.1111/maps.12271

Blinova, A. I., Herd, C. D. K., & Duke, M. J. M. (2014b). Testing variations within the Tagish Lake meteorite-II: Whole-rock geochemistry of pristine samples. *Meteoritics & Planetary Science*, *49*(6), 1100–1118. https://doi.org/10.1111/maps.12303

Boctor, N. Z., Kurat, G., & Alexander, C. M. O. D. (2003). Sulfide-Oxide Assemblage in Tagish Lake Carbonaceous Chondrite. *34th Lunar and Planetary Science Conference*, abstract no. 1705. http://adsabs.harvard.edu/abs/2003LPI....34.1705B

Boctor, Nabil Z., Kurat, G., Alexander, C. M. O., & Prewitt, C. T. (2002). Sulfide Mineral Assemblages in Boriskino CM Chondrite. *33rd Lunar and Planetary Science Conference*, abstract no. 1534.

Bose, M., Root, R. A., & Pizzarello, S. (2017). A XANES and Raman investigation of sulfur speciation and structural order in Murchison and Allende meteorites. *Meteoritics & Planetary Science*, *52*(3), 546–559. https://doi.org/10.1111/maps.12811

Brandon, A. D., Humayun, M., Puchtel, I. S., & Zolensky, M. E. (2005). Re-Os isotopic systematics and platinum group element composition of the Tagish Lake carbonaceous chondrite. *Geochimica Et Cosmochimica Acta*, *69*(6), 1619–1631. https://doi.org/10.1016/j.gca.2004.10.005

Brearley A. J. (2006) The action of water. In *Meteorites and the Early Solar System II* (eds. D. S. Lauretta and H. Y. McSween). University of Arizona Press, Tucson, pp. 584–624.

Brearley, A. J., & Martinez, C. (2010). Ubiquitous Exsolution of Pentlandite and Troilite in Pyrrhotite from the TIL 91722 CM2 Carbonaceous Chondrite: A Record of Low Temperature Solid State Processes. *41st Lunar and Planetary Science Conference*, abstract no. 1689.

Brearley, A. J., & Martinez, C. (2010). *Ubiquitous Exsolution of Pentlandite and Troilite in Pyrrhotite from the TIL 91722 CM2 Carbonaceous Chondrite: A Record of Low Temperature Solid State Processes*. *41st*

Lunar and Planetary Science Conference, Abstract no. 11689.

https://www.lpi.usra.edu/meetings/lpsc2010/pdf/1689.pdf

Brown, P. G., Hildebrand, A. R., Zolensky, M. E., Grady, M., Clayton, R. N., Mayeda, T. K., Tagliaferri, E., Spalding, R., MacRae, N. D., Hoffman, E. L., Mittlefehldt, D. W., Wacker, J. F., Bird, J. A., Campbell, M. D., Carpenter, R., Gingerich, H., Glatiotis, M., Greiner, E., Mazur, M. J., McCausland, P. JA., Plotkin, H., Mazur, T. R. (2000). The fall, recovery, orbit, and composition of the Tagish Lake meteorite: A new type of carbonaceous chondrite. *Science*, *290*(5490), 320–325. https://doi.org/10.1126/science.290.5490.320

Brown, P. G., ReVelle, D. O., Tagliaferri, E., & Hildebrand, A. R. (2002). An entry model for the Tagish Lake fireball using seismic, satellite and infrasound records. *Meteoritics & Planetary Science*, *37*(5), 661–675. https://doi.org/10.1111/j.1945-5100.2002.tb00846.x

Bullock, E. S., Gounelle, M., Lauretta, D. S., Grady, M. M., & Russell, S. S. (2005a). Mineralogy and texture of Fe-Ni sulfides in CI1 chondrites: Clues to the extent of aqueous alteration on the CI1 parent body. *Geochimica Et Cosmochimica Acta*, *69*(10), 2687–2700. https://doi.org/10.1016/j.gca.2005.01.003

Bullock, E. S., Grady, M. M., Russell, S. S., & Gounelle, M., (2005b). Fe-Ni Sulphides Within a CM1 Clast in Tagish Lake. *36th Lunar and Planetary Science Conference,* abstract no.1883.

Bullock, E. S., McKeegan, K. D., Gounelle, M., Grady, M. M., & Russell, S. S. (2010). Sulfur isotopic composition of Fe-Ni sulfide grains in CI and CM carbonaceous chondrites. *Meteoritics & Planetary Science*, *45*(5), 885–898. https://doi.org/10.1111/j.1945-5100.2010.01052.x

Burgess, R., Wright, I. P., & Pillinger, C. T. (1991). Determination of sulphur-bearing components in C1 and C2 carbonaceous chondrites by stepped combustion. *Meteoritics*, *26*(1), 55–64. https://doi.org/10.1111/j.1945-5100.1991.tb01015.x

Busemann, H., Young, A. F., Alexander, C. M. O., Hoppe, P., Mukhopadhyay, S., & Nittler, L. R. (2006). Interstellar chemistry recorded in organic matter from primitive meteorites. *Science*, *312*(5774), 727–730. https://doi.org/10.1126/science.1123878

Chennaoui Aoudjehane, H., Agee, C. B., Ziegler, K., Garvie, L. A. J., Irving, A., Sheikh, D., Carpenter, P. K., Zolensky, M., Schmitt-Kopplin, P., & Trif, L. (2021). Tarda (C2-Ung): A New and Unusual Carbonaceous Chondrite Meteorite Fall from Morocco. *52nd Lunar and Planetary Science Conference*, Abstract no. 1928. https://www.hou.usra.edu/meetings/lpsc2021/pdf/1928.pdf

Chyba, C., & Sagan, C. (1992). Endogenous production, exogenous delivery and impact-shock synthesis of organic molecules: An inventory for the origins of life. *Nature*, *355*(6356), Article 6356. https://doi.org/10.1038/355125a0

Clayton, R. N., & Mayeda, T. K. (2001). Oxygen Isotopic Composition of the Tagish Lake Carbonaceous Chondrite. *32nd Lunar and Planetary Science Conference*, abstract no. 1885. http://adsabs.harvard.edu/abs/2001LPI....32.1885C

Cooper, G. W., Onwo, W. M., & Cronin, J. R. (1992). Alkyl phosphonic acids and sulfonic acids in the Murchison meteorite. *Geochimica et Cosmochimica Acta*, *56*(11), 4109–4115. https://doi.org/10.1016/0016-7037(92)90023-C

Craig J. R. 1973. Pyrite-pentlandite assemblages and other low temperature relations in the Fe-Ni-S system. *American Journal of Science* 273-A:496–510.

Davidson, J., Alexander, C. M. O., Bates, H. C., King, A. J., Foustoukos, D. I., Schrader, D. L., Bullock, E. S., Greenwood, R. C., Busemann, H., Morino, P., Riebe, M. E. I., Rüfenacht, M., Schönbächler, M., & Clay, P. (2020). Coordinated Studies of Samples Relevant for Carbonaceous Asteroid Sample Return: CM

Chondrites Aguas Zarcas and Meteorite Hills 00639. *51st Lunar and Planetary Science Conference*, Abstract no. 1623. http://www.lpi.usra.edu/meetings/lpsc2020/pdf/1623.pdf

Degrigny, C. (2010). Use of electrochemical techniques for the conservation of metal artefacts: A review. *Journal of Solid State Electrochemistry*, *14*(3), 353–361. https://doi.org/10.1007/s10008-009-0896-0

Dey, S., Yin, Q.-Z., & Zolensky, M. (2021). Exploring the Planetary Genealogy of Tarda—A Unique New Carbonaceous Chondrite. *52nd Lunar and Planetary Science Conference*, Abstract no. 2517. https://www.hou.usra.edu/meetings/lpsc2021/pdf/2517.pdf

Dreibus, G., Palme, H., Spettel, B., Zipfel, J., & Wanke, H. (1995). Sulfur and Selenium in Chondritic Meteorites. *Meteoritics*, *30*(4), 439–445. https://doi.org/10.1111/j.1945-5100.1995.tb01150.x

Drews, M. J., González-Pereyra, N. G., Mardikian, P., & Viviés, P. de. (2013). The application of subcritical fluids for the stabilization of marine archaeological iron. *Studies in Conservation*, *58*(4), 314–325. https://doi.org/10.1179/2047058412Y.0000000079

Durazzo, A., & Taylor, L. (1982). Exsolution in the Mss-Pentlandite System—Textural and Genetic-Implications for Ni-Sulfide Ores. *Mineralium Deposita*, *17*(3), 313–332.

Etschmann, B., Pring, A., Putnis, A., Grguric, B. A., & Studer, A. (2004). A kinetic study of the exsolution of pentlandite (Ni, $Fe)_9S_8$ from the monosulfide solid solution (Fe, Ni)S. *American Mineralogist*, *89*(1), 39–50. https://doi.org/10.2138/am-2004-0106

Farquhar, J., Savarino, J., Jackson, T. L., & Thiemens, M. H. (2000). Evidence of atmospheric sulphur in the martian regolith from sulphur isotopes in meteorites. *Nature*, *404*(6773), 50–52. https://doi.org/10.1038/35003517

Fegley, B., Jr., Lauretta, S. D., & Kremser, T. D. (1995). *The origin of troilite and pyrrhotite in chondrites: I. Iron sulfide formation kinetics in H_2S-H_2 gas mixtures. 20th Symposium on Antarctic Meteorites*, 59–62.

Gao, X., & Thiemens, M. H. (1993). Isotopic composition and concentration of sulfur in carbonaceous chondrites. *Geochimica et Cosmochimica Acta*, *57*(13), 3159–3169. https://doi.org/10.1016/0016-7037(93)90300-L

Genge, M. J., & Grady, M. M. (1999). The fusion crusts of stony meteorites: Implications for the atmospheric reprocessing of extraterrestrial materials. *Meteoritics & Planetary Science*, *34*(3), 341–356. https://doi.org/10.1111/j.1945-5100.1999.tb01344.x

Gilmour, C. M., Herd, C. D. K., & Beck, P. (2019). Water abundance in the Tagish Lake meteorite from TGA and IR spectroscopy: Evaluation of aqueous alteration. *Meteoritics & Planetary Science*, *54*(9), 1951–1972. https://doi.org/10.1111/maps.13362

Glavin, D. P., Elsila, J. E., Burton, A. S., Callahan, M. P., Dworkin, J. P., Hilts, R. W., & Herd, C. D. K. (2012). Unusual nonterrestrial L-proteinogenic amino acid excesses in the Tagish Lake meteorite. *Meteoritics & Planetary Science*, *47*(8), 1347–1364. https://doi.org/10.1111/j.1945-5100.2012.01400.x

Godlevskiy M. N., Likhachev A. P., Chuvikina N. G., and Andronov A. D. (1971) Hydrothermal synthesis of pentlandite. *Dokl. Akad. Nauk. SSSR* 196, 146-149.

González, N. G., Mardikian, P., Näsänen, L., & Drews, M. J. (2013). *The use of subcritical fluids for the stabilisation of archaeological iron: An overview*. Woodhead Publishing. https://doi.org/10.1533/9781782421573.5.434

Grady, M. M., Verchovsky, A. B., Franchi, I. A., Wright, I. P., & Pillinger, C. T. (2002a). Light element geochemistry of the Tagish Lake CI2 chondrite: Comparison with CI1 and CM2 meteorites. *Meteoritics & Planetary Science*, *37*(5), 713–735. https://doi.org/10.1111/j.1945-5100.2002.tb00851.x

Greshake, A., Krot, A. N., Flynn, G. J., & Keil, K. (2005). Fine-grained dust rims in the Tagish Lake carbonaceous chondrite: Evidence for parent body alteration. *Meteoritics & Planetary Science*, *40*(9–10), 1413–1431. https://doi.org/10.1111/j.1945-5100.2005.tb00410.x

Grossman L. and Larimer J. W. 1974. Early chemical history of the solar system. *Reviews of Geophysics and Space Physics, 12*, 71–103.

Harries, D., & Langenhorst, F. (2013). The nanoscale mineralogy of Fe,Ni sulfides in pristine and metamorphosed CM and CM/CI-like chondrites: Tapping a petrogenetic record. *Meteoritics & Planetary Science*, *48*(5), 879–903. https://doi.org/10.1111/maps.12089

Herd, C. D. K., Blinova, A., Simkus, D. N., Huang, Y., Tarozo, R., Alexander, C. M. O., Gyngard, F., Nittler, L. R., Cody, G. D., Fogel, M. L., Kebukawa, Y., Kilcoyne, A. L. D., Hilts, R. W., Slater, G. F., Glavin, D. P., Dworkin, J. P., Callahan, M. P., Elsila, J. E., De Gregorio, B. T., & Stroud, R. M. (2011). Origin and Evolution of Prebiotic Organic Matter As Inferred from the Tagish Lake Meteorite. *Science*, *332*(6035), 1304–1307. https://doi.org/10.1126/science.1203290

Herd, C. D. K., Hilts, R. W., Skelhorne, A. W., & Simkus, D. N. (2016). Cold curation of pristine astromaterials: Insights from the Tagish Lake meteorite. *Meteoritics & Planetary Science*, *51*(3), 499–519. https://doi.org/10.1111/maps.12603

Herndon J. M., Rowe M. W., Larson E. E., and Watson D. E. (1975) Origin of magnetite and pyrrhotite in carbonaceous chondrites. *Nature, 253*, 516–518.

Hewins, R. H., Bourot-Denise, M., Zanda, B., Leroux, H., Barrat, J.-A., Humayun, M., Goepel, C., Greenwood, R. C., Franchi, I. A., Pont, S., Lorand, J.-P., Cournede, C., Gattacceca, J., Rochette, P., Kuga, M., Marrocchi, Y., & Marty, B. (2014). The Paris meteorite, the least altered CM chondrite so far. *Geochimica Et Cosmochimica Acta*, *124*, 190–222. https://doi.org/10.1016/j.gca.2013.09.014

Hildebrand, A. R., McCausland, P. J. A., Brown, P. G., Longstaffe, F. J., Russell, S. D. J., Tagliaferrii, E., Wacker, J. F., & Mazur, M. J. (2006). The fall and recovery of the Tagish Lake meteorite. *Meteoritics & Planetary Science*, *41*(3), 407–431. https://doi.org/10.1111/j.1945-5100.2006.tb00471.x

Hilts, R. W., Herd, C. D. K., Simkus, D. N., & Slater, G. F. (2014). Soluble organic compounds in the Tagish Lake meteorite. *Meteoritics & Planetary Science*, *49*(4), 526–549. https://doi.org/10.1111/maps.12272

Holt, M. C., & Herd, C. D. K. (2022). Fe-Ni sulfides in Tagish Lake: Implications for nebular and parent body conditions of formation. *Meteoritics & Planetary Science*, *57*(6), 1267–1287. https://doi.org/10.1111/maps.13819

Howard, K. T., Alexander, C. M. O., Schrader, D. L., & Dyl, K. A. (2015). Classification of hydrous meteorites (CR, CM and C2 ungrouped) by phyllosilicate fraction: PSD-XRD modal mineralogy and planetesimal environments. *Geochimica et Cosmochimica Acta*, *149*, 206–222. https://doi.org/10.1016/j.gca.2014.10.025

Huss, G. R., Meshik, A. P., Smith, J. B., & Hohenberg, C. M. (2003). Presolar diamond, silicon carbide, and graphite in carbonaceous chondrites: Implications for thermal processing in the solar nebula. *Geochimica et Cosmochimica Acta*, *67*(24), 4823–4848. https://doi.org/10.1016/j.gca.2003.07.019

Isaksson, E., Kekonen, T., Moore, J., & Mulvaney, R. (2005). The methanesulfonic acid (MSA) record in a Svalbard ice core. *Annals of Glaciology, 42*, 345-351. doi:10.3189/172756405781812637

Izawa, M. R. M., Flemming, R. L., King, P. L., Peterson, R. C., & McCausland, P. J. A. (2010). Mineralogical and spectroscopic investigation of the Tagish Lake carbonaceous chondrite by X-ray diffraction and infrared reflectance spectroscopy. *Meteoritics & Planetary Science*, *45*(4), 675–698. https://doi.org/10.1111/j.1945-5100.2010.01043.x

Kaplan, I. R., & Hulston, J. R. (1966). The isotopic abundance and content of sulfur in meteorites. *Geochimica et Cosmochimica Acta*, *30*(5), 479–496. https://doi.org/10.1016/0016-7037(66)90059-7

Keene, S. (1993). *Real-time survival rates for treatments of archaeological iron.* Getty Conservation Institute.

Keller, L. P., & Flynn, G. J. (2001). Matrix Mineralogy of the Tagish Lake Carbonaceous Chondrite: TEM and FTIR Studies. *32nd Lunar and Planetary Science Conference,* Abstract no. 1639. http://adsabs.harvard.edu/abs/2001LPI....32.1639K

Kergourlay, F., Rémazeilles, C., Neff, D., Foy, E., Conforto, E., Guilminot, E., Reguer, S., Dillmann, Ph., Nicot, F., Mielcarek, F., Rebière, J., & Refait, Ph. (2011). Mechanisms of the dechlorination of iron archaeological artefacts extracted from seawater. *Corrosion Science*, *53*(8), 2474–2483. https://doi.org/10.1016/j.corsci.2011.04.003

Kerraouch, I., Bischoff, A., Zolensky, M. E., Pack, A., Patzek, M., Hanna, R. D., Fries, M. D., Harries, D., Kebukawa, Y., Le, L., Ito, M., & Rahman, Z. (2021a). The polymict carbonaceous breccia Aguas Zarcas: A potential analog to samples being returned by the OSIRIS-REx and Hayabusa2 missions. *Meteoritics & Planetary Science*, *56*(2), 277–310. https://doi.org/10.1111/maps.13620

Kerraouch, I., Bischoff, A., Zolensky, M. E., Hellmann, J. L., Woefer, E., King, A. J., Patzek, M., Marrocchi, Y., Pack, A., Ludwig, T., & Trieloff, M. (2021b). The Metal-Rich Lithology Within the Aguas Zarcas Breccia:

characterization, Origin, and Evolution. *84th Annual Meeting of the Meteoritical Society*, LPI Contribution No. 2609, id.6201

Kerraouch, I., Bischoff, A., Zolensky, M. E., Pack, A., Patzek, M., Wölfer1, E., Burkhardt, C., & Fries, M. (2020). Characteristics of a New Carbonaceous, Metal-Rich Lithology Found in the Carbonaceous Chondrite Breccia Aguas Zarcas. *51st Lunar and Planetary Science Conference,* Abstract no. 2011

Kimura, M., Grossman, J. N., & Weisberg, M. K. (2011). Fe-Ni metal and sulfide minerals in CM chondrites: An indicator for thermal history. *Meteoritics & Planetary Science*, *46*(3), 431–442. https://doi.org/10.1111/j.1945-5100.2010.01164.x

Kitakaze, A., Sugaki, A., Itoh, H., & Komatsu, R. (2011). A Revision of Phase Relations in the System Fe-Ni-S From 650 Degrees to 450 degrees C. *Canadian Mineralogist*, *49*(6), 1687–1710. https://doi.org/10.3749/canmin.49.6.1687

Kminek, G., Botta, O., Glavin, D. P., & Bada, J. L. (2002). Amino acids in the Tagish Lake meteorite. *Meteoritics & Planetary Science*, *37*(5), 697–701. https://doi.org/10.1111/j.1945-5100.2002.tb00849.x

Kosyakov V. I., Sinyakova E. F. and Shestakov V. A. (2003). Dependence of sulfur fugacity on the composition of phase associations in the Fe–FeS–NiS–Ni system at 873 K. *Geochem. Int. 7*, 660–669.

Krot, A. N., Hutcheon, I. D., Yurimoto, H., Cuzzi, J. N., McKeegan, K. D., Scott, E. R. D., Libourel, G., Chaussidon, M., Aleon, J., & Petaev, M. I. (2005). Evolution of oxygen isotopic composition in the inner solar nebula. *Astrophysical Journal*, *622*(2), 1333–1342. https://doi.org/10.1086/428382

Krot, A. N., Meibom, A., Weisberg, M. K., & Keil, K. (2002). The CR chondrite clan: Implications for early solar system processes. *Meteoritics & Planetary Science*, *37*(11), 1451–1490. https://doi.org/10.1111/j.1945-5100.2002.tb00805.x

Labidi, J., Farquhar, J., Alexander, C. M. O., Eldridge, D. L., & Oduro, H. (2017). Mass independent sulfur isotope signatures in CMs: Implications for sulfur chemistry in the early solar system. *Geochimica et Cosmochimica Acta*, *196*, 326–350. https://doi.org/10.1016/j.gca.2016.09.036

Lauretta, D. (2005). Sulfidation of an Iron–Nickel–Chromium–Cobalt– Phosphorus Alloy in 1% H_2S–H_2 Gas Mixtures at 400–1000°C. *Oxidation of Metals*, *64*, 1–22. https://doi.org/10.1007/s11085-005-5703-4

Lauretta, D. S., Kremser, D. T., & Fegley, B. (1996a). The rate of iron sulfide formation in the solar nebula. *Icarus*, *122*(2), 288–315. https://doi.org/10.1006/icar.1996.0126

Lauretta, D. S., Lodders, K., & Fegley, B. (1997). Experimental simulations of sulfide formation in the solar nebula. *Science*, *277*(5324), 358–360. https://doi.org/10.1126/science.277.5324.358

Lauretta, D. S., Lodders, K., & Fegley, B. (1998). Kamacite sulfurization in the solar nebula. *Meteoritics & Planetary Science*, *33*(4), 821–833. https://doi.org/10.1111/j.1945-5100.1998.tb01689.x

Lauretta, Dante S., Fegley, B., Jr., Lodders, K., & Kremser, D. T. (1996b). The kinetics and mechanism of iron sulfide formation in the solar nebula. *Antarctic Meteorite Research*, *9*, 111.

Lauretta, Dante S., Kremser, D. T., & Fegley, B., Jr. (1996c). A comparative study of experimental and meteoritic metal-sulfide assemblages. *Antarctic Meteorite Research*, *9*, 97.

Lee, M. (1993). The Petrography, Mineralogy and Origins of Calcium-Sulfate Within the Cold Bokkeveld Cm Carbonaceous Chondrite. *Meteoritics*, *28*(1), 53–62. https://doi.org/10.1111/j.1945-5100.1993.tb00248.x

Lodders, K. (2003). Solar system abundances and condensation temperatures of the elements. *Astrophysical Journal*, *591*(2), 1220–1247. https://doi.org/10.1086/375492

Mardikian, P. (n.d.). New perspectives regarding the stabilization of terrestrial and marine archaeological iron. *Iron, Steel & Steam, Fremantle, Australia, June 26-27 2006. Special Publication, Australian National Centre of Excellence for Maritime Archaeology No. 13. Ed M. McCarthy.* Retrieved May 25, 2021, from https://www.academia.edu/37535703/New_perspectives_regarding_the_stabilization_of_terrestrial_and_marine_archaeological_iron

Marrocchi, Y., Avice, G., & Barrat, J.-A. (2021). The Tarda Meteorite: A Window into the Formation of D-type Asteroids. *The Astrophysical Journal Letters*, *913*(1), L9. https://doi.org/10.3847/2041-8213/abfaa3

Mathias, C., Ramsdale, K., & Nixon, D. (2004). Saving archaeological iron using the Revolutionary Preservation System. In *Metal 04: Proceedings of the international conference on metals conservation, Canberra, Australia, 4-8 October 2004* (pp. 28–42, ill.). https://www.bcin.ca/bcin/detail.app?id=242311

McCubbin, F. M., Herd, C. D. K., Yada, T., Hutzler, A., Calaway, M. J., Allton, J. H., Corrigan, C. M., Fries, M. D., Harrington, A. D., McCoy, T. J., Mitchell, J. L., Regberg, A. B., Righter, K., Snead, C. J., Tait, K. T., Zolensky, M. E., & Zeigler, R. A. (2019). Advanced Curation of Astromaterials for Planetary Science. *Space Science Reviews*, *215*(8), 48. https://doi.org/10.1007/s11214-019-0615-9

Meteoritical Bulletin Database. 2021. https://www.lpi.usra.edu/meteor/metbull.php?code=69696

Mikouchi, T., Kasama, T., Zolensky, M. E., & Tachikawa, O. (2001). Transmission Electron Microscopy of the Matrix Minerals in the Tagish Lake Carbonaceous Chondrite. *32nd Lunar and Planetary Science Conference,* Abstract no. 1371. http://adsabs.harvard.edu/abs/2001LPI....32.1371M

Mittlefehldt, D. W. (2002). Geochemistry of the ungrouped carbonaceous chondrite Tagish Lake, the anomalous CM chondrite Bells, and comparison with CI and CM chondrites. *Meteoritics & Planetary Science*, *37*(5), 703–712. https://doi.org/10.1111/j.1945-5100.2002.tb00850.x

Monster, J., Anders, E., & Thode, H. G. (1965). 34S/32S ratios for the different forms of sulphur in the Orgueil meteorite and their mode of formation. *Geochimica et Cosmochimica Acta*, *29*(7), 773–779. https://doi.org/10.1016/0016-7037(65)90030-X

Mungall, E. L., Wong, J. P. S., & Abbatt, J. P. D. (2018). Heterogeneous Oxidation of Particulate Methanesulfonic Acid by the Hydroxyl Radical: Kinetics and Atmospheric Implications. *ACS Earth and Space Chemistry*, *2*(1), 48–55. https://doi.org/10.1021/acsearthspacechem.7b00114

Nakamura, T., Noguchi, T., Zolensky, M. E., & Tanaka, M. (2003). Mineralogy and noble-gas signatures of the carbonate-rich lithology of the Tagish Lake carbonaceous chondrite: Evidence for an accretionary breccia. *Earth and Planetary Science Letters*, *207*(1–4), 83–101. https://doi.org/10.1016/S0012-821X(02)01127-5

Naldrett A. J. (1989) *Magmatic Sulphide Deposits*. Oxford University Press, Oxford.

Noguchi, T., Nakamura, T., & Nozaki, W. (2002). Mineralogy of phyllosilicate-rich micrometeorites and comparison with Tagish Lake and Sayama meteorites. *Earth and Planetary Science Letters*, *202*(2), 229–246. https://doi.org/10.1016/S0012-821X(02)00777-X

Paterakis, A. B., & Hickey-Friedman, L. (2011). Stabilization of iron artifacts from Kaman-Kalehöyük: A comparison of chemical and environmental methods. *Studies in Conservation*, *56*(3), 179–190.

Paterakis, A. B., & Mariano, M. (2013). *Oxygen absorbers and desiccants in the protection of archaeological iron: Maintaining some control*. Historic Scotland.

Paterakis, A. B., & Mariano, M. (2016). *Oxygen absorption for the protection of archaeological iron: Improving maintenance*. ICOM Committee for ConservationMetals Working Group.

Pearson, V. K., Sephton, M. A., Franchi, I. A., Gibson, J. M., & Gilmour, I. (2006). Carbon and nitrogen in carbonaceous chondrites: Elemental abundances and stable isotopic compositions. *Meteoritics & Planetary Science*, *41*(12), 1899–1918. https://doi.org/10.1111/j.1945-5100.2006.tb00459.x

Pizzarello, S., & Huang, Y. S. (2002). Molecular and isotopic analyses of Tagish Lake alkyl dicarboxylic acids. *Meteoritics & Planetary Science*, *37*(5), 687–696. https://doi.org/10.1111/j.1945-5100.2002.tb00848.x

Pizzarello, S., Huang, Y. S., Becker, L., Poreda, R. J., Nieman, R. A., Cooper, G., & Williams, M. (2001). The organic content of the Tagish Lake meteorite. *Science*, *293*(5538), 2236–2239. https://doi.org/10.1126/science.1062614

Rai, V. K., & Thiemens, M. H. (2007). Mass independently fractionated sulfur components in chondrites. *Geochimica et Cosmochimica Acta*, *71*(5), 1341–1354. https://doi.org/10.1016/j.gca.2006.11.033

Ralchenko, M., Britt, D. T., Samson, C., Herd, C. D. K., Herd, R. K., and McCausland, P. J. A., 2014. Bulk Physical Properties of the Tagish Lake Meteorite Frozen Pristine Fragments *45th Lunar and Planetary Science Conference* Abstract no. 1021

Rau, H. (1976). Energetics of Defect Formation and Interaction in Pyrrhotite Fe1-Xs and Its Homogeneity Range. *Journal of Physics and Chemistry of Solids*, *37*(4), 425–429. https://doi.org/10.1016/0022-3697(76)90024-X

Rimmer, M., Thickett, D., Watkinson, D., & Ganiaris, H. (2013). *Guidelines for the storage and display of archaeological metalwork* [Monograph]. English Heritage. http://www.english-heritage.org.uk/publications/guidelines-storage-display-archaeological-metalwork/Storage_Display_Metalwork_2ndPP.pdf

Rubin, A. E., Trigo-Rodríguez, J. M., Huber, H., & Wasson, J. T. (2007). Progressive aqueous alteration of CM carbonaceous chondrites. *Geochimica et Cosmochimica Acta*, *71*(9), 2361–2382. https://doi.org/10.1016/j.gca.2007.02.008

Russell, S. D. J., Longstaffe, F. J., King, P. L., & Larson, T. E. (2008). *Whole-Rock, Clay Mineral, and Olivine Oxygen and Hydrogen Isotope Compositions of the Tagish Lake Carbonaceous Chondrite*. *39*, 1709.

Scarlett, T. (2016). Potential applications of supercritical carbon dioxide extraction and impregnation for the stabilization and conservation of industrial heritage artifacts. *Department of Social Sciences Publications*. https://digitalcommons.mtu.edu/social-sciences-fp/88

Schrader, D. L., Connolly, H. C., Lauretta, D. S., Zega, T. J., Davidson, J., & Domanik, K. J. (2015). The formation and alteration of the Renazzo-like carbonaceous chondrites III: Toward understanding the genesis of ferromagnesian chondrules. *Meteoritics & Planetary Science*, *50*(1), 15–50. https://doi.org/10.1111/maps.12402

Schrader, D. L., Davidson, J., & Mccoy, T. J. (2016). Widespread evidence for high-temperature formation of pentlandite in chondrites. *Geochimica Et Cosmochimica Acta*, *189*, 359–376. https://doi.org/10.1016/j.gca.2016.06.012

Schrader, D. L., Davidson, J., McCoy, T. J., Zega, T. J., Russell, S. S., Domanik, K. J., & King, A. J. (2021). The Fe/S ratio of pyrrhotite group sulfides in chondrites: An indicator of oxidation and implications for return samples from asteroids Ryugu and Bennu. *Geochimica et Cosmochimica Acta*, *303*, 66–91. https://doi.org/10.1016/j.gca.2021.03.019

Selwyn, L. S., & Logan, J. A. (1993). *Stability of treated iron: A comparison of treatment methods*. ICOM Committee for Conservation.

Shewman, R. W., & Clark, L. A. (1970). Pentlandite phase relations in the Fe–Ni–S system and notes on the monosulfide solid solution. *Canadian Journal of Earth Sciences*, *7*(1), 67–85. https://doi.org/10.1139/e70-005

Siauw, A., & Norman, A. (2006). The S isotope composition of methanesulfonic acid in Arctic aerosols. *AGU Fall Meeting Abstracts*.

Simkus, D. N., Aponte, J. C., Elsila, J. E., Hilts, R. W., McLain, H. L., & Herd, C. D. K. (2019). New insights into the heterogeneity of the Tagish Lake meteorite: Soluble organic compositions of variously altered specimens. *Meteoritics and Planetary Science*, *54*(6), 1283–1302. https://doi.org/10.1111/maps.13276

Simon, S. B., & Grossman, L. (2003). Petrography and mineral chemistry of the anhydrous component of the Tagish Lake carbonaceous chondrite. *Meteoritics & Planetary Science*, *38*(5), 813–825. https://doi.org/10.1111/j.1945-5100.2003.tb00044.x

Singerling, S. A., & Brearley, A. J. (2018). Primary iron sulfides in CM and CR carbonaceous chondrites: Insights into nebular processes. *Meteoritics & Planetary Science*, *53*(10), 2078–2106. https://doi.org/10.1111/maps.13108

Singerling, S. A., & Brearley, A. J. (2020). Altered primary iron sulfides in CM2 and CR2 carbonaceous chondrites: Insights into parent body processes. *Meteoritics & Planetary Science*, *55*(3), 496–523. https://doi.org/10.1111/maps.13450

Sjøgren, A., & Buchwald, V. F. (1991). Hydrogen Plasma Reactions in a D.C. Mode for the Conservation of Iron Meteorites and Antiquities. *Studies in Conservation*, *36*(3), 161–171. https://doi.org/10.2307/1506422

Takir, D., Howard, K. T., Stockstill-Cahill, K. R., Hibbitts, C. A., Abreu, N., Zolensky, M. E., & Fries, M. (2020). Spectroscopy and Mineralogy of Aguas Zarcas. *51st Lunar and Planetary Science Conference*, Abstract #2533. http://www.lpi.usra.edu/meetings/lpsc2020/pdf/2533.pdf

Thunberg, J. C., Watkinson, D. E., & Emmerson, N. J. (2021). Desiccated Microclimates for Heritage Metals: Creation and Management. *Studies in Conservation*, *66*(3), 127–153. https://doi.org/10.1080/00393630.2020.1799599

Toulmin P. and Barton P. B. Jr. 1964. A thermodynamic study of pyrite and pyrrhotite. *Geochimica et Cosmochimica Acta 28*, 641–671.

Tunney, L. D., Herd, C. D. K., & Hilts, R. W. (2020). Organic contamination on the surface of meteorites as a function of space and time: A case study of the Buzzard Coulee H4 chondrite. *Meteoritics & Planetary Science*, *55*(8), 1899-1923. https://doi.org/10.1111/maps.13551

Tunney, L. D., Hill, P. J. A., Herd, C. D. K., Hilts, R. W., & Holt, M. C. (2022a). Distinguishing between terrestrial and extraterrestrial organic compounds in the CM2 Aguas Zarcas carbonaceous chondrite: Implications for intrinsic organic matter. *Meteoritics & Planetary Science*, *57*(4), 883–911. https://doi.org/10.1111/maps.13803

Tunney, L. D., Hill, P. J. A., Herd, C. D. K., & Hilts, R. W. (2022b). Organic compounds in the Tarda C2 ungrouped carbonaceous chondrite: Evaluating the sources of contamination in a desert fall. *Meteoritics & Planetary Science*, *57*(4), 850–865. https://doi.org/10.1111/maps.13800

Vaughan D. J. and Craig J. R. 1997. Sulfide ore mineral stabilities, morphologies, and intergrowth textures. In *Geochemistry of Hydrothermal Ore Deposits*, 3rd edn., edited by Barnes H. L. New York: John Wiley and Sons. pp. 367–434.

Visser, R., John, T., Patzek, M., Bischoff, A., & Whitehouse, M. J. (2019). Sulfur isotope study of sulfides in CI, CM, C2(ung) chondrites and volatile-rich clasts—Evidence for different generations and reservoirs of sulfide formation. *Geochimica et Cosmochimica Acta*, *261*, 210–223. https://doi.org/10.1016/j.gca.2019.06.046

Watkinson, D., & Lewis, M. T. (2005). Desiccated Storage of Chloride-Contaminated Archaeological Iron Objects. *Studies in Conservation*, *50*(4), 241–252. https://doi.org/10.2307/25487756

Wetherill G. W., and Chapman C. R. 1988. Asteroids and meteorites. *Meteorites and the Early Solar System*, eds Kerridge, J. F., and Matthews, M. S. University of Arizona Press, Tucson, AZ.

Yang, X., Hanna, R. D., Davis, A. M., Neander, A. I., & Heck, P. R. (2021). A Possible Record of an Active Asteroid: Discovery of a Compact Lithology in the Aguas Zarcas Cm Chondrite. *84th Annual Meeting of the Meteoritical Society.* LPI Contribution No. 2609, id.6075

Zolensky, M. E., & Thomas, K. L. (1995). Iron and iron-nickel sulfides in chondritic interplanetary dust particles. *Geochimica et Cosmochimica Acta*, *59*(22), 4707–4712. https://doi.org/10.1016/0016-7037(95)00329-0

Zolensky, M. E., Nakamura, K., Gounelle, M., Mikouchi, T., Kasama, T., Tachikawa, O., & Tonui, E. (2002). Mineralogy of Tagish Lake: An ungrouped type 2 carbonaceous chondrite. *Meteoritics & Planetary Science*, *37*(5), 737–761. https://doi.org/10.1111/j.1945-5100.2002.tb00852.x

Zolensky, Michael E., Krot, A. N., & Benedix, G. (2008). Record of low-temperature alteration in asteroids. In G. J. MacPherson, D. W. Mittlefehldt, J. H. Jones, & S. B. Simon (Eds.), *Oxygen in the Solar System* (Vol. 68, pp. 429–462). Mineralogical Soc Amer & Geochemical Soc. https://doi.org/10.2138/rmg.2008.68.15

Appendices

Appendix A

Table A.1. Major and minor element compositions of Fe-Ni sulfides in Tagish Lake.

Sample	Area	Line		Mineral	Si (wt%)	Cr (wt%)	Fe (wt%)	Co (wt%)	Ni (wt%)	Mn (wt%)	P (wt%)	S (wt%)	Total	Fe/S (at%)
11h	TL-11h area1	55		pyrrhotite	0	0.05	58.15	0.15	2.65	0.06	0	39.94	101.00	0.836
	TL-11h area1	56		pyrrhotite	0.02	0.04	58.08	0	1.74	0.06	0	39.57	99.51	0.843
	TL-11h area5	63		pentlandite	0	0.03	30.82	0.77	35.19	0	0	33.74	100.55	0.524
	TL-11h area5	64		pentlandite	0	0.01	30.78	0.75	35.35	0	0	33.88	100.77	0.521
	TL-11h area6	65		pyrrhotite	0.01	0.04	59.34	0	1.71	0.03	0	39.50	100.63	0.862
	TL-11h area6	66		pyrrhotite	0.03	0.04	59.04	0	1.67	0.03	0	39.92	100.73	0.849
	TL-11h area7	67		pentlandite	0	0.02	29.65	1.34	36.12	0	0	33.76	100.89	0.504
	TL-11h area7	68		pentlandite	0	0.02	30.95	1.27	34.54	0	0	34.07	100.85	0.521
	TL-11h area8	69		pyrrhotite	0.02	0.12	59.14	0	1.9	0.01	0	39.87	101.06	0.852
	TL-11h area8	70		pentlandite	0.21	0.05	29.48	1.49	33.89	0.01	0	32.57	97.70	0.520
	TL-11h area11	78		pentlandite	0	0.02	30.42	1.15	35.54	0	0	33.58	100.71	0.520
	TL-11h area11	79		pyrrhotite	0.01	0.02	59.11	0	1.79	0	0	39.55	100.48	0.858
	TL-11h area12	80		pentlandite	0	0.02	30.03	0.91	35.53	0	0	33.74	100.23	0.511
	TL-11h area12	81		pentlandite	0	0.03	30.19	0.87	35.19	0	0	33.58	99.86	0.516
			average	pyrrhotite	0.02	0.05	58.81	0.03	1.91	0.03	0.00	39.73	100.57	0.850
			1σ		0.01	0.03	0.55	0.06	0.37	0.02	0.00	0.21	0.56	0.010
			average	pentlandite	0.03	0.03	30.29	1.07	35.17	0.00	0.00	33.62	100.20	0.517
			1σ		0.07	0.01	0.55	0.28	0.68	0.00	0.00	0.45	1.07	0.007
11i	TL-11i area1	82		pentlandite	0.00	0.02	28.53	0.72	36.24	0.00	0.00	33.75	99.26	0.485
	TL-11i area1	83		pentlandite	0.00	0.02	28.19	0.69	35.81	0.00	0.00	33.35	98.06	0.485
	TL-11i area2	84		pentlandite	0.00	0.00	31.43	0.62	33.46	0.00	0.00	33.54	99.05	0.538
	TL-11i area2	85		pentlandite	0.00	0.00	31.26	0.61	33.50	0.00	0.00	33.60	98.97	0.534
	TL-11i area3	87		pyrrhotite	0.01	0.03	59.24	0.00	1.52	0.03	0.00	38.91	99.74	0.874
	TL-11i area4	88		pyrrhotite	0.01	0.05	59.28	0.13	0.94	0.03	0.00	39.24	99.68	0.867
	TL-11i area4	89		pyrrhotite	0.03	0.06	58.86	0.15	0.91	0.04	0.00	39.02	99.07	0.866
	TL-11i area6	92		pyrrhotite	0.09	0.07	58.69	0.07	1.65	0.01	0.01	39.16	99.75	0.860
	TL-11i area6	93		pyrrhotite	0.03	0.06	58.67	0.07	1.61	0.02	0.00	39.22	99.68	0.859
	TL-11i area7	94		pentlandite	0.02	0.04	36.46	0.79	28.17	0.02	0.00	34.86	100.36	0.600
	TL-11i area8	96		pyrrhotite	0.03	0.13	53.28	0.03	6.48	0.00	0.00	39.91	99.86	0.766
	TL-11i area8	97		pyrrhotite	0.20	0.11	49.73	0.15	9.97	0.00	0.00	38.63	98.79	0.739
	TL-11i area10	101		pyrrhotite	0.01	0.04	58.57	0.00	1.36	0.00	0.00	39.12	99.10	0.860
	TL-11i area12	104		pyrrhotite	0.01	0.04	58.70	0.00	1.78	0.02	0.00	39.38	99.93	0.856
			average	pyrrhotite	0.05	0.07	57.22	0.07	2.91	0.02	0.00	39.18	99.51	0.839
			1σ		0.06	0.03	3.37	0.06	3.15	0.02	0.00	0.35	0.41	0.050

			average	pentlandite	0.00	0.02	31.17	0.69	33.44	0.00	0.00	33.82	99.14	0.529
			1σ		0.01	0.02	3.31	0.07	3.21	0.01	0.00	0.60	0.82	0.048
11v chip1	TL-11v area1	106		pyrrhotite	0.03	0.29	59.98	0.00	0.64	0.21	0.00	38.91	100.06	0.885
	TL-11v area1	107		pyrrhotite	0.03	0.32	59.83	0.00	0.61	0.27	0.00	38.89	99.95	0.883
	TL-11v area4	112		pyrrhotite	0.82	0.05	58.61	0.00	0.90	0.02	0.01	37.29	97.70	0.902
	TL-11v area4	113		pyrrhotite	0.03	0.04	60.22	0.00	1.01	0.00	0.00	39.24	100.54	0.881
	TL-11v area5	114		pyrrhotite	0.14	0.05	57.79	0.00	2.80	0.03	0.00	38.18	98.99	0.869
			average	pyrrhotite	0.21	0.15	59.29	0.00	1.19	0.11	0.00	38.50	99.45	0.884
			1σ		0.34	0.14	1.04	0.00	0.91	0.12	0.00	0.78	1.13	0.012
11v chip2	TL-11v area5	115		pyrrhotite	0.11	0.04	57.76	0.00	2.89	0.00	0.00	38.38	99.18	0.864
	TL-11v area5	116		pyrrhotite	0.12	0.05	58.64	0.00	2.40	0.03	0.00	38.57	99.81	0.873
			average	pyrrhotite	0.12	0.05	58.20	0.00	2.65	0.02	0.00	38.48	99.50	0.869
			1σ		0.01	0.01	0.62	0.00	0.35	0.02	0.00	0.13	0.45	0.006
4	TL4 area3	61		pyrrhotite	0.00	0.04	58.31	0.05	2.63	0.03	0.00	38.63	99.69	0.867
	TL4 area3	62		pyrrhotite	0.00	0.03	59.38	0.00	1.67	0.02	0.00	38.82	99.92	0.878
	TL4 area3	63		pyrrhotite	0.00	0.02	58.70	0.00	2.24	0.00	0.00	38.55	99.51	0.874
	TL4 area3	64		pyrrhotite	0.00	0.04	57.94	0.05	2.64	0.00	0.00	38.62	99.29	0.861
	TL4 area3	65		pyrrhotite	0.00	0.03	59.16	0.00	1.50	0.00	0.00	38.66	99.35	0.878
	TL4 area3	66		pyrrhotite	0.00	0.03	58.71	0.00	2.19	0.00	0.00	38.51	99.44	0.875
	TL4 area3	71		pyrrhotite	0.00	0.04	58.60	0.00	2.08	0.02	0.00	38.26	99.00	0.879
	TL4 area3	72		pyrrhotite	0.00	0.05	58.89	0.00	1.88	0.02	0.00	38.25	99.09	0.884
	TL4 area3	75		pyrrhotite	0.00	0.04	58.56	0.03	2.37	0.02	0.00	38.39	99.41	0.876
	TL4 area3	76		pyrrhotite	0.00	0.04	59.11	0.00	1.60	0.00	0.00	38.72	99.47	0.876
	TL4 area4	78		pentlandite	0.00	0.02	35.12	0.90	29.47	0.00	0.00	32.88	98.39	0.613
	TL4 area4	79		pentlandite	0.00	0.03	35.15	0.93	29.60	0.00	0.00	32.69	98.40	0.617
	TL4 area5	80		pentlandite	0.00	0.01	28.70	0.69	36.30	0.00	0.00	32.69	98.39	0.504
	TL4 area5	81		pentlandite	0.00	0.03	28.52	0.69	36.01	0.00	0.00	32.47	97.72	0.504
	TL4 area9	93		pentlandite	0.06	0.05	29.37	1.27	34.41	0.00	0.00	32.48	97.64	0.519
	TL4 area11	105		pyrrhotite	0.01	0.05	60.90	0.00	0.36	0.00	0.00	37.98	99.30	0.921
	TL4 area11	106		pyrrhotite	0.00	0.05	60.18	0.11	0.95	0.03	0.00	37.92	99.24	0.911
			average	pyrrhotite	0.00	0.04	59.04	0.02	1.84	0.01	0.00	38.44	99.39	0.882
			1σ		0.00	0.01	0.82	0.03	0.68	0.01	0.00	0.29	0.25	0.017
			average	pentlandite	0.01	0.03	31.37	0.90	33.16	0.00	0.00	32.64	98.11	0.552
			1σ		0.03	0.01	3.45	0.24	3.39	0.00	0.00	0.17	0.39	0.058
5b	TL5b area1	56		pyrrhotite	0.15	0.04	57.77	0.00	0.98	0.00	0.00	38.95	97.89	0.852
	TL5b area1	57		pyrrhotite	0.03	0.04	57.90	0.00	1.31	0.00	0.00	39.38	98.66	0.844
	TL5b area1	58		pyrrhotite	0.02	0.04	58.65	0.00	1.21	0.02	0.00	39.44	99.38	0.854
	TL5b area4	60		pyrrhotite	0.09	0.55	57.95	0.00	0.67	0.05	0.00	39.15	98.46	0.850

	TL5b area5	63		pyrrhotite	0.04	0.08	58.51	0.02	1.28	0.06	0.00	38.94	98.93	0.863
	TL5b area5	64		pyrrhotite	0.03	0.07	58.21	0.04	1.63	0.04	0.00	38.85	98.87	0.860
	TL5b area5	66		pyrrhotite	0.02	0.07	58.52	0.03	1.44	0.05	0.00	38.49	98.62	0.873
	TL5b area5	68		pyrrhotite	0.04	0.08	59.10	0.00	1.03	0.05	0.00	38.52	98.82	0.881
	TL5b area5	69		pyrrhotite	0.01	0.06	58.63	0.03	1.10	0.04	0.00	38.67	98.54	0.871
	TL5b area5	70		pyrrhotite	0.03	0.07	58.74	0.00	1.00	0.03	0.00	38.88	98.75	0.867
	TL5b area5	71		pyrrhotite	0.11	0.07	58.05	0.05	1.16	0.06	0.00	38.39	97.89	0.868
	TL5b area5	74		pyrrhotite	0.02	0.06	58.29	0.06	0.97	0.06	0.00	38.74	98.20	0.864
	TL5b area5	75		pyrrhotite	0.03	0.07	58.66	0.00	0.87	0.04	0.00	38.72	98.39	0.870
	TL5b area5	76		pyrrhotite	0.03	0.07	58.61	0.00	0.78	0.06	0.00	38.83	98.38	0.866
	TL5b area6	77		pyrrhotite	0.02	0.07	59.36	0.06	0.84	0.03	0.00	39.13	99.51	0.871
	TL5b area7	78		pyrrhotite	0.02	0.03	59.09	0.08	0.52	0.02	0.00	39.02	98.78	0.869
	TL5b area7	79		pyrrhotite	0.02	0.02	59.15	0.09	0.54	0.00	0.00	38.84	98.66	0.874
	TL5b area7	80		pyrrhotite	0.03	0.02	59.27	0.07	0.55	0.00	0.00	38.74	98.68	0.878
	TL5b area7	81		pyrrhotite	0.06	0.01	59.09	0.05	0.56	0.02	0.00	38.78	98.57	0.875
	TL5b area7	82		pyrrhotite	0.08	0.02	58.75	0.09	0.55	0.02	0.00	38.26	97.77	0.881
	TL5b area7	83		pyrrhotite	0.08	0.02	58.68	0.05	0.55	0.02	0.00	38.55	97.95	0.874
	TL5b area7	85		pyrrhotite	0.04	0.02	58.94	0.06	0.47	0.00	0.00	38.97	98.50	0.868
	TL5b area7	86		pyrrhotite	0.03	0.04	58.74	0.09	0.45	0.00	0.00	39.01	98.36	0.865
	TL5b area7	87		pyrrhotite	0.04	0.02	58.76	0.03	0.45	0.00	0.00	38.94	98.24	0.866
			average	pyrrhotite	0.04	0.07	58.64	0.04	0.87	0.03	0.00	38.84	98.53	0.867
			1σ		0.03	0.11	0.44	0.03	0.35	0.02	0.00	0.28	0.43	0.010
10a	TL10a area2	91		pentlandite	0.00	0.04	30.71	0.79	33.41	0.02	0.00	33.12	98.09	0.532
	TL10a area2	92		pentlandite	0.00	0.03	30.87	0.79	33.55	0.02	0.00	33.13	98.39	0.535
	TL10a area4	99		pyrrhotite	0.00	0.06	58.88	0.00	1.79	0.05	0.00	39.37	100.15	0.859
	TL10a area4	100		pyrrhotite	0.00	0.06	59.20	0.00	1.85	0.05	0.00	39.36	100.52	0.863
	TL10a area6	134		pyrrhotite	0.05	0.16	53.09	0.08	6.42	0.00	0.00	39.57	99.37	0.770
	TL10a area8	138		pyrrhotite	0.00	0.08	58.50	0.00	1.77	0.04	0.00	39.09	99.48	0.859
	TL10a area8	139		pyrrhotite	0.00	0.07	58.69	0.00	1.71	0.07	0.00	38.85	99.39	0.867
	TL10a area11	162		pyrrhotite	0.02	0.03	58.59	0.00	1.51	0.00	0.00	39.07	99.22	0.861
	TL10a area12	164		pyrrhotite	0.01	0.07	58.67	0.02	1.80	0.00	0.00	39.32	99.89	0.857
			average	pyrrhotite	0.01	0.08	57.95	0.01	2.41	0.03	0.00	39.23	99.72	0.848
			1σ		0.02	0.04	2.15	0.03	1.77	0.03	0.00	0.24	0.48	0.034
			average	pentlandite	0.00	0.04	30.79	0.79	33.48	0.02	0.00	33.13	98.24	0.534
			1σ		0.00	0.01	0.11	0.00	0.10	0.00	0.00	0.01	0.21	0.002
1/3	TLp-1/3 area1	166		pyrrhotite	0.00	0.05	56.99	0.00	3.13	0.00	0.00	39.77	99.94	0.823
	TLp-1/3 area2	169		pyrrhotite	0.02	0.12	57.74	0.07	1.72	0.00	0.00	39.90	99.57	0.831
	TLp-1/3 area7	182		pyrrhotite	0.00	0.35	59.19	0.00	0.24	0.11	0.00	39.73	99.62	0.855
	TLp-1/3 area7	183		pyrrhotite	0.00	0.35	58.76	0.00	0.62	0.14	0.00	39.80	99.67	0.848
	TLp-1/3 area7	184		pyrrhotite	0.00	0.35	59.32	0.00	0.26	0.11	0.00	39.61	99.65	0.860

	TLp-1/3 area7	185		pyrrhotite	0.00	0.35	59.55	0.00	0.26	0.10	0.00	39.64	99.90	0.862
	TLp-1/3 area8	186		pyrrhotite	0.00	0.03	59.60	0.04	0.77	0.00	0.00	39.90	100.34	0.857
	TLp-1/3 area8	187		pentlandite	0.00	0.02	31.34	1.01	34.23	0.00	0.00	33.16	99.76	0.543
	TLp-1/3 area9	189		pyrrhotite	0.00	0.06	59.02	0.09	0.90	0.03	0.00	39.36	99.46	0.861
	TLp-1/3 area9	191		pyrrhotite	0.00	0.06	58.76	0.07	1.06	0.05	0.00	39.25	99.25	0.860
	TLp-1/3 area9	192		pyrrhotite	0.01	0.06	58.43	0.09	0.99	0.04	0.00	39.30	98.92	0.854
	TLp-1/3 area10	193		pyrrhotite	0.34	0.04	57.02	0.09	1.42	0.03	0.06	39.06	98.06	0.838
	TLp-1/3 area10	194		pyrrhotite	0.09	0.04	57.23	0.18	1.62	0.02	0.02	39.58	98.78	0.830
	TLp-1/3 area14	199		pentlandite	0.00	0.03	32.13	0.43	30.02	0.01	0.00	36.78	99.40	0.501
	TLp-1/3 area14	200		pentlandite	0.00	0.04	32.48	0.44	30.88	0.00	0.00	35.38	99.22	0.527
	TLp-1/3 area14	201		pentlandite	0.00	0.03	31.00	0.49	33.57	0.00	0.00	34.76	99.85	0.512
			average	pyrrhotite	0.04	0.16	58.47	0.05	1.08	0.05	0.01	39.58	99.43	0.848
			1σ		0.10	0.15	0.98	0.06	0.82	0.05	0.02	0.27	0.61	0.014
			average	pentlandite	0.00	0.03	31.74	0.59	32.18	0.00	0.00	35.02	99.56	0.521
			1σ		0.00	0.01	0.68	0.28	2.04	0.01	0.00	1.50	0.30	0.018
1/6	TLp-1/6 area1	204		pyrrhotite	0.01	0.06	57.94	0.00	1.68	0.00	0.00	39.87	99.56	0.834
	TLp-1/6 area1	205		pyrrhotite	0.10	0.06	57.52	0.00	1.51	0.00	0.00	39.72	98.91	0.831
	TLp-1/6 area2	206		pyrrhotite	0.04	0.04	57.82	0.00	1.37	0.00	0.00	39.69	98.96	0.836
	TLp-1/6 area3	209		pyrrhotite	0.04	0.07	58.08	0.00	1.25	0.00	0.00	39.71	99.15	0.840
	TLp-1/6 area4	210		pyrrhotite	0.01	0.06	58.32	0.00	1.66	0.00	0.00	39.91	99.96	0.839
	TLp-1/6 area4	211		pyrrhotite	0.05	0.08	58.11	0.04	1.46	0.00	0.00	39.92	99.66	0.836
	TLp-1/6 area5	212		pyrrhotite	0.00	0.05	58.91	0.05	0.98	0.06	0.00	39.81	99.86	0.849
	TLp-1/6 area5	213		pyrrhotite	0.02	0.06	58.54	0.06	1.22	0.07	0.00	39.99	99.96	0.841
	TLp-1/6 area6	214		pyrrhotite	0.01	0.06	59.13	0.11	0.94	0.04	0.00	39.41	99.70	0.861
	TLp-1/6 area6	215		pyrrhotite	0.01	0.07	59.18	0.15	0.91	0.02	0.00	39.44	99.78	0.861
	TLp-1/6 area7	216		pyrrhotite	0.00	0.08	58.26	0.13	1.58	0.03	0.00	39.53	99.61	0.846
	TLp-1/6 area7	217		pyrrhotite	0.00	0.10	58.09	0.26	1.92	0.04	0.00	39.42	99.83	0.846
	TLp-1/6 area8	218		pyrrhotite	0.04	0.07	57.70	0.10	2.91	0.01	0.00	39.28	100.11	0.843
	TLp-1/6 area8	219		pyrrhotite	0.00	0.08	58.77	0.12	1.73	0.01	0.00	39.50	100.21	0.854
	TLp-1/6 area9	220		pentlandite	0.00	0.02	30.38	0.79	34.86	0.00	0.00	33.26	99.31	0.524
	TLp-1/6 area9	221		pentlandite	0.00	0.02	29.10	0.79	35.99	0.00	0.00	33.19	99.09	0.503
	TLp-1/6 area10	222		pyrrhotite	0.02	0.03	59.34	0.12	1.51	0.01	0.00	39.47	100.50	0.863
	TLp-1/6 area10	223		pyrrhotite	0.01	0.02	59.23	0.14	1.35	0.02	0.00	39.55	100.32	0.860
	TLp-1/6 area11	224		pentlandite	0.00	0.03	30.88	0.76	33.51	0.00	0.00	32.97	98.15	0.538
	TLp-1/6 area11	225		pyrrhotite	0.04	0.12	57.60	0.08	1.87	0.02	0.00	39.47	99.20	0.838
	TLp-1/6 area11	226		pyrrhotite	0.00	0.07	56.21	0.14	3.51	0.03	0.00	39.02	98.98	0.827
	TLp-1/6 area11	227		pentlandite	0.00	0.11	30.77	0.80	33.77	0.00	0.00	32.80	98.25	0.539
	TLp-1/6 area11	228		pyrrhotite	0.00	0.11	55.78	0.18	4.61	0.03	0.00	39.00	99.71	0.821
	TLp-1/6 area11	229		pentlandite	0.00	0.04	30.99	0.77	33.71	0.00	0.00	32.99	98.50	0.539
	TLp-1/6 area11	230		pyrrhotite	0.00	0.06	56.51	0.11	3.22	0.00	0.00	39.07	98.97	0.830
	TLp-1/6 area12	231		pentlandite	0.00	0.02	28.26	0.79	36.37	0.00	0.00	32.83	98.27	0.494
	TLp-1/6 area12	232		pentlandite	0.00	0.03	28.39	0.76	36.19	0.00	0.00	32.87	98.24	0.496
	TLp-1/6 area13	233		pentlandite	0.00	0.01	30.07	0.71	34.61	0.00	0.00	33.07	98.47	0.522

TLp-1/6 area13	234		pentlandite	0.00	0.01	30.71	0.69	34.71	0.00	0.00	33.13	99.25	0.532
TLp-1/6 area14	235		pyrrhotite	0.01	0.06	59.34	0.09	1.15	0.00	0.00	40.07	100.72	0.850
TLp-1/6 area14	236		pyrrhotite	0.01	0.08	58.66	0.09	1.30	0.00	0.00	39.92	100.06	0.843
TLp-1/6 area15	237		pyrrhotite	0.00	0.02	58.61	0.04	1.68	0.03	0.00	39.95	100.33	0.842
TLp-1/6 area15	238		pyrrhotite	0.01	0.03	58.86	0.07	1.30	0.02	0.00	40.16	100.45	0.841
		average	pyrrhotite	0.02	0.06	58.19	0.09	1.78	0.02	0.00	39.62	99.77	0.843
		1σ		0.02	0.03	0.96	0.07	0.90	0.02	0.00	0.33	0.53	0.011
		average	pentlandite	0.00	0.03	29.95	0.76	34.86	0.00	0.00	33.01	98.61	0.521
		1σ		0.00	0.03	1.08	0.04	1.10	0.00	0.00	0.16	0.47	0.018
total		average	pyrrhotite	0.04	0.08	58.42	0.05	1.63	0.03	0.00	39.15	99.39	0.857
		1σ		0.09	0.09	1.40	0.06	1.33	0.04	0.01	0.56	0.74	0.025
		average	pentlandite	0.01	0.03	30.70	0.83	34.05	0.00	0.00	33.47	99.09	0.527
		1σ		0.04	0.02	1.92	0.24	2.16	0.01	0.00	0.90	1.00	0.031

Appendix B

Table B.1: Major and minor element compositions of Fe-Ni sulfides in Aguas Zarcas

Sample	Area	Line		Mineral	Si (wt%)	Cr (wt%)	Fe (wt%)	Co (wt%)	Ni (wt%)	Mn (wt%)	P (wt%)	S (wt%)	Total	Fe/S (at%)
MET11791-1	MET11791/1 area1 sulfide1	**57**		pyrrhotite	0.00	0.04	60.20	0.24	1.70	0.02	0.00	37.71	99.91	0.917
	MET11791/1 area1 sulfide1	**58**		pyrrhotite	0.00	0.04	60.39	0.23	1.61	0.01	0.00	37.80	100.08	0.917
	MET11791/1 area1 sulfide1 R	**166**		pyrrhotite	0.04	0.68	60.46	0.00	0.61	0.02	0.00	37.97	99.78	0.914
	MET11791/1 area1 sulfide2	**62**		pyrrhotite	0.00	0.01	59.43	0.24	2.03	0.06	0.00	38.15	99.92	0.894
	MET11791/1 area1 sulfide2	**63**		MSS	0.00	0.03	59.51	0.13	2.71	0.05	0.00	36.48	98.91	0.936
	MET11791/1 area2 sulfide1 R1	**167**		pyrrhotite	0.39	0.24	58.00	0.04	1.86	0.00	0.00	38.19	98.72	0.872
	MET11791/1 area2 sulfide1 R2	**168**		pyrrhotite	0.05	0.04	59.01	0.00	2.31	0.00	0.00	38.68	100.09	0.876
	MET11791/1 area2 sulfide1 R4	**170**		pyrrhotite	0.01	0.06	59.73	0.03	1.35	0.00	0.01	38.85	100.04	0.883
	MET11791/1 area2 sulfide2	**68**		pyrrhotite	0.01	0.04	59.92	0.03	1.48	0.00	0.00	38.53	100.01	0.893
	MET11791/1 area2 sulfide2 R	**171**		pyrrhotite	0.02	0.09	59.03	0.00	2.43	0.00	0.00	37.51	99.08	0.903
	MET11791/1 area2 sulfide3	**70**		pyrrhotite	0.00	0.15	60.61	0.00	0.42	0.10	0.00	38.78	100.06	0.897
	MET11791/1 area2 sulfide3 R	**172**		pyrrhotite	0.01	0.18	59.93	0.00	0.98	0.07	0.00	38.60	99.77	0.891
	MET11791/1 area3 sulfide2	**78**		pyrrhotite	0.09	0.23	59.55	0.00	0.52	0.00	0.00	38.57	98.96	0.886
	MET11791/1 area3 sulfide2 R	**175**		pyrrhotite	0.07	0.40	60.30	0.00	0.48	0.00	0.00	39.25	100.50	0.882
	MET11791/1 area4 sulfide2	**87**		pyrrhotite	0.00	0.01	59.77	0.00	1.47	0.02	0.00	37.79	99.06	0.908
	MET11791/1 area4 sulfide2	**88**		pyrrhotite	0.00	0.02	60.26	0.00	0.91	0.02	0.00	37.97	99.18	0.911
			average	pyrrhotite	0.05	0.15	59.77	0.05	1.34	0.02	0.00	38.29	99.68	0.896
			1σ		0.10	0.18	0.69	0.10	0.67	0.03	0.00	0.50	0.53	0.015
AZ-PT2	AZ-PT/2 area1 sulfide1 R	**176**		pentlandite	0.12	0.04	30.51	2.16	33.21	0.00	0.00	33.29	99.33	0.526
	AZ-PT/2 area1 sulfide2	**92**		pentlandite	0.00	0.03	33.56	0.74	31.52	0.00	0.00	32.94	98.79	0.585
	AZ-PT/2 area1 sulfide2	**93**		pentlandite	0.00	0.03	33.52	0.65	31.42	0.01	0.00	33.03	98.66	0.583
	AZ-PT/2 area2 sulfide2	**96**		pyrrhotite	0.00	0.02	60.10	0.05	0.63	0.01	0.00	38.47	99.28	0.897
	AZ-PT/2 area2 sulfide2	**97**		pyrrhotite	0.01	0.03	60.34	0.03	0.59	0.00	0.00	38.46	99.46	0.901
	AZ-PT/2 area3 sulfide4	**111**		pyrrhotite	0.03	0.05	59.42	0.05	0.84	0.00	0.00	38.59	98.98	0.884
			average	pyrrhotite	0.01	0.03	59.95	0.04	0.69	0.00	0.00	38.51	99.24	0.894
			1σ		0.02	0.02	0.48	0.01	0.13	0.01	0.00	0.07	0.24	0.009

			average	pentlandite	0.04	0.03	32.53	1.18	32.05	0.00	0.00	33.09	98.93	0.565
			1σ		0.07	0.01	1.75	0.85	1.01	0.01	0.00	0.18	0.36	0.033
AZ-PT1	AZ PT1 area2	59		pentlandite	0.16	0.03	31.53	0.63	32.82	0.00	0.00	32.97	98.14	0.549
	AZ PT1 area2 R1	261		pentlandite	0.03	0.03	31.47	0.65	33.01	0.00	0.00	33.42	98.61	0.540
	AZ PT1 area5	68		pyrrhotite	0.02	0.02	59.21	0.10	1.48	0.00	0.00	38.15	98.98	0.891
	AZ PT1 area5	69		pyrrhotite	0.01	0.03	59.63	0.14	1.71	0.00	0.00	38.62	100.14	0.886
	AZ PT1 area6 R1	263		pentlandite	0.00	0.04	34.24	0.87	31.22	0.00	0.00	33.39	99.76	0.589
	AZ PT1 area7	71		pentlandite	0.05	0.02	29.69	1.89	33.38	0.00	0.00	32.83	97.86	0.519
	AZ PT1 area7	72		pentlandite	0.02	0.02	30.30	1.89	33.66	0.00	0.00	33.50	99.39	0.519
	AZ PT1 area7 R1	264		pentlandite	0.05	0.04	30.05	1.87	33.62	0.00	0.00	33.51	99.14	0.515
	AZ PT1 area10	78		pyrrhotite	0.00	0.03	60.53	0.00	0.97	0.08	0.00	38.81	100.42	0.895
	AZ PT1 area10	79		pyrrhotite	0.00	0.03	60.72	0.00	0.50	0.00	0.00	38.85	100.10	0.897
	AZ PT1 area11	80		alloy	0.01	0.32	93.32	0.09	5.09	0.00	0.39	0.00	99.22	
	AZ PT1 area12	82		pyrrhotite	0.00	0.04	61.71	0.00	0.21	0.00	0.00	38.88	100.84	0.911
	AZ PT1 area12	83		pyrrhotite	0.00	0.04	61.26	0.00	0.45	0.00	0.00	38.84	100.59	0.905
			average	pyrrhotite	0.01	0.03	60.51	0.04	0.89	0.01	0.00	38.69	100.18	0.898
			1σ		0.01	0.01	0.95	0.06	0.61	0.03	0.00	0.28	0.65	0.009
			average	pentlandite	0.05	0.03	31.21	1.30	32.95	0.00	0.00	33.27	98.82	0.538
			1σ		0.06	0.01	1.66	0.64	0.91	0.00	0.00	0.29	0.74	0.028
AZ-PT3	AZ PT3 area1	87		pyrrhotite	0.00	0.03	60.38	0.13	1.25	0.00	0.00	38.47	100.26	0.901
	AZ PT3 area1	88		pyrrhotite	0.01	0.03	60.40	0.08	0.82	0.00	0.00	38.65	99.99	0.897
	AZ PT3 area2	91		pentlandite	0.06	0.03	32.81	0.49	32.56	0.00	0.00	33.34	99.29	0.565
	AZ PT3 area2 R1	267		pyrrhotite	0.01	0.05	59.74	0.06	1.69	0.00	0.00	38.86	100.41	0.882
	AZ PT3 area5	98		pyrrhotite	0.01	0.02	60.61	0.00	0.49	0.00	0.00	38.67	99.80	0.900
	AZ PT3 area5	99		pyrrhotite	0.01	0.04	59.75	0.20	1.94	0.00	0.00	38.52	100.46	0.890
	AZ PT3 area8 R1	271		pentlandite	0.14	0.03	30.28	1.71	33.12	0.00	0.02	32.66	97.96	0.532
	AZ PT3 area9	106		pentlandite	0.00	0.02	35.96	0.66	29.89	0.00	0.00	33.56	100.09	0.615
	AZ PT3 area9	107		pentlandite	0.08	0.03	35.54	0.70	29.49	0.00	0.00	32.77	98.61	0.622
	AZ PT3 area10	109		pentlandite	0.00	0.02	33.84	0.61	32.41	0.00	0.00	33.72	100.60	0.576
	AZ PT3 area11	110		pyrrhotite	0.01	0.05	60.38	0.07	1.26	0.00	0.00	38.78	100.55	0.894
	AZ PT3 area11	111		pyrrhotite	0.00	0.03	59.00	0.16	2.35	0.00	0.00	38.59	100.13	0.878
	AZ PT3 area13	114		pyrrhotite	0.00	0.03	60.39	0.00	0.69	0.00	0.00	38.68	99.79	0.896
	AZ PT3 area13	116		pyrrhotite	0.01	0.03	60.06	0.07	1.06	0.00	0.00	38.46	99.69	0.896
	AZ PT3 area14	117		pyrrhotite	0.00	0.02	60.74	0.00	0.66	0.00	0.00	38.62	100.04	0.903
	AZ PT3 area14	118		pyrrhotite	0.00	0.01	59.39	0.22	1.45	0.00	0.00	38.48	99.55	0.886
	AZ PT3 area15	119		pentlandite	0.02	0.03	31.69	0.97	33.48	0.00	0.00	33.56	99.75	0.542
	AZ PT3 area15	120		pentlandite	0.00	0.04	31.84	0.95	33.32	0.00	0.00	33.09	99.24	0.552
	AZ PT3 area15	121		pentlandite	0.00	0.03	31.67	0.93	33.71	0.00	0.00	33.46	99.80	0.543
			average	pyrrhotite	0.01	0.03	60.08	0.09	1.24	0.00	0.00	38.62	100.06	0.893
			1σ		0.01	0.01	0.54	0.08	0.58	0.00	0.00	0.13	0.33	0.008
			average	pentlandite	0.04	0.03	32.95	0.88	32.25	0.00	0.00	33.27	99.42	0.569

			1σ		0.05	0.01	2.01	0.38	1.64	0.00	0.01	0.39	0.84	0.034
MET11791-3	MET11791-3 area1	122		pentlandite	0.01	0.04	34.62	0.69	31.03	0.00	0.00	33.60	99.99	0.592
	MET11791-3 area2	123		pyrrhotite	0.02	0.04	60.79	0.00	0.51	0.00	0.00	38.79	100.15	0.900
	MET11791-3 area2	125		pyrrhotite	0.04	0.06	59.26	0.00	0.94	0.00	0.00	38.13	98.43	0.892
	MET11791-3 area3	126		alloy	0.01	0.19	93.56	0.17	4.81	0.00	0.39	0.00	99.13	
	MET11791-3 area3	127		alloy	0.03	0.15	92.81	0.14	5.64	0.00	0.30	0.00	99.07	
	MET11791-3 area3 R1	273		pentlandite	0.00	0.06	33.26	0.45	33.06	0.00	0.00	33.64	100.47	0.568
	MET11791-3 area5	134		pyrrhotite	0.00	0.00	60.87	0.05	0.65	0.00	0.00	38.72	100.29	0.902
	MET11791-3 area5	135		pyrrhotite	0.00	0.02	61.02	0.00	0.46	0.00	0.00	38.60	100.10	0.908
	MET11791-3 area7	139		pyrrhotite	0.00	0.00	60.98	0.00	0.34	0.00	0.00	38.91	100.23	0.900
	MET11791-3 area7	140		pyrrhotite	0.00	0.00	60.52	0.00	0.35	0.00	0.00	38.79	99.66	0.896
			average	pyrrhotite	0.01	0.02	60.57	0.01	0.54	0.00	0.00	38.66	99.81	0.900
			1σ		0.02	0.03	0.67	0.02	0.23	0.00	0.00	0.28	0.71	0.005
			average	pentlandite	0.01	0.05	33.94	0.57	32.05	0.00	0.00	33.62	100.23	0.580
			1σ		0.01	0.01	0.96	0.17	1.44	0.00	0.00	0.03	0.34	0.017

Appendix C

Table C.1: Major and minor element compositions of Fe-Ni sulfides in Tarda.

Sample	Area	Line		Mineral	Si (wt%)	Cr (wt%)	Fe (wt%)	Co (wt%)	Ni (wt%)	Mn (wt%)	P (wt%)	S (wt%)	Total	Fe/S (at%)
MET11800/1/1	MET11800-1-1 area2 R1	277		pentlandite	0.10	0.04	32.32	1.51	30.06	0.00	0.02	34.58	98.63	0.536
	MET11800-1-1 area3 R1	278		alloy	0.04	0.07	93.70	0.18	5.55	0.00	0.38	0.02	99.94	3122.333
	MET11800-1-1 area3 R2	279		pyrrhotite	0.03	0.04	53.88	0.38	6.11	0.00	0.00	39.14	99.58	0.790
	MET11800-1-1 area4	148		pyrrhotite	0.01	0.84	59.44	0.00	0.24	0.28	0.00	39.28	100.09	0.869
	MET11800-1-1 area4 R1	280		pentlandite	0.00	0.03	32.86	1.28	31.56	0.04	0.02	34.47	100.26	0.547
	MET11800-1-1 area5A	150		pyrrhotite	0.02	0.02	58.97	0.05	0.92	0.03	0.00	39.89	99.90	0.849
	MET11800-1-1 area7	161		pentlandite	0.25	0.05	32.71	1.96	30.42	0.00	0.00	34.16	99.55	0.550
	MET11800-1-1 area8B	164		pyrrhotite	0.02	0.04	59.89	0.03	0.48	0.04	0.00	40.04	100.54	0.859
	MET11800-1-1 area8B	165		pyrrhotite	0.03	0.04	59.97	0.00	0.23	0.00	0.00	40.07	100.34	0.859
	MET11800-1-1 area9A	166		pyrrhotite	0.07	0.04	59.15	0.07	0.87	0.00	0.00	38.91	99.11	0.873
	MET11800-1-1 area9A	168		pentlandite	0.03	0.02	29.72	1.33	35.17	0.00	0.00	33.27	99.54	0.513
	MET11800-1-1 area9A R1	285		pentlandite	0.03	0.05	28.81	0.90	35.36	0.00	0.00	33.15	98.30	0.500
	MET11800-1-1 area9C R1	286		pyrrhotite	0.01	0.16	59.92	0.00	0.51	0.07	0.00	40.02	100.69	0.860
	MET11800-1-1 area10 R1	287		pyrrhotite	0.03	0.07	55.32	0.74	4.68	0.00	0.00	39.85	100.69	0.797
	MET11800-1-1 area11	288		pyrrhotite	0.03	0.05	59.27	0.00	0.92	0.00	0.00	39.70	99.97	0.857
	MET11800-1-1 area13A	177		pentlandite	0.03	0.03	36.70	1.06	26.50	0.00	0.00	35.29	99.61	0.597
	MET11800-1-1 area13A	289		pentlandite	0.06	0.04	31.79	1.37	33.27	0.00	0.00	34.23	100.76	0.533
	MET11800-1-1 area13A	290		pentlandite	0.04	0.04	33.32	0.85	31.85	0.00	0.00	34.39	100.49	0.556
	MET11800-1-1 area13B	181		pyrrhotite	0.15	0.12	58.95	0.00	0.78	0.04	0.00	39.34	99.38	0.860
	MET11800-1-1 area13B	291		pyrrhotite	0.09	0.19	58.88	0.00	0.67	0.03	0.03	39.69	99.58	0.852
	MET11800-1-1 area13B	292		pentlandite	0.04	0.06	35.61	0.98	28.95	0.03	0.00	35.17	100.84	0.581
	MET11800-1-1 area13C	293		pentlandite	0.17	0.03	31.80	2.04	30.65	0.02	0.00	33.87	98.58	0.539
	MET11800-1-1 area13C	297		pentlandite	0.26	0.08	36.16	2.01	26.04	0.03	0.00	33.86	98.44	0.613
			average	pyrrhotite	0.04	0.15	58.51	0.12	1.49	0.04	0.00	39.63	99.99	0.848
			1σ		0.04	0.24	2.00	0.24	1.97	0.08	0.01	0.40	0.54	0.028
			average	pentlandite	0.09	0.04	32.89	1.39	30.89	0.01	0.00	34.22	99.55	0.551
			1σ		0.09	0.02	2.49	0.44	3.05	0.02	0.01	0.68	0.95	0.034
MET11800/1/2	MET11800-1-2 area1A	55		troilite?	0.02	0.07	63.68	0.00	2.47	0.00	0.00	35.21	101.45	1.038

	MET11800-1-2 area1A	56		alloy	0.02	0.04	84.11	0.91	14.38	0.00	0.00	0.05	99.51	945.444
	MET11800-1-2 area1B	57		pyrrhotite	0.00	0.02	60.26	0.13	0.93	0.02	0.00	38.87	100.23	0.890
	MET11800-1-2 area2A	61		alloy	0.01	0.05	86.93	0.71	11.84	0.00	0.10	0.15	99.79	323.9259
	MET11800-1-2 area2B	62		pentlandite	0.13	0.14	37.39	1.10	25.37	0.00	0.00	35.14	99.27	0.611
	MET11800-1-2 area3A	65		troilite?	0.02	0.06	60.63	0.06	3.60	0.00	0.00	34.00	98.37	1.024
	MET11800-1-2 area3B	67		pentlandite	0.12	0.04	31.24	1.34	31.53	0.00	0.00	33.50	97.77	0.536
	MET11800-1-2 area3C	68		pyrrhotite	0.19	0.02	52.92	0.69	6.76	0.00	0.00	37.84	98.42	0.803
	MET11800-1-2 area 5A	73		pyrrhotite	0.01	0.03	58.37	0.18	2.05	0.05	0.00	39.45	100.14	0.849
	MET11800-1-2 area 5A	74		pyrrhotite	0.01	0.03	59.19	0.04	1.18	0.06	0.00	39.60	100.11	0.858
	MET11800-1-2 area6	77		pyrrhotite	0.03	0.05	58.67	0.00	1.19	0.07	0.00	39.46	99.47	0.854
			average	pyrrhotite	0.04	0.04	59.10	0.16	2.60	0.03	0.00	37.78	99.74	0.902
			1σ		0.07	0.02	3.26	0.24	2.06	0.03	0.00	2.27	1.09	0.092
			average	pentlandite	0.13	0.09	34.32	1.22	28.45	0.00	0.00	34.32	98.52	0.573
			1σ		0.01	0.07	4.35	0.17	4.36	0.00	0.00	1.16	1.06	0.053
MET11800/2/1	MET11800-2-1 area2	83		pyrrhotite	0.35	0.05	58.96	0.00	0.85	0.00	0.00	38.37	98.58	0.882
	MET11800-2-1 area6	91		pentlandite	0.28	0.05	37.95	1.66	23.52	0.00	0.25	34.69	98.40	0.628
	MET11800-2-1 area9A	99		pyrrhotite	0.12	0.02	57.46	0.16	1.65	0.04	0.00	38.49	97.94	0.857
	MET11800-2-1 area10	102		pyrrhotite	0.08	0.04	56.63	0.06	4.01	0.00	0.00	37.64	98.46	0.864
	MET11800-2-1 area10	103		pyrrhotite	0.04	0.05	50.98	0.26	9.47	0.00	0.00	38.29	99.09	0.764
	MET11800-2-1 area11A	107		pyrrhotite	0.13	0.21	58.23	0.00	0.95	0.00	0.00	38.65	98.17	0.865
	MET11800-2-1 area11B	109		pyrrhotite	0.10	0.03	59.09	0.00	1.05	0.00	0.00	38.61	98.88	0.879
	MET11800-2-1 area12	110		pyrrhotite	0.08	0.22	59.16	0.00	0.82	0.06	0.00	38.86	99.20	0.874
			average	pyrrhotite	0.13	0.09	57.22	0.07	2.69	0.01	0.00	38.42	98.62	0.855
			1σ		0.10	0.09	2.91	0.10	3.20	0.03	0.00	0.39	0.47	0.041
			average	pentlandite	0.28	0.05	37.95	1.66	23.52	0.00	0.25	34.69	98.40	0.628
			1σ											

Appendix D

Table D.1: Organic and inorganic compounds detected in solutions of $NaHSO_4$, H_2SO_4, and MSA in acetonitrile as well as the acetonitrile and hot water extractions of doped Allende samples from prepared group 1.

Sample	Retention Time (min)	Quality	Compound
blank	3.327	91	teta-Butyldimethylsilanol
	3.512	72	teta-Butyldimethylsilanol
	8.175	83	Disiloxane, 1,3-bis(1,1-dimethylethyl)-1,1,3,3-tetramethyl-
NaHSO4 + MTBSTFA	3.218	91	Acetamide
	3.425	64	teta-Butyldimethylsilanol
	3.501	78	teta-Butyldimethylsilanol
	5.223	90	teta-Butyldimethylsilanol
	8.208	92	Disiloxane, 1,3-bis(1,1-dimethylethyl)-1,1,3,3-tetramethyl-
	10.802	80	Tris(trimethylsilyl)borate
H2SO4 + MTBSTFA	3.218	91	Acetamide
	3.403	94	Silane, chloro(1,1-dimethylethyl)dmethyl-
	3.501	91	teta-Butyldimethylsilanol
	3.773	46	Silane, chloro(1,1-dimethylethyl)dmethyl-
	4.013	83	Cyclotrisiloxane, hexamethyl-
	4.253	86	Disiloxane, 1,3-dichloro-1,1,3,3-tetramethyl-
	4.602	64	Bis-N,N-(trimethylsilyl)formamide
	5.234	78	Chloromethyldimethylisopropoxysilane
	5.92	80	Indol-2-one, 5-chloro-1,3-dihydro-
	6.16	40	Tetramethyl-1,3-bis[(2Z)-pent-2-en-1-yloxy]disiloxane
	7.87	53	3,4-Dihydrocoumarin, 6-amino-4,4-dimethyl-
	8.11	43	3H-1,2,4-Triazole-3-thione, 5-amin-1,2-dihydro-
	8.208	92	Disiloxane, 1,3-bis(1,1-dimethyletyl)-1,1,3,3-tetramethyl-
	9.527	70	Tetrasiloxane, 1,7-dichloro-1,1,3,3,5,5,7,7-octamethyl-
	10.802	80	Tris(trimethylsilyl)borate
	13.155	68	Tetrasiloxane, decamethyl-
	14.179	87	Sulfuric acid, bis(tert-butyldimethylsilyl) ester
	21.295	56	9,12-Octadecadienoic acid, tert-butyldimethylsilyl ester, (Z,Z)-
MSA + MTBSTFA	3.403	91	Silane, chloro(1,1-dimethylethyl)dimethyl-
	3.512	83	teta-Butyldimethylsilanol
	4.612	94	teta-Butyldimethylsilanol
	6.127	91	Cyclotetrasiloxane, octamethyl-
	8.219	92	Disiloxane, 1,3-bis(1,1-dimethylethyl)-1,1,3,3-tetramethyl-

	9.527	64	Trimethylsilyl methansulfonate
	10.802	80	Tris(trimethylsilyl)borate
blank	3.447	87	teta-Butyldimethylsilanol
	3.556	59	teta-Butyldimethylsilanol
	6.149	37	Benzenesulfonamide, N-(3-chloropropyl)-N-methyl-
	8.186	94	Disiloxane, 1,3-bis(1,1-dimethylethyl)-1,1,3,3-tetramethyl-
	9.472	50	Hexamethyldisilazane
0.1	3.316	90	teta-Butyldimethylsilanol
	3.446	83	teta-Butyldimethylsilanol
	3.566	72	teta-Butyldimethylsilanol
	6.105	43	Benzenesulfonamide, N-(3-chloropropyl)-N-methyl-
	8.175	78	Bis-N,N-(trimethylsilyl)formamide
	11.619	40	Butanoic acid, 4-[(trimethylsilyl)oxy]-, trimethylsilyl ester
0.2	3.457	90	teta-Butyldimethylsilanol
	3.599	72	teta-Butyldimethylsilanol
	6.127	91	Cyclotetrasiloxane, octamethyl-
	8.175	94	Disiloxane, 1,3-bis(1,1-dimethylethyl)-1,1,3,3-tetramethyl-
1.1	3.327	91	teta-Butyldimethylsilanol
	3.457	91	teta-Butyldimethylsilanol
	3.588	72	teta-Butyldimethylsilanol
	6.127	91	Cyclotetrasiloxane, octamethyl-
	8.175	93	Disiloxane, 1,3-bis(1,1-dimethylethyl)-1,1,3,3-tetramethyl-
1.2	3.326	91	teta-Butyldimethylsilanol
	3.457	91	teta-Butyldimethylsilanol
	3.599	72	teta-Butyldimethylsilanol
	6.127	91	Cyclotetrasiloxane, octamethyl-
	8.175	93	Disiloxane, 1,3-bis(1,1-dimethylethyl)-1,1,3,3-tetramethyl-
1.3	3.327	91	teta-Butyldimethylsilanol
	3.555	72	teta-Butyldimethylsilanol
	6.116	91	Cyclotetrasiloxane, octamethyl-
	8.165	96	Disiloxane, 1,3-bis(1,1-dimethylethyl)-1,1,3,3-tetramethyl-
1.4	3.327	91	teta-Butyldimethylsilanol
	3.457	91	teta-Butyldimethylsilanol
	3.599	72	teta-Butyldimethylsilanol
	6.127	91	Cyclotetrasiloxane, octamethyl-
	8.175	96	Disiloxane, 1,3-bis(1,1-dimethylethyl)-1,1,3,3-tetramethyl-
1.5	3.327	91	teta-Butyldimethylsilanol

	3.457	91	teta-Butyldimethylsilanol
	3.599	72	teta-Butyldimethylsilanol
	6.127	91	Cyclotetrasiloxane, octamethyl-
	8.176	91	Disiloxane, 1,3-bis(1,1-dimethylethyl)-1,1,3,3-tetramethyl-
1.6	3.457	91	teta-Butyldimethylsilanol
	3.588	72	teta-Butyldimethylsilanol
	6.127	91	Cyclotetrasiloxane, octamethyl-
	8.186	83	Disiloxane, 1,3-bis(1,1-dimethylethyl)-1,1,3,3-tetramethyl-
	11.63	83	tert-Butyl-[2-(tert-butyldimethylsilyl)oxyethoxy]dimethylsilane

Appendix E

E.1 Survey Questions

1. Is the corrosion of iron meteorites a concern in the collection?
2. Is the storage area climate controlled? If so, what methods are employed?
3. Does the collection employ the use of microclimates?
4. What is considered the ideal relative humidity in the broader collections space?
5. If microclimates are employed:
    1. What methods and materials are used? (storage boxes, desiccants, bags, oxygen absorbers, etc?)
    2. Sizes and quantities of each?
    3. Are multiple specimens stored together?
    4. What is the target relative humidity?

5. Was accessibility a factor in choosing this type of microclimate?

6. How often are conditions for the meteorites reassessed?

7. Were any other methods employed in conservation of the specimens?

Follow-up questions may include:

1. How long ago were these conditions implemented?

2. Were these changes successful in halting or limiting the corrosion of the specimens?

E.2 Survey Responses:

E.2.1 Tim McCoy and Catharine Hawks at the Smithsonian Natural History Museum:

We have not invested time or energy in working with establishing microclimates for iron meteorites. From this, I assume you mean isolating individual irons in sealed containers with some type of moisture getter that could prevent rusting. We do, of course, control the climate in our meteorite storage room, as we do throughout the building, typically to keep temperature and humidity within a comfortable range for everyone. In extreme cases, we have isolated a small number of iron meteorites in dry nitrogen storage cabinets that eliminate both atmospheric oxygen and humidity.

In the long-term, iron meteorites are inherently unstable on the surface of the Earth and will deteriorate. Microclimates may help in some aspects, but our decision to not employ extraordinary measures was driven in large part by the seminal work that Roy Clarke and Vagn Buchwald took in our collection. In first identifying akageneite as the dominant weathering product, they noted that many of the particularly rust-prone meteorites had been buried at some point and inundated by Cl-bearing fluids in the soil. At that point, these were deprived of oxygen and rusting minimized. With exposure to

atmospheric oxygen - not just humidity - the formation of akageneite commenced. While microclimates might reduce humidity, they will not reduce atmospheric oxygen. In those cases, isolation in gaseous nitrogen is the most expedient solution.

Depending upon the size of your collection, you may want to consider a commercially available product, such as one of the systems from Heritage Packaging https://heritagepackaging.squarespace.com/products.

These can be fabricated to create anoxic environments, so might be an option if a full-scale room is not viable. There are variants that have been used for pest control in museums, but are generally not designed for long-term use.

E.2.2 Carolyn Leckie at the Canadian Museum of Nature:

Below I have listed a few general preservation resources, that I am sure you are already familiar with

- 1992 benchmark Butterworth book on Care & Conservation of Geological Collections
    - Unfortunately, a 2018 JAIC paper suggest that not much has progressed WRT specifics & more research is needed
- There are some good NASA references, but I doubt the situation is very comparable (I have some in an old email I could dig up for you)
- I would also suggest that you might want to reach out to some other institutions with good collections, that may have better established protocols, such as
- One of the big American institutions who have good meteorite collections and strong conservation programs
- Also Brendt Hyde, at The ROM seems pretty active in research and collection care or meteorites

E.2.3 Lu Allington-Jones at the Natural History Museum (UK):

The meteorite storage area is climate controlled using the HVAC system, but since the area also contains staff offices and a non-iron meteorite collections, the levels are not ideal for irons. The HVAC system aims for 18-21 degrees C and 40-50% RH.

As far as I know the irons are stored at low humidity (0 to 10%RH) using artsorb or RPA oxygen scavengers in Escal™ barrier film bags. A very few are stored in glass microclimates.

As far as I am aware the anoxic environments at low RH are working well. A lot of them were bagged up in 2013 and I have not heard about any deterioration problems. We also have a low oxygen and low RH active positive pressure nitrogen enclosure (Cranbourne meteorite) in a glass display case which has been effective over several years.

One warning about the barrier film enclosures is that air exchange rate is not zero. It is best to have a look at the manufacturer's figures and try to calculate how long they will last. We use Escal™ NEO which I calculated would last 10 years before oxygen levels rose too much. We have some fossil enclosures which use RPK rather than RPA (because we did not want them to dry out) which are still at 0% oxygen after 8 years. Also the sachets must be replaced every time an enclosure is open because the reaction is finite and does not work like buffering materials such as Artsorb. Controlling the humidity rather than oxygen and humidity is much easier since the water molecule is larger than oxygen and barrier films are more effective against it. One bonus of the RP system over Artsorb, however, is that it also absorbs atmospheric pollutants.

E.3 Rubric for Prioritization

Ranked list of meteorites which require most immediate treatment:

1) Those exhibiting signs of the advanced stages of active corrosion causing immediate threat to the integrity of the specimen. If left unchecked could result in the complete loss of the specimen.

    a) Advanced stages of active corrosion include weeping (yellow-brown liquid droplets on the surface of the metal which dry to form spherical shells), cracking (may be of varying lengths and orientations or form a network; may contain fresh corrosion products), blisters and flakes (rounded prices of the outer corrosion layer may lift off and fall away completely, with orange crystals potentially left behind as corrosion continues), and delamination (the outer layer of corrosion lifts away completely from the metal core, possibly resulting in objects breaking apart entirely).

2) Those exhibiting signs of more mild corrosion which will progress to more advanced stages and cause specimen damage if not quickly addressed.

    a) Surface corrosion, often a yellow-brown crust, indicates the beginning of the formation of the mineral akaganéite (β-FeOOH), which is believed to be primarily responsible for the long-term instability of iron

3) All other iron and stony-iron meteorites.

    a) Metal which is not currently actively corroding could begin corroding in the event of a sustained high-humidity event. Given sufficient time and resources, the proper storage of all metallic meteorites should be considered.

Specimens will be prioritized beginning with those in category 1, then proceeding down the list. As there are a large number of specimens within categories 1 and 2, the criteria below will be used, in order, to determine which of these should be treated first:

1. Unstable Specimens

    a. Specimens which have been in the UAB Meteorite Collection for ≤10 years, having experienced extensive amounts of corrosion in this relatively short period of time.

2. Specimens of high research or cultural value, regardless of whether corrosion is currently active.

    a. The damage of such specimens would represent a significant loss to the collection, and thus it is imperative to ensure even mild corrosion is halted or prevented, as corrosion cannot be reversed once it begins.

3. Meteorites where a limited amount of sample or number of specimens are available within the collection.

    a. The loss of one specimen or a portion of one specimen where only one or two (perhaps small) samples are available could result in the complete loss of a particular meteorite from the collection. These specimens should be protected regardless of corrosion extent to ensure they remain represented in the collection.